ANL-6725
Chemical Separations Processes
for Plutonium and Uranium
(TID-4500, 28th Ed.)
AEC Research and
Development Report

ARGONNE NATIONAL LABORATORY
9700 South Cass Avenue
Argonne, Illinois 60440

CHEMICAL ENGINEERING DIVISION SUMMARY REPORT

April, May, June, 1963

S. Lawroski, Division Director
R. C. Vogel, Associate Division Director
Milton Levenson, Associate Division Director
V. H. Munnecke, Assistant Division Director

Preceding Quarterly Reports:

ANL-6687	January, February, March, 1963
ANL-6648	October, November, December, 1962
ANL-6596	July, August, September, 1962

Operated by The University of Chicago
under
Contract W-31-109-eng-38
with the
U. S. Atomic Energy Commission

DISCLAIMER

ANNOUNCEMENT

Change in Schedule of Chemical Engineering Division Summary Reports

This report, Chemical Engineering Division Summary Report, April, May, June, 1963 is the last in the series of quarterly progress reports that has been issued by the Chemical Engineering Division. Instead of reporting the work of the division on a quarterly basis, the work will be reported henceforth on a semiannual basis. The first Chemical Engineering Division Semiannual Summary Report will be for the period July through December, 1963.

TABLE OF CONTENTS

TABLE OF CONTENTS

LIST OF TABLES

LIST OF TABLES

LIST OF TABLES

LIST OF FIGURES

LIST OF FIGURES

LIST OF FIGURES

LIST OF FIGURES

LIST OF FIGURES

SUMMARY

CHEMICAL ENGINEERING DIVISION SUMMARY REPORT

I. Chemical-Metallurgical Processing (pages 31 to 111)

The melt refining process is a process by which EBR-II fuel is purified while in the molten condition. Major development work on this process has been completed, but work is continuing on related problems.

An experiment was conducted to investigate the behavior of fission product iodine after it is condensed on a Fiberfrax fume trap in the melt refining process, the melt refining furnace is opened, and the trap is exposed to the argon atmosphere of the EBR-II Fuel Cycle Facility. To simulate a high burnup fuel, a 20-g specimen of uranium-fissium alloy was spiked with uranium triiodide and cesium metal, and was lightly irradiated to produce iodine-131 tracer activity. The specimen was then melt refined with a Fiberfrax cover in place. The Fiberfrax was transferred from the melt refining furnace to a quartz tube furnace. Temperature gradients similar to those expected in the plant facility as a result of fission product heating were maintained in the Fiberfrax. A slowly flowing argon stream passed over the Fiberfrax and then through charcoal traps for collection and determination of the iodine activity. With a gradient in the Fiberfrax of 680 to 315 C, the rate of iodine release was nearly constant over the period of 30 hr, with about 0.16 percent of the total activity in the Fiberfrax being released each hour. At 150 C, this rate was reduced substantially. The behavior of the activity was consistent with previous indications that the volatilized iodine activity is either cesium iodide or a material containing both of these elements.

To prepare for possible future necessity of removing nitrogen from the argon atmosphere in the EBR-II Fuel Cycle Facility, studies were begun of the removal of nitrogen from argon with hot titanium sponge. Various Inconel, 300 series stainless steels, and Hastelloy steels have been tested and evaluated for the containment of titanium sponge metal in argon at 900 C. The steel most resistant to attack by titanium was Type 316 stainless steel. However, because of its superior high-temperature strength, Hastelloy X has been selected as the structural material for the high-temperature equipment. However, those parts of the high-temperature vessels which would come into contact with the titanium sponge will be lined with Type 316 stainless steel.

Work continued on the development of the skull reclamation process* for the recovery and purification of fissionable material present in the crucible residues (skulls) remaining after melt refining operations. The effects of various process changes have been elucidated in small-scale (100 g of uranium) demonstration runs. An attempt to precipitate zirconium as a carbide from the uranium-magnesium-zinc solution present after the uranium-reduction step was unsuccessful. High uranium losses in the supernatant solution removed after precipitation of the uranium-zinc intermetallic compound were traced to excessive stirring (originally done to prevent accumulation of crystals on the vessel walls). Stirring in this step will be discontinued. The rate of extraction of ruthenium in the noble metal-extraction step was increased by increase in temperature within the permissible range of 650 to 800 C and by increase in the degree of mixing of the flux and metal phases.

Operation of the large-scale integrated skull processing equipment has been started. Principal attention is being given to the materials handling operations and, in particular, to the transfers of molten metal and salt phases required in the process. According to present plan, the two uranium precipitation steps are to be conducted in a beryllia crucible. Two large thixotropically cast beryllia crucibles ($11\frac{1}{2}$-in. OD by 10-in. ID by 20 in. high) were each unexpectedly wetted by the metal process solutions; therefore, it was not possible to remove the uranium product concentrate for retorting. This wetting is contrary to experience with small beryllia crucibles of the same type. Discussions with representatives of the manufacturer of these crucibles have revealed differences in the methods of preparation of the large and small crucibles which are believed to be responsible for differences in the wetting behavior. Until properly prepared beryllia crucibles are obtained, all process steps up to retorting are being performed in the single, large tungsten crucible (12-in. OD by $9\frac{1}{2}$-in. ID by 19 in. high) used for the noble metal-extraction and oxide-reduction steps. The durability and high corrosion resistance of this crucible have been gratifying. A number of advantages of using a single crucible for all operations prior to retorting have become apparent, and this method of operation may prove to be superior to the two-crucible method.

Further results have been obtained on separation processes for fast breeder reactor fuels containing uranium and plutonium. One type of separation under study involves equilibration of the fuel constituents between liquid magnesium-zinc alloys and molten magnesium chloride at 800 C. Neptunium and curium were found to exhibit approximately the

*The process consists of oxidation of the skull material and removal of the skull oxides as a powder, extraction of noble metal impurities into zinc from a slurry of skull oxides in a halide flux, reduction of the uranium oxides by (and dissolution of the uranium in) a magnesium-zinc solution at 800 C, precipitation of a uranium-zinc intermetallic compound by cooling the solution to 500 to 525 C, decomposition of the intermetallic compound to yield uranium metal by the addition of magnesium, and retorting of the uranium product to evaporate residual magnesium and zinc.

same distribution behavior as observed for uranium and plutonium in earlier experiments. Both neptunium and curium tend to favor the metal phase, with distribution coefficients (w/o in flux/w/o in metal) having minimum values of about 0.02 at 10 w/o magnesium in the metal phase. With 100 percent magnesium in the metal phase, the distribution coefficients for neptunium and curium are about 0.9 and 0.6, respectively. Protactinium favors the metal phase more strongly, with distribution coefficients lower by about a factor of ten than those for neptunium and curium. Preliminary results for chromium indicate distribution coefficients of about 10^{-2} for 100 percent zinc, and of 10^{-1} for zinc-40 w/o magnesium in the metal phase.

A liquid metal process has been developed for separating plutonium from EBR-II depleted uranium blanket material. In this process, the blanket material is dissolved in a magnesium-zinc solution; later, uranium is selectively precipitated from solution. A demonstration run of the blanket process was made with lightly irradiated uranium but with no plutonium present to obtain information on fission product behavior. Although in the EBR-II Fuel Cycle Facility the blanket material may be cooled for a considerable time before processing, thereby allowing decay of most of the iodine activity, it was of considerable interest to determine if the iodine activity present would appear in the furnace off-gases and thereby create an off-gas handling problem. Considerable iodine activity (about one-quarter of the total) was volatilized and was found condensed on the upper walls and top flange of the furnace chamber, but little iodine activity (about 0.1 percent of the total) was found in the furnace off-gases (as shown by trapping the iodine in a charcoal filter unit). No serious off-gas handling problem due to iodine is evident. Some of the iodine in solution was removed by a mechanism other than volatilization, probably by a drossing reaction.

As expected, ruthenium largely accompanied uranium through the process, while the rare earths, yttrium, and barium and strontium appeared predominantly in the plutonium product supernatant solution. The bulk of the zirconium and tellurium activities were not accounted for, only small percentages being found with either the uranium or the magnesium-zinc "product" solution. It is believed that these activities were removed by sorption on solid surfaces.

The dilute plutonium product solution of the blanket process (about 0.1 w/o plutonium in a 50 w/o magnesium-zinc solution) must be concentrated by a factor of at least ten before it may be used for enriching the core material. Preliminary work on this evaporation step has been started on a 10-kg scale with cerium as a stand-in for plutonium.

Corrosion testing of tungsten and a 30 w/o tungsten-molybdenum alloy has been carried out in a zinc-halide flux system employed in the skull reclamation process at a temperature 200 C higher than that used in

the process (1000 C versus 800 C). After 500 hr at 1000 C, tungsten was found, by metallographic examination, to have been attacked intergranularly to a depth of 2 to 4 mils, and the molybdenum-tungsten alloy to a depth of 2 to 8 mils. Grain sizes were not greatly affected. Sharp edges remained on the specimens, and dimensional changes were less than 1 percent.

Several experiments were made to determine the effects of small amounts of added impurities on the stability of uranium-containing magnesium-zinc systems. Beryllium added to the extent of 0.05 w/o, slightly over its solubility value, and aluminum added to the extent of 1 w/o had no effect on uranium concentrations. Silicon caused direct precipitation of the uranium. Stainless steel had no effect up to a concentration of 0.1 percent, but at a concentration of 1 percent caused a slight (less than 5 percent) decrease in uranium concentration. This slight decrease in uranium concentration is believed to have been caused by reaction with elements, such as carbon or silicon, which are present at low concentrations in stainless steel.

In order to take advantage of the good mechanical properties of porous coarse-grained crucibles (such as Alundum) for the containment of metal and salt systems, sealing the pores of such crucibles by impregnating the inner surfaces with a slurry of low-melting oxides has been attempted. Subsequent firing of the crucible fuses the oxides, thereby sealing the pores. When properly applied to smooth surfaces, the coatings have been impervious and strongly adherent, but imperfections in the coatings have persisted in coatings applied to slightly rough surfaces.

Various combinations of plasma-sprayed coatings and substrate materials are being evaluated for use as container materials in liquid metal-salt processes. In preliminary thermal cycle tests (twelve cycles between 300 and 800 C), no deterioration of tungsten-coated silicon carbide (nitride- or oxide-bonded), Alundum, and Type 430 stainless steel was evident, nor of Alundum and Type 430 stainless steel when sprayed with beryllia.

Construction and testing of equipment for the preparation of 500-g batches of uranium monocarbide by precipitation from liquid metal solution have been completed. The process consists of dissolution of uranium metal in zinc-magnesium alloy, addition of carbon, removal of the supernatant liquid metal, and retorting of the uranium monocarbide product to eliminate the remaining zinc and magnesium.

New methods for the preparation of carbides are also being developed. It has been found that uranium monocarbide can be prepared by the reaction of magnesium carbide with uranium halides in molten chloride solutions.

Work has continued on the preparation of uranium monosulfide through the reaction of hydrogen sulfide with hydrided-dehydrided uranium metal, followed by homogenization at 1900 C. In recent preparations, the oxygen content of the uranium monosulfide product has been reduced to less than 0.1 w/o, and the sulfur-to-uranium ratio has been within 3 percent of the stoichiometric value.

Further investigation of the zinc-magnesium reduction of thorium dioxide suspended in a molten halide flux has indicated that a thorium dioxide-to-flux weight ratio of less than 0.2 is required for complete reduction under the following conditions: a flux consisting of 10 m/o magnesium fluoride in magnesium chloride, 10 w/o magnesium in the zinc at the end of the reduction, a temperature of 850 C, a period of 4 hr, and mixing at 1000 rpm. A brief study of crucible materials indicated that the use of graphite, silicon carbide, and alumina may result in contamination of the thorium product, but that tungsten appears to be a satisfactory crucible material.

Plutonium dioxide is also reduced to the metal by the zinc-magnesium reduction technique. The reduction of plutonium dioxide, unlike that of uranium and thorium oxides, was rapid and complete in fluxes of widely varying composition. The extent of plutonium dioxide reduction appears to be governed by the distribution coefficient of plutonium between the metal and the flux.

Previous data on the reactions of the higher uranium oxides and the oxychlorides with molten chlorides had indicated the formation of a uranium(V) species in solution which was tentatively identified as UO_2^+ ion. Comparison of the visible and near-infrared absorption spectrum of this species with the spectrum reported for the isoelectronic ion NpO_2^{++} showed corresponding peaks. The ratios of wavelengths of the corresponding peaks are nearly constant. The UO_2^+ ion is formed by the thermal decomposition of uranyl chloride:

$$2\ UO_2Cl_2 \rightleftharpoons 2\ UO_2Cl + Cl_2.$$

Through a combination of spectrophotometric measurements of the UO_2^+ ion and manometric determinations of the amount of chlorine evolved, the stoichiometry of the reaction was confirmed, and molar absorptivity data for UO_2^+ were obtained. A preliminary value of about 10^{-6} atm at 650 C was determined for the equilibrium constant of this reaction by determining the optical absorbance of UO_2^+ as a function of the chlorine pressure.

A series of tests was performed while the Argon Cell contained nitrogen at a pressure equal to the outside pressure to determine the effect of opening penetrations into the Argon Cell on the composition of the cell atmosphere. Three small penetrations were opened for periods up to

4 min without a significant increase in the oxygen concentration of the cell atmosphere. The opening of a 6-ft-diameter penetration into the cell caused the oxygen concentration of the cell atmosphere to rise to 300 ppm in $4\frac{1}{2}$ min.

A glovebox purification system was received at Idaho, leak tested, and successfully operated. Air leakage into the associated glovebox was found to be 0.015 percent per day of the glovebox-glovebox purification system volume. A second glovebox atmosphere purification system and two gas analytical instrument panelboards were tested and shipped to the Idaho site for installation.

The top shielding plug of the Argonne fuel-transfer coffin was modified to overcome binding at sliding surfaces. The plug assembly was found to function satisfactorily after the modifications had been completed.

Tests were made to determine the behavior of sodium-coated fuel pins while contained in a stainless steel melt refining charging tray. The temperature of the tray was maintained at 450 C in one experiment and at 300 C in another experiment. The sodium coating evaporated from the fuel pins in both experiments and condensed on the cold areas of the test stainless steel containers. No interaction occurred between the pins and the stainless steel containers.

A second skull-oxidation furnace is being designed which will allow the heater-cover assembly to be disposed of in a standard waste container if the heater attached to the cover should fail. The furnace atmosphere control system was successfully tested during the oxidation of 12 skulls which ranged in weight from 300 to 1300 g.

Tests with inductive heating and mixing have demonstrated that greater than 80 percent reduction of uranium oxide by 5 w/o magnesium-zinc alloy can be obtained in 2 hr at 800 C. The weight of the skull oxide charge used in the tests was $2\frac{1}{2}$ kg.

Studies on the collection of metal vapors have continued. With an improved apparatus, four runs were made in which 2-kg charges of magnesium-zinc were distilled at rates of 25, 32, 48, and 62 g/min. In the first three runs, no loss of magnesium-zinc occurred. In the fourth run, 17 g of magnesium-zinc distillate escaped from the graphite enclosure and deposited on the Fiberfrax insulators.

The solubility of plutonium in liquid zinc may be represented by the empirical equation

$$(458 \text{ to } 752 \text{ C}) \quad \log (\text{a/o plutonium}) = 8.612 - 10090T^{-1} + 1.461 \times 10^{6}T^{-2} \quad .$$

Two activation methods for the determination of oxygen in sodium are being investigated. The first involves irradiation by fast (14.5-MeV) neutrons to produce nitrogen-16 activity by the reaction

$$ {}_0n^1 + {}_8O^{16} \rightarrow {}_7N^{16} + {}_1H^1 \quad . $$

The second method involves triton irradiation to produce fluorine-18 activity by the reaction

$$ {}_1T^3 + {}_8O^{16} \rightarrow {}_9F^{18} + {}_0n^1 \quad . $$

The tritons are produced <u>in situ</u> by thermal neutron irradiation of lithium (added to the sodium sample) by the reaction

$$ {}_0n^1 + {}_3Li^6 \rightarrow {}_1T^3 + {}_2H^4 \quad . $$

The solubility of carbon in liquid sodium is being measured as a function of temperature and oxygen content as a first step in a basic study of the transport of carbon by liquid sodium.

The thermodynamics of the plutonium-zinc and plutonium-cadmium systems are being studied by means of a high-temperature galvanic cell method. The activity coefficient of saturated solutions of plutonium in liquid zinc may be represented by the equation

$$ \log \gamma_{Pu} = 5.312 - 9713T^{-1} \quad . $$

The activity coefficient of saturated solutions of plutonium in liquid cadmium may be represented by the equation

$$ \log \gamma_{Pu} = 4.786 - 6473T^{-1} \quad . $$

An optical absorption method is being developed to study the thermodynamics of binary solutions of the alkali metals.

Rare earth metal-cadmium systems are being studied by the effusion method. The following sequences of intermediate phases are found in binary systems of cadmium with lanthanum, cerium, praseodymium, and neodymium: lanthanum-cadmium system: $LaCd_{11}$, La_2Cd_{17}, La_3Cd_{13}, $LaCd_2$, and LaCd; cerium-cadmium, praseodymium-cadmium, and neodymium-cadmium system: MCd_{11}, MCd_6, M_3Cd_{13}, M_4Cd_{13}, MCd_2, and MCd.

II. Fuel Cycle Applications of Volatility and Fluidization Techniques (pages 112 to 190)

In the conceptual flowsheet of the fluid-bed fluoride volatility process, the uranium and plutonium content of spent oxide fuels will be recovered by fluorination to produce the volatile hexafluorides of uranium and plutonium. Laboratory-scale work has been concerned with the fluorination of U_3O_8 in a $1\frac{1}{2}$-in.-diameter fluid-bed fluorinator. This work is being performed to develop and test apparatus and procedures for use in future work in which plutonium will be handled. The oxide U_3O_8 is being used because it is the product which will be obtained in a proposed oxidative "decladding" step for removing the uranium and plutonium from stainless steel-clad and Zircaloy-clad fuel elements.

In the experimental work, the powdered U_3O_8 is injected into the fluid bed with the fluidizing nitrogen stream. Fluorine is brought into the bed just above the point at which the powder enters and the fluorination reaction occurs as the U_3O_8 and fluorine mix. This report covers experimental investigation of the effect of variables such as temperature, U_3O_8 elutriation from the fluidized bed, and duration of the fluorination period upon the reaction. A reaction scheme employing two periods at a reaction temperature of 500 C has been developed; in the first period, the U_3O_8 is fed into the bed and fluorination is carried out with 20 v/o fluorine in the gas phase; in the second period a gas phase containing 100 percent fluorine is recirculated through the fluid bed for a period of 5 hr. By means of this reaction scheme, more than 99 percent of the U_3O_8 fed to the reactor was converted to uranium hexafluoride.

The oxidation of uranium dioxide, which results in the formation of a finely divided U_3O_8 powder, is being considered as part of a decladding step for stainless steel- and Zircaloy-clad fuel elements. Fuel-element mockups consisting of $5\frac{1}{2}$-in.-long sections of $\frac{1}{2}$-in.-diameter stainless steel or Zircaloy tubing packed with uranium dioxide pellets were oxidized in a fluid bed at 450 C with air as the oxidant and fluidizing gas. Slots ($\frac{1}{8}$ in. x $\frac{1}{32}$ in.), with intervals of $\frac{3}{8}$ in. between ends of slots, were milled along the length of the cladding tubes to promote splitting of the cladding. It was found that the time necessary to completely split open a section of cladding along the slit line was dependent on the thickness of the tubing. For 10- and 20-mil wall thicknesses of stainless steel, the tubing split open along its entire length after 2 and 4 hr of oxidation, respectively. For 30-mil Zircaloy, the tubing was completely split after 6 hr of oxidation. Complete removal of the U_3O_8 product was accomplished by 1-2 hr of further oxidation.

Rates have been measured by means of a thermobalance for the reaction of U_3O_8 with fluorine over the temperature range from 300 to 400 C. Two samples of U_3O_8 were used; one was an analytical standard sample, the other a commercially produced material. The commercially

produced material is also being used in the fluid bed fluorination work. The data have been treated by a diminishing-sphere kinetic model which relates the reaction rate constant k (in units of min^{-1}) directly to a function of the fraction of the oxide remaining after a reaction time t. The reaction rate constants for the commercially produced material were slightly higher than those for the analytical standard sample at the same temperatures. An average value of 30 kcal/mole was calculated for the activation energy of this reaction which, within experimental error, is the same for both materials used. Equations are given which relate the change in reaction rate constant with temperature. An estimate of the time required to completely convert a particle of U_3O_8, of about 10-micron diameter, to uranium hexafluoride, based on an extrapolation of the rate constant to 500 C, was less than 2 min.

The study of the effect that the addition of helium to plutonium hexafluoride has on the decomposition of plutonium hexafluoride by gamma irradiation has been continued. Additional data have given G values of 7.2 ± 1.1 and 5.8 ± 0.8 for experiments in which one atmosphere and two atmospheres of helium, respectively, were added. A comparison of these G values with the G value of 7.5 ± 0.7 obtained for the decomposition of plutonium hexafluoride alone indicates that helium does not significantly influence the decomposition.

Engineering-scale investigation of a fluid-bed fluoride volatility process for the recovery of uranium and plutonium from discharged uranium dioxide fuels was continued. In this process the oxides are directly fluorinated to the hexafluorides, which are then decontaminated and separated by volatility techniques. Emphasis has been placed, for the sake of process simplicity, on the batch reaction of oxide charges in a single vessel. The major objectives have been to demonstrate short batch fluorination time (less than 20 hr) and satisfactory fluorine utilization efficiencies (greater than 75 percent).

The latest and most successful runs have employed a two-zone, oxidation-fluorination technique. In this technique, the lower (oxidation) zone of the reactor consists of a bed of uranium dioxide pellets with fused alumina grain filling the voids of the bed (fluidized-packed bed); the upper (fluorination) zone consists of a fluidized bed of fused alumina grain that extends above the fluidized packed bed. By passing an oxygen-nitrogen mixture through the lower zone, U_3O_8 fines (10 to 20 μ) are produced and transported to the upper fluidization zone, where they are fluorinated to uranium hexafluoride vapor.

In recent studies the two-zone oxidation-fluorination scheme was used successfully with 12-in.-deep, fluidized packed beds of uranium dioxide. Caking was avoided, and both high production rates and high fluorine utilization efficiencies were attained. In this work, emphasis was placed on optimizing process control by regulation of the input of the reagent gases: oxygen and fluorine.

A two-zone run was carried out in the 3-in.-diameter fluid-bed reactor in which a 12-in.-deep, fluidized packed bed of uranium dioxide pellets was completely fluorinated. Improved control of the reaction was evidenced by more uniform rates of production of uranium hexafluoride and by higher fluorine utilization efficiency for the complete batch operation. Ninety percent of the product was collected in 8.2 hr of fluorination, corresponding to a production rate of 54 lb UF_6/(hr)(sq ft) and a fluorine efficiency of 79 percent. A final period of time to complete the fluorination by recycling fluorine extended the total processing time to 12.5 hr and reduced the overall fluorine utilization efficiency to 75 percent. The continuous monitoring of fluorine in the process off-gas with a newly installed gas thermal conductivity cell assisted in improving process control. From the results of this run, it is apparent that optimum conditions were approached more closely than in previous runs: The fluorination zone was maintained at 500 C, and the temperature gradient in the oxidation zone was from 480 C at the top of the bed to 340 C at the bottom; the gas flow to the oxidation zone was 1.0 scfm (at 1 atm and 25 C) and contained 8 percent oxygen in nitrogen; the gas flow in the fluorination zone was 1.5 scfm and contained 9 to 15 percent fluorine in nitrogen at the inlet; a small amount of gas (about 2 percent of the total gas flow) was added in pulses at a frequency of 2 pulses/min.

Work has been started on the evaluation of the two-zone technique for the processing of stainless steel-clad uranium dioxide pellets. Short lengths (~1 in.) of stainless steel tubing with both ends open are used to contain uranium dioxide pellets and thereby simulate a charge of sheared fuel elements. Longer element sections with longitudinal perforations or slits are also being evaluated.

In two experiments carried out in the 3-in.-diameter fluid-bed reactor, removal of uranium dioxide from the stainless steel tubing was complete with a 1.5-in.-deep fluidized packed section and 95 percent complete with a 6-in. packed section. These results were obtained in 8.5 and 13.5 hr, respectively. Operating conditions for both runs were similar: oxidation was carried out at 450 C with 22 percent oxygen, and fluorination was carried out at 500 C with 4 to 10 percent fluorine. In each run, uranium dioxide removal from the cladding was enhanced by passage of fluorine through the fluidized packed bed with the system on total off-gas recycle.

The method of removal of uranium dioxide fuel from cladding by oxidation is also being studied separately from the fluorination. A series of twelve experiments has been completed as an initial examination of the extent of removal of uranium dioxide from simulated stainless steel-clad fuel elements sheared to a 1-in. length. The $\frac{1}{2}$-in.-diameter stainless steel-clad segments were charged to the 2-in.-diameter fluid-bed reactor as random-packed beds of 40 segments. The removal of uranium depends both on the oxidation of the uranium dioxide pellets to U_3O_8 and on the

physical disengagement of the U_3O_8 from the pellets and cladding as fines, which are then mixed with the fluid bed of inert fused alumina grain. Air at a superficial gas rate of about 0.75 ft/sec was the oxidizing gas. Gas pulsing (with air) was only partially beneficial for improving the rate of removal of oxide and for improving temperature uniformity in the system. Pulses of 1-sec duration were used at two frequencies, 0.5 pulse/min and 6 pulses/min; in most runs the fluidizing gas was cut off during the pulsing to enhance the pulse effect. Variations in the pulsing technique over the range of conditions tried produced little difference in results. Runs were carried out at constant temperatures in a range from 350 to 550 C. An optimum overall rate of removal appeared to occur at temperatures between 400 and 500 C.

Since the separation of oxide from the cladding involves two successive steps, chemical oxidation and physical removal, the chemical reaction was observed independently of removal by determination of the oxygen consumption with a gas thermal conductivity cell calibrated for oxygen-nitrogen mixtures. From the gas analysis, it was found that the oxidation reaction had virtually ceased after 7 hr at 550 C and after 9 hr at 450 C. However, only partial removals of uranium oxide were achieved in these runs.

Difficulty in obtaining complete physical removal has been encountered in all tests made thus far Reasonable rates of removal have been obtained up to 50 to 80 percent removal, but overall removals greater than about 80 percent have not been obtained Somewhat higher removals were obtained in tubing elements located at the top of the fluidized packed bed than at the bottom of the bed.

Additional experiments were made with alternate steps of oxidation and reduction of the uranium dioxide. This technique is capable of promoting the pulverization of uranium dioxide and thus may assist in enhancing the removal. (This oxidation-reduction method may have an advantage over the oxidation-fluorination method described above in that the cladding metal is not fluorinated.)

Two oxidation-reduction experiments were conducted on the same type of charge of stainless steel-clad uranium dioxide pellets as was used in a previous experiment in which the removal of uranium dioxide by oxidation alone was attempted. The reduction was performed at 550 C with a mixture of 5 v/o of hydrogen in nitrogen This reducing gas was passed through the reactor after the initial oxidation had been completed at 450 C. After reduction of the U_3O_8 residues, the uranium dioxide was reoxidized at 450 C. However, the removals of 80 percent obtained in these two experiments were not significantly different from those obtained when oxidation alone was used. The incomplete removals were apparently due to insufficient circulation of the inert fluid-bed material and insufficient

motion of the individual fuel segments in spite of gas pulsing (pulses of 0.5-sec duration at a rate of 2 pulses/min).

In two additional experiments, which were performed at the same oxidation and reduction temperatures, the fluidized packed bed of fuel elements was divided into four individual packed sections which were each approximately $1\frac{1}{2}$ in. deep and which were separated from each other by support plates. The fluid bed was continuous between these bed sections. This procedure, combined with gas pulsing, improved the inert material circulation and the motion of the fuel segments, and resulted in an almost complete removal of the uranium oxides from the stainless steel cladding after a reaction time of about 13 hr. The separation obtained in one run was 100 percent and in the other, 99 percent.

The results of these two experiments indicate that a separation of uranium dioxide from stainless steel cladding is achievable by an oxidation-reduction-reoxidation process if the inert fluid-bed material and especially the motion of the fuel segments are not restricted. Further effort is planned to develop a satisfactory practical means of carrying out the oxidative separation.

Construction is under way of a facility for engineering-scale investigation of the several steps of a fluid-bed fluoride volatility process for recovery of fissionable materials from spent nuclear reactor fuel of the uranium dioxide type and for reconstitution of the oxide fuel material after it is freed from fission products. In this process, the dioxides of uranium and plutonium are fluorinated to form the volatile hexafluoride products. Subsequently, the hexafluorides are further purified by fractional distillation and converted back to dioxides by reaction with steam and hydrogen. The fluorination equipment is now being installed. Because of its high toxicity, the radioactive plutonium must be completely contained. Therefore, all equipment is being installed inside a large glovebox, 17 ft high by 25 ft long.

In the present period, the process piping and valve installations in the large alpha containment box and in the fluorine gas storage and supply system located in the fluorine cabinet have been completed. Current work is concerned chiefly with the installation of the instrumentation and auxiliary lines inside of the box. The installation and mounting of the fluorine pump has also begun. Testing of process valves under extended use has been started.

The elevator lifts which provide personnel with access to glove ports at all levels of the large alpha box have been received and installed.

The Phase II subcontract for installation of services and ventilation has been awarded. The completion date for this work is in early September, 1963.

Glovebox enclosures used for handling of plutonium and its compounds are equipped with filters to prevent the escape of particulate plutonium. Since plutonium hexafluoride reacts with moisture in the air to form a solid reaction product (PuO_2F_2), an investigation of the factors which affect the filtration of products of the hydrolysis of plutonium hexafluoride is being carried out.

In order to provide a basis for the analysis of experimental filtration data, mathematical models were developed to estimate the effects on filtration of particle agglomeration and of loading of the filters. Data previously reported on filter penetration have been analyzed and correlated on the basis of these estimates.

A basic investigation of the mixing of fluidized particles in the voids of a packed bed of larger, nonfluidized bodies was carried out in support of the development of the fluid-bed fluoride volatility process which involves the use of inert fluidized particles to remove heat generated by the fluorination of a fluidized packed bed of uranium dioxide pellets. Copper and nickel shot (-40 +50, -100 +120, -120 +200, and -140 +170 mesh) and spherical ($\frac{3}{16}$ in.-, $\frac{1}{4}$ in.-, $\frac{3}{8}$ in.-, and $\frac{1}{2}$ in.-diameter) and cylindrical ($\frac{1}{4}$ in. x $\frac{1}{4}$ in., $\frac{3}{8}$ in. x $\frac{3}{8}$ in., and $\frac{1}{2}$ in. x $\frac{1}{2}$ in.) packings were used as bed materials. Diffusion coefficients were determined as a measure of the rate of particle movement during the mixing process.

It was found that, consistent with a random-walk model for eddy diffusion in flow through packed beds, the rate of mixing was proportional to the size of the packing. At a given gas velocity, mixing decreased with increased fluidized particle size. When -40 +50 mesh copper-nickel shot was used as the fluidized material in the voids of $\frac{3}{8}$-in.-diameter spherical packing over a range of gas velocity from 1.8 to 2.9 ft/sec, the mixing diffusivities increased from 0.17×10^{-4} to 1.8×10^{-4} ft^2/sec. The diffusivity of -140 +170 mesh copper-nickel shot with the same packing increased from 1.7×10^{-4} to 16.7×10^{-4} ft^2/sec as the fluidizing gas velocity increased from 0.62 to 3.0 ft/sec.

Mixing rates were higher for a fluidized bed without the presence of the fixed packing. Also, for fluidization without packing, mixing increased with increased height of the fluidized bed, whereas in the case of the fluidized packed bed, the baffling by the fixed packing resulted in more uniform fluidization, and solids mixing was found to be independent of bed height.

An empirical correlation was developed for fluidization in beds containing spherical packing, which relates the diffusivity of the fluidized solids to the packing size, the fluidized particle size, and the gas rate.

Development work on a fluid-bed volatility process scheme for the recovery of enriched uranium from low uranium-high alloy fuel is in progress. The first fuel to be studied is uranium-zirconium fuel. In the process scheme, the zirconium is separated as the volatile tetrachloride during hydrochlorination of the alloy, and the uranium is recovered as the hexafluoride in a subsequent fluorination step. The reactions are conducted in an inert fluidized bed (currently, fused alumina grain is being used as the bed material) which serves as a heat transfer medium.

In current studies in the 1½-in.-diameter fluid-bed system, further evaluation of the hydrogen chloride-fluorine reaction sequence was made using, for the first time, miniature multiplate fuel element subassemblies (normal uranium-Zircaloy alloy clad with Zircaloy; overall uranium content about one percent). Two runs were completed, one with high-purity, Type RR Alundum and one with the less costly, Type 38 Alundum (Norton Company granular fused aluminas) as fluid-bed material. One charge of -14 +20 mesh, Type 38 Alundum was used as the filter bed for both runs.

Hydrochlorination of each subassembly was completed in about 7 hr. Alloy temperatures to 750 C were noted, while the maximum fluid-bed temperature was only 500 C. The reactor walls in the fluid-bed zone were maintained in the range from 300 to 415 C.

By use of a modified fluorination procedure, a lower initial temperature (250 instead of 350 C) and a relatively high initial fluorine concentration (50 percent instead of 5 to 10 percent), reduction of the concentration of uranium in the final beds to a level of <0.01 w/o (the current goal) was achieved for both Type RR and Type 38 Alundum. This is the first time that these levels have been obtained for hydrogen chloride-fluorine cycles in the absence of other reagents. The concentration of uranium in the filter bed remained at 0.007 w/o after each run.

Correlation of the loss of uranium during hydrochlorination with absolute temperature now suggests that a major part of the uranium is lost as vapor (probably as uranium tetrachloride) rather than as particulate solids. The rate of loss of uranium correlates with the lowest temperature maintained in that part of the reactor system that is downstream of the fluid bed. Losses ranged from 0.13 mg/hr at 320 C to 8.7 mg/hr at 390 C. Changing the alumina in the packed-bed filter section from -40 +60 mesh to a more coarse fraction, -14 +20 mesh, produced no noticeable effect on the uranium losses sustained during hydrochlorination. This tends to substantiate the belief that uranium is lost as a vapor. Pressure buildup associated with the packed-bed filter was found to be relieved by use of the more coarse -14 +20 mesh bed material.

Inspection of a multiplate fuel element subassembly after one stoichiometric equivalent of hydrogen chloride had been fed to the reactor showed that the extent of hydrochlorination of the subassembly decreased

gradually with increase in distance from the gas inlet. The upper portion of the plates appeared completely unreacted.

Infrared and mass spectrometric analyses of the contents of the hexafluoride collection traps indicate that the same minor constituents, including chlorine mono- and trifluorides, were present for both the hydrogen chloride-fluorine cycle and the hydrogen chloride-phosgene-fluorine cycle, although no quantitative data are available for the latter. The data obtained in the current run indicated that about 7 percent of the chlorine initially associated with the uranium after hydrochlorination was converted to chlorine trifluoride during fluorination.

Adaptability of the fluid-bed hydrolysis scheme to the conversion of aluminum chloride vapor (simulated waste from the processing of aluminum-based alloy fuels) to the more readily stored oxide has been demonstrated. Three experiments (total run duration of 9.5 hr) were conducted in the 6-in.-diameter column (used previously for hydrolysis of zirconium tetrachloride) at 300 C with aluminum trichloride feed rates of 4 kg/hr and the steam rate adjusted at four times the stoichiometric requirement Sand was used as the starting bed material Operations were trouble-free, and excellent overall mass balances were obtained. No trace of aluminum was found in the off-gas stream, indicating that hydrolysis was complete within the unit.

Excessive fines formation in recent zirconium tetrachloride hydrolysis studies is now presumed to be associated with the presence of unsublimable material in the as-supplied solid tetrachloride.

Installation has been completed of the pilot-plant facility for the fluid-bed volatility reprocessing of highly enriched uranium-alloy fuel. Final leak-checking is in progress. Shakedown and operation of this facility with nonirradiated fuel material is scheduled for the ensuing quarter.

Design of the bench-scale facility for high-activity-level studies on the fluid-bed volatility process for highly enriched uranium alloy fuels is nearly complete. Fabrication of the equipment and procurement will start next quarter. Installation of the facility during the latter half of 1963 is planned.

Process development studies of a fluid-bed scheme for preparing dense uranium dioxide particles directly from uranium hexafluoride were continued in a 3-in.-diameter Monel column. The scheme involves reaction of the hexafluoride with a mixture of steam and hydrogen ($UF_6 + H_2 + 2H_2O \rightarrow UO_2 + 6HF$) in the presence of a starting bed of uranium oxide maintained at 650 to 700 C

A method of up-grading (densifying) low-density (<7.0 g/cc) uranium dioxide is being sought; therefore, a study was made in which the

course of the increase in density of a starting bed of low density was observed. The established technique of alternating uranium hexafluoride feed periods with periods in which steam and hydrogen only were fed (residual fluoride cleanup period) was used.

An unexpectedly large density increase and no overall particle growth were observed over the scheduled 8-hr run period, during which time 0.84 bed equivalent of dioxide was produced. The anticipated density increase (based on previous results) was about 12 percent, whereas a 24 percent increase to 8.6 g/cc was obtained; the expected increase in average particle size due to deposition of new material was about 19 percent. These anomalous results suggest that sintering of the entire particle is occurring, and not just the surface as was previously believed.

III. Calorimetry (pages 191 to 200)

Refinements in the calculations have led to slight revisions in the derived thermal data for the formation of uranium hexafluoride from the elements at 25 C. The revised data are: standard energy of formation, ΔEf°_{298}, -520.7_9(c), $-509\ 5_1$(g), standard enthalpy of formation ΔHf°_{298}, -522.5_7(c), $-510\ 7_0$(g); Gibbs energy of formation, ΔGf°_{298}, $-491\ 8_9$(c), -490.7_2(g). The uncertainty intervals are $\pm\ 0.4_4$ for uranium in the crystalline state and $\pm\ 0.4_6$ in the gaseous state

Preliminary investigation is in progress to develop satisfactory techniques for the determination of the heat of formation of uranium monosulfide. It has been found that, with proper protection of the sample from fluorine before ignition, the fluorine bomb calorimetric method will very likely be suitable.

Preliminary investigation has been in progress to develop satisfactory techniques for the determination of the heats of formation of tetrafluoromethane (CF_4) and silicon carbide. Satisfactory techniques have been found, and the calorimetric system is being calibrated preparatory to the calorimetric studies.

A critique of the available literature data for the heats of formation of hydrogen fluoride gas and its aqueous solutions is being made.

The furnace component of the 1500 C enthalpy calorimeter has been disassembled. It was found that the three silver heat shields and three of the five aluminum heat shields had melted to a considerable extent. Modifications and simplifications have been made to the furnace core, and the furnace has been reassembled. Experiments have been performed to obtain heat transfer data across the $\frac{3}{4}$-in. dust shield containing bubbled aluminum oxide.

IV. Reactor Safety (pages 201 to 223)

The air oxidation of uranium at temperatures above 500 C is being investigated in order to determine the nature and degree of protectiveness of oxide films formed. In current studies, uranium specimens are heated by induction in a closed loop apparatus. The rate of the initial reaction is determined by measurements of pressure decrease, with a pressure transducer. Studies have been performed with the following oxidants: pure oxygen at 500 and 600 C, dry air between 500 and 1000 C, and 20 v/o oxygen-80 v/o argon mixture between 500 and 1000 C. The results of these experiments were integrated with the results of previous studies of the uranium-air reaction in which a once-through flow method was used, and in which the oxygen and nitrogen depletion was measured by means of a mass spectrometer.

The character of the oxidation reaction (linear, parabolic, or cubic rate law) found for a particular gas mixture and temperature was consistent; however, there was considerable scatter in the values of the rate constants and the times of transition from one reaction stage to another. At 500 C, the reaction of uranium with each of the gases followed the same nearly linear rate law. At 600 C, a linear rate was found in pure oxygen; however, the reaction rate in air and in the oxygen-argon mixture was initially parabolic and later became linear (paralinear). At 700, 800, 900, and 1000C, the uranium-air reaction remained paralinear; however, the parabolic period of the reaction was much longer at 900 and 1000 C than at the lower temperatures. The characteristics of the reaction of uranium with oxygen-containing gases suggested that the reaction rate is controlled by an adsorption equilibrium at the oxide-gas interface and by the diffusion of oxygen ions through oxide film. The transition from a parabolic to a linear reaction probably occurs when the protective oxide film begins to crack.

Studies of the oxidation and ignition of plutonium are continuing. Results of ignition-temperature determinations with specimens of cubes and foils of pure plutonium indicated that the variation of ignition temperature with changes in specific area were not continuous. Ignition occurred at approximately 500 C for specimens of low specific area and at approximately 300 C for specimens of high specific area. Discontinuities in ignition temperature occurred very sharply at a specific area of 1.5 sq cm/g in air and of 6.0 sq cm/g in oxygen. The two regimes of ignition were consistent with a change in isothermal oxidation kinetics which had previously been shown to occur just above 300 C.

The experimental program to determine rates of reaction of molten reactor fuel and cladding metals with water is continuing. A method of study is under development in which the energy contained in the light beam from a ruby laser heats single particles of metal in a water environment. The laser heating method will replace the condenser-discharge

experiment. Experimental development of the method is progressing along three lines: (1) Means are being developed of (a) focusing the laser beam on metal particles contained within a glass reaction cell and (b) measuring the efficiency of energy transfer. (2) A rapid-response two-color optical pyrometer is being constructed to determine the temperatures reached by the heated particles. (3) Microanalytical apparatus to determine the quantity of hydrogen generated by metal-water reaction in closed glass reaction cells has been constructed and tested.

Studies of metal-water reactions initiated by a nuclear transient have been continued. In these studies, small fuel specimens were submerged in water in high-pressure autoclaves which were placed at the center of TREAT and subjected to severe nuclear transients. Studies reported previously included experiments with specimens of clad SPERT-ID fuel and unclad SL-1 fuel (both are aluminum-uranium alloys) reacting in room-temperature water. Four additional experiments have now been completed in water which was initially heated to 285 C (saturation pressure 1000 psi) prior to the reactor transients. The energy supplied in two transients was calculated to be only enough to melt the specimens. Only 0.2 to 0.4% metal-water reaction occurred in these runs, in agreement with results in room-temperature water. In the other two experiments, the nuclear energy input was calculated to bring the specimen temperature somewhat above 1200 C. The extents of metal-water reaction in these two tests were 76 and 89%, which was considerably greater than was observed for similar earlier runs in room-temperature water ($<$20% reaction). The large increase in reaction may have been due in part to higher peak fuel temperatures resulting from a decreased heat-loss rate during heating in saturated water compared with the greater heat-loss rates occurring in subcooled water in previous experiments. The reactions, however, did not generate an explosive pressure rise.

Two TREAT experiments were performed, in each of which three SPERT-ID fuel specimens were arranged at the end of a long alumina tube. The metal-water reaction per gram of metal was identical with that obtained in previous experiments with single specimens. There was no indication that a violent water hammer was generated during the experiment such as that observed in the destructive transient recently conducted in the SPERT-1 reactor.

Particle size determinations were performed on the residue from all of the TREAT experiments with the SPERT-ID and the SL-1 fuel material. The results showed that the surface area exposed to the water increased by a factor of about 100 when the nuclear energy input exceeded 450 and 530 cal/g for SPERT material and SL-1 material, respectively. The increased surface area coincided with an increase in the extent of metal-water reaction.

A method has been developed for comparing the quantity of metal-water reaction occurring in TREAT experiments with that estimated to have occurred in the SPERT-1 and SL-1 meltdowns. This procedure utilizes an estimate of the percentage of the reactor core which was completely melted and an estimate of the peak fission energy density at the center of the core. This information defined a sphere of melting in which the fission energy at the center of the sphere was a peak value (500 cal/g for SL-1 and 380 cal/g for SPERT-1) and the fission energy at the periphery of the sphere was 220 cal/g, the energy required to heat aluminum to its melting point and fully melt it. The sphere was then segmented mathematically into regions and each region was assigned an average temperature. The extent of chemical reaction was calculated by reference to TREAT results in which specimens reached a temperature similar to those reached in the SPERT-1 and SL-1 meltdowns. A summation over the sphere of melting then yielded an estimate of the total quantity of metal-water reaction. Results calculated from TREAT data yielded 2 MW-sec of chemical energy for the SPERT-1 excursion and 26 MW-sec of chemical energy for the SL-1 excursion. These values may be compared with estimates of the extent of metal-water reaction based on the post-transient collection and analysis of alpha-alumina in the reactor debris, namely, 3-4 MW-sec of chemical energy for the SPERT-1 excursion and 24 ± 10 MW-sec for the SL-1 excursion.

V. Energy Conversion (pages 224 to 242)

Bimetallic cells are simple concentration cells with a common anode-cathode electrolyte. The internal cell resistance can be made very low, with a resulting capability of high current density (100-500 ma/sq cm) output at one-half open-circuit voltage.

Temperature-emf-composition data for the lithium-bismuth cell have been obtained over the temperature range from 750 to 1150 K. Similar data for the lithium-tin system are being determined. The lithium-tin cell delivers lower voltages than does a lithium-bismuth cell; however, since the tin vapor pressure is lower than that of bismuth, separation of the metals by vaporization at high temperature would be easier. The lithium-tin cell is especially attractive because the lithium appears to be regenerated thermally as virtually a pure lithium phase.

The anomalous double exothermic break above the eutectic halt in the cooling curve of binary mixtures of liquid lithium hydride and lithium chloride has been explained. Resolution of this anomaly has shifted the lithium chloride solid-liquid equilibrium temperatures to lower values in the phase diagram. Values for excess chemical potentials and activity coefficients which have been calculated indicate that the system is close to an ideal solution.

The solubility of liquid lithium metal in liquid lithium chloride was 1.3 a/o at 610 C as determined by an isopiestic equilibration. This may be compared with a literature value of 0.5 ± 0.2 a/o at 650 C. Work on a transpiration apparatus for the study of liquid-gas phase equilibria is complete.

A 100-g batch of relatively highly pure uranium monosulfide has been prepared for use in thermoelectric parameter measurements and for use by the Calorimetry Group for measuring the heat of formation of uranium monosulfide.

The Seebeck coefficient has been measured as a function of temperature for two specimens of uranium monosulfide (a sintered pellet containing negligible insolubles and a slab fabricated from a melted ingot containing one percent insolubles). The coefficients for both samples showed a temperature dependence. The magnitude of the Seebeck coefficient values were similar to those previously reported for other uranium monosulfide specimens.

The presence of higher sulfides such as U_2S_3 and U_3S_5 in uranium monosulfide results in a decrease in Seebeck coefficient values with increasing temperature; a change in the sign of the Seebeck coefficient occurs at approximately 600 C.

A linear increase in resistivity with increasing temperature was found for a thorium monosulfide specimen. For a 50-50 m/o US-ThS solid solution, the resistivity was found to be virtually constant with temperature.

The Seebeck coefficient as a function of temperature was also measured for a sintered specimen of uranium monophosphide. A temperature dependency was shown. The magnitude of the Seebeck coefficient values was similar to those obtained with uranium monosulfide.

VI. Determination of Nuclear Constants (pages 243 to 246)

The program for the measurement of neutron cross sections of elements of importance to fast reactor technology has been continued. Preliminary data on the capture cross section of rhenium-187 were obtained, and studies of neutron total cross sections of rhenium as a function of neutron energy have begun. The total neutron cross sections of gadolinium have been determined as a function of neutron energy between 9 and 1880 keV. The neutron capture cross sections of erbium-170 have been determined for neutron energies between 0.34 and 1.9 MeV. The cross section data for the three elements are presented in graphical form.

CHEMICAL ENGINEERING DIVISION
SUMMARY REPORT

April, May and June, 1963

I. CHEMICAL-METALLURGICAL PROCESSING*

Pyrometallurgical processes for the recovery of fissionable material from discharged reactor fuels offer promise of achieving a reduction in the reprocessing costs associated with nuclear power. The principal characteristics of pyrometallurgical processes which are likely to result in lower costs are their simplicity, compactness, low-volume dry wastes, and capability for handling short-cooled fuels, with a resulting reduction in fuel inventories. Among the pyrometallurgical processes under development are melt refining (a simple melting procedure for metallic fuels), and various processes for core and blanket materials which utilize liquid metal solvents as processing media. Pyrometallurgical techniques also show promise for the preparation of various reactor-fuel materials, including metals and carbides. The melt refining process is presently in the most advanced state of development, and it will be used for the recovery of enriched uranium from the first core loading of the second Experimental Breeder Reactor (EBR-II),** located in Idaho.

A. Pyrometallurgical Development

1. Melt Refining
(R. K. Steunenberg, L. Burris, Jr.)

The fuel used in the first core loading of EBR-II consists of approximately 50 percent enriched uranium alloyed with about 5 w/o noble metal fission product elements which improve the stability of the alloy under irradiation. The fuel pins are clad with stainless steel, thermally bonded by a small amount of sodium in the annulus. The pins are declad mechanically, chopped, and charged to a lime-stabilized zirconia crucible in which they are melted and liquated under an argon atmosphere at 1400 C for a period of 3 to 4 hr. During this treatment, approximately two-thirds of the fission products are removed by volatilization and selective oxidation by the crucible. The purified metal product is top-poured into a mold to form an ingot from which new fuel pins are prepared by injection casting. A mixture of oxidized and unpoured metal remains in the crucible as a skull from which uranium is recovered by a separate process (see Skull Reclamation Process) employing liquid metal solvents.

*A summary of this section is given on pages 11 to 17.

**Melt refining will be performed in the Fuel Cycle Facility, which is adjacent to the EBR-II reactor building.

During melt refining, a Fiberfrax* fume trap on top of the crucible is used to collect volatilized sodium and condensable fission products. The experimental work during the quarter has been concentrated on an attempt to estimate the amount of fission product iodine that may be released to the cell atmosphere when the fume trap is removed from the melt refining furnace in the EBR-II Fuel Cycle Facility.

a. Release of Iodine from a Fiberfrax Fume Trap
(N. R. Chellew, D. M. Meyer)

During the melt refining step in the EBR-II Fuel Cycle Facility, much of the fission product iodine is expected to condense on a Fiberfrax cover located over the melt refining crucible. This fume trap is described in previous Summary Reports (ANL-6145, p. 32, and ANL-6287, p. 90). After the melt refining operation is completed, the furnace will be allowed to cool to an equilibrium temperature, and gaseous fission products, primarily xenon-133 and krypton-85, will be removed by evacuation before the furnace is refilled with argon and opened. If the fume trap is kept on top of the crucible during this period, it is estimated that fission product decay heat from the melt refining skull will raise the temperature of the inner surface of the Fiberfrax fume trap to about 700 C. Under these conditions the outer surface of the $\frac{7}{8}$-in.-thick Fiberfrax would have a temperature of about 350 C. If the fume trap is lifted away from the crucible, however, the fume trap is expected to cool to a temperature of 150 to 200 C.

The objective of the experimental work was to estimate the amount of fission product iodine that would be released from the fume trap when the melt refining furnace was opened with the fume trap at temperatures approximating each of the two conditions of fission product heating mentioned above.

Experimental

In this investigation an attempt was made to simulate the EBR-II plant conditions as closely as possible. Previous studies with 7-g charges of highly irradiated EBR-II prototype fuel (see Summary Report ANL-6569, p. 26) had indicated that the iodine which had volatilized during melt refining had condensed as cesium iodide. In the present work, high burnup of a fuel sample weighing about 20 g was simulated by placing uranium triiodide and cesium metal in separate holes in a natural uranium-5 percent fissium capsule and sealing uranium plugs in the holes by electron beam welding. The ratios of cesium and iodine to uranium alloy in

*A product of the Carborundum Corporation prepared from amorphous fibers and colloidal silica binder. The reported composition in w/o is: Al_2O_3 (51.2), SiO_2 (47.4), B_2O_3 (0.7), and Na_2O (0.7).

this capsule were, respectively, about four and thirteen times higher than those for EBR-II fuel irradiated to 2 total a/o burnup. The capsule was lightly irradiated in a thermal flux to produce iodine-131 and cesium-134 activity, and was cooled about 20 days to allow decay of the 30-hr tellurium-131 parent.

The apparatus used in the experiment is illustrated in Figure I-1. It consisted of (1) an induction furnace to melt the fuel with a one-inch-thick Fiberfrax cover in place,* (2) a separate quartz tube furnace into which the Fiberfrax fume trap could be moved after melt refining

Figure I-1

APPARATUS FOR STUDY OF IODINE RELEASE FROM A FIBERFRAX FUME TRAP

(not to scale)

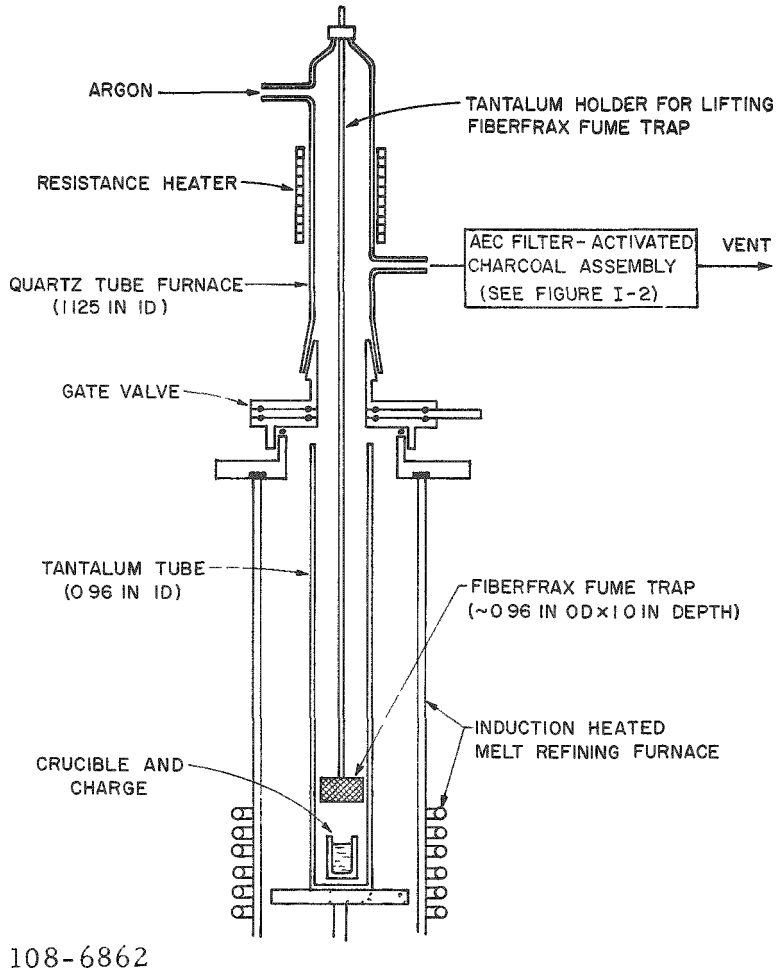

*During this step the temperature gradient in the Fiberfrax (bottom surface, 1015 C; top surface, 540 C) approximated that observed in the fume trap during tests of the plant-scale melt refining furnace.

was completed; the Fiberfrax fume trap could then be isolated and heated by a resistance heater to simulate fission product heating, and (3) an assembly of AEC filters and activated charcoal beds* to collect the iodine activity removed from the isolated Fiberfrax cover by a slow-flowing stream of argon. A diagram of this assembly is shown in Figure I-2. Two similar filter assemblies, A and B, were used and were alternated so that measurements of gamma activities could be made without interrupting the run.

Figure I-2

AEC FILTER-ACTIVATED CHARCOAL ASSEMBLY FOR COLLECTION OF IODINE RELEASED FROM A FIBERFRAX FUME TRAP

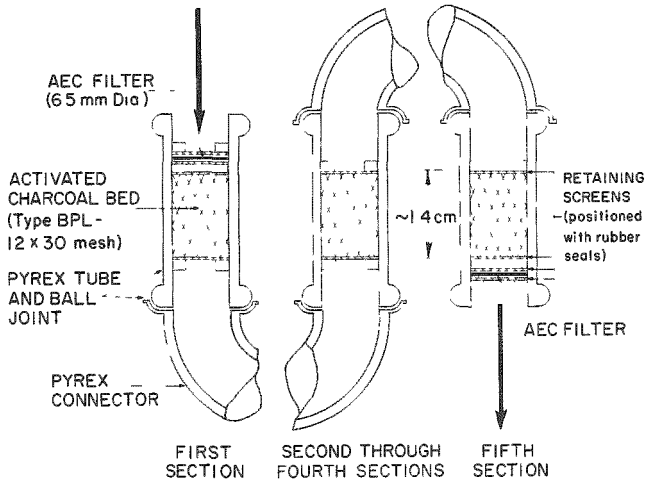

108-6886

In the experiment, the lightly irradiated 19.97-g fuel capsule and 0.21 g of sodium (to simulate the sodium present as a thermal bonding medium in the EBR-II fuel element) were charged to a small lime-stabilized zirconia crucible, the Fiberfrax fume trap was placed in its lower position, and the charge was melt refined for one hour at 1400 C. Previous results (see Summary Report ANL-6569, p. 26) had shown that one hour of melt refining on a small scale (7 g) is sufficient to remove over 98 percent of the iodine activity. After the melt refining furnace had cooled overnight, the Fiberfrax was withdrawn into the upper section of the apparatus, and radioactive krypton and xenon were removed by evacuating the system to 7 μ. The Fiberfrax fume trap was then isolated from the lower section of the apparatus by closing the metal gate valve shown in Figure I-1 and was placed at a position in the quartz tube furnace which would allow the desired temperature gradient to be obtained. One atmosphere of argon was then added to the system.

Figure I-3 shows the appearance of the Fiberfrax trap after the melt refining operation. The blackening of the zone facing the melt is associated with chemical reaction between the Fiberfrax and the sodium and cesium volatilized during melt refining.

---

*A similar AEC filter-activated charcoal filter assembly was found to be effective in removing iodine activity from a similar gas stream in previous experiments (see ANL-6596, p. 30).

Figure I-3

FIBERFRAX FUME TRAP AFTER MELT REFINING EXPERIMENT

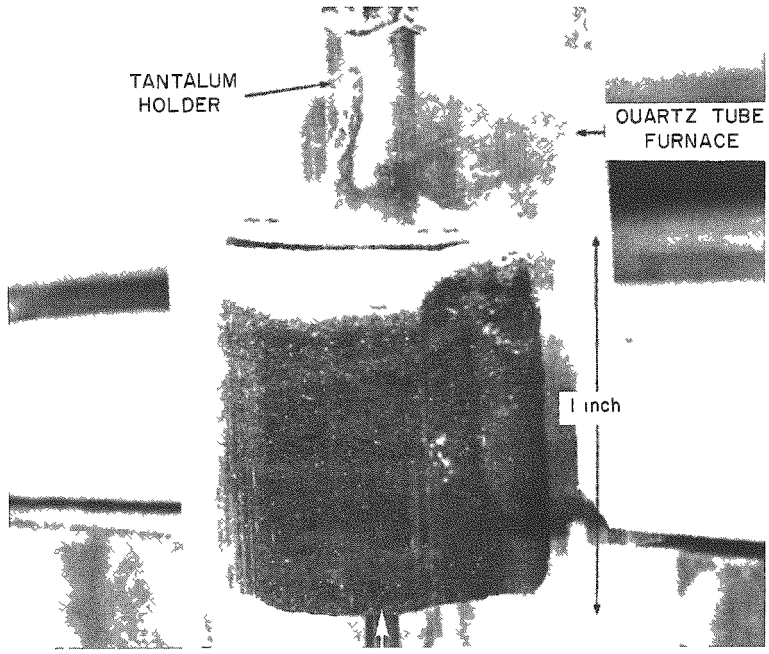

108-6076B

After the Fiberfrax fume trap was isolated, argon containing 6 ppm moisture and 2.2 ppm oxygen* was passed over the surface of the Fiberfrax (in order to sweep away released iodine) and then through the activated charcoal filter assemblies. The flow rate was held constant at about 6.6 ft/min over the sides of the Fiberfrax and at about 34 ft/min through the filter assemblies. At frequent intervals, one of the two filter assemblies (Filter A and Filter B) was removed from the system, and the gamma activities present were measured with a 256-channel analyzer. While an assembly was being counted, it was replaced with the other one so that the argon-transported activity was collected continuously, except for overnight periods when the bed was cooled to room temperature and maintained in a static argon atmosphere. On completion of the experiment, the apparatus was dismantled. Samples for the determination of activity retained by the Fiberfrax and condensed on the walls of the quartz tube were then obtained by leaching techniques.

Results

The analytical results obtained when the Fiberfrax was reheated are summarized in Table I-1. Since it was considered likely that

*The argon atmosphere in the argon cell of the EBR-II Fuel Cycle Facility is circulated through the process cell to provide heat removal, and provisions have been made to remove oxygen and water vapor so as to maintain the oxygen level below 20 ppm and the water below 5 ppm.

Table I-1

DISTRIBUTION OF IODINE IN EXPERIMENTAL APPARATUS AFTER REHEATING OF FIBERFRAX FUME TRAP USED IN MELT REFINING EXPERIMENT

Experimental Conditions

Melt Refining Step

Crucible:	Lime-stabilized zirconia
Charge:	Lightly irradiated U-5 w/o fissium (19.731 g) spiked with cesium (0.187 g), uranium triiodide (0.033 g of iodine), and sodium (0.21 g)
Fiberfrax Temperature:	Bottom area (facing melt), 1015 C; top area, 540 C; Fiberfrax outgassed at 1000 C prior to use

Iodine Collection Step

Argon Flow through Carbon Assembly:	34 ft/min (max)
Fiberfrax Temperature:	Indicated below

Fiberfrax Temperature	Time (hr)	Iodine Activity (μC)[a] Collected by Filter Assemblies (cumulative)	Volatilized to Walls of Apparatus	Retained by Fiberfrax
Constant at 680 C, 315 C[b]	34.2	47.7	117.9	691.2
Constant at 150 C, 110 C[b]	5.5	2.8		
Varying[c]	17.7	7.9		
Total Activity		58.4	117.9	691.2

[a]Appropriate corrections for decay have been applied.

[b]Temperatures apply to bottom and top areas of fume trap, respectively; bottom area faced the melt during the refining operation.

[c]Cooling to room temperature for overnight holding periods and reheating to experimental temperatures.

the rate of iodine release would be much greater at the higher temperature (680 to 315 C), the major portion of the experiment was conducted at this temperature. Preliminary results were obtained for only a short time at the lower temperature (150 to 110 C) because of the analytical limitation imposed by the short (8-day) half-life of the iodine-131 activity. Of the 867 μC of iodine-131 accounted for, about 80 percent was retained by the Fiberfrax, 14 percent was found on the walls of the apparatus, and the remainder was collected in the activated charcoal filters.

Since an appreciable amount of the iodine released from the Fiberfrax was retained on the walls of the quartz apparatus, which were heated at elevated temperatures for extended periods of time, it appears likely that much of the iodine was condensed in a form other than the elemental form. Qualitative analyses of all samples after more than 99 percent of the iodine-131 had decayed showed that cesium-134 (produced by activation of the added cesium) was the only additional gamma-active element present. These observations suggest that the iodine found in the Fiberfrax, on the walls of the apparatus, and in the charcoal filters was primarily cesium iodide. Under actual process conditions in the Fuel Cycle Facility, a fraction of the total iodine similar to the fraction found on the quartz walls in this experiment would probably condense largely on cooler surfaces in or near the melt refining furnace and would not be transported readily throughout the argon-atmosphere cell.

The rates of iodine-131 collection by the carbon filter assemblies for the two conditions of Fiberfrax heating are shown in Figure I-4. The cumulative percentage of activity collected is based on the amount of activity originally present in the Fiberfrax. At the higher temperature (gradient from 680 C to 315 C), the rate appeared to be constant after an initial period of more rapid release. The greater rate during the initial period might have resulted from more rapid removal of the activity

Figure I-4

CUMULATIVE IODINE ACTIVITY RELEASED TO FILTER ASSEMBLIES DURING REHEATING OF FIBERFRAX FUME TRAP USED IN MELT REFINING EXPERIMENT

Initial Iodine Concentration in Fiberfrax: 867.5 μC

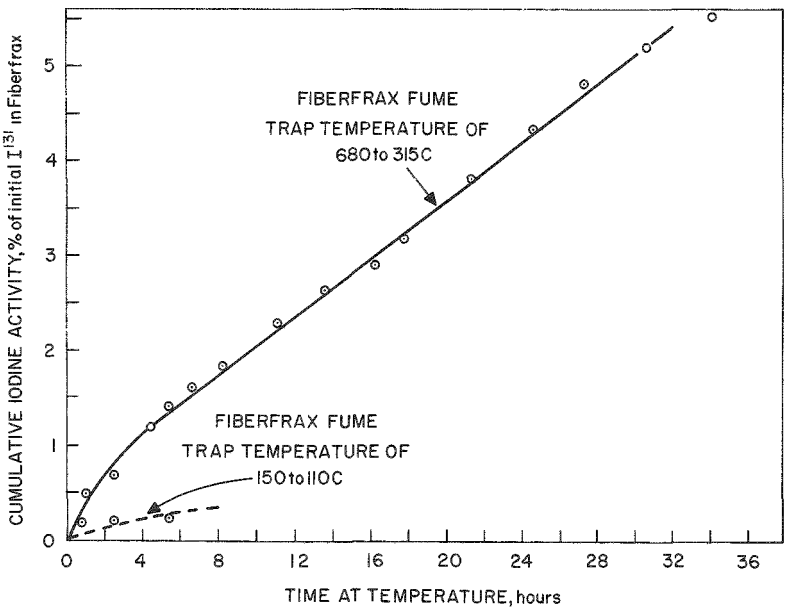

108-6846

which had been deposited on the outer surfaces of the Fiberfrax during melt refining. Comparison of the collection rates at the higher temperatures with the much slower rates of iodine collection at the lower temperature (gradient from 150 C to 110 C) indicates that the rate of iodine release from Fiberfrax to the argon stream is primarily dependent upon the temperature.

Distribution data for the iodine-131 and ratios of the cesium and iodine activities in the two charcoal filter assemblies are presented in Table I-2. Of the total iodine activity collected in each assembly, over 50 percent was retained by the inlet AEC filter. In each filter assembly, the quantity of iodine collected by the granular charcoal decreased

Table I-2

ACTIVITY DISTRIBUTION IN AEC FILTER-ACTIVATED CHARCOAL ASSEMBLIES[a] USED FOR STUDY OF IODINE RELEASE FROM FIBERFRAX

Experimental Conditions: See Table I-1

	Filter Assembly A[b]			Filter Assembly B[b]		
Component	Bed Depth (cm)	I^{131}[c] Activity (μC)	Cs^{134}[c]/I^{131} Activity Ratio (arbitrary units)	Bed Depth (cm)	I^{131}[c] Activity (μC)	Cs^{134}[c]/I^{131} Activity Ratio (arbitrary units)
Section I						
Inlet AEC Filter		15.08			21.95	
Activated Carbon	1.28	8.18	(1.0)[d]	1.35	6.45	(1.0)[c]
Pyrex Connector		0.07			0.02	
Section II						
Activated Carbon	1.24	1.39	1.6	1.49	0.65	1.7
Pyrex Connector		0.04			0.02	
Section III						
Activated Carbon	1.16	0.89	1.6	1.45	0.49	1.4
Pyrex Connector		0.03			0.01	
Section IV						
Activated Carbon	1.36	0.83	1.6	1.16	0.25	1.4
Pyrex Connector		0.03			0.01	
Section V						
Activated Carbon	1.27	0.82	1.4	1.17	0.25	1.2
Outlet AEC Filter		0.28			0.69	
Total Activity		27.64			30.79	

[a] A diagram of an assembly is shown in Figure I-2.

[b] Appropriate decay corrections have been applied to the activities listed. Estimated precision of analyses (relative %): iodine-131, ±5; cesium-134, ±10.

[c] These results are total values for the three heating conditions listed in Table I-1.

[d] Cesium analyses used to calculate the activity ratios are considered questionable because of handling problems associated with sample preparation.

sharply after penetrating the first bed section (approximately 1.3 cm), and the quantities collected in Sections II to V were similar. The ratio of cesium activity to iodine activity remained nearly constant throughout all of the activated charcoal sections of the assembly. This observation suggests that much of the iodine collected was transported in the effluent argon from the quartz furnace as particulate material, probably consisting of cesium iodide or of reaction products formed at elevated temperatures from cesium, iodine, and contaminants in the argon. Since an appreciable amount of the iodine activity penetrated the inlet AEC filter, which type of filter is reported to be efficient for particles larger than 0.35 μ, some of the iodine-bearing particles were very small.

In summary, the results indicate that the rate of iodine release to the argon atmosphere of the Fuel Cycle Facility from a Fiberfrax fume trap used for melt refining will depend primarily upon the temperature of the trap at the time the furnace is opened. If the Fiberfrax trap has a temperature gradient of about 700 to 300 C, it is estimated that approximately 0.16 percent of the activity in the trap will be released to the cell atmosphere during each hour of exposure. Because of the different size and geometry of the melt refining equipment in the EBR-II Fuel Cycle Facility, this result cannot be applied directly to the plant-scale operation. However, it might be expected that less than 0.5 percent of the total iodine activity present in the Fiberfrax fume trap would be released to the argon cell for each hour of exposure to the argon atmosphere.

b. Removal of Nitrogen from Argon with Titanium Sponge
(M. Kyle, P. Nelson, and J. Arntzen)

A method is under development for removing nitrogen from the argon atmosphere of the argon atmosphere cell of the EBR-II Fuel Cycle Facility by gettering the nitrogen on hot titanium sponge (see ANL-6648, pp. 38-40). Two sets of experimental equipment are presently being constructed: (1) equipment for a study of the kinetics of nitrogen removal from argon on hot titanium sponge, and (2) a pilot plant for obtaining overall process performance data and information on component reliability. Studies will be conducted with argon containing initial nitrogen concentrations of between 50 and 5000 ppm.

Containment of Titanium Sponge

Several Inconel, stainless steel, and Hastelloy alloys were evaluated for the containment of titanium sponge in 400-hr tests at 900 C, the probable operating temperature of the pilot plant. (Nitrogen reacts with titanium at practical reaction rates at temperatures above 850 C.) In these tests, particles of sponge and a coupon of the test material were placed in intimate contact in an alumina crucible. At the conclusion of the tests, particles of the titanium sponge adhered to the coupons. Metallurgical examinations of the coupons were made in areas of particle adherence.

A thin reaction layer was present on all materials except Type 316 stainless steel (Table I-3). In addition to this reaction layer, grain-boundary precipitation of an undetermined phase was present in some materials. Since titanium forms compounds with iron, nickel, and chromium, the presence of a zone of interaction is not unexpected. (Titanium is frequently added to alloys of the types tested as a deoxidant, hardening agent, or carbon scavenger.)

Table I-3

CORROSION OF INCONEL, STAINLESS STEEL, AND HASTELLOY ALLOYS BY TITANIUM SPONGE

Test Conditions

Time:	400 hr
Temperature:	900 C
Atmosphere:	Argon
Charge:	$\frac{1}{4}$-in. particles of solid titanium sponge (99.4% Ti, melting point 1800 C). The particles were placed on or in contact with a coupon of the material under test in an alumina crucible.

Static conditions

Material	Depth of Reaction Zone[a] (mils)
Inconel 702	3 to 4
Inconel 718	3 to 4
Inconel 750	4 to 5
Inconel 800	3 to 4[b]
Stainless Steel Type 304	4 to 5[b]
Stainless Steel Type 310	2 to 4[b]
Stainless Steel Type 316	<1[b]
Hastelloy C	5 to 7
Hastelloy X	5 to 7

[a]At the conclusion of each test, particles of the titanium sponge adhered to all of the coupons. The depth of the reaction zone was measured in the area of adherence.

[b]In addition to a reaction layer, grain-boundary precipitation of undetermined phase was observed.

Type 316 stainless steel, although possessing very good resistance to reaction with titanium sponge, does not possess the required strength at the elevated temperature to be used. Hastelloy X will be used

as the structural material for the high-temperature vessels of the initial pilot-plant unit. However, those parts of the Hastelloy X vessels which would come in direct contact with titanium sponge will be lined with Type 316 stainless steel. Other vessels of the system which will be operated at lower temperatures will be fabricated of Type 310 stainless steel, primarily because of its good resistance to external oxidation by air.

2. Processes Employing Liquid Metal Solvents

Several processes are being developed which employ liquid metals and salts as processing media. Further small-scale demonstration runs have been made in investigation of the skull reclamation process for recovering the fissionable material remaining in the crucible residue (skull) after a melt refining operation. Equipment development studies and large-scale demonstration experiments are also now being conducted in essentially full-scale integrated process equipment.

Demonstrations of a liquid metal process for the extraction of plutonium from EBR-II blanket material have been continued. Laboratory development work is underway on processes for other fuel materials, including those which will contain plutonium as a fissionable material.

Supporting fundamental studies of liquid metals and molten salts of process interest are in progress. These studies include both the chemical reactions involved in process steps and engineering operations important to process development, such as distillation, heat transfer, mass transfer, and mixing characteristics of liquid metals and salts.

a. Development of the Skull Reclamation Process

The skull reclamation process is being developed as an auxiliary to melt refining for processing the first fuel loading of the EBR-II reactor. The process has two purposes: (1) recovery of fissionable materials from the skull remaining in the crucible after melt refining, and (2) separation of fission products from uranium. The recovered and purified uranium will be returned to the main EBR-II fuel cycle. The skull reclamation process provides for disposal of all non-volatile fission products in the EBR-II fuel cycle.

The flowsheet for the skull reclamation process has been presented previously (see ANL-6596, p. 46). For reference purposes, this flowsheet is again presented in Figure I-5.* Results of a study of containment materials for the skull reclamation process are presented in a following section of this report.

---

*Figure I-5, which is a revised version of the previously published flowsheet, presents the process conditions and process reagents now being evaluated.

Figure I-5

FLOWSHEET FOR SKULL RECLAMATION PROCESS

(Relative weights based on a 120-g uranium charge)

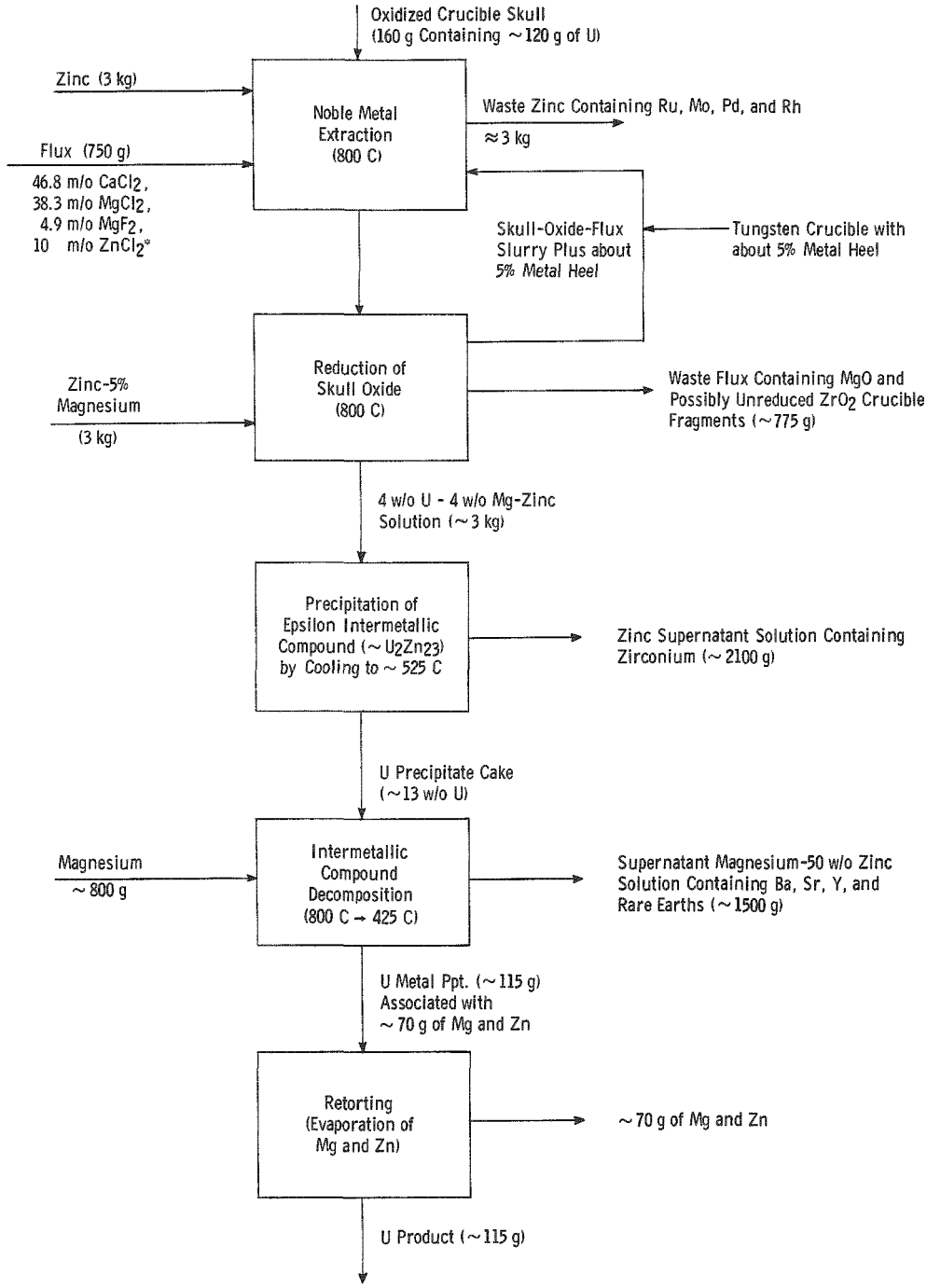

*After reaction of all of the $ZnCl_2$ with uranium and magnesium metal heel from the reduction step, the flux composition would become $CaCl_2$ 47.5 m/o, $MgCl_2$ 47.5 m/o, MgF_2 5.0 m/o. However, an excess of $ZnCl_2$ (about 2 m/o) is employed.

108-6855

(1) Partial Oxidation of Crucible Skulls
(R. D. Pierce and K. R. Tobias)

The charge material to the skull reclamation process is oxidized skull material (skull oxides). In order to remove the skull material from the zirconia melt refining crucible, the skull material is oxidized and is thereby converted to a powder which can be readily poured from the crucible. The possibility of using partial oxidation to free the skull, rather than complete oxidation as is now being done, was investigated briefly.

Partial oxidation of the skull material was attempted in upright crucibles in the same equipment that is being used for complete oxidation of skull material (see p. 94). In this equipment the crucible is dumped by partially rotating the crucible around a horizontal axis, much as water is spilled by a water wheel. In this work, the partially oxidized skull was in the form of a tight-fitting cup. Although the skull material was no longer adhering to the walls of the crucible, it frequently wedged in the crucible when an attempt was made to dump it out. Thus, partial oxidation in the present equipment is not an attractive alternative to the present method of skull removal.

The oxidation of skulls from inverted crucibles was next attempted in two experiments in the semi-works. The advantage of having the crucible inverted was that any loosened material dropped into the receiver. The oxidations were performed at about 600 C in an atmosphere of about 20 percent oxygen in argon. In the first experiment, the zirconia crucible was free-standing in the furnace, thus permitting some oxygen penetration through the crucible walls and oxidation at the skull-crucible interface. The skull material fell into the receiver when about 25 percent of it had been oxidized. In the second experiment, the zirconia crucible was contained in a close-fitting stainless steel can. The oxidation was stopped when about 22 percent of the skull had been oxidized. Later examination showed that much of the skull material had fallen into the receiver, but a cup-like portion which had fallen only part way was found wedged in the crucible. This "cup" appeared to be nearly broken and probably would have fallen free with very little additional oxidation.

These two experiments indicate than an appreciable percentage, about 25 percent, of the skull material must be oxidized before the skull is completely freed from the crucible. The resultant mixture of metal and oxide might have some advantage over an all-oxide charge in the subsequent process (principally in the extraction of noble metals), but because of the large fraction of oxide this advantage seems small. Therefore, no further development of the procedure for partial oxidation and no design and construction of new oxidation equipment seem warranted.

(2) Small-scale Demonstrations of the Skull Reclamation Process

(R. D. Pierce, K. R. Tobias)

Small-scale (100 to 150 g of uranium) demonstrations of the skull reclamation process are in progress in equipment located inside an argon-atmosphere glovebox (shown in Summary Report ANL-6543, pp. 32 to 35). These demonstration runs are being made to expose and rectify any process difficulties and to establish permissible ranges of process variations. The determination of optimum flowsheet conditions in these small-scale runs will permit emphasis to be given to process mechanics and equipment performance in large integrated process equipment, operation of which is discussed in a following section of this report.

Removal of Zirconium as the Carbide

Some removal of zirconium, in addition to that achieved in the intermetallic compound precipitation step, may be necessary if an excessive amount of zirconia crucible fragments is frequently present in the skull oxides. A suggested method of increasing the zirconium-removal capability of the skull reclamation process is precipitation as the carbide from the uranium-magnesium-zinc solution present at the conclusion of the uranium oxide-reduction step (see ANL-6687, p. 32). It was expected that any zirconium carbide formed would be suspended in the overlying molten salt phase and discarded in this phase.

To test this method, carbon was added to the reduction solution in a demonstration run (Run BJ-20). Carbon addition resulted in removal of only about 10 percent of the zirconium from solution, and also precipitated some uranium and cerium. The uranium content of the waste flux after carbon addition was about an order of magnitude higher than normal (4 percent instead of about 0.4 percent). About 20 percent of the cerium was also removed in the flux, whereas usually about ten percent of the cerium is removed. It was concluded that the addition of carbon during this step would be of little value for zirconium removal.

Investigation of High Uranium Losses in Waste Zinc Solution of the Intermetallic Compound Precipitation Step

In several runs, as much as 20 percent of the uranium has been found in the waste zinc from the intermetallic compound precipitation step. This high loss of uranium has been traced to the gentle agitation which has been employed during crystallization of the intermetallic compound. This agitation was employed to avoid accumulation of crystals on the crucible walls during cooling. To evaluate the possible effect of

agitation, the precipitation of the zinc-uranium intermetallic was performed three times in one run: first, without stirring; second, with the same stirring as had been used in preceding runs; and finally, again without stirring. After each performance of the step, the waste ingot was melted, sampled, and then recombined with the cake for another performance of the step. The uranium contents of the waste ingots are summarized in Table I-4. In the absence of stirring, the uranium content of the transferred zinc solution was slightly greater than the solubility of uranium, which is 0.03 to 0.04 percent at the transfer temperature; with stirring, the loss was excessive. Therefore, elimination of stirring in this step is recommended.

Table I-4

EFFECT OF AGITATION ON URANIUM LOSS IN THE INTERMETALLIC COMPOUND PRECIPITATION STEP OF THE SKULL RECLAMATION PROCESS

(Run BJ-19)

Precipitation in a 3-in.-ID beryllia crucible with a 2-in. x $\frac{3}{4}$-in. slant-blade agitator deflecting downward.[a]

Agitation (rpm)	Initial and Transfer Temperature of Solution (C)	Cooling Time (hr)	Time Held at Transfer Temperature (hr)	Uranium Content of Transferred Zinc Waste Solution (%)	Calculated Percent Loss[b] of Uranium in Transferred Zinc Waste Solution
0	814 to 528	1.8	1.0	0.049	0.8
200	815 to 522	1.7	0.7	0.58	9.7
0	819 to 527	1.8	2.5	0.060	1.0

[a]The bottom of the agitator blade was 2 in. above the bottom of the container; the top of the blade was just below the surface of the liquid.

[b]Based on an original uranium concentration of 4 percent and on 80 percent transfer of the zinc waste solution.

Effects of Temperature and Agitation on Noble Metal Extraction

Poor extraction of ruthenium reported in ANL-6648, p. 40, was attributed to a lack of oxidizing power in the molten salt phase (caused by the absence of traces of water). This hypothesis appeared to be confirmed when good ruthenium removals (near 100 percent) were again achieved by the addition of a small quantity of water or of a zinc chloride oxidant to the flux phase in the noble metal extraction step. However, in the runs in which good ruthenium extraction was obtained, the quantity of zinc used was reduced in order to increase the concentration of ruthenium in the zinc extract and thereby effect an improvement in the accuracy of ruthenium analyses. The resultant change in zinc volume lowered the

flux-metal interface from several inches above the agitator down to near the agitator. The belief has grown that this change in mixing conditions may have contributed substantially to the improvement in ruthenium extraction. Therefore, two experiments (Runs BJ-22A and BJ-23A) have been made to evaluate the effects of both agitation and temperature on the rate of ruthenium extraction (believed to be representative of the extraction of all noble metals) in the noble metal-extraction step. The effect of temperature was studied in order to determine the lowest practical operating temperature.

In these experiments, one conducted initially at 650 C and the other initially at 725 C, the stirring speed was increased in three steps, 500, 800, and 1000 rpm ($1\frac{1}{2}$ hr at each stirring speed at the initial temperatures). The agitator was located just below the metal-salt interface. The skull oxide employed was from a common batch of material. Zinc chloride, now a standard constituent of the flux to insure oxidation of any metallic uranium present, was present in the flux at an initial concentration of 1.5 m/o.* In the final 2 hr of each run, the temperature was raised to 800 C and the melt was stirred at 1000 rpm to insure good extraction of noble metals and permit continuation of the run through the balance of the skull reclamation steps.

The data obtained are presented in Figure I-6. The extraction rate of ruthenium was found to be higher at both the higher temperature (725 C) and the higher stirring speeds. However, difficulty in sampling of the zinc extract or in solution stability (insofar as ruthenium is concerned) seemed to occur at 800 C, and low ruthenium concentrations in the zinc extract were obtained. Absorption of ruthenium on the surfaces of the tungsten crucible, molybdenum-30 percent tungsten agitator, tantalum thermocouple well, or tantalum sampling tubes could account for the sharp decreases in ruthenium concentration at 800 C. It is known that ruthenium absorbs on tantalum sampling tubes, and although measures have been taken in the analytical processes to remove absorbed ruthenium from the sampling tubes, the analytical problem remains a difficult one. The reappearance of high ruthenium concentrations (see Figure I-6) in the waste zinc ingots, which were remelted and heated to 800 C in tungsten for sampling, refutes the supposition of ruthenium absorption on tungsten. To obtain further information on the stability of solutions of ruthenium in zinc in tungsten crucibles, the waste ingot from Run BJ-22A has been remelted and held in a tungsten crucible at 650 and 800 C. The samples from this holding experiment have not been analyzed.

Completed Demonstration Runs

Results are available for two demonstration runs (Run BJ-18 and Run BJ-20). Both of these runs varied from the flowsheet shown in Figure I-5. In Run BJ-18, a skull which had not been oxidized

*The composition of the flux on a zinc chloride-free basis was 47.5 m/o $MgCl_2$, 47.5 m/o $CaCl_2$, and 5.0 m/o MgF_2.

was used. In the noble metal-extraction step for this run, the uranium was oxidized into the molten salt phase with zinc chloride, which was present in the salt at an appropriate concentration. Under these conditions, the noble metal extraction was performed at 650 C rather than at 800 C, the temperature used for processing skull oxide. This lower temperature was used to avoid excessive vaporization of zinc chloride. This is feasible because the noble metals remain in the zinc phase and the more difficult extraction of noble metals from an oxide matrix is not encountered. In Run BJ-20, carbon was added after the reduction step in an attempt to precipitate zirconium carbide. The effects of this carbon addition were previously discussed on p. 44.

Figure I-6

EFFECTS OF TEMPERATURE AND STIRRING RATE ON RUTHENIUM EXTRACTION IN THE NOBLE METAL EXTRACTION STEP

Equipment Description:

Tungsten crucible having four integral mixing baffles - 4 1/4-in.-ID, 2-in. by 3/4-in. molybdenum-30 percent tungsten slant-blade agitator, deflecting downward and located just below metal-salt interface.

Tantalum thermocouple well and sampling tubes.

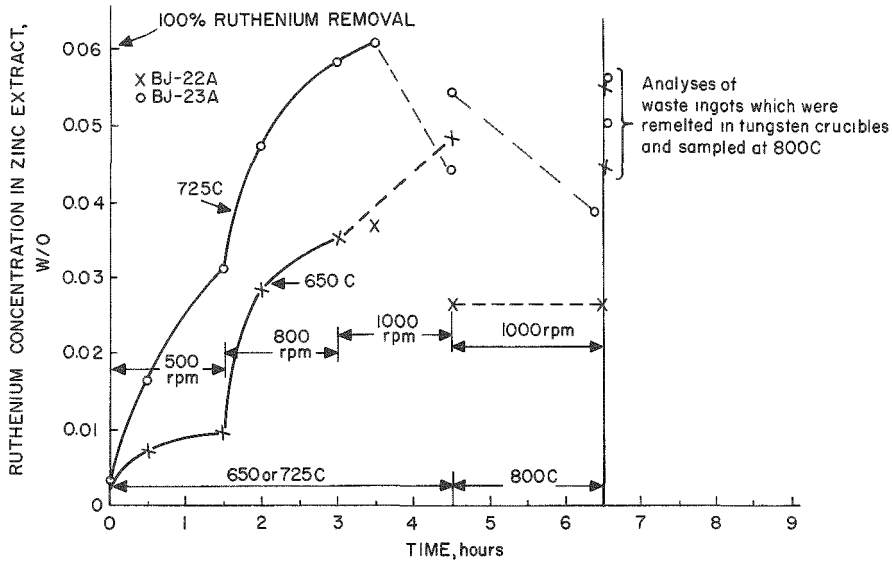

108-6837

The uranium material balances for these runs are given in Table I-5. Of necessity, some of the figures in Table I-5 were estimated or calculated by material-balance calculations. For example, in Run BJ-18, because it is difficult to obtain a reliable sample of a uranium-fissium skull, the charged uranium in the skull was determined from the amount of uranium present in the metal and flux phases after the reduction step. As pointed out previously, the high uranium loss in the waste flux phase of Run BJ-20 (tenfold higher than usual) was caused by the addition of carbon. In both runs, high uranium losses were experienced

in the supernatant solutions of the intermetallic compound precipitation step. As discussed earlier in this report, it is now known that these losses can be reduced to about 1 percent by elimination of stirring in this step. However, as a consequence of these high losses, the yields of uranium product in these runs were low, about 80 percent.

Table I-5

URANIUM MATERIAL BALANCES FOR SKULL RECLAMATION PROCESS DEMONSTRATION RUNS BJ-18 AND BJ-20

(See Figure I-5 for flowsheet and text for modifications)

	Weight of Uranium (g)	
	Run BJ-18	Run BJ-20
Charge		
Uranium-Fissium Skull	(76)[a]	None
Uranium-Fissium Skull Oxide	None	118
Heels	(2)[a]	(45)[a,b]
Uranium Slug	None	8
Total	(78)	(181)
Waste Ingots		
Zinc from Noble Metal Extraction Step	0.5	0.3
Flux from Reduction Step	0.4	3.9
Supernatant Solution from Intermetallic Compound Precipitation Step	13.2	27.7
Supernatant Solution from Intermetallic Compound Decomposition Step	0.8	1.5
Heels	(4.7)[a]	33.0
Samples	0.8	7.4
Product	58	97.3
Total	78.4	171.1

[a]Values in parentheses were estimated by material balance.

[b]This value was much higher than typical as a result of an iron-addition step used in the preceding run (Run BJ-19) in an attempt to increase the removal of zirconium.

For each run, the product composition has been compared with that of the charge (see Table I-6). Ruthenium removals were very good; the removals of the other elements, although adequate, were

somewhat lower than usual. These lower removals are in part due to the lower scale of Run BJ-18 (78 g versus the design scale of 130 g of uranium). Since the percent removal values were calculated by simple comparison of charge and product compositions, they may, because of the low uranium recoveries and the large input of recycle material in Run BJ-20, be somewhat lower than the removals actually achieved. The zirconium removal in Run BJ-20, in which a large amount of zirconium was charged, was not good enough. It is believed that this zirconium content, which resulted from a very high introduction of zirconia crucible fragments, is about four to seven times larger than will be encountered with EBR-II melt refining skulls.

Table I-6

FISSION PRODUCT REMOVALS EFFECTED IN RUNS BJ-18 AND BJ-20

	Run BJ-18			Run BJ-20		
	Composition, w/o, Oxygen-free Basis		Percent of Component	Composition, w/o, Oxygen-free Basis		Percent of Component
Component	Charge	Product	Removed[a]	Charge	Product	Removed
Ce	4.0	1.1	73	6.0	1.8	70
Zr	1.1	0.5	55	13.4	3.9	71
Ru	1.7	0.15	91	1.6	0.12	92
Mo	2.1	0.83	60	2.0	0.83	59
U	91.1	97.4	-	77.0	93.4	-

[a]These removals are based on product and charge concentrations, which implies 100 percent recovery of uranium. Since actual uranium recoveries were only about 80 percent in these runs, these are minimum values for fission product removals; a higher recovery of uranium would give higher apparent removals.

(3) Engineering-scale Integrated Equipment for Skull Reclamation Process

(I. O. Winsch, D. Grosvenor, G. Rogers, P. Mack)

Engineering-scale integrated equipment is currently being operated for equipment demonstration as well as for purposes of process demonstration. The design of the equipment was illustrated in the preceding quarterly report (ANL-6687, p. 35) by photographs. The equipment, which was sized for processing about 2.5 kg of skull oxide per batch, consists essentially of two large crucibles (about 13 in. in OD by 19 in. high), one tungsten and one beryllia, in which the process operations are performed. The crucibles are heated by radiation-cooled induction coils and are centrally located within two large furnaces (24 in. in OD by 36 in. high) covered with bell jars. Enclosure within the furnaces allows an argon atmosphere to be maintained over the process systems and allows pressurization of the furnaces, which is required for the transfer of molten metals and salts to a waste container or to the adjacent crucible. The bell jar covers have three nozzles, one of which is used for a stirrer, the other two of which are used for insertion of transfer pipes and other equipment used for sampling, liquid-level measurement, and temperature measurement.

Equipment performance, which has been of principal interest, is being determined by performing the necessary process

operations in the course of making skull reclamation process runs. Three runs have been completed in the equipment, but analytical data are not yet available for them.

Noble Metal Extraction

The noble metal-extraction step is performed in the tungsten crucible at 800 C by contacting a slurry of skull oxides in a halide flux with zinc to leach or extract the noble metal fission product elements, molybdenum, ruthenium, rhodium, and palladium. The scale of operation is such that 2.4 kg of skull material, 12 kg of halide flux,* and 35 kg of zinc may be charged. The phases are mixed for 4 hr at 800 C, after which the system is cooled to about 525 C to freeze the flux phase. The still-molten zinc phase is then transferred by pressure through a heated transfer line to a waste container. Since the solubilities of molybdenum and ruthenium are exceeded at the transfer temperature, the zinc phase is stirred during the transfer to suspend the precipitated molybdenum and ruthenium particles.

The percentages of zinc transferred in three operations were 92.5, 96.7, and 93.3, which are regarded as very good. In these tests, it was found that the frozen flux creates an effective barrier to transmission of gas pressure to force the molten zinc phase out through the transfer pipe. A high-resistance route exists along the agitator shaft, which is rotated slowly during freezing of the flux. Consequently, a pressure of about 12 psig was required to effect zinc transfer, rather than the 7 psig calculated to be necessary. It was shown that, if desirable, the transfer pressure could be lowered by maintaining an opening through the flux by means of an open-end pipe having its top opening above the flux phase and its bottom opening in the zinc phase. This pipe was kept open during freezing of the flux to provide a direct path for gas through the frozen flux phase. An agitator shaft with vanes, which would be rotated slowly while the flux was solidifying, could also provide an effective opening through the flux phase.

Reduction Step

The reduction of uranium oxides from the flux phase is also effected at 800 C in the tungsten crucible, the flux phase being contacted with a 5 percent magnesium-zinc alloy. As the uranium oxides are reduced, the uranium metal dissolves in the zinc-magnesium phase. The uranium concentration of the zinc-magnesium phase approaches 4 w/o at

*Composition of flux: 47.5 m/o $MgCl_2$, 47.5 m/o $CaCl_2$, and 5 m/o MgF_2. If uranium metal is present in the charge, zinc chloride also is added to the flux to oxidize uranium into the flux.

complete reduction. The reduction step was effected without difficulty, but results of sample analyses are needed before it is known whether the agitation was sufficiently vigorous to effect complete reduction.

Following the reduction, a high-temperature (800 C) separation and transfer of the phases from the crucible is required, the flux phase being sent to waste and the uranium-bearing metal phase to the large beryllia crucible in the adjacent bell jar furnace. An automatic method of separating and transferring the phases, which leaves behind a small heel of each phase in the tungsten crucible, was initially given a trial. Development of this phase separation procedure was reported in a previous Summary Report (ANL-6543, p. 39). Difficulty was experienced in the automatic phase separation of the flux from the zinc-magnesium-uranium phase. This difficulty was caused by solidification of material in the transfer lines at points of low temperatures along the transfer tubes. This condition is being remedied by adding more electrical heaters. In addition, it was found that the flux at 800 C severely corroded a stainless steel section of the flux transfer line, which was employed between the bell jar furnace and the waste receiver. Therefore, a new flux transfer line is being fabricated entirely of a 70 percent molybdenum-30 percent tungsten alloy.

Because of the inability to effect the automatic phase separation, each phase was separately transferred. By the use of a bubbler-type liquid-level gauge to locate the interface and to indicate the total depth and weight of each liquid, it was possible to effect a carefully controlled, sequential transfer of the two phases. The desired weight of the zinc-magnesium-uranium phase was first transferred through a pipe extending to near the bottom of the vessel. The transfer pipe was then raised so that its open end was just above the interface and then the flux phase was transferred. This method of phase separation and transfer worked so well that it will merit consideration in the design of the final plant equipment.

Uranium Precipitation Steps

After the uranium-zinc product solution is transferred to the adjacent beryllia crucible, it is first cooled to between 500 and 525 C to precipitate uranium as a uranium-zinc intermetallic compound (the epsilon phase, which is approximately U_2Zn_{23}). The supernatant liquid is then pressure-siphoned to waste, and sufficient magnesium is added to the precipitated uranium-zinc intermetallic compound to decompose it, and thereby liberate uranium metal, which precipitates. The resultant supernatant metal, a 50 percent magnesium-zinc solution, is then removed by pressure siphoning.

Removals of the supernatant have been lower than previously achieved on a smaller scale (around 80 percent instead of 90 to 95 percent). Since much better phase separations have been achieved in previous work, the poor phase separations in these early runs are attributed to impure atmospheres and lack of experience with the new equipment. When operational procedures have been improved sufficiently, the glovebox will be closed and a dry air atmosphere, to be changed later to an inert atmosphere, will be maintained around the equipment.

Of much greater concern in these steps was wetting of the beryllia crucible by the liquid metal solutions. As a result of this wetting, it was not possible to remove the precipitated uranium cake after the second uranium-precipitation step. Two large thixotropically cast beryllia crucibles had been procured from the Brush Beryllium Co., and both were wetted by the metal solutions.

Wetting of the beryllia is contrary to previous experience with small (4-in. OD by 9 in. high) thixotropically cast beryllia crucibles. In discussions with representatives from the Brush Beryllium Co., it was ascertained that the method of fabrication of the large crucibles had differed from the method used to fabricate the previously tested small crucibles. The small crucibles had been fired in an electric furnace under controlled-temperature, controlled-atmosphere conditions. The large crucibles were fired at a slightly lower temperature (1470 instead of 1550 C) in a gas furnace instead of in an inert atmosphere, and the resulting moist atmosphere and lower temperature are believed to have caused poor sintering of fine beryllia particles. This would result in a rough and porous surface susceptible to wetting by the liquid metal. Evidence that the differences in firing conditions were indeed responsible for wetting of the large crucibles is that small beryllia crucibles fired in the gas-fired furnace also were wetted by the liquid metal. New beryllia crucibles fabricated under the proper firing conditions are being procured.

Operation in a Single Tungsten Crucible

The lack of a satisfactory large beryllia crucible led to consideration of performing all process steps in the tungsten crucible. This method of process operation has a number of advantages:

1) An entire furnace unit is eliminated.

2) The high-temperature separation of flux and metal phases after the reduction step is eliminated. Until the process step in which the uranium product phase is removed, only waste solutions of flux or metals are removed from the tungsten crucible.

The disadvantages of this procedure are:

1) possible contamination of the uranium product with residual flux;

2) difficulty in removing the uranium product phase from the crucible.

At the present time, uranium is being removed from the tungsten crucible by dissolving it to a 12 percent concentration in a 12 percent magnesium-zinc alloy.

One run has been completed with the tungsten crucible used for all process steps. All process steps were performed without difficulty except that for removal of the uranium product. A 98 percent removal of the zinc extract was effected, waste flux was easily removed, and 74 and 81 percent removals of the zinc-magnesium supernatant solutions were realized. Dissolution of the uranium product in magnesium-zinc alloy and its removal did not go well because the agitator could not be extended far enough into the crucible to give good agitation. This situation is being remedied. Because new beryllia crucibles will not be available for several months, operation with only the tungsten crucible will be continued for some time.

General Observations

The large tungsten crucible has proved to be very durable. Freezing and remelting of entire charges were accomplished with no adverse effects. Salt and metal vapors within the bell jars have caused corrosion of the stainless steel parts. This corrosion is accelerated by absorption of water vapor by the salts when the furnaces are opened. Plans are being made to close up the glovebox which contains the furnaces so that an argon cover atmosphere can be employed. This will eliminate problems caused by the absorption of water by the hygroscopic salts which are used.

b. Processes for Plutonium Reactor Fuels
(R. K. Steunenberg)

Fuels containing uranium and plutonium are used in fast breeder reactor cores and blankets. A critical separation in the processing of fuels of this type by pyrometallurgical methods is the removal of rare earth fission products from plutonium. A promising technique for effecting this, as well as other pertinent separations, involves selective extractions from zinc-magnesium solutions by means of molten halide fluxes. Previous work has indicated that plutonium-rare earth separation factors in these systems are large enough to provide adequate separations by using multistage contacting equipment. However, additional work is needed to

determine the behavior of other fission products such as zirconium, the metals used in fuel cladding alloys, and transplutonium elements generated during irradiation of a fast reactor fuel.

Molten Salt Extraction Studies

(J. B. Knighton, J. D. Schilb, J. W. Walsh)

Further investigations have been conducted on the separation of constituents of irradiated reactor fuels through equilibration between liquid magnesium-zinc alloys and molten magnesium chloride. Distribution coefficients, K_d = (w/o in flux)/(w/o in metal), as a function of magnesium concentration in the metal phase have been reported previously for thorium, uranium, plutonium, americium, curium, barium, yttrium, cerium, praseodymium, neodymium, zirconium, vanadium, and iron (see ANL-6687, p. 41; ANL-6648, p. 48, and preceding Summary Reports). The effects of variables such as temperature, concentration, and composition of the flux and metal phases have also been described (see ANL-6596, p. 59; ANL-6648, p. 46). During the past quarter, additional distribution data have been obtained for neptunium, curium, protactinium, and chromium.

Neptunium

The distribution coefficients for neptunium between magnesium chloride and zinc-magnesium alloy at 800 C have been determined. Preliminary results were reported previously in ANL-6687, p. 43. The tracer-level neptunium-239 (half-life, 2.35 days) used in the determinations was prepared by neutron irradiation of highly depleted uranium. The uranium was not removed prior to the experiments.

Three separate experiments have been completed. In the first, NpE-1, which used tracer-level neptunium, the equilibrium was approached from the zinc-rich side of the zinc-magnesium phase. In the second, NpE-2, macro amounts (~0.2 w/o) of neptunium-237, in the form of neptunium dioxide, were spiked with neptunium-239. The equilibrium was again approached from the zinc-rich side. The third experiment, NpE-3, utilized neptunium dioxide spiked with neptunium-239 tracer, and equilibrium was approached from the magnesium-rich side.

Filtered samples of the metal and salt phases were obtained by withdrawing the samples through porous tantalum filters into tantalum tubes. The neptunium contents of the samples were determined by gamma counting.

The conditions of these experiments and the distribution coefficients as a function of magnesium concentration in the metal phase

Figure I-7

DISTRIBUTION OF NEPTUNIUM BETWEEN MAGNESIUM CHLORIDE AND ZINC-MAGNESIUM ALLOY

Conditions

Temp:	800 C
Mixing Rate:	300 rpm
Crucible:	Tantalum
Atmosphere:	Argon

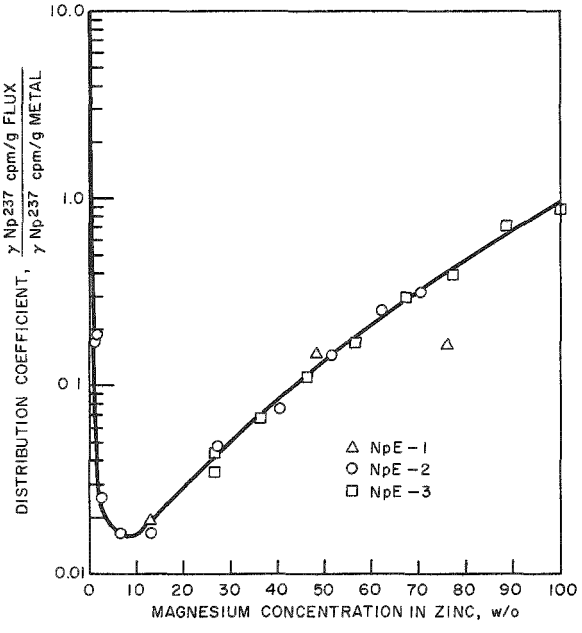

108-6863

are presented in Figure I-7. The results show that neptunium exhibits the same general behavior as plutonium and curium. The data from the three neptunium experiments are in good agreement, and they indicate that changes in the neptunium concentration from tracer level to 0.2 w/o in the metal phase had no appreciable effect on the distribution coefficients.

Curium

Further measurements of the distributions of curium between magnesium chloride and zinc-magnesium alloy at 800 C have been made. (Preliminary data were reported in ANL-6687, p. 41.) In this study, two experiments were performed. In one, CmE-1, equilibrium was approached from the zinc-rich side, and in the other, CmE-2, equilibrium was approached from the magnesium-rich side. Approximately 0.1 mg of curium-244 (half-life, 17.6 yr) was used in each experiment. In each experiment, the curium was added as the trifluoride carried on about 100 mg of lanthanum trifluoride. Samples of the metal and flux phases were obtained by the method described previously in the neptunium experiments. The specific activity of curium in the samples was determined by alpha counting of the curium-244 isotope.

The distribution coefficients for curium (Figure I-8) show the same general dependence upon the magnesium concentration in the metal phase as do those of the other actinide and lanthanide metals, with a minimum value at about 10 w/o magnesium. The absolute values of the distribution coefficients for curium are very similar to those for plutonium, with both elements favoring the metal phase.

Although the agreement of the data obtained in the two curium experiments is adequate, the results indicate that a small systematic error may be present in either or both sets of data. The source of this discrepancy has not yet been established.

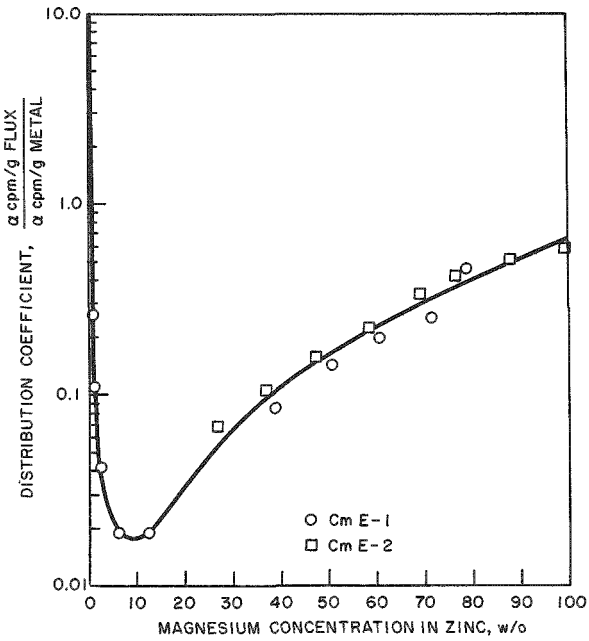

108-6876

Figure I-8

DISTRIBUTION OF CURIUM BETWEEN ZINC-MAGNESIUM ALLOY AND MAGNESIUM CHLORIDE

Conditions

Temp:	800 C
Mixing Rate:	300 rpm
Crucible:	Tantalum
Atmosphere:	Argon

Protactinium

Two experiments were performed in order to obtain distribution coefficients of protactinium between magnesium chloride and zinc-magnesium alloy at 800 C. Equilibrium was approached from the zinc-rich side in the first experiment and from the magnesium-rich side in the second. The tracer protactinium-233 (half-life 27.4 days) used in the experiments was prepared by neutron irradiation of thorium-232. The flux and metal phases were sampled by the technique described previously. The specific activity of protactinium in the samples was determined by gamma counting of the protactinium-233 isotope.

The data for the experiment in which equilibrium was approached from the zinc-rich side (Figure I-9) show a fair degree of self-consistency, although scatter exists in the region of about 5 to 10 w/o magnesium. The results from the reverse experiment, which are not shown, scattered randomly, although the results were of the same order of magnitude as those shown in Figure I-9. No explanation for the scatter has been found.

The results from the first experiment indicate that protactinium behaves in a manner typical of the actinide elements, with the distribution coefficient reaching a minimum value at a magnesium concentration of about 10 w/o in the metal phase. The absolute values of the distribution coefficients are about an order of magnitude lower than those for plutonium. Additional experiments have been planned in order to obtain more reliable data on the distribution of protactinium.

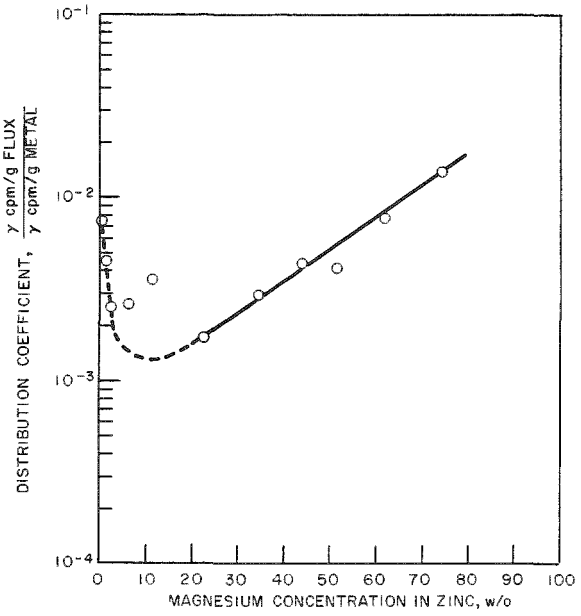

108-6864

Figure I-9

DISTRIBUTION OF PROTACTINIUM BETWEEN MAGNESIUM CHLORIDE AND ZINC-MAGNESIUM ALLOY

Conditions

Temp:	800 C
Mixing Rate:	300 rpm
Crucible:	Tantalum
Atmosphere:	Argon

Chromium

Chromium is of interest as a constituent of stainless steel, which is frequently used as a fuel cladding material. A single experiment was performed in which an attempt was made to measure the distribution behavior of chromium between magnesium chloride and zinc-magnesium alloy. Chromium-51 tracer (half-life, 27.8 days) was prepared by neutron irradiation of naturally occurring chromium. The sampling techniques were identical with those described above, and the specific activity of the chromium tracer was determined by gamma counting. The results, presented in Figure I-10, show that chromium exhibits a preference for the metal phase.

Figure I-10

DISTRIBUTION OF CHROMIUM BETWEEN MAGNESIUM CHLORIDE AND ZINC-MAGNESIUM ALLOY

Conditions

Temp:	800 C
Mixing Rate:	300 rpm
Crucible:	Tantalum
Atmosphere:	Argon

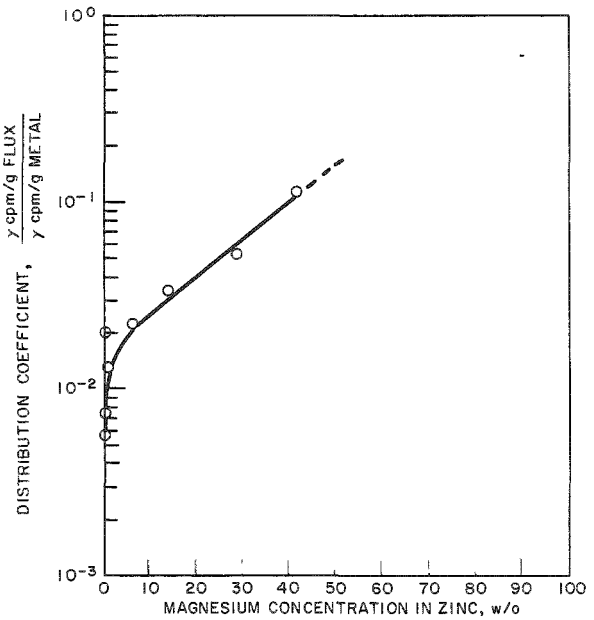

108-6871

Chromium is like iron and unlike the actinide and lanthanide elements in not distributing to the flux phase at very low magnesium concentrations. Above about 42 w/o magnesium, the data showed considerable scatter and are not included in Figure I-10 since their reliability in this region is questionable.

c. Recovery of Plutonium from EBR-II Blanket Material (I. O. Winsch, T. F. Cannon, P. J. Mack)

In the presently proposed blanket process (see Summary Report ANL-6477, p. 47), uranium blanket material (from the EBR-II reactor) containing about one percent plutonium is dissolved in a 12 to 14 w/o magnesium-zinc alloy at 800 C to produce a 12 to 14 w/o uranium solution. The addition of magnesium to an approximately 50 w/o concentration precipitates the uranium from solution while the plutonium remains in solution. The uranium solubility in the supernatant phase is decreased by cooling to about 400 C prior to removal of the plutonium-bearing supernatant phase. Isolation of the plutonium from this latter phase is to be accomplished by evaporating the magnesium and zinc.

(1) Experiments Using Irradiated Uranium Blanket Materials

Previous blanket-process-demonstration runs (see ANL-6596, p. 66, and preceding Summary Reports) have demonstrated that it should be possible to recover about 90 to 95 percent of the plutonium from a uranium-1 w/o plutonium blanket material in a magnesium-zinc supernatant. Subsequent recovery of the plutonium product would be accomplished by distilling the magnesium-zinc solvent. The seventh of a series of blanket-process-demonstration runs has been completed with the use of irradiated uranium blanket rods. The purpose of this run was to determine the behavior of iodine and fission products in the blanket process. Even though it is expected that blanket material will be stored for a long time, thus permitting essentially complete decay of iodine-131 and other short-lived isotopes, the behavior of iodine is of interest because it may occasionally be desirable to process short-cooled blanket material.

Depleted uranium blanket rods and small sections of these rods to be used as control samples were encapsulated in aluminum cans and irradiated in the CP-5 reactor at a flux of about 6×10^{13} n/cm^2-sec for a period of about one hour. A cooling period of about 20 days was allowed before decanning and processing of the material. Because of the expected variability of both the irradiation time of EBR-II blanket material (between 2 and 20 yr) and the cooling time of this material, it is difficult to specify the level of iodine activity which will be encountered. However, it was calculated that after 15 days of cooling, the most active blanket material (that next to the core) will have an iodine level of less than one-hundredth that of the core material. The level of iodine activity employed

in the experiment was about the same as that calculated for the most active blanket material. In order to facilitate analytical work, plutonium was not used in this experiment. Inactive fission product elements were added* to bring the concentration of fission product elements up to expected process levels. Molybdenum, the element with the highest fission yield, would have a maximum concentration of about 600 ppm in discharged blanket material, which would result in a concentration of about 70 ppm in the 13 w/o uranium dissolver solution. All fission product analyses were, therefore, performed by radiochemical methods.

A schematic diagram of the equipment employed is shown in Figure I-11. The argon atmosphere in the dissolver was changed nine times during the course of the run (see conditions in Table I-7) by exhausting the argon before each sampling operation through an activated-charcoal trap (of 4-in. OD by 7 in. long), and then venting the gas to the building exhaust system. Since the blanket-dissolution and subsequent steps would be effected in a closed system in production operations, changing the atmosphere several times created a maximum off-gas-handling problem. Glass wool filters were placed on the inlet and outlet sides of the activated-charcoal bed to remove particulate iodine activity. A 16-in.-long, 1-in.-wide nickel strip was located on the wall of the furnace chamber and on the underside of the water-cooled flange to obtain an indication of the proportion of iodine depositing in the upper section of the furnace.

Figure I-11

EXPERIMENTAL EQUIPMENT FOR PROCESSING LIGHTLY IRRADIATED URANIUM BY THE EBR-II BLANKET PROCESS

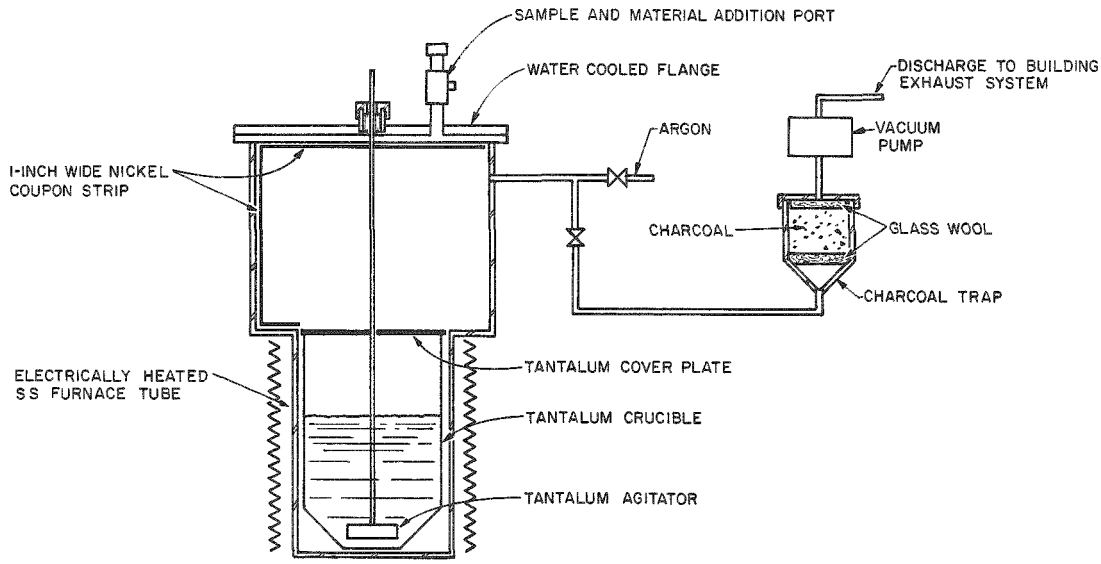

108-6842

*Elements added were: strontium, zirconium, molybdenum, ruthenium, rhodium, palladium, tellurium, barium, lanthanum, cerium, and neodymium.

The distribution of volatilized iodine activity was as follows:

		Percent of the Total Iodine Activity in the Charge
Underside of upper water-cooled flange (~200 C)		11.8
Upper furnace walls (200 to 700 C)		12.0
Tantalum cover plate over crucible (~700 C)		0.5
Activated-charcoal trap[a] (room temperature)		0.03
Inlet section of charcoal	0.018	
Exit section of charcoal	0.004	
Inlet glass wool filter (room temperature)		0.08
Outlet glass wool filter (room temperature)		0.006

[a]Charcoal trap was 4 in. deep and 4 in. in diameter.

Based on analyses of dissolved 1-in. squares of nickel strip and on the assumptions that iodine was symmetrically deposited on the upper cylindrical section of the furnace and uniformly deposited on the upper water-cooled flange, it was calculated that about 24 percent of the iodine charged was deposited on the furnace walls. Because of the presence of a cover plate over the crucible, it is believed that iodine could have reached the upper furnace walls only by vaporization, probably as a volatile compound, from the melt.

The gradual decrease in iodine activity through the activated-charcoal bed is more characteristic of the removal of particulate-carried iodine activity than of adsorption of molecular iodine. Previous experience on adsorption of molecular iodine in a charcoal bed (see ANL-6596, p. 38) showed essentially complete iodine adsorption to have occurred in the first inch of the charcoal bed.

The concentration of iodine in the off-gases was low in this experiment, despite frequent changes of the argon atmosphere, and there should not be a serious iodine-handling problem in blanket-processing operations. The use of at least one charcoal trap in the off-gas line and controlled disposal of off-gases from a tall stack should be adequate to avoid an off-gas-handling problem. The maximum iodine activity in the gases discharged during this experiment from the stack (i.e., the building exhaust system) was about one-quarter the maximum permissible iodine concentration in air.

The concentrations of iodine and other fission products in samples of the metal solution taken during the run are shown in Table I-7. The changes in the concentrations of these elements during the course of the run are discussed below.

Table I-7

SUMMARY OF BLANKET PROCESS DEMONSTRATION RUN 7

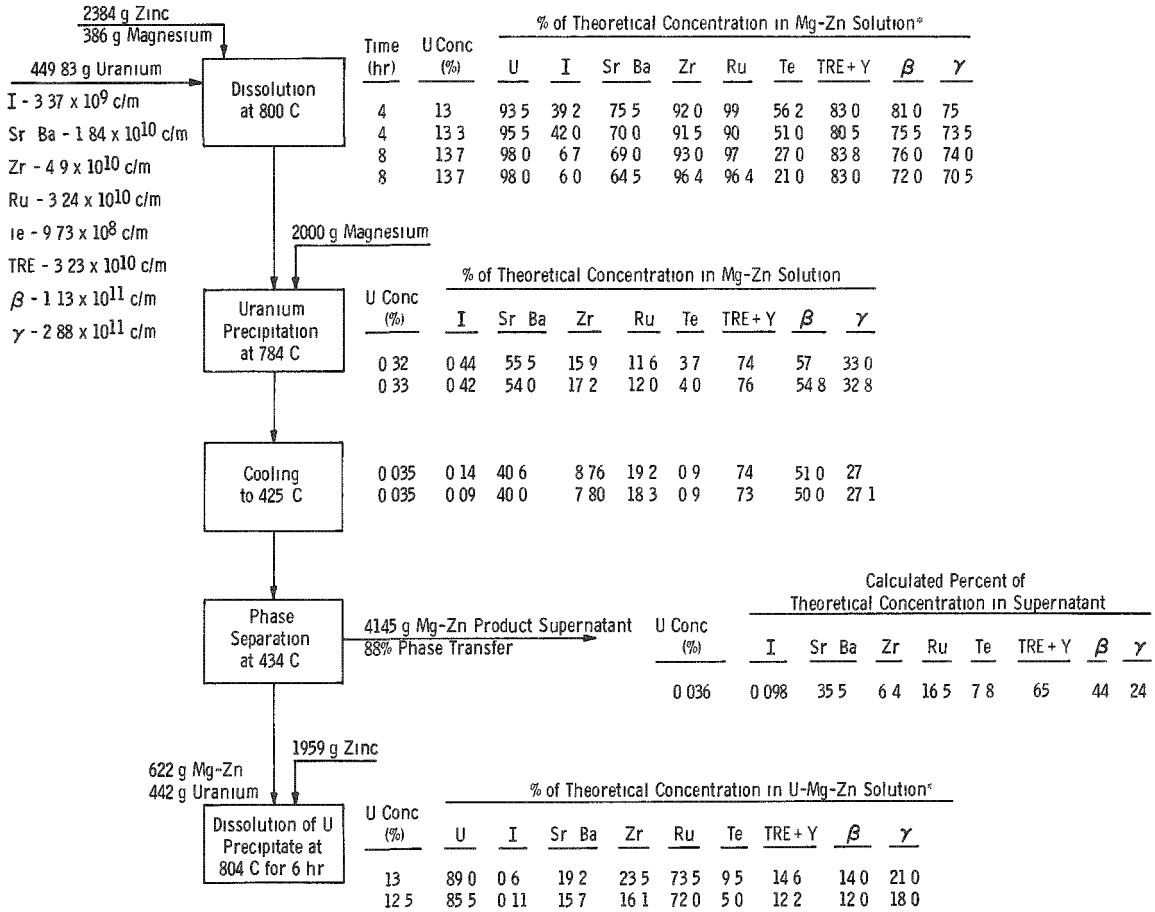

*Analyses of duplicate samples are given
**Uranium Concentration based on analysis of samples of supernatant at 425 C

108-6892

Iodine

The concentration of iodine in the magnesium-zinc dissolver solution decreased during the course of dissolution of the uranium charge (from about 40 percent to about 6 percent of that charged). Less than one percent of the iodine charged was found in the metal solution samples of succeeding steps; thus, virtually all of the iodine activity which was accounted for was the 24 percent found on the upper furnace surfaces. Because of the many active metals present in the dissolver solution (for example, magnesium, uranium, strontium, barium, and cesium), it is

unreasonable to believe that iodine would exist in the molecular state. Rather it would be expected to form inorganic compounds, for example, MgI_2, which would be highly insoluble in the zinc solution. Therefore, its disappearance from solution, if it were in solution, is believed to have occurred by agglomeration with other insoluble materials as a surface dross. The high initial values can be accounted for by the fact that thief samples, rather than filtered samples, were taken. This made possible inclusion of fine particulate matter in the sample.

Barium and Strontium

When dissolution had been completed, 65 to 70 percent of the charged barium and strontium activity was found in the dissolver solution. The bulk of this activity remained in the supernatant solution on precipitation of the uranium. Of the barium and strontium charged, 50 to 55 percent was finally accounted for in the product supernatant phase and the uranium precipitate phase. Barium and strontium are also believed to have been removed from solution through drossing reactions, e.g., with oxygen present as an atmosphere impurity or other less stable oxides present as impurities in the metal solution or tantalum container.

Zirconium

About 90 percent of the zirconium activity charged was present in the dissolver solution when dissolution was completed. The bulk of the zirconium disappeared from solution on precipitation of the uranium, but only a small portion of it reappeared in solution when the uranium was later redissolved. Considerable analytical difficulty was encountered in the zirconium analyses of the redissolved uranium solution.

Ruthenium

Essentially all of the charged ruthenium was found in the dissolver solution. As expected, the bulk of the ruthenium then precipitated with the uranium and was later recovered when the uranium was redissolved. The overall ruthenium material balance was between 90 and 95 percent.

Tellurium

The behavior of tellurium paralleled that of iodine; that is, tellurium was gradually lost from the dissolver solution, and little was found in either of the product solutions. There was very little tellurium activity deposited on the nickel sample plates. Drossing reactions or absorption on crucible walls would account for its disappearance also.

Rare Earths and Yttrium

Eighty to 85 percent of the theoretical concentration of these elements was found in the solution from the dissolution step. The amount finally accounted for in the product streams was 80 percent. As expected, most of the rare earth elements remained in the magnesium-zinc supernatant solutions on precipitation of the uranium.

Total Beta and Gamma Activities

Changes in these activities reflect changes in the concentrations of the individual activities.

Uranium Behavior

The behavior of uranium was not significantly different from that found in previous demonstration runs. Uranium dissolution was essentially complete after 8 hr at 800 C. The percentages of uranium in solution at 784 and 425 C, after the addition of magnesium to precipitate it from solution, are in agreement with solubility values. Transfer of 88 percent of the magnesium-zinc product supernatant is good for this scale of operations. However, on redissolution of the uranium for material-balance data, only 85 to 89 percent of the charged uranium was put into solution. The redissolution was accomplished in a 12 percent magnesium-zinc solution, whose volume was small compared with the previous 50 percent magnesium-zinc supernatant solution. It is believed that some of the uranium may have adhered to the crucible walls above the level of the final uranium solution and thus escaped redissolution.

(2) Concentration of Simulated Plutonium Product Solutions by Evaporation

(I. O. Winsch, T. F. Cannon, P. J. Mack)

The final step of the EBR-II blanket process is an evaporation in which the plutonium-magnesium-zinc product solution is concentrated by evaporation from an initial plutonium concentration of about 0.1 w/o to a final concentration of between 1 and 10 w/o plutonium. The final product solution will be fed into the core fuel cycle by adding it at an appropriate point into the recovery process for the core fuel material. Since the plutonium-recovery process for plutonium-bearing core materials has not been selected, the required degree of concentration of the product solution of the blanket process has not been firmly established.

The equipment being employed for the evaporation of simulated product solutions is a slightly modified version of that previously described in Summary Report ANL-6145, p. 62. For convenience a diagram of the modified equipment is shown in Figure I-12. The capacity of

the still pot of the metal evaporation unit is about 3.2 liters, which is equivalent to 14 kg of the dilute plutonium-50 w/o magnesium-zinc solution which is charged to the still pot. Evaporation is conducted at a pressure of about 40 mm Hg pressure. The temperature increases as the more volatile constituent, zinc, is removed. The temperature of the material in the still pot is determined by a top-entering immersion thermocouple. The tip of this thermocouple is at the same distance above the bottom of the crucible as the final desired solution level. When there is a sharp rise in the thermocouple temperature, this indicates that the solution level has dropped just below the thermocouple tip.

Figure I-12

METAL EVAPORATION UNIT

(Still pot volume = 3.2 liters)

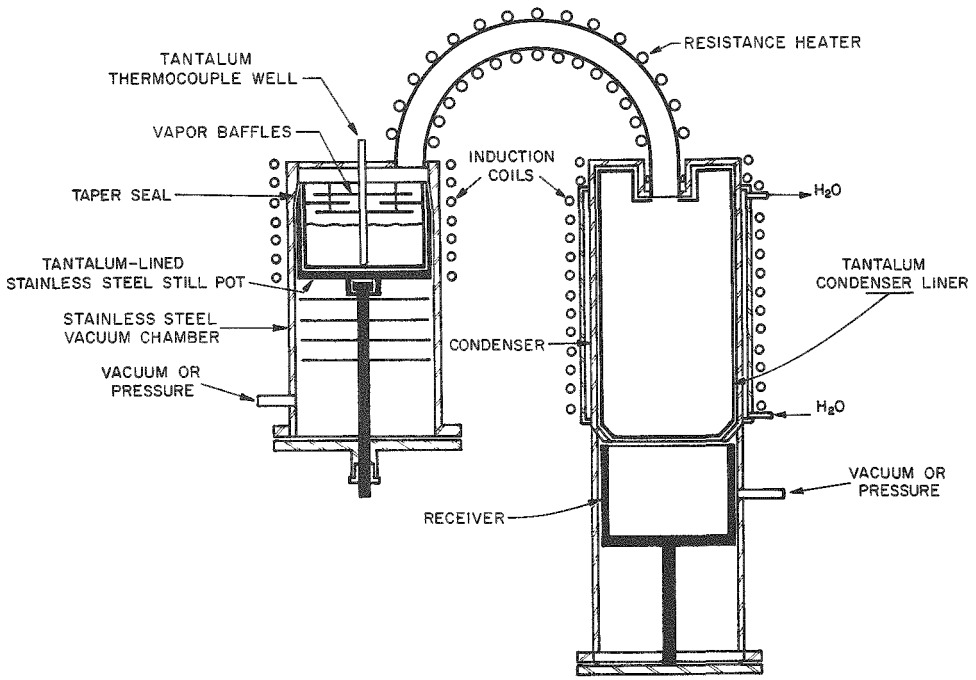

108-6848

The unit was fabricated of Type 304 stainless steel. However, tantalum liners are used to cover those parts of the still pot and condenser where zinc-containing metal solutions are evaporated or where zinc vapors are condensed. Zinc vapors, which are not excessively corrosive, are allowed to come in contact with Type 304 stainless steel above the still pot and in the vapor line between the still pot and the condenser.

Four preliminary runs have been completed in the metal evaporation unit with charges of 50 w/o magnesium-zinc alloys. The charges were simulated product solutions from inactive (i.e., no plutonium was present) blanket-processing runs and contained uranium at or slightly

above its solubility value at 405 to 425 C, namely, 0.03 to 0.04 w/o. Two of these charges contained cerium at an initial concentration of about 0.5 percent as a stand-in for plutonium. The fates of uranium (which, per se, is not very important) and of cerium, i.e., entrainment and deposition on baffles and still pot walls, are indicative of the probable fate of plutonium during evaporation.

The results of the four runs are given in Table I-8. The large percentages of cerium and uranium which were deposited on the still pot walls in Runs 3 and 4 (between 12 and 40 percent, being larger in the run in which a larger percentage of material was evaporated) are especially noteworthy. They indicate that a considerable amount of liquid had splashed against or spattered onto the walls and had evaporated from the walls. The still pot walls above the liquid level were undoubtedly hotter than the liquid itself; therefore, any zinc or magnesium that came into contact with the walls was rapidly vaporized, whereas cerium and uranium, which have comparatively high melting points (790 and 1130 C, respectively), remained on the wall as solids. Plutonium, which has a melting point of 640 C, might flow back into the solution when present. The comparatively small amount of deposition of material on the vapor baffles probably is the result of less liquid being splashed onto the baffles and a greater opportunity for the liquid to drop back into solution before vaporizing since the baffles are not directly heated.

Table I-8

ENTRAINMENT OF URANIUM AND CERIUM DURING EVAPORATION OF 50 w/o MAGNESIUM-ZINC SOLUTIONS

(Uranium was present in all charges at a concentration of 0.03 to 0.04 w/o; cerium was added to the charges of Runs 3 and 4 to a concentration of 0.5 and 0.4 w/o, respectively.)

Distillation Conditions

Pressure: 38-44 mm Hg
Temperature: 750-780 C

Run No.	Charge (kg)	Percent of Charge Material Evaporated	Average Evaporation Rate (kg/hr)	Entrainment of U and Ce Solutes (% of that in charge)					
				Vapor Baffles		Still Pot Walls		Condensate	
				U	Ce	U	Ce	U	Ce
1	10	84	1.8	N.D.[a]	-	N.D.[a]	-	2.0	-
2	9	72	2.2	N.D.[a]	-	N.D.[a]	-	1.4	-
3	15	54	2.2	0.14	0.9	18	12	0.2	0.2
4	15.3	96	1.6	4.0	1.9	31	40	3.0	0.2

[a]Not determined.

Only 0.2 percent of the cerium originally present in the still pot was carried over into the condensates. However, up to three percent of the uranium charged was found in the condensates. This is probably associated with the fact that uranium is precipitated from solution during the course of the evaporation, making possible its entrainment in particulate form, and, therefore, at concentrations higher than its solubility value. The high entrainment values in Run 4 as compared to Run 3 are probably the result of the more complete evaporation of the charge material in Run 4.

In the evaporation runs, the fraction of solute materials deposited on the still pot walls is indicative of a deposition of plutonium that would be large in relation to process requirements. The small volume of plutonium that will be present [only 5 cc in a 10-kg charge (530 cc) of blanket material] could create a problem in collecting the plutonium from such deposits. Heating the still pot from the bottom, rather than from the sides, would probably be an improvement, because there would be increased opportunity for bathing the still pot walls with reflux material.

d. Materials and Equipment Evaluation
(P. A. Nelson)

Studies are in progress to evaluate the compatability of various materials with liquid metal and fused salt systems of the types contemplated for reprocessing reactor fuels. Selection of materials for EBR-II processing equipment is the main objective, but data of more general interest are also being accumulated. Included in this report are studies of the corrosion of tungsten and a 30 percent tungsten-molybdenum alloy at 1000 C in the zinc-halide salt systems of the skull reclamation process, a study of the stability of uranium-zinc solutions, and evaluations of ceramic and metallic coating materials.

(1) Corrosion Studies
(M. Kyle, M. Deerwester)

Corrosion of Tungsten and Molybdenum-30 w/o Tungsten Alloy in Zinc-Halide Flux Systems

Both tungsten and molybdenum-30 w/o tungsten alloy are being tested as containment materials for zinc-halide flux systems. Most of the previous testing was done at temperatures of 800 or 850 C for 100 to 500 hr (see ANL-6596, p. 70, and ANL-6648, p. 66). In an effort to determine a practical limit of these materials for containment of zinc-halide flux systems, the materials have been tested at a higher temperature.

A run has been made at 1000 C for 500 hr to test the corrosion resistance of pressed-and-sintered tungsten and arc-cast molybdenum-30 w/o tungsten (MoW) to conditions of the noble metal leach step of the skull reclamation process. The conditions of the run and the results obtained are presented in Table I-9. After the test, sharp edges were still present on all of the specimens. Metallographic examination showed that tungsten was attacked to a depth of about 2 mils. There was some evidence that cavitation had occurred to a slightly greater depth. The exposure conditions did not greatly affect grain size, indicating that grain growth is not a problem with tungsten, even at 1000 C.

Table I-9

CORROSION OF TUNGSTEN AND MOLYBDENUM-30 w/o TUNGSTEN ALLOY EXPOSED TO THE SALT-METAL SYSTEM OF THE NOBLE METAL EXTRACTION STEP

Conditions

Time:	500 hr
Temp:	1000 C
Metal Phase:	40 g zinc
Flux Phase:	20 g of composition (m/o) of 46.6 LiCl, 46.6 $MgCl_2$, 4.8 MgF_2, 2.0 $ZnCl_2$
Containment:	Mo-30 w/o W welded capsule enclosed in a 310 SS capsule
Specimen Size:	0.09 x 0.09 x 1.5 in.; W, 3.9 g; MoW, 2.7 g

One capsule containing all six specimens was contained in a rocking furnace which was oscillated through 180° at 2 cycles/min.

	Specimen Thickness		
Material	Initial (mils)	Change (mil)	Photomicrograph Results
W	90.1	+0.4	Some 2- to 4-mil cavitation with 2-mil intergranular attack
W	89.0	-0.7	
W	89.5	-0.5	
MoW	86.8	+0.3	2- to 8-mil intergranular attack. No obvious molybdenum leaching.
MoW	90.7	-0.3	
MoW	90.7	-0.9	

The molybdenum-30 w/o tungsten alloy withstood attack better than anticipated. This is probably attributable to the method of testing. Initial testing of the molybdenum-tungsten alloy at 850 C

(see ANL-6596, pp. 71-72) had indicated that leaching of the molybdenum occurred. In one of these tests, a 500-hr test at 850 C, the final molybdenum concentration in zinc was calculated from the weight loss of the specimen to be 0.015 w/o (assuming that all of the weight loss was as molybdenum). This concentration is somewhat lower than the molybdenum solubility in zinc, namely, 0.022 w/o at 850 C.

These initial tests were run in alumina crucibles so that all the molybdenum present in solution could have come only from the test specimen. In the tests whose results are given in Table I-9, it was necessary to contain the test specimens in a molybdenum-tungsten capsule having a large surface area compared to that of the specimen itself. The ratio of exposed molybdenum-30 percent tungsten area to the zinc volume was 10 sq cm/cc as compared with 0.029 sq cm/cc for the previous tests made in alumina crucibles. In the capsule test, the molybdenum solubility limit of 0.022 w/o would have been reached by molybdenum leaching from the surfaces of the capsule and corrosion specimens to a depth of only 0 005 mil (50 percent removal of molybdenum to this depth). It may be concluded that the rate of attack of the molybdenum-tungsten alloy by molybdenum-saturated zinc solutions is very low. However, as indicated by the previous tests in alumina crucibles, slow leaching of molybdenum from the alloy may be expected by zinc which is not saturated with molybdenum.

The performance of the welded molybdenum-tungsten corrosion capsule was satisfactory. The capsule and lid were machined from bar stock and the closure was made by conventional inert gas Heliarc welding. Satisfactory techniques for welding the molybdenum-tungsten alloy make possible the fabrication of leak-tight, high-temperature corrosion capsules, and also may be useful in the fabrication of process equipment from this alloy.

(2) Materials Demonstration Runs
(G. A. Bennett, N. Quattropani)

A series of experiments to determine the effect of small amounts of added impurities on the stability of uranium-containing zinc-5 w/o magnesium solutions has been completed. In these experiments, known amounts of impurities were added to the metallic solutions contained in a pressed-and-sintered tungsten crucible, which is apparently inert to dissolved uranium (see ANL-6569, pp. 52 and 53). The temperature was maintained at 800 C, and mixing was effected by means of a molybdenum-30 w/o tungsten agitator (also inert to dissolved uranium according to the above reference) rotated at 530 rpm.

Runs of this type have been made to determine the effects of added silicon, Type 304 stainless steel, aluminum, and beryllium.

(Silicon, aluminum, and beryllium might be introduced into solution by reduction of oxide crucibles containing one or more of these elements. Stainless steel might be introduced as fuel cladding fragments.) With the exception of the beryllium additions, the runs were made in four stages: Stage I a "blank" stage in which no added impurity was present (to establish the initial concentration and sampling reliabilities); Stage II a stage with 500 ppm of added impurity; Stage III a stage with 1000 ppm of total added impurity; Stage IV a stage with one or two percent of total added impurity.

Because of the low density of beryllium (1.85 g/cc) and its relative insolubility in the solution (estimated at 0.03 w/o at 800 C), special precautions were taken to insure its dissolution. A known weight of beryllium rod was held under the surface of the molten metal during the dissolution period by means of a tantalum tube to which the beryllium was fastened. In two separate beryllium additions, 0.027 w/o was added in the first addition and a total of 0.051 w/o (probably beyond the solubility limit) had been added after the second addition. No later additions of beryllium were made. The beryllium content of the solution as determined spectrographically was 0.04 percent (order of magnitude accuracy).

Analytical results, although not yet complete are available and are shown in Figures I-13 to -16. These results may be summarized as follows:

(1) The addition of silicon to zinc-magnesium caused direct precipitation of uranium from solution (see Figure I-13) Since essentially all of the silicon reacted in Stages II and III (less than 50 ppm of silicon was left in solution after each stage), it was calculated that between 0.7 and 0.9 atom of silicon caused the precipitation of one atom of uranium. Examination of the uranium-silicon phase diagram indicates that the probable compounds formed were U_2Si_3 and USi. Silicon addition to a one percent concentration (a considerable excess on the basis of formation of USi) caused essentially complete precipitation of the uranium, the final uranium concentration being about 0.02 percent.

(2) No effect of stainless steel addition on uranium concentration was observable for additions of up to 1000 ppm stainless steel (see Figure I-14) as determined from colorimetric uranium analyses (accuracy, ±5 percent). Fifteen separate analyses of samples (taken during the blank, 500 ppm, and 1000 ppm periods of the run) showed a uranium concentration of 2.00 ± 0.04 percent (±2 percent deviation). This is in agreement with the calculated initial uranium concentration of 2.00 percent. However, when Type 304 stainless steel was added to give a two percent concentration of stainless steel, the uranium concentration dropped slightly to an average value of 1.94 percent. This slight decrease can probably be attributed to the reaction of uranium with impurities in the

stainless steel, the principal possibility being silicon. Differential colorimetric uranium analyses, accurate to ±1%, are being obtained to check the validity of this apparent decrease.

Figure I-13

STABILITY OF SOLUTIONS OF URANIUM IN FIVE PERCENT MAGNESIUM-ZINC ALLOY IN PRESENCE OF SILICON

Test Temperature: 800 C
Crucible: Baffled Pressed-and-sintered Tungsten
Stirrer: Mo-30 w/o W
Stirring Speed: 530 rpm

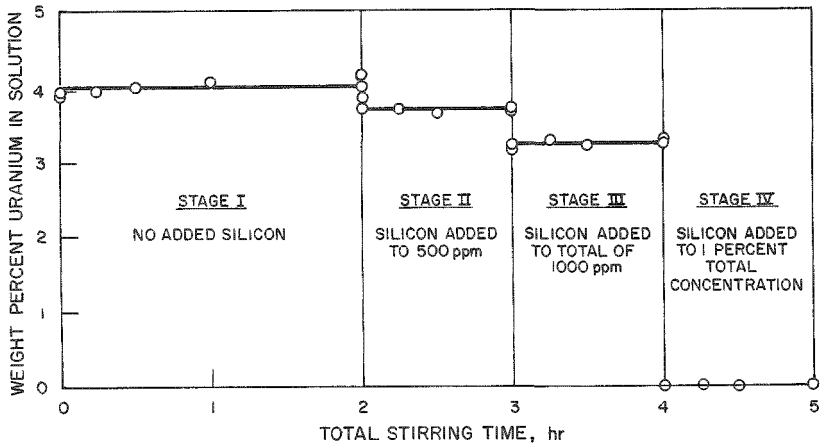

	Initial Concentration	
	Wt(g)	Percent
Zn	3409	91.00
Mg	187.0	5.00
U	149.46	4.00

108-6872

Figure I-14

STABILITY OF SOLUTIONS OF URANIUM IN FIVE PERCENT MAGNESIUM-ZINC ALLOY IN THE PRESENCE OF 304 STAINLESS STEEL

Test Temperature: 800 C
Crucible: Baffled Pressed-and-sintered Tungsten
Stirrer: Mo-30 w/o W
Stirring Speed: 530 rpm

Solid points indicate duplicate samples with analyses agreeing within 2 percent.

	Initial Concentration	
	Wt(g)	Percent
Zn	3403	93.00
Mg	182.81	5.00
U	73.12	2.00

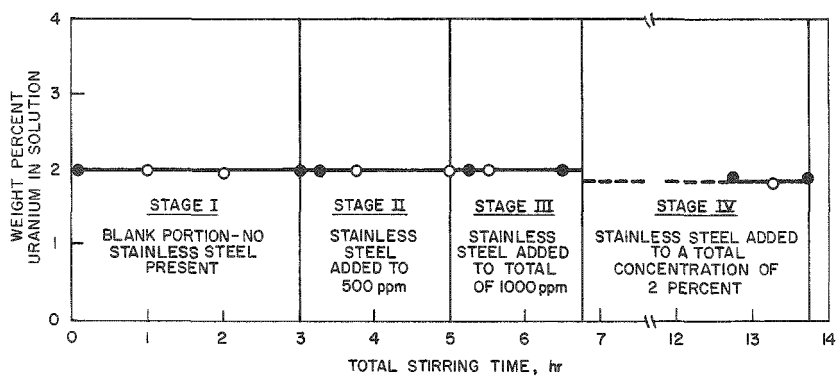

108-6866

(3) No effect of aluminum addition on uranium concentration was observable for additions of aluminum up to one percent total aluminum concentration. The data shown in Figure I-15 are based on differential color analyses (estimated accuracy, ±1%) for the first two stages of the experiment, and on colorimetric analyses (estimated accuracy, ±5%) for the last two stages of the experiment. This probably accounts for several high uranium concentration values (only one of which exceeds the estimated analytical accuracy) shown for the last two stages of the run. The uranium concentrations for these last two stages are being checked by differential colorimetric analysis.

Figure I-15

STABILITY OF SOLUTIONS OF URANIUM IN FIVE PERCENT MAGNESIUM-ZINC ALLOY IN THE PRESENCE OF ALUMINUM

Test Temperature: 800 C
Crucible: Baffled Pressed-and-sintered Tungsten
Stirrer: Mo-30 w/o W
Stirring Speed: 530 rpm

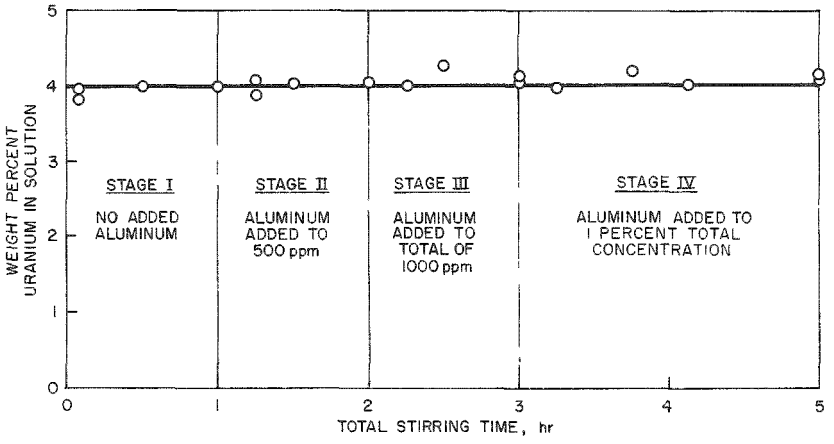

	Initial Concentration	
	Wt(g)	Percent
Zn	3400	91.00
Mg	186.84	5.00
U	149.45	4.00

108-6884

(4) The dissolved uranium and the added beryllium did not react, as was indicated by the preliminary single-aliquot colorimetric analytical results for uranium shown in Figure I-16. The variation of analyses of samples taken throughout the run did not exceed the estimated 5 percent analytical accuracy. The uranium content of a few samples is being determined by means of differential colorimetric analysis.

(3) Fabrication of Ceramic Containers

(P. A. Nelson, Z. D. Jastrzebski,* W. Pehl, and M. Deerwester)

A need for large ceramic vessels is envisioned for future large-scale liquid metal processes. Beryllia, alumina, and magnesia are among the ceramic materials which are sufficiently inert to

*Consultant from Lafayette College, Pennsylvania.

process systems (magnesium-zinc and halide salt systems) to be considered as container materials. No commercial source of large crucibles of these materials having good resistance to thermal and mechanical shock and low permeability to halide salts has been found. Crucibles formed by ramming or casting and containing large prefired aggregates have good mechanical properties but, unfortunately, also have high porosity and are easily wet and penetrated by molten magnesium-zinc solutions. On the other hand, low-porosity crucibles formed by slip casting or isostatic pressing from very fine, highly reactive powders have poor thermal and mechanical shock resistance.

Figure I-16

STABILITY OF SOLUTIONS OF URANIUM IN FIVE PERCENT MAGNESIUM-ZINC ALLOY IN THE PRESENCE OF BERYLLIUM

	Initial Concentration	
	Wt(g)	Percent
Zn	3402.5	92.09
Mg	186.81	5.06
U	105.3	2.85

Test Temperature: 800 C
Crucible: Baffled, Pressed-and-sintered Tungsten
Stirrer: Mo-30 w/o W
Stirring Speed: 530 rpm

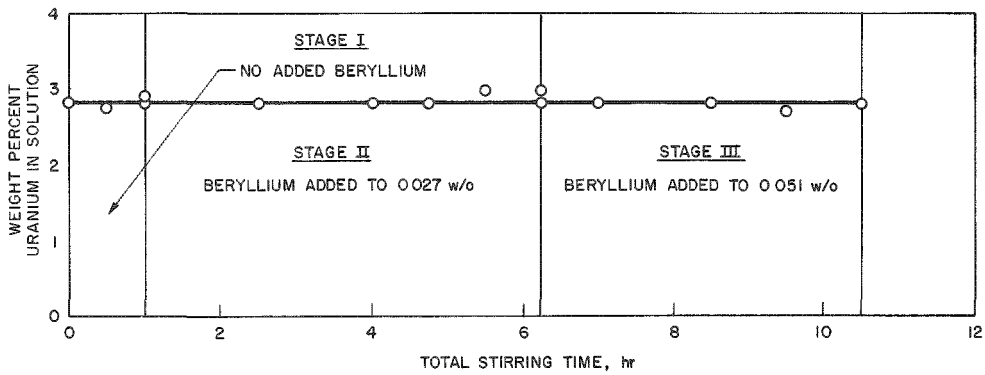

108-6869

In order to take advantage of the good mechanical properties of porous, coarse-grained alumina crucibles, an attempt is being made to seal the pores of these crucibles by coating or impregnating the inner surfaces with a slurry or thin paste containing a finely divided mixture of low-melting oxides. Subsequent firing of the crucible fuses the coating or impregnating material, thereby sealing the pores.

In the last summary report (ANL-6687, p. 50) it was reported that Alundum crucibles that had been coated twice with an alcohol

slurry of Al_2O_3-41 percent CaO-7 percent MgO mixture (and fired after each coating at 1300 to 1500 C) were impervious to water. In the cases reported, the slurry was formed by premelting the proper mixture of Al_2O_3, $CaCO_3$, and $MgCO_3$ (CO_2 is driven off during melting), and then crushing and ball-milling the melted product. In recent coating tests, the coating material was made by premelting and ball-milling a mixture of oxides to obtain, it was thought, the same coating material. (The only change in procedure was the use of calcium and magnesium oxides instead of carbonates.) However, alumina crucibles coated with this material (especially with heavy coatings of this material) developed cracks during the firing operation at 1400 C. In one firing, an uncoated crucible which was fired at the same time as a coated crucible was unaffected, while the coated crucible cracked.

Later tests have confirmed the supposition that the difference in coating preparation was the primary cause of cracking of alumina crucibles coated with the oxide mixture. Three crucibles coated with a new batch of coating material prepared from alumina and carbonates of calcium and magnesium did not crack on firing, and each was rendered impervious to water with two rather thin (5- to 10-mil) coatings.

One of these coated alumina crucibles was tested for its ability to contain zinc-5 percent magnesium-4 percent uranium solution at 800 C in argon atmosphere. No noticeable leakage of liquid metal occurred during the 10-hr holding period, and no cracks were evident. However, the frozen melt adhered tightly to the crucible coating, indicating that wetting had occurred. On remelting of the metal, in order to pour it out, the crucible cracked. The surface of the coating had been blackened below the liquid level (indicating oxygen depletion), but otherwise it appeared unaffected. Examination of several crucible fragments indicated that the coating had adhered very tightly to the substrate and that penetration by the melt had occurred only to a minor extent through a few flaws in the coating.

The other two coated crucibles were tested for their ability to contain a molten salt of the composition (in m/o): LiCl-47.5 $MgCl_2$-5 MgF_2 at 800 C. One crucible successfully contained the salt during a 2-hr run. However, a small amount of the flux leaked from the second crucible at two flaws in the coating which had not been evident in tests with water.

Application of the coating material to crucibles cast from cement-bonded castable alumina has not resulted in an impervious coating because of roughness and air pockets on the surface of the cast shape.

It is concluded that although the coating adheres well to alumina and has a measure of corrosion resistance to EBR-II process systems, the application of the coating requires extreme care. Coatings of this type appear to be limited, at present, to application on rather smooth surfaces.

(4) Testing of Plasma-sprayed and Vapor-deposited Coating Materials
(G. A. Bennett, W. A. Pehl, N. Quattropani)

Although pressed-and-sintered tungsten crucibles have been shown to be satisfactory for the noble metal-extraction and -reduction steps of the skull reclamation process, and although thixotropically cast beryllia crucibles have shown promise of being satisfactory for the precipitation and retorting steps, fabrication of crucibles from each of these materials is expensive, and the size of such crucibles may be limited. A possible method of overcoming both of these problems is to plasma-spray coating materials having good corrosion resistance on other, less expensive materials which can be fabricated into large shapes. Spraying may be done in air or in an inert gas chamber. Various spraying techniques, such as the use of graded coatings (i.e., coating layers of increasing proportions of coating material and decreasing proportions of substrate material), deposition of an intermediate layer, or plasma fusion (which is really a welding operation), may be employed to increase bonding and reduce the susceptibility of the coated crucible to thermal shock. By proper use of available techniques, it may be possible to obtain adherent coatings even though the coating materials have coefficients of thermal expansion which differ from those of the substrate materials. The limitations of these methods for crucible fabrication appear to be primarily geometrical, i.e., the crucible being coated must be of sufficient diameter (approximately 10 in.) to permit positioning of the spray gun at the proper distance from all surfaces to be coated.

In order to survey the applicability of plasma spraying to the coating of crucibles which must contain molten flux and uranium-zinc-magnesium solutions, samples of possible substrate materials (each sample was approximately 3 sq in. in area) were sent to Western Gear Corporation, Lynwood, California, for coating by the various plasma-spray techniques. The substrate materials, which were silicon carbide, graphite, Alundum, and Type 430 stainless steel, were selected because of their fabricability into large equipment, their low cost, and, in some cases, the compatibility of their coefficients of thermal expansion with those of the coating materials. The coating materials consisted of tungsten, beryllia, zirconium diboride, and tantalum monoboride. The last two coating materials may have resistance to attack by oxide fluxes. The coating thickness and powder particle sizes (10 mils and 12 to 44 μ, respectively) were those recommended by the Western Gear Corporation.

The coated samples were tested by thermal cycling between 300 and 800 C for a total of twelve times in an argon atmosphere. At the conclusion of the run, all samples were visually examined for coating adherence. The results are given in Table I-10.

Table I-10

PERFORMANCE OF PLASMA-SPRAYED COATINGS SUBJECTED TO THERMAL CYCLING BETWEEN 300 AND 800 C

Except when noted, the following conditions were employed:

Spraying Conditions	Coating Thickness:	10 mils
	Powder Particle Size:	12-44 μ
	Spray Density:	93% theoretical (minimum)
	Glovebox Atmosphere:	5% H_2-95% Argon
Sintering Conditions	In argon for 3 hr at ~1200 C	
Thermal Cycling Conditions	Twelve cycles between 300 and 800 C	

Substrate Material	Coating Material	Spraying Technique	Observed Change after Thermal Cycling
Silicon Nitride-bonded Silicon Carbide	Tungsten	Inert atmosphere box	None
	Tungsten[a]	Inert atmosphere box	None
	Tungsten[b]	Inert atmosphere box	None
	Tungsten	Sprayed in air	None
	Tantalum Monoboride	Inert atmosphere box	Separation of coating
Oxide-bonded Silicon Carbide	Tungsten	Inert atmosphere box	None
Type CS Graphite	Tungsten	Inert atmosphere box	None
	Zirconium Diboride	Inert atmosphere box	Coating powdered during cycling
Type 430 Stainless Steel	Tungsten[c]	Inert atmosphere box	Coating cracked at corners
	Tungsten	Graded coating[d]	None
	Tungsten	Intermediate layer of 1-2 mils molybdenum	Separation of coating
	Tungsten	Intermediate layer of 1-2 mils tantalum	Separation of coating
	Tungsten	Brazing technique[e]	None[f]
	Beryllium Oxide	Brazing technique[e]	Could not achieve adherence during plasma spraying
	Beryllium Oxide	Sprayed in air	None
Alundum	Tungsten	Inert atmosphere box	None
	Tungsten	Graded coating[d]	None
	Tungsten	Intermediate layer of 1-2 mils titanium	None
	Beryllium Oxide	Sprayed in air	None

[a]Tungsten layer: 30 mils.

[b]Tungsten particle size: 8 μ.

[c]Sintered in H_2 at ~1150 C for 3 hr.

[d]Composition of spray material varied from 100 percent substrate material to 100 percent coating, in 8 equal increments.

[e]Nibrobraz No. 120 used.

[f]Two samples.

No obvious deterioration was noted, either visually or photomicrographically, for tungsten-coated specimens of the following materials: nitride-bonded or oxide-bonded silicon carbide, graphite, and Alundum. For coating silicon carbide with tungsten, spraying in air was as satisfactory a technique as the more complicated and expensive techniques of graded coatings or plasma fusion. The latter methods appear to be necessary, however, for coating of Type 430 stainless steel with tungsten. Satisfactory adherence of beryllium oxide on either Alundum or Type 430 stainless steel appears obtainable by simple spraying in air.

Test crucibles of tungsten-coated silicon carbide and tungsten-coated stainless steel are being obtained for evaluation under process conditions.

A tantalum-clad thermocouple was coated with tungsten by a vendor who used the vapor-deposition technique. However, part of the coating was easily peeled from the substrate, and further peeling occurred after four temperature cycles between 300 and 800 C.

e. Supporting Chemical Investigations
(R. K. Steunenberg)

Certain fundamental studies of molten salts and liquid metals are being conducted in order to supply data for process use and to gain a fuller understanding of the basic principles involved. During the quarter, additional results have been obtained on the nature of the species formed when uranium oxides are added to molten chloride solvents.

Reactions of Uranium Oxides in Molten Chloride Media
(M. D. Adams, D. A. Wenz, J. S. Tait)

It was reported previously (see Summary Report ANL-6569, p. 54) that a uranium(V) species tentatively identified as the UO_2^+ ion is formed by the reactions of higher uranium oxides or oxychlorides with molten halide salts. A characteristic absorption spectrum for this species in the visible and near-infrared regions has been observed in the following solvents: (1) equimolar lithium chloride-magnesium chloride, (2) the binary eutectic at 59 m/o lithium chloride and 41 m/o potassium chloride, and (3) the ternary eutectic at 30 m/o sodium chloride, 20 m/o potassium chloride, and 50 m/o magnesium chloride.

Further identification of the uranium(V) species as UO_2^+ ion has been provided by comparing its spectrum with that of the isoelectronic neptunyl ion, NpO_2^{++}.[1] The two spectra have the same general characteristics, and the ratios of the wavelengths of the corresponding peaks are nearly constant.

[1] Cohen, D., and Taylor, B., Some Observations of Np(VI) in Chloride Solutions, J. Inorg. and Nuclear Chem. 22, 151-3 (1961).

The UO_2^+ ion is formed by the thermal decomposition of uranyl chloride in molten chloride solvents at temperatures above about 600 C:

$$2UO_2Cl_2 \rightleftharpoons 2UO_2Cl + Cl_2. \quad (1)$$

An investigation of Reaction 1 is being made to obtain additional information on the UO_2^+ ion and its spectrum. Two solvent systems are being used, the lithium chloride-potassium chloride eutectic, and the ternary sodium chloride-potassium chloride-magnesium chloride eutectic.

Preliminary molar absorptivity values at 650 C for the UO_2^+ species and equilibrium data for Reaction 1 have been determined with a Cary Model 14 spectrophotometer modified to accommodate a one-centimeter square quartz cell at temperatures up to about 800 C. For this study, the apparatus shown schematically in Figure I-17 was connected to the spectrophotometer cell. This apparatus permitted simultaneous measurement of the optical absorptivity of the salt solution and determination of the amount of chlorine evolved by Reaction 1. Each spectrophotometer cell was provided with a stopcock through which the chlorine could be

Figure I-17

APPARATUS FOR THE COLLECTION AND MEASUREMENT OF GAS EVOLVED FROM MOLTEN SALT SOLUTIONS

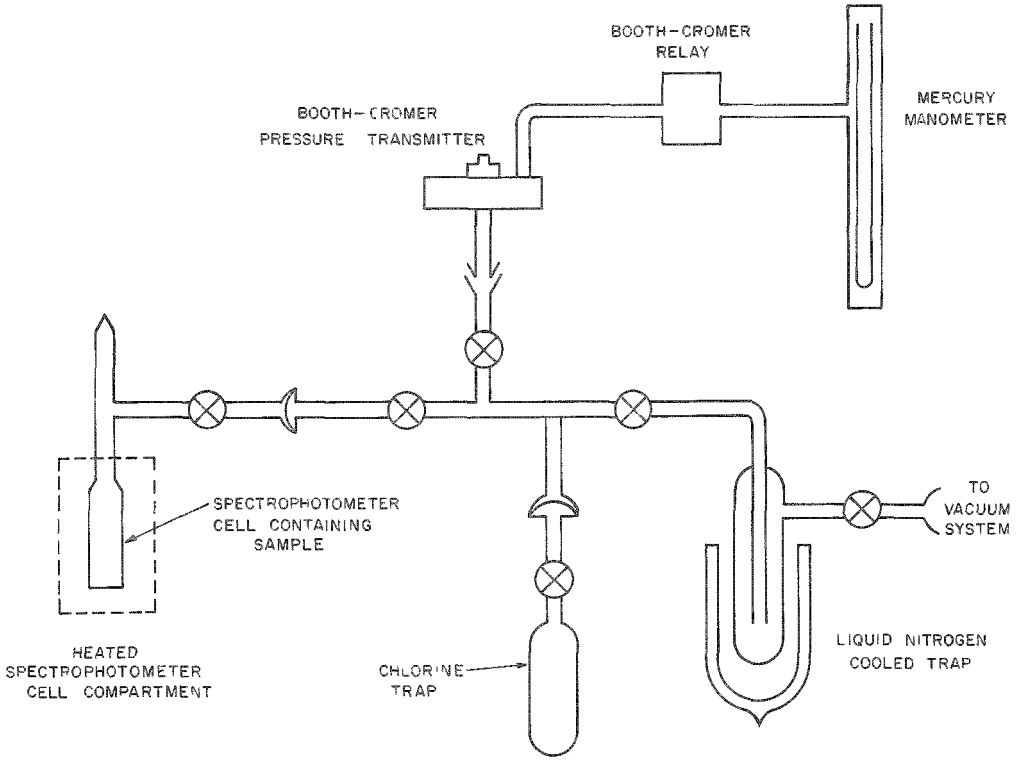

108-6851

removed and condensed in a liquid nitrogen cold trap. The chlorine was then warmed to room temperature and expanded into a section of the apparatus having a known volume, and its quantity was determined by pressure measurement.

In each determination, uranyl chloride was added to the molten chloride solvent, and the amount of chlorine produced was determined. The quantity of chlorine collected proved to be directly proportional to the absorbance of the UO_2^+ peaks. When the uranium concentration in the salt had been determined by chemical analysis, it was then possible to compute molar absorptivity values in the two solvents. The spectra based on these values are presented in Figure I-18.

Figure I-18

MOLAR ABSORPTIVITY OF UO_2^+ ION IN THE VISIBLE AND NEAR-INFRARED REGIONS

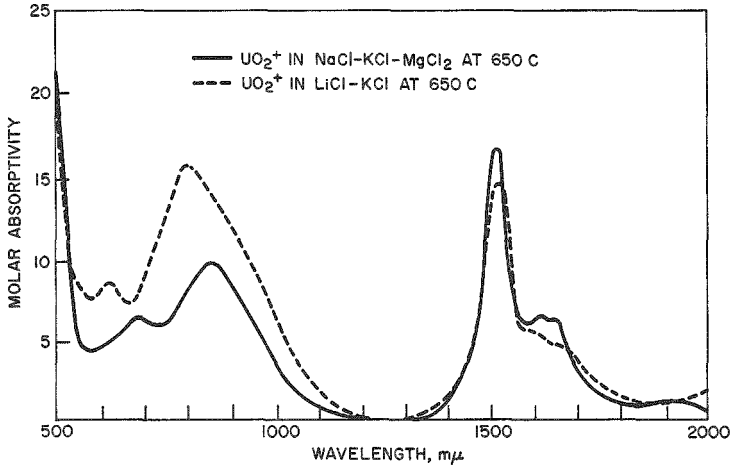

108-6880

The results of these experiments indicate that the molar absorptivities can be measured with good precision (about 3 percent) in solutions of uniform composition. However, small changes in the proportions of the components of the solvents used had a marked effect on the molar absorptivities.

By determining equilibrium chlorine pressures over the salt as a function of the optical absorbance, it is possible to determine the equilibrium constant for Reaction 1:

$$K_{eq} = \frac{(UO_2Cl)^2 \, (P_{Cl_2} \, [atm])}{(UO_2Cl_2)^2}.$$

At 650 C, a preliminary value of K_{eq} is about 10^{-6} atm in the lithium chloride-potassium chloride eutectic.

3. Reactor Materials
(R. K. Steunenberg)

Pyrometallurgical methods show promise as simple, economical procedures for producing nuclear fuel materials. Refractory compounds of the actinide elements that are of interest as high-performance reactor fuels can be prepared by reactions of the actinide elements with carbon or other elements in liquid metal media. Other new synthetic methods for the preparation of refractory compounds such as the carbides and sulfides of uranium and plutonium are being investigated.

An effective procedure for the preparation of metallic fuel materials is the direct reduction of actinide oxides or halides from a molten halide flux by liquid metal solutions containing magnesium.

The experimental work during the past quarter has been concentrated mainly on the preparation of uranium carbides and sulfides, and the direct reduction of thorium and plutonium oxides to the respective metals.

a. Preparation of Uranium Monocarbide
(E. J. Petkus, J. F. Lenc, T. R. Johnson, J. P. LaPlante, M. A. Bowden)

Construction and testing of equipment for the preparation of uranium monocarbide on a 500-g scale by the reaction of uranium and carbon in liquid metal solutions has been completed. The principal component is a helium-vacuum glovebox, shown in Figure I-19. This glovebox can be evacuated with the metal covers of the glove ports in place. After the box is filled with high-purity helium at atmospheric pressure, the covers are removed to permit use of the gloves. The other major components are a reaction-phase transfer furnace (shown in position under the glovebox in Figure I-19) and a vacuum retorting furnace which can be attached to a part on the floor of the glovebox. Materials can be transferred into and out of the glovebox through a vacuum lock, thereby avoiding contamination of the materials or the box by the atmosphere. The connection between the furnaces and the glovebox can also be evacuated and filled with high-purity helium, then opened to permit transfers of materials between these components without exposure to air.

This equipment is presently being used to develop procedures for the preparation of 500-g batches of high-purity, stoichiometric uranium monocarbide. Particular attention is being given to reducing the oxygen and nitrogen content of the product to low levels. Subsequent evaluation of the product for fabrication into reactor fuel shapes will be performed by the Metallurgy Division.

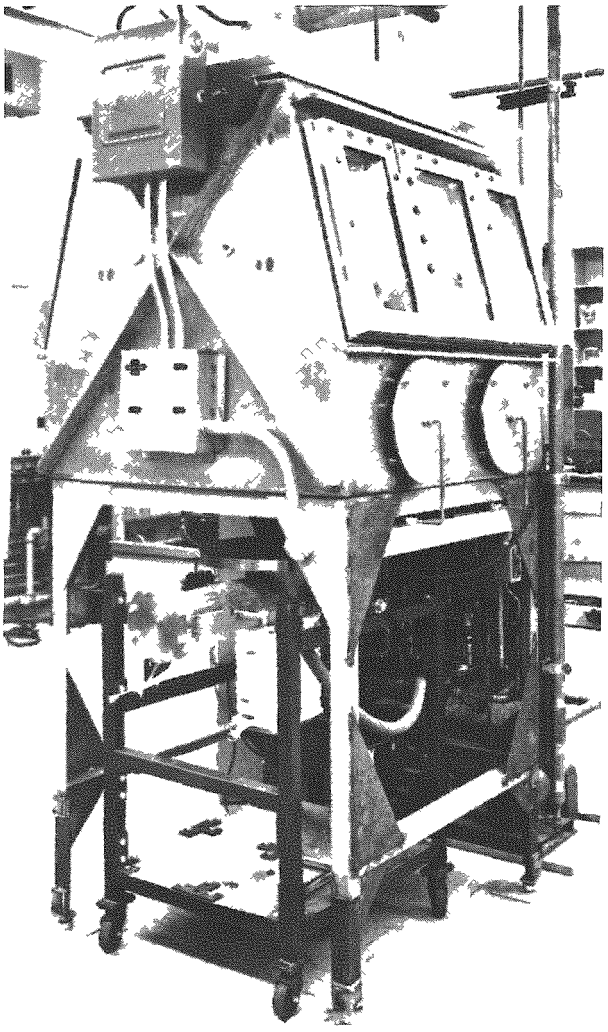

Figure I-19

VACUUM GLOVEBOX FOR URANIUM MONOCARBIDE PREPARATION

108-6086

The preparative method currently under investigation includes the following steps: (1) dissolution of metallic uranium in zinc containing a low concentration of magnesium, (2) addition to the metal solution of degassed activated charcoal in the amount required to form uranium monocarbide, (3) a phase separation to remove the bulk of the supernatant liquid metal from the precipitated uranium monocarbide, and (4) retorting under vacuum to remove residual zinc and magnesium from the product. Analytical data are not yet available for the 500-g batches of material recently prepared.

b. Development of New Methods for Preparation of Uranium Carbide
(J P. LaPlante, H. E Griffin)

Attempts are being made to develop new methods for the preparation of uranium-carbon compounds with different, but reproducible uranium-to-carbon ratios, and to determine the effects of impurities and of various carbon-to-uranium ratios on the physical properties of the product.

Several scouting experiments were performed, in which magnesium carbide, prepared by the reaction of magnesium chloride and calcium carbide,[2] was added to uranium tetrafluoride or magnesium uranate dissolved in a flux (32.4 m/o sodium chloride-19.3 m/o potassium chloride-48.3 m/o magnesium chloride). The reaction vessel consisted of a quartz tube open to the atmosphere, and the temperature range was about 460 to 750 C. The magnesium carbide appeared to react readily with the dissolved uranium compounds, as evidenced by an immediate change in the color of the flux from yellow or brown to white, and the formation of a black precipitate. The precipitate has been found to react with water, but has not been completely characterized.

An additional experiment was performed in which magnesium carbide was added to uranium tetrafluoride dissolved in a flux composed of 35.0 m/o lithium chloride and 65.0 m/o magnesium chloride. A black product that precipitated from the solution was separated from the bulk of the flux by filtration in an inert atmosphere. An X-ray diffraction pattern of the product indicated the major phase to be uranium monocarbide.

Plans are being made to perform additional experiments under more closely controlled conditions in order to characterize the product more fully and to determine its purity.

c. Preparation of Uranium Monosulfide
(S. Vogler, J. P. LaPlante, J. A. Trischan)

The major objective of this work is to prepare uranium monosulfide that is suitable for evaluation as a reactor fuel material. A product of controlled composition and satisfactorily low impurity content is desired. To fulfill this objective, it is necessary to characterize by various physical and chemical methods the uranium monosulfide prepared.

Procedure

The preparative method of Eastman and coworkers[3] was chosen for the initial work. This procedure consists of three steps: (1) bulk uranium metal is hydrided and dehydrided until a finely divided reactive powder is formed, (2) the uranium powder is heated with the stoichiometric quantity of hydrogen sulfide required to form uranium monosulfide, and (3) the resulting mass of unreacted uranium and higher sulfides is ground, sieved, mixed, and then heated in vacuum to about 1900 C to form homogeneous uranium monosulfide.

---

[2]Schneider, A., The Preparation and Thermal Stability of Magnesium Carbides, MgC_2 and Mg_2C_3, Z. anorg. u. allgem. Chem. 279, 94 (1955).

[3]Eastman, E. D., Brewer, L., Bromley, L. A., Gilles, P. W., and Lofgren, N. A., Preparation and Properties of the Sulfides of Thorium and Uranium, J. Am. Chem. Soc. 72, 4019 (1950).

Results

A series of uranium monosulfide preparations on a 40-g scale has been completed, and the products have been analyzed. Some of the results are presented in Table I-11. Common impurities in the product are the oxides and oxysulfides of uranium, which are insoluble in dilute sulfuric acid when present as a separate phase. Thus a rough estimate of the purity of the product can be obtained readily by dissolving the uranium monosulfide in dilute sulfuric acid and weighing the insoluble material. However, more reliable analytical data on the oxygen and nitrogen contents were obtained by direct determinations of these elements.

Table I-11

COMPOSITION OF URANIUM MONOSULFIDE SAMPLES

Run No.	Insolubles[a] (w/o)	Oxygen (w/o)	Nitrogen (w/o)	Total Uranium[b] (w/o)	S/U (atomic ratio)[d]	X-ray Results (Å)[c]	X-ray Results Minor Phases
12	0.42	0.23		87.50	1.06	5.480	
13A	3.2	0.22		88.20	0.98	5.480	
15	1.03	0.061	0.077	87.46	1.06	5.481	
16-1	0.04	0.089		87.79	1.03	5.487	
16-2	0.04		0.0095			5.487	
16-3	0.25	0.42		87.77	1.03	5.487	
17-1	2.02	0 078	0.083	87.18	1.08	5.482	Possibly U_3S_5
17-2	1.95			86.65	1.14	5.484	U_3S_5, U_2S_3
18-1	0.1	0.24	0.063	86.86	1.12	5.481	Possibly U_3S_5
18-2	2.8			86.81	1.12	5.484	Possibly U_3S_5
19-1	0.0	0.085	0.0035	88.22	0.99	5.484	
19-2	0.0	0.084		88.11	1.00	5.487	
20-1	0.0		0.027	87.85	1.03	5.485	
20-2	0.0			87.83	1.03	5.487	

[a]In dilute sulfuric acid.

[b]Determined by ignition of the sulfide to U_3O_8.

[c]Lattice parameter.

[d]Calculated value, based on uranium weights corrected for uranium content of the insolubles.

The uranium contents of the products were determined by igniting samples of the sulfide to uranosic oxide, from which the amounts of uranium were calculated. By making corrections for the uranium content of the insoluble material, it was possible to compute the sulfur content and the sulfur-to-uranium ratio of the uranium sulfide.

The products from Runs 19 and 20 in Table I-11 appear to be satisfactory on the basis of the insolubles content and the uranium content. The products from Run 20 showed an oxygen content greater than 0.1 w/o, but the specific values are not listed in Table I-11 because of poor precision of the results. The oxygen contents found for the products from

Runs 19 and 20 cannot be attributed to the phase that is insoluble in sulfuric acid. It is believed that this oxygen may be present as a solid solution in the uranium monosulfide. This possibility has been discussed by Cater.* In those instances for which a substantial part of the oxygen content cannot be accounted for by the presence of insolubles, values calculated for the sulfur contents of the products may be in error. In order to obtain unambiguous results, direct determinations of the sulfur content will be made in future experiments.

The nitrogen contents of the products varied considerably (from 0.0035 to 0.083 w/o). In general, the higher nitrogen contents were associated with smaller lattice parameters. This effect is attributed to the formation of solid solutions of uranium mononitride and uranium monosulfide. An exception to this behavior was found for Run 19-1, in which a small lattice parameter was observed in a sample with a low nitrogen content.

Analyses of several samples of uranium monosulfide showed approximately 1000 ppm carbon to be present in each sample. The source of the carbon is believed to be carbon monoxide or carbon dioxide present as an impurity in the hydrogen sulfide. These impurities can be removed by holding the hydrogen sulfide under vacuum at liquid nitrogen temperature for at least one hour. This purification step will be used in all future experiments.

Several of the uranium monosulfide products were also analyzed spectrographically for metallic impurities. The results indicated that impurity levels in the uranium metal and the uranium monosulfide product do not differ greatly.

Table I-12

EFFECT OF REHEATING ON INSOLUBLES AND OXYGEN CONTENTS OF URANIUM MONOSULFIDE

	Insolubles (w/o)[a]		Oxygen (w/o)	
Run No.	Initial	Reheated	Initial	Reheated
13A[b]	3.2	0.56	0.22	0.15
15[b]	1.03	0.066	0.058	0.34
17-2[c]	1.95	0.0	-	-
18-2[d]	2.8	0.83	-	-

[a] In dilute sulfuric acid.
[b] Material from this run arc-melted in argon-helium mixture.
[c] Material from this run heated in vacuum at 1915 C for 4 hr.
[d] Material from this run heated in vacuum at 1900 C for 6 hr.

Effect of Reheating

Several samples that were known to contain oxygen were reheated in vacuum at 1900 C or arc-melted to determine whether the amount of oxygen would thereby be decreased. The results from several such samples, presented in Table I-12, show that the insolubles content of the uranium monosulfide is reduced by reheating in vacuum or by arc-melting. The results of the direct oxygen analyses show a less definite effect and suggest that the principal effect of reheating is the formation of solid solutions.

*E. D. Cater, The Vaporization, Thermodynamics, and Phase Behavior of Uranium Monosulfide, ANL-6140 (March 1960).

d. Reduction of Thorium Dioxide

(W. H. Hauschildt,* J. B. Knighton, J. W. Walsh)

The objective of this work is to develop a practical method for the reduction of thorium dioxide to the metal by means of a liquid metal-flux technique. The thorium dioxide, suspended in a molten halide flux of the proper composition, is reduced to the metal by liquid magnesium-zinc alloy. Previous work on this problem has been reported in previous Summary Reports (ANL-6477, p. 43; ANL-6569, p. 66; ANL-6648, p. 90; ANL-6687, p. 59). Further investigations have been made of the relationship between the weight ratio of thorium dioxide feed to flux and the reduction of thorium dioxide. The suitability of various materials for use as crucibles in the reduction process was evaluated briefly.

Figure I-20

EFFECT OF THORIUM DIOXIDE TO FLUX WEIGHT RATIO ON THE REDUCTION OF THORIUM DIOXIDE

Temperature:	850 C
Mixing Rate:	1000 rpm
Magnesium Concentration:	~10 w/o in Zn (600 g)
Duration of Reduction:	4 hr
Atmosphere:	Argon
Crucible:	Tantalum
Flux:	10 m/o MgF_2 - 90 m/o $MgCl_2$ (300 g)

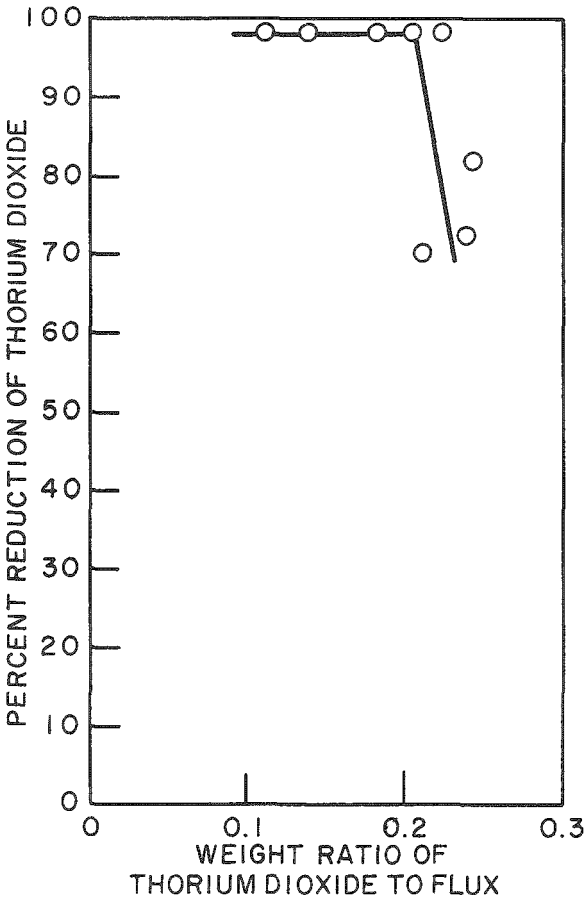

108-6849

A correlation between the weight ratio of thorium dioxide to flux and the extent of reduction is shown in Figure I-20. The flux (300 g) consisted of 10 m/o magnesium fluoride and 90 m/o magnesium chloride, the zinc phase (600 g) contained about 10 w/o magnesium at the completion of reduction, and the reaction was carried out for 4 hr at 850 C in a baffled tantalum crucible. The amount of thorium dioxide varied from about 30 to 80 g. It appears that for complete reduction under these conditions, a thorium dioxide-to-flux weight ratio of less than 0.2 is required.

Preliminary reductions were performed in crucibles made of the following materials: pressed-and-sintered tungsten, ATJ graphite, silicon nitride-bonded silicon carbide (Norton Crystolon 401), and

*Dow Chemical Co.

alumina (Norton Alundum 213). Thorium dioxide reductions were carried out for 4 hr at 850 C with the 10 m/o magnesium fluoride-90 m/o magnesium chloride flux, and about 10 w/o magnesium in the magnesium-zinc alloy. The product ingot for each reduction was retorted to remove the zinc and magnesium, and the resulting thorium metal sponge was arc-melted. Analyses of the products from the reduction in tungsten showed the tungsten content to be below the limit of detection (<500 ppm). Reduction in either graphite or silicon carbide appeared to increase the carbon content of the product, which was 0.34 percent for the former and 0.18 percent for the latter, compared with about 0.025 percent for reductions performed in tungsten and alumina. The silicon content of the product from the silicon carbide crucible was one weight percent or more, as determined by spectrographic analyses. Use of the alumina crucible resulted in a product containing one percent or more aluminum. Although tantalum and tungsten appear to be satisfactory crucible materials from the viewpoint of integrity and lack of product contamination, it would be desirable to use materials that are less expensive and more easily fabricated.

e. Reduction of Plutonium Dioxide
(J. B. Knighton, J. D. Schilb, J. W. Walsh)

The development of reduction procedures for uranium and thorium oxides by zinc-magnesium alloys in the presence of fluxes prompted a study to determine whether this technique could be extended to the reduction of plutonium dioxide. One previous experiment, reported in Summary Report ANL-6287, p. 57, had given a preliminary indication that plutonium dioxide could be reduced by this procedure.

Effect of Flux Composition

The rate and extent of reduction of uranium and thorium oxides are strongly dependent on the composition of the flux. Four plutonium dioxide reduction experiments were carried out with fluxes which had resulted in both good and poor reductions of uranium and thorium oxides. The amount of plutonium dioxide used was sufficient to produce a 1.0 w/o plutonium concentration in the zinc-5 w/o magnesium alloy on complete reduction. (Plutonium at a concentration of 1.0 w/o is well below the saturation concentration of plutonium in zinc at 800 C.)

The experimental conditions and results of these experiments are presented in Table I-13. The reduction of plutonium dioxide, unlike that of uranium and thorium oxides, was rapid and complete in all the fluxes used. The reduction appeared to be relatively independent of the flux composition and did not require magnesium chloride as a major constituent, as is required for uranium and thorium oxide reductions. This difference in reduction behavior may represent a method of separating plutonium from uranium and thorium.

Table I-13

EFFECT OF FLUX COMPOSITION ON REDUCTION OF PLUTONIUM DIOXIDE

Experimental Conditions

Temperature:	800 C
Mixing Rate:	800 rpm
Crucible:	Tantalum
Atmosphere:	Argon
Metal:	600 g Zn-5 w/o Mg
Flux:	300 g (of specified composition)
PuO_2:	7.13 g (1.0 w/o Pu in metal phase at 100% reduction)

Flux Composition	Pu Conc after 120 min (w/o)		Percent Reduction of PuO_2[a]
	In Metal	In Flux	
95 m/o $MgCl_2$-5.0 m/o MgF_2	0.95	0.0109	99.5
47.5 m/o LiCl-47.5 m/o $CaCl_2$-5.0 m/o MgF_2	0.88	0.0007	99.94
47.5 m/o KCl-47.5 m/o $CaCl_2$-5.0 m/o MgF_2	0.97	0.0034	99.9
47.5 m/o KCl-47.5 m/o LiCl-5.0 m/o MgF_2	0.95	0.0038	99.4

[a]Based on amount of plutonium remaining in the flux after 120 min.

Effect of Magnesium Concentration

Six additional plutonium dioxide-reduction experiments were conducted, with a 47.5 m/o calcium chloride-47.5 m/o magnesium chloride-5.0 m/o magnesium fluoride flux and zinc-magnesium alloy with magnesium concentrations ranging from 1 to 70 w/o. The results are presented in Table I-14. The optimum reductions occurred at about 10 w/o magnesium.

Table I-14

EFFECT OF MAGNESIUM CONCENTRATION ON REDUCTION OF PLUTONIUM DIOXIDE

Conditions

Temperature:	800 C
Mixing Rate:	800 rpm
Crucible:	Tantalum
Atmosphere:	Argon
Metal:	600 g Zn-Mg (of specified composition)
Flux:	300 g 47.5 m/o $CaCl_2$-47.5 m/o $MgCl_2$-5 m/o MgF_2
PuO_2:	7.13 g (1.0 w/o Pu in metal phase at 100% reduction)

Mg (w/o) in Mg-Zn Alloy	Pu Conc after 120 min (w/o)		% Reduction at 120 min[a]	$K_d = \frac{\text{Pu conc in flux, w/o}}{\text{Pu conc in metal, w/o}}$
	In Metal	In Flux ($\times 10^2$)		($\times 10^2$)
1	0.90	4.00	98.0	4.40
3	0.89	1.23	99.4	1.38
5	0.98	1.11	99.3	1.13
10	0.92	0.995	99.5	1.08
40	0.90	3.60	98.2	4.00
70	0.81	13.0	93.5	16.1

[a]Based on plutonium remaining in flux phase.

The distribution coefficients,

$$K_d = \frac{\text{Pu conc in flux, w/o}}{\text{Pu conc in metal, w/o}},$$

for plutonium between magnesium chloride and zinc-magnesium alloy (see ANL-6569, p. 40) show a minimum at about 10 w/o magnesium. These distribution coefficients and the distributions obtained in the six plutonium dioxide reduction experiments are compared in Figure I-21. The distribution coefficient curve for the reduction experiments, shown as the dashed line, is displaced nearly uniformly below the curve for a magnesium chloride flux. This downward displacement is in agreement with the results obtained in other distribution experiments (see ANL-6596, p. 64) when the magnesium chloride concentration in the flux was lowered by dilution. It therefore appears that the distribution coefficient for plutonium between the two phases is the factor which limits the extent of plutonium dioxide reduction.

Figure I-21

DISTRIBUTION OF PLUTONIUM BETWEEN ZINC-MAGNESIUM ALLOY AND MAGNESIUM CHLORIDE

Conditions

Temp:	800 C
Mixing Rate:	300 rpm, solid curve 800 rpm, dashed curve
Atmosphere:	Argon
Crucible:	Tantalum

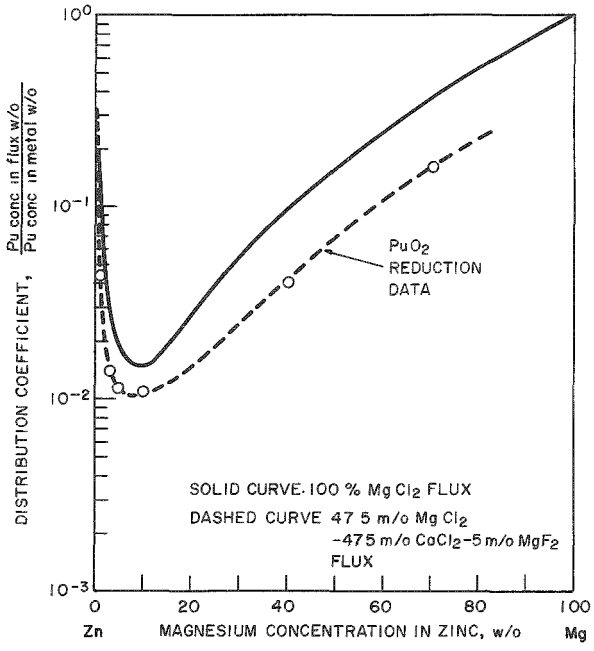

108-6865

Analyses of filtered metal samples and flux samples showed considerable scatter, and were biased toward low material balances. It was found that the reduction data based on the flux samples were reliable and that the apparent plutonium losses had resulted from interactions with impurities, causing a small percentage of the plutonium to precipitate from the liquid metal solution. For example, in one experiment, analysis of the filtered metal samples indicated that the reduction was only 90 percent complete, whereas analysis of the flux samples showed 99 percent removal of the plutonium from the flux. When two pie-shaped samples of the ingot were dissolved and analyzed, however, 100 percent of the theoretical amount of plutonium was found in the metal phase, thereby indicating that about 10 percent of the plutonium had precipitated.

The liquid metal-flux method for the reduction of plutonium dioxide to the metal appears to be highly satisfactory, and it has the advantage of a substantial reduction in the neutron hazard in that the (α,n) reaction is much less efficient in plutonium oxides than in the fluorides. Although this technique may be useful for the practical production of plutonium metal or for the recovery of plutonium from scrap that is generated by existing processes, no further experimental work is planned on this aspect of the problem. Serious consideration of a process of this type would require much additional work on techniques for recovering the reduced metal, scale-up problems, engineering feasibility, and economic factors. However, further studies will be made of this technique as a step in the reprocessing of uranium and plutonium oxide and carbide reactor fuels by pyrometallurgical methods.

B. Fuel-processing Facilities for EBR-II

(J. H. Schraidt, M. Levenson, L. F. Coleman)

A direct-cycle fuel-reprocessing plant based on pyrometallurgical procedures was designed and is being constructed as part of the Experimental Breeder Reactor No. II (EBR-II) Project. Melt refining, liquid metal extraction, and processes involving fractional crystallization from liquid metal systems are methods being examined for the recovery and purification of EBR-II fuels. Based on these studies, process equipment is being designed and tested.

1. Status of Fuel Cycle Facility

a. Building and Building Services

(J. O. Ludlow, M. A. Slawecki, H. L. Stethers)

(1) Operation during Argon Cell Leak Tests

The air in-leakage rate of the Argon Cell has been determined in a series of tests (see ANL-6687, p. 63). For the last test of the series the air in the Argon Cell was replaced with nitrogen. Residual oxygen (one percent) was further reduced by operating the Argon Cell atmosphere-purification system. The air in-leakage rate was periodically determined by measuring the increase in the oxygen level of the cell atmosphere during various testing periods when the argon-purification system was not in operation. The results of the leak tests indicated an air in-leakage rate of less than 0.006 cfm at a pressure in the Argon Cell of -4 in. water.

While the cell was filled with nitrogen, investigations were undertaken to determine the effect that opening of certain penetrations into the Argon Cell would have on the composition of the cell atmosphere. The tests were necessary because similar openings will be made immediately after the cell is filled with argon to replace shielding plugs in fill

and vent penetrations and may be made again at some later date. The penetrations into the cell were opened one at a time while the pressure in the cell was near atmospheric pressure. The openings were maintained for various periods of time up to 5 min. The passages that were opened included a horizontal penetration in the wall (of 5-in. diameter by 5 ft long), a vertical penetration in the roof of the cell (of 7-in. diameter by 5 ft long), and both ends of one of the small (2-sq ft opening) transfer locks mounted horizontally in the wall between the Argon Cell and the Air Cell. The opening of these penetrations caused no significant change in the oxygen level of the cell atmosphere. When both ends of the large (6-ft-diameter) transfer lock, which is mounted vertically in the floor, were opened for $4\frac{1}{2}$ min, the oxygen level in the Argon Cell increased from 10 to about 300 ppm. No detectable increase in the inventory of the gas in the Argon Cell occurred during these tests.

During the nine-week period that the Argon Cell contained nitrogen, operation of the cell pressure-control system and the argon-purification system provided an opportunity for operational testing of the equipment and for training of operators. During this period the cell pressure-control system was operated continuously, and it was found possible to maintain the pressure in the cell at set point pressures which were varied between +0.5 and -6 in. water (usually -4 in.). The effects of changes in the rates of heat evolution in the Argon Cell and in outside temperature and barometric pressure were noted. The rates of heat evolution in the cell varied from 100,000 to 370,000 Btu/hr. The overall pressure-control system of the Argon Cell, which includes emergency exhaust and emergency fresh gas (argon) feed systems, operated satisfactorily and is considered adequate for maintaining the cell pressure within controlled limits under plant processing conditions.

Toward the end of the air in-leakage tests, a bearing failed in the compressor used in the argon-purification system. The bearing was removed and is being studied to determine the probable cause of its failure. To remove the bearing, it was first necessary to remove the compressor from its enclosure. The removal was difficult and the compressor enclosure is being redesigned to overcome this difficulty.

(2) Purification System for Inert Atmosphere Glovebox

Two inert atmosphere glovebox systems will be used for work associated with fuel processing. One glovebox system will be installed in the Fuel Cycle Facility; the other will be installed in the Laboratory and Service Building. Each system will include a purification system to remove oxygen and water vapor continuously from the argon used in the glovebox (see ANL-6687, p. 68). The components of the system are mounted on a portable base and consist of a Molecular Sieves* dryer, a palladium

*A product of the Linde Co., Division of Union Carbide.

catalyst bed, a blower, and a control panel. Each system will also include analytical instruments to determine the concentrations of oxygen, water vapor, and nitrogen in the glovebox atmosphere.

One purification system was installed and leak tested in the Fuel Cycle Facility. The associated gloveboxes were then purged with argon and tests started to determine the in-leakage rate. The tests showed that air leakage into the gloveboxes when they are not being used is 0.015 percent of the system volume per day or 0.037 cu ft per day. Nitrogen in the system was reduced to 0.6 percent or lower by the initial purging. The oxygen has been reduced to 2 ppm while water in the system has been decreasing slowly as the box continues to out-gas.

The second purification system for removing water vapor and oxygen from gloveboxes has been fabricated, tested, and shipped to the Idaho site.

The purification system was connected to a 30-cu ft glovebox for testing. The glovebox atmosphere was continuously monitored for water vapor and oxygen content while the glovebox gas was being circulated through the purification system at a rate of approximately 7 cu ft/min. Test results indicated that the atmosphere in the 30-cu ft glovebox can be maintained at an oxygen content of less than 3 ppm and a water vapor content of less than 3 ppm.

Two analytical instrument panelboards* have been received, successfully tested, and shipped to the Idaho site. Each instrument panelboard consists of a water vapor analyzer, with a range of 0-1000 ppm of water vapor, an oxygen analyzer, with a range of 0-1000 ppm of oxygen, and a nitrogen analyzer, with a range of 0-10 percent nitrogen.

b. Cell Transfer Locks
(G. J. Bernstein, A. A. Chilenskas, J. Graae)

Air Cell Hatch Cover and Drive

The cover for the 7-ft square hatch connecting the Air Cell to the Transfer Cell is being installed. The cover is designed to support 10,000 lb, and to be opened and closed by means of a remotely operated electric motor drive, which operates a chain hoist. Limit switches stop the drive automatically in the open and closed positions of the hatch cover. The motor drive is identical with those provided for the window shutters (see ANL-6687, p. 65). A slip clutch, which is also identical with those used in the window shutter drives, prevents overloading the mechanism. Both the motor drive unit and the chain hoist can be remotely replaced.

*A product of Manufacturers Engineering and Equipment Corp.

c. Miscellaneous Cell Service Equipment
(J. Graae, H. Stethers, M. Slawecki)

Storage Racks for Fuel Subassemblies

A storage rack for four fuel subassemblies has been designed, and two such racks have been ordered. The rack will fit into a 12-in.-diameter by 10-ft-deep storage pit; ten such storage pits are provided in the floor of the Air Cell. Four pits will be modified to provide piping for coolant air to the bottom of the pits. The piping in each pit terminates in a ball joint which fits a companion socket on the bottom of the storage rack. Racks will be installed in two of the pits; temporary closures equipped with sockets will be placed on the ball joints in the other two pits. This procedure permits the latter pits to be used for other storage purposes until such time as expanded requirement for subassembly storage makes it necessary to install additional racks in those pits.

Cooling air will be supplied by a blower located outside the Air Cell. Each rack will consist of a cluster of four storage tubes. A valve, located at the bottom of each tube, will automatically open when a fuel subassembly is placed into the tube, thereby admitting cooling air. An orifice in the valve will permit passage of some cooling air even when the valve is closed. This prevents overloading of the blower, which will be of the positive-displacement lobe-type.

2. Service Equipment Development

a. Interbuilding Fuel Transfer Coffins
(G. J. Bernstein, A. A. Chilenskas)

Fuel subassemblies containing spent or reconstituted fuel will be transported between the Reactor Building and the Air Cell of the Fuel Cycle Facility in 20-ton interbuilding fuel-transfer coffins (see ANL-6687, p. 65). One coffin, which was designed and built by a commercial fabricator, has been delivered to Idaho. A second coffin, which was designed by personnel of Argonne National Laboratory, is currently being built at Argonne.

Tests of the Argonne coffin revealed difficulty in the operation of the large shielding plug which seals the top of the coffin. This plug is driven by a horizontal screw shaft which passes through a seal plate. When the plug and the coffin body were filled with lead, the mating surfaces warped, which caused binding of the plug. These surfaces have been refinished, and additional support bearings have been provided for the screw shaft. The plug assembly has been installed and functions satisfactorily.

The gas-circulation blower, the blower motor, valves, and piping are being prepared for installation. The completed coffin will be tested with a resistance-heated subassembly to determine the heat-removal performance and the pressure drop in the circulating coolant gas.

b. Interaction of Fuel Pins and Pin Charger
(W. E. Miller, H. Stethers)

Spent fuel pins, after decanning, will be sheared to approximately $1\frac{1}{2}$-in. lengths. These sheared pins will be collected in a pin charger for transfer to the crucible in the melt refining furnace. The sheared pins will have a surface layer of the sodium that is used for thermal bonding of the fuel pins to their stainless steel jackets. The pins may be at an elevated temperature due to radioactive decay.

The pin charger consists of a closed, shallow, rectangular box with a pouring spout at one end. The surfaces contacted by the pins are stainless steel. The pins normally lie on the bottom of the box, which is held in a horizontal position until the pins are to be poured. For proper operation of the pin charger, the pins must slide or roll along the bottom of the pin charger when it is tilted in the pouring operation. Several experiments were made to determine if interactions between a heated stainless steel plate and bare or sodium-coated pins would prevent free movement of the pins.

In the first experiment, bare uranium-fissium pins were used. To remove any oxide coating, the pins were polished inside a glovebox (argon atmosphere containing 3 ppm oxygen, 3 ppm water, and less than one percent nitrogen) and were then placed on a stainless steel plate at 550 C within the glovebox. The pins were on the plate for 3 hr, during which time the temperature of the plate was maintained at 550 C. No interaction between the pins and plate was noted. When the hot plate was tipped, the pins rolled and slid freely.

In the next experiment, sodium-coated pins were used. The pins were polished inside the glovebox and were then placed in a sodium bath at 450 C. In about $1\frac{1}{2}$ hr the pins became wetted with sodium. They were then removed from the sodium bath and placed in a rectangular stainless steel box with a removable top cover. The bottom of the box was heated until its temperature reached 450 C. This temperature was maintained for 2 hr, when the top cover of the box was removed. All the sodium had evaporated from the pins and had deposited on the underside of the cover. The experiment was repeated. However, in this experiment the bottom of the box was heated to only 300 C. After the temperature had reached 300 C, the top cover of the box was removed at $\frac{1}{2}$-hr intervals and the condition of the sodium film on the pins was observed. During these

observation periods the pins were moved around on the tray to see whether any sticking of the pins to the stainless steel had occurred. No sticking was observed. The experiment was terminated after 3 hr, since all the sodium had evaporated from the pins and was found deposited on the removable top cover.

The stainless steel surfaces were not wetted by the sodium during the experiments with sodium-coated pins. Therefore, the effect of such wetting on the interaction between the pins and the stainless steel surfaces is not yet known.

In plant operation it is possible that portions of the pin charger will become coated with sodium by condensation of the metal on the cooler surfaces of the charger. However, it should be possible to remove the sodium deposits by heating the entire tray to vaporize the sodium.

c. Miscellaneous Service Equipment Development
(G. Bernstein, A. Chilenskas, W. Miller, M. Slawecki)

(1) Exhaust Air Prefilter

Approximately 5000 cfm of building air flows through openings in the Air Cell wall, through the Air Cell, and into the Transfer Cell. From this area, the air enters a 24-in. square duct which connects to the building exhaust air duct. In order to reduce the possibility of particulate contamination of the building duct, a prefilter has been designed for installation in the Transfer Cell. The prefilter consists of a plenum approximately 5 ft high, $3\frac{1}{2}$ ft wide, and 2 ft deep covering the 24-in. duct opening in the Transfer Cell wall. The face of the plenum is a hinged door which contains six standard commercial 20 x 20 x 1-in. fiberglass filters. The door containing the filters will be remotely removable through the Air Cell floor hatch by means of the operating manipulator. This operation will permit the remote replacement of the filters.

3. Process Equipment Development

a. Skull Oxidation Equipment
(W. E. Miller, M. A. Slawecki, H. L. Stethers)

After the melt refining step is carried out, a skull remains in the zirconia crucible. The skull contains significant quantities of fissionable material which will be recovered by means of the skull reclamation process. The skull will be removed from the melt refining crucible by converting the metallic skull to an oxide powder which can be poured out of the crucible. Equipment is being developed for the oxidation of skulls and for the transfer of oxide powders.

The control system (see ANL-6687, p. 70) for the skull oxidation furnace was used to control the oxidation of twelve skulls ranging in weight from 300 to 1300 g. Some of the skulls contained cerium and some did not. The system worked satisfactorily in all cases. The oxidized material was removed from the crucibles by means of a dumper that is being developed for this purpose No crucible fragments were visible in any of the oxide products. A small amount of oxide (about 1 to 5 g) remained in each crucible after the oxide powder was dumped.

It has been proposed that partially oxidized skulls be used in the skull reclamation process. In order to determine the degree of oxidation that is required before a skull can be removed from a crucible, two fissium-cerium skulls were partially oxidized. The oxidations were carried out in the oxidation furnace with the crucible held in a secondary container in the normal, upright position.

A 479-g skull, contained in a zirconia crucible, was oxidized 37 percent. The steel container holding the zirconia crucible was placed in the dumper and inverted, and 237 g of material fell out. A metal cup or skull remnant was retained in the crucible. The crucible in its steel container was placed back in the oxidation furnace and 10 percent of the residual skull material was oxidized. After this additional oxidation, the container and crucible were inverted by hand; however, only a small amount of material fell out. While the crucible was inverted, the steel, secondary container was removed The bottom of the crucible, which had broken away from the side walls during oxidation, was also removed. A metal cup, which was wedged against the cylindrical portion of the crucible, remained. Figure I-22 shows the remainder of the crucible which contained the wedged metal cup. The tape fastened around the crucible was added, before the crucible bottom was removed, to keep the fragmented, upper section of the crucible intact The residual metal cup weighed about 200 g and was essentially unoxidized metal.

Figure I-22

PARTIALLY OXIDIZED MELT REFINING SKULL

(Bottom of crucible became separated during the run and is not shown)

In a second experiment, a 540-g skull was oxidized to the extent of 50 percent. Results similar to those described above were obtained.

The results of these experiments indicate the following:

(1) Partial oxidation (50% or less) does not completely destroy the integrity of the skull, even though such oxidation loosens the skull from the crucible wall.

(2) When a skull is partially oxidized in a standard melt refining crucible maintained in an upright position during oxidation, only a portion of the skull material falls out of the crucible when it is inverted.

If oxidation occurs in an inverted crucible (see p. 43), the skull will fall out at a degree of oxidation which is probably less than that required to assure release from a crucible in which oxidation took place in an upright position. However, the equipment required to oxidize the skull in an inverted crucible and to collect the oxide as it falls from the crucible is considerably more complex than the equipment now being developed for skull oxidation. The use of partially oxidized skull material rather than fully oxidized material in the skull reclamation process does not offer any significant advantage that would justify the development of an inverted oxidation furnace.

A second skull oxidation furnace is being designed. The shape of the second furnace will differ from that of the first (see Summary Report ANL-6477, p. 87). In the new design, a coiled resistance heater element, which is used to heat the skull, is made part of a removable cover. The diameter of the cover is less than 12 in., which will permit the cover to fit a standard waste container. The heater-cover assembly can be discarded in the event that the heater fails and requires replacement.

b. Skull Oxide Processing Equipment
(G. Bernstein, W. E. Miller, T. W. Eckels, J. Harast)

In the skull reclamation process molten flux or molten metal wastes must be removed at the completion of each process step. Present design concepts envision transferring this material from the skull reclamation furnace through a removable, heated transfer line into a waste pail. Approximately 5 gal of waste material will be transferred in each step.

c. Inductive Heating and Mixing
(A. A. Chilenskas, M. A. Slawecki, P. Kelsheimer, E. Johnston)

The skull reclamation process requires the heating and mixing of molten metal-molten salt systems at temperatures up to about

800 C. Because a high radiation field is associated with this process, it is necessary to carry out the process remotely. Appreciable simplification and greater reliability of plant equipment is anticipated if inductive mixing can be used instead of mechanical mixing.

Preliminary work has been concluded which has demonstrated that vigorous mixing of molten metal charges can be obtained using 60-cycle power (see ANL-6596, pp. 104 to 105). To determine whether or not an acceptable degree of mixing of molten metal with molten salt can be achieved by inductive mixing, the reduction step of the skull reclamation process was chosen for the study. In this step, skull oxide (mainly U_3O_8), magnesium, zinc, and salt are mixed for several hours at 800 C. The reduction of the uranium oxide to uranium and its dissolution into the metal phase are used as a measure of the effectiveness of the mixing.

Two runs were attempted on a scale that is presently planned for plant operation. In these runs 5-kg charges of skull oxide were used. Because the graphite crucibles employed in these runs failed, the tests were continued on a reduced ($2\frac{1}{2}$-kg) scale until tungsten crucibles could be obtained. Two runs, IM-17 and IM-19, were thus made in an unbaffled graphite crucible. The charge data and crucible-coil configuration for these runs are given in Figure I-23.

Figure I-23

INDUCTIVE HEATING AND MIXING APPARATUS

(Used for reduction of skull oxide in Runs IM-17 and IM-19)

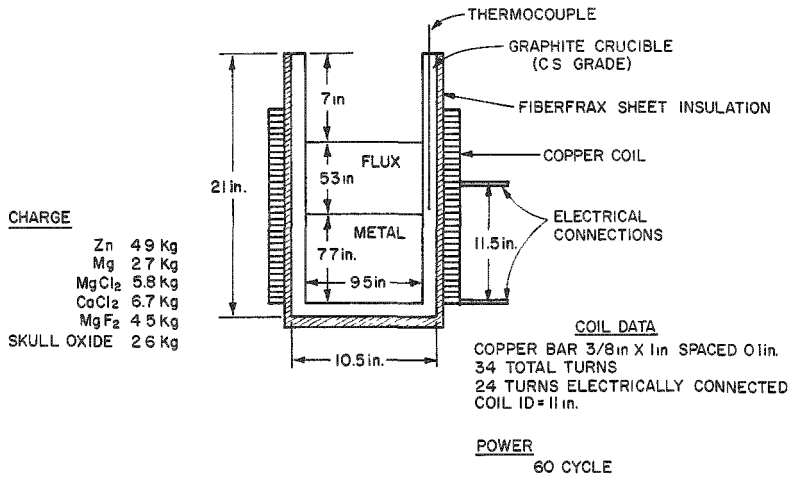

108-6856

Mixing was induced in the melt by means of a power input to the coil of about 15 kW at 60 cycles. Calculations showed that about one-half of this power was consumed as a resistance loss in the coil while

the other half was absorbed by the charge. The power was applied intermittently to prevent excessive heating and to maintain the charge temperature between about 770 and 830 C. This was accomplished by turning the power off when the charge temperature reached 830 C and turning the power on when the charge cooled to 770 C. In Run IM-17, the power was on for a total of 2.7 hr, whereas the time that the charge was between 770 and 830 C was 4.4 hr. In Run IM-19 some of the insulation surrounding the crucible was removed to increase the cooling rate. In this run, the power was on for a total of 2 hr, whereas the time that the charge was at temperature was 3 hr.

The metal phase was periodically sampled by means of quartz tubes, and the samples were analyzed for uranium. A plot of uranium concentration in the metal phase as a function of mixing time is shown in Figure I-24. The values shown in the plot indicate that in Run IM-17 about 86 percent reduction was obtained, whereas in Run IM-19 about 80 percent reduction was obtained. The actual reduction may have been greater than that indicated by the analytical values, since it is known (see Summary Report ANL-6379, p. 56) that loss of uranium from the metal solution can occur by interaction of the uranium with the graphite to form insoluble uranium carbide. Future investigations of skull oxide reductions will be done in tungsten crucibles.

Figure I-24

OVERALL RATE OF REDUCTION AND DISSOLUTION OF SKULL OXIDE

(Runs IM-17 and IM-19)

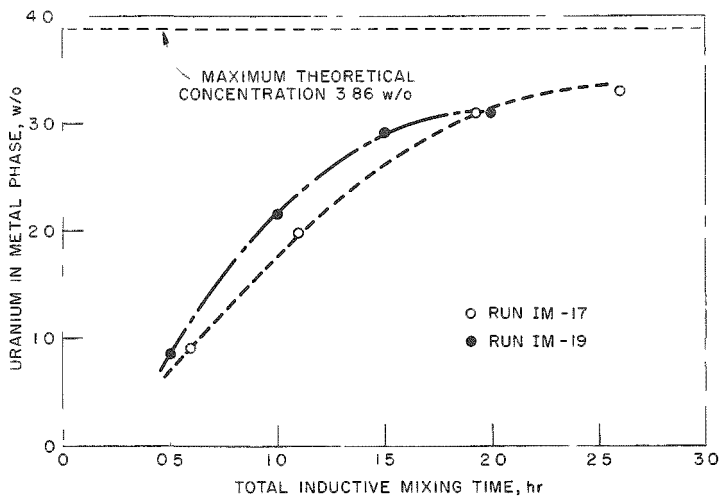

108-6888

Examination of the crucible after the runs showed that some skull oxide had deposited on the crucible wall above the normal salt level, thereby effectively removing a small fraction of the oxide from the

metal-salt phases. It is believed that this deposition was caused by salt foaming which occurred when the skull oxide was added to the molten salt. This difficulty can be corrected by degassing the skull oxide prior to its addition to the molten salt or by adding the skull oxide to the salt in small increments rather than in single batches as was done in Runs IM-17 and IM-19.

d. Collection of Metal Vapors
(W. E. Miller, H. L. Stethers)

The product from the uranium precipitation step of the skull reclamation process is a precipitate of uranium in residual magnesium-zinc alloy. Distillation is a convenient means of removing the magnesium-zinc alloy from the uranium. Work was continued on the development of a distillation apparatus (2-kg distillate scale) suitable for remote operation (see ANL-6687, p. 73).

Figure I-25

MAGNESIUM-ZINC DISTILLATION APPARATUS

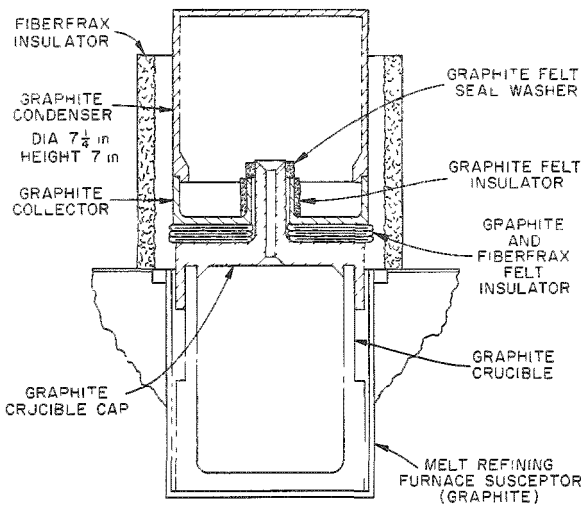

108-6897

Additional tests were carried out with the apparatus shown in Figure I-25. The apparatus was heated in an induction furnace which had been used for development of the melt refining process. In the first of two runs, the graphite felt seal washer shown in the figure was not used. In this run, one kg of 50 w/o magnesium-zinc was distilled at one mm absolute pressure. Of the charge, six percent was found in the condenser, 90 percent was found in the collector, and 4 percent was found between the collector and the crucible cap. There was no measurable loss of distillate from the condenser and collector enclosure, other than that found between the collector and the cap. The condenser could be lifted easily from the collector, and the crucible cap could be lifted easily from the crucible. The collector was bonded to the crucible cap by metal which had condensed in the annulus between the crucible cap spout and the collector.

In the second run, a graphite felt seal washer was used as shown in Figure I-25. (Liquid magnesium-zinc does not penetrate graphite felt.) The magnesium-zinc was distilled under conditions that were identical with those of the preceding run. After the run had been completed, all the distillate was found in the condenser-collector, and all parts of the apparatus were separated easily. No deposit of metal was found between the

cap and collector as had been found in the first run. In the first run, molten metal apparently had trickled down the outside of the cap spout and entered the annulus between the spout and the collector. In both runs the distillation rate was about 25 g/min. The final crucible temperature in each run was 750 C.

The modified apparatus was used to make four additional runs which had two primary objectives. The first was to determine the maximum distillation rate which could be achieved with this apparatus. The rate is limited by the heat dissipation capability of the condenser since uncondensed vapors would escape from the graphite enclosure. The second objective was to determine whether or not any of the condensate would re-evaporate from the condenser when the apparatus was heated to 1150 C. It is intended in plant operations that the uranium which remains in the crucible will be melted to consolidate it for ease of removal and handling.

In each run, 2 kg of 50 w/o magnesium-zinc was charged to the crucible. Distillation was performed at one mm pressure and at a temperature range from 660 to 700 C. In the first three runs distillation rates of 25, 32, and 48 g/min were tested. At the conclusion of each run all of the distillate was found in the condenser-collector, indicating no loss during distillation and no reboiling when the crucible temperature was raised to 1150 C. In the fourth run the distillation rate of 62 g/min exceeded the capacity of the condenser, and 17 g of metal escaped from the graphite enclosure and deposited on the Fiberfrax insulators.

C. Chemistry of Liquid Metals

(I. Johnson, H. M. Feder)

The chemistry of liquid metal systems is being investigated to provide basic concepts and data for the design of methods for the reprocessing of nuclear fuels and to provide a basis for the development of liquid alkali metal technology. The results of these studies may also provide data for the testing of theories of liquid metal solutions.

1. Solubilities in Liquid Metals

Of prime importance in the practical design of fuel-reprocessing methods are the solubilities of the metals whose separations are being attempted. These solubilities need to be known as a function of both temperature and solvent composition. Since the solubility of a metallic phase in a liquid metal solvent is related to the difference in free energy of formation of the metallic phase and the partial excess free energy of the solute in the saturated solution, information on the temperature coefficient of the solubility gives information on the corresponding enthalpy and entropy differences. The systematization of such data for a wide variety of different systems will furnish the empirical relations which may lead to the resolution of the factors governing the energetics of formation of liquid metal

solutions. For such fundamental applications, it is necessary to know the constitution and the thermodynamic properties of the solid phases in equilibrium with the saturated liquid phase.

Solubility of Plutonium in Liquid Zinc
(M. G. Chasanov and P. D. Hunt)

The solubility of plutonium in molten zinc was determined by direct sampling of the saturated solution by means of tantalum sample tubes fitted with tantalum filters. The results of this experiment, in which 20.7 g of plutonium (99.85 percent plutonium) were added to 300 g zinc (99.995 percent zinc) contained in a magnesia crucible, are given in Table I-15. The data may be represented by the empirical equation

$$(458 \text{ to } 752 \text{ C}) \log (\text{a/o plutonium}) = 8.612 - 10090\ T^{-1} + 1.461 \times 10^{6}\ T^{-2}.$$

The relative standard deviation is 4 percent. These data are compared in Figure I-26 with earlier solubility data reported by Elliott and Sweezer (in Summary Report ANL-5789, p. 91). The slightly higher solubilities found by Elliott and Sweezer may be the result of shorter equilibration times coupled with the fact that the samples were obtained only on cooling the melt.

Table I-15

SOLUBILITY OF PLUTONIUM IN LIQUID ZINC

(Data in chronological order)

Temp (C)	Plutonium Content (w/o)	Temp (C)	Plutonium Content (w/o)
481	0.0230	608	0.384
501	0.0356	725	3.27
650	0.962	530	0.0737
602	0.352	458	0.0134
752	4.82	632	0.641
701	2.35	571	0.185

Solubility of Rare Gases in Liquid Alkali Metals
(S. K. Dhar)

The solubility of rare gases in liquid alkali metals is being studied in order to gain a better understanding of the electronic structure of metals and to check the validity of the existing theories of solution in molten metals, which are based on several statistical mechanical approaches.

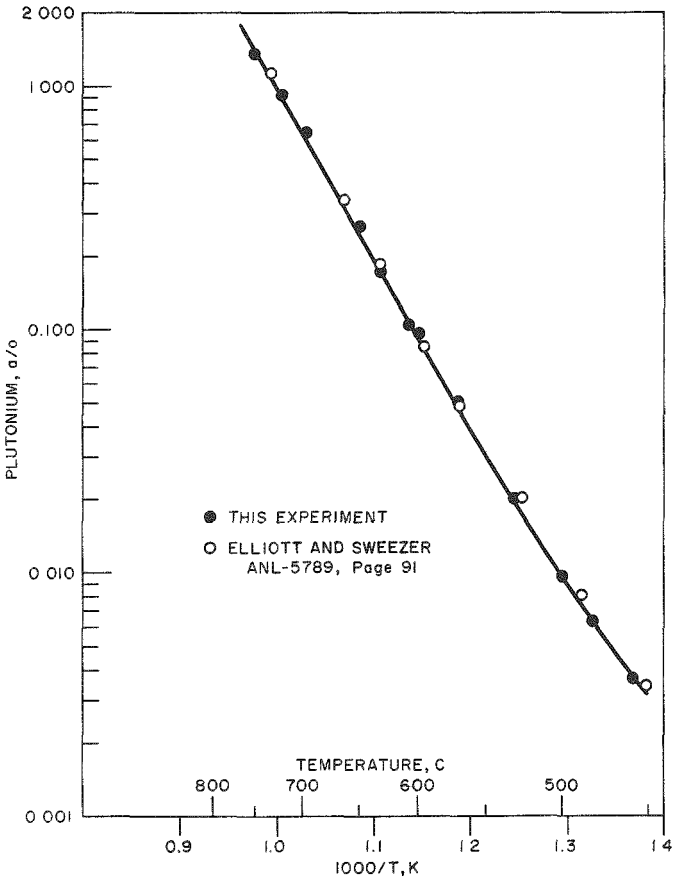

Figure I-26

SOLUBILITY OF PLUTONIUM IN LIQUID ZINC

108-6873

Analysis of data reported in the literature on the solubilities of rare gases in molten metals indicated the desirability of having an apparatus capable of yielding significant solubility data in the region below 10^{-10} atom fraction of gas in the metal. The apparatus that has been constructed for the present studies is designed to make possible the determination of solubilities down to 10^{-15} atom fraction of the gas in the metal.

The apparatus consists of two interconnected vessels, each having a capacity of 3.5 kg of sodium. In one vessel, the liquid metal is saturated with the rare gas solute; in the other, the dissolved gas is removed from solution by sparging with a suitable gas or mixture of gases. The eluted rare gas is collected by adsorption on charcoal which is cooled by liquid nitrogen. The apparatus is completely self-enclosed, and all operations are carried out by external manipulations.

The system, which is being tested for leaks, will be used first for the determination of krypton-85 in sodium at temperatures up to 500 C and pressures up to 10 atm.

2. Liquid Sodium Coolant Chemistry

The utilization of liquid alkali metals as heat transfer media in high-power-density fast nuclear reactors as well as in other power sources makes essential a continuing advancement in alkali metal technology. To insure a sound technological advance, a comprehensive fundamental research program is needed. A basic program has been started to elucidate the chemistry of the reactions that occur in liquid alkali metal solutions; special emphasis will be given to liquid sodium, since its practical importance is greatest.

Sodium of high, known purity is required for significant research in this area. Thus the closely related problems of purification, analysis, and metal handling are of importance in this research. Because results of high-temperature corrosion studies indicate that high purities may also be required for practical systems, basic information relevant to the purification and analysis of sodium may have immediate practical use.

The high chemical reactivity of liquid sodium makes it very prone to contamination. Liquid sodium contaminated with oxygen and carbon has been found to be more corrosive to structural materials than pure sodium; oxygen facilitates mass transfer whereas carbon causes carburization. The two impurities when present together promote, under some conditions, extensive carbon transfer.

a. Sodium Purification
(G. Lutz, K. E. Anderson)

The removal of oxygen from sodium is generally accomplished by cold trapping, hot trapping, or distillation. The effectiveness of these procedures probably increases in the order given. For the preparation of sodium with a low oxygen content for use in the studies discussed below, a small (one liter per day) apparatus has been designed in which oxygen removal is accomplished by cold trapping followed by distillation. The receiver has been designed so that the purified sodium can be transferred to the experimental apparatus without contamination.

b. Sodium Analysis
(G. Lutz, K. E. Anderson)

The analyses of sodium for oxygen and carbon are of immediate importance in the studies of the carbon-oxygen-sodium system that are being undertaken (see Section c below). Several methods have been used by other investigators for the determination of oxygen in sodium. In all these methods, the sodium is separated from the very small amount of

sodium oxide present, which is then analyzed either chemically or by flame photometry. Of the various separation methods, distillation of the sodium (under reduced pressure) or dissolution in mercury have been used most often by other investigators. The accuracy of these methods is good when the oxygen content of the sodium is greater than about 100 ppm. When the oxygen content is in the range from 10 to 20 ppm, the accuracy is poor. When the oxygen concentration is less than 10 ppm, the analytical results are open to serious question. Since high-purity sodium is to be used in the present program of study, it is desirable to develop analytical methods which will give accurate results with sodium samples containing from 100 ppm oxygen to less than 10 ppm oxygen.

Two activation methods are being considered. In the first method, $_7N^{16}$ (7.35-sec half-life) is produced by fast (14.5-MeV) neutron irradiation by the reaction $_0n^1 + {}_8O^{16} \rightarrow {}_7N^{16} + {}_1H^1$. Preliminary studies indicate that this method may be useful for analysis of sodium containing oxygen in the range of 1 to 10 ppm.

The second method under investigation involves the production of F^{18} from O^{16} by triton irradiation. A small amount (0.1 percent) of lithium is added to the sodium and the tritons are produced <u>in situ</u> by the thermal neutron irradiation of the lithium by the reaction $_0n^1 + {}_3Li^6 \rightarrow {}_1T^3 + {}_2H^4$. The tritons thus produced react with the oxygen in the sodium to form F^{18} by the reaction $_1T^3 + {}_8O^{16} \rightarrow {}_9F^{18} + {}_0n^1$. The fluorine activity (112-min half-life) is separated chemically from the sodium and counted. Theoretical calculations indicate that this method is suitable down to less than 1 ppm.

Two crucial steps in this method require development. These are (1) the addition of lithium to the sodium sample and (2) the chemical separation of the fluorine activity from the large amount of sodium activity (Na^{24}) produced by the neutron irradiation. The method which appears satisfactory for the separation of the fluoride activity involves the following steps. The irradiated sample is dissolved in water, fluoride carrier is added, and the fluoride is precipitated as barium fluoride by addition of barium ions. The precipitate is dissolved in an ammoniacal EDTA solution. Sodium carrier is added and excess barium ion to re-precipitate BaF_2. This is repeated until sufficient decontamination is achieved. Preliminary results indicate that each pass yields a 500-fold separation of fluoride from sodium and a 70 percent yield of fluoride.

The development of a method of alloying lithium with sodium will proceed as soon as suitable inert atmosphere glovebox facilities are in operation. These facilities have been assembled and are presently being tested.

c. Carburization Reaction in Liquid Sodium

A potentially serious problem associated with the use of liquid sodium in nuclear reactors is the tendency of metals to carburize or decarburize. This is caused by the basic instability of many metallic systems with respect to graphite. Thus, ordinary steel is a metastable system of ferrite (α-Fe) and cementite (Fe_3C). The thermodynamically stable system would consist of ferrite containing a smaller concentration of carbon and graphite. Liquid sodium can act as a path for the transformation of the metastable system to the stable system, thus effecting a decarburization. Similarly, many ferrous alloys containing nickel and chromium are not stable if carbon is available for reaction with the alloy. Thus, sodium may also act as a medium for the transport of carbon to the alloy to form the more stable carbide system. In either case, whether it be carburization or decarburization, undesired changes in the mechanical properties of the container materials result.

The mechanism by which liquid sodium can act as a medium for the transport of carbon is not understood. Whether carbon exists in liquid sodium as single atoms, ions, or more complex molecular species is not known. The role of dissolved oxygen is not known although it is believed to be significant.

A basic study of the transport of carbon by liquid sodium has been started. As a first step in this study the solubility of graphite in liquid sodium will be measured as a function of temperature and oxygen content. To facilitate the carbon analyses, carbon enriched with carbon-14 (5568-yr half-life, 0.15-MeV beta) will be used. The conventional dry-oxidation method for the analysis of carbon will also be used. Apparatus has been constructed to carry out both types of analyses. An apparatus to equilibrate graphite and sodium has been assembled and is undergoing testing. The apparatus is constructed so that procedures, such as sampling and sodium charging, can be done in a dry inert atmosphere glovebox.

3. Thermodynamic Studies

Thermodynamic functions are being measured for elements that are of importance to pyrometallurgical separations processes and for elements that are particularly useful for the testing of theories of metallic systems. Several methods are being used. Galvanic cells have proved to be especially useful for the measurement of activities in liquid metal solutions as well as for the determination of the free energy of formation of the equilibrium solid phase in solid-liquid two-phase alloys. For systems composed of several well-defined intermetallic phases, measurement of the decomposition pressure by the Knudsen effusion method is proving to be very useful. Systems in which only a small difference in electrochemical potential of the components exists and in which both components have

nearly the same vapor pressure are not readily studied by either the galvanic cell method or the effusion method. For such systems a vapor-phase optical absorption method is being developed.

The galvanic cell method is being used to study systematically binary plutonium alloys with the low-melting B-subgroup metals. Results of studies of the plutonium-zinc and plutonium-cadmium systems are presented below. The effusion method is being used to study the binary rare earth metal-zinc and -cadmium systems. Results for binary systems of cadmium with lanthanum, cerium, praseodymium, and neodymium are given below. The optical method will be used to study the thermodynamics of binary alkali metal systems. The basic principles of the method and pertinent experimental details are discussed below.

Thermodynamic Studies of the Plutonium-Zinc System
(I. Johnson, M. G. Chasanov, and R. Yonco)

Galvanic cell data for the plutonium-zinc system were reported in ANL-6687, p. 79. These quantities have been combined with the plutonium-zinc solubility data reported above to compute the activity coefficient of plutonium in a saturated zinc solution. This activity coefficient may be represented by the empirical equation

$$(420 \text{ to } 670 \text{ C}) \quad \log \gamma_{Pu} = 5.312 - 9713\ T^{-1}.$$

Within experimental error, the relative partial molal enthalpy and excess partial molal entropy of plutonium in zinc solution are constant over this temperature range, and have the following values:

$$\bar{L}_{Pu} = -44.4 \text{ kcal/g-atom Pu}; \qquad \bar{S}^{xs}_{Pu} = -24.3 \text{ cal/deg-g-atom Pu}.$$

These partial molal excess quantities are markedly more negative than those for uranium in liquid zinc solution,[4] thus reflecting the greater deviation from ideality of plutonium in zinc solution.

Thermodynamics of the Plutonium-Cadmium System
(I. Johnson, M. G. Chasanov, and R. Yonco)

Thermodynamic quantities for the plutonium-cadmium system are being determined by emf measurements made on the galvanic cell

$$Pu/PuCl_3\,(0.5 \text{ w/o})\text{-KCl-LiCl(eutectic)}/\text{Pu-Cd(2-phase alloy)}.$$

The cell reaction consists of dissolution of plutonium into the fused salt at the pure plutonium anode and deposition of plutonium into the saturated

---

[4] Johnson, I., and Feder, H. M., Thermodynamics of Nuclear Materials, I.A.E.A., Vienna, 1962, pp. 319-329.

liquid alloy electrode. The phase diagram for this system is not completely known; however, Winsch, Nelson, and Paul (see Summary Report ANL-5959, p. 120) have reported (from solubility data) that a peritectic reaction occurs at 404 C. The intermetallic compounds at the cadmium-rich end of the diagram have not yet been identified, although the most cadmium-rich intermetallic is probably $PuCd_{11}$.

The cell assembly used for these studies is identical to that described in ANL-6687, p. 80, for the plutonium-zinc galvanic cell. The details of the preparation of the electrolyte, a mixture of LiCl-KCl eutectic and $PuCl_3$, and the operating procedure for the cell are similar to those reported for the plutonium-zinc system. A small cylinder of plutonium was welded to a tungsten wire to provide the anode; the cathode consisted of liquid cadmium saturated with plutonium and contained in a small thoria crucible. A tungsten lead wire was used for the cathode. The plutonium used was high-purity material, produced by electrorefining, furnished by G. B. O'Keefe of the Metallurgy Division.

The data for the emf as a function of cell temperature, shown in Figure I-27, were obtained over a period of two weeks during which the cell operated in a reversible manner. The data can be represented by the empirical equations:

$$(358 \text{ to } 403 \text{ C})\ E\ (V) = 0.6999 - 0.5746 \times 10^{-3}\ T, \quad \sigma = 1 \text{ mV};$$

$$(403 \text{ to } 570 \text{ C})\ E\ (V) = 0.5783 - 0.3949 \times 10^{-3}\ T, \quad \sigma = 0.7 \text{ mV}.$$

The intersection of the lines representing these equations, 403 C, is in excellent agreement with the peritectic at 404 C found by Winsch, Nelson, and Paul.

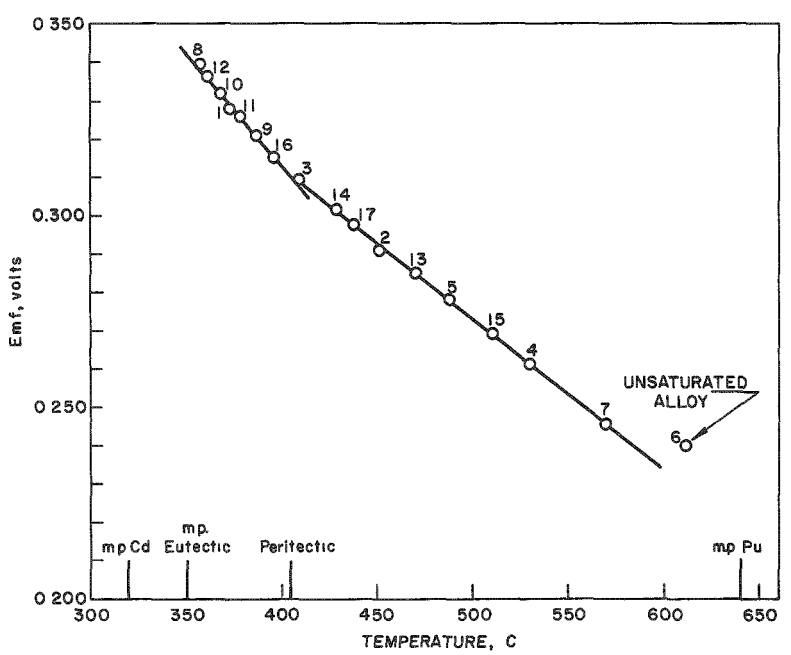

108-6889

Figure I-27

EMF OF PLUTONIUM-CADMIUM GALVANIC CELL VERSUS TEMPERATURE

(Data points numbered chronologically)

The cell data can be combined with the solubility data to compute the activity coefficient of plutonium in saturated liquid cadmium solutions. The activity coefficient over the range from 358 to 570 C can be represented by the empirical equation

$$(358 \text{ to } 570 \text{ C}) \quad \log \gamma_{Pu} = 4.786 - 6473\ T^{-1}.$$

Thermodynamics of Binary Alkali Metal Solutions (Optical Absorption Method)
(F. Cafasso, V. Khanna, and R. Murray)

The various theories of liquid solutions which have been useful in understanding the thermodynamic behavior of aqueous and organic solutions have not been very useful in understanding liquid metal solutions. This is likely due to the fact that many factors necessary for an adequate description of metallic solutions are basically different from the factors controlling interactions in nonmetallic systems. Most likely an understanding of metallic solutions will be accomplished by the fusion of basic electronic theory with theories of many-body interactions. Significant progress is being made in this area, and the time is approaching when confrontation of the theories developed by this fusion with experimental data should occur. The electronic theory of metals has been most highly developed for the alkali metals; the validity of first-principle calculations for more complex metals is far more uncertain. Thus, the first tests of theory and experiment will be best made by comparing the results for binary alkali metal solutions.

Surprisingly, practically no information has been published on the thermodynamics of binary solutions of the alkali metals. This may be due partly to the fact that the binary system most commonly used, namely, the sodium-potassium system, is very nearly ideal, and thus other alkali metal systems were assumed also to be nearly ideal. Inspection of the phase diagrams for the binary alkali metal systems shows that this assumption is far from being justified. Three types of phase diagrams are found in the literature.[5]

1. Diagrams which exhibit either a simple eutectic (e.g., the sodium-rubidium system) or both a simple eutectic and a single compound which has an incongruent melting point (e.g., the sodium-potassium and sodium-cesium systems).

2. Diagrams which exhibit a continuous series of solid solutions (e.g., the potassium-rubidium, potassium-cesium, and rubidium-cesium systems).

---

[5]Hansen, M., and Anderko, K., Constitution of Binary Alloys, McGraw-Hill, New York, N. Y. (1958).

3. Diagrams which exhibit extended solubility gaps in either the liquid state (e.g., the lithium-sodium system) or both the solid and liquid states (e.g., lithium-potassium, lithium-rubidium, and lithium-cesium systems).

For those systems in which compound formation occurs or in which large immiscibility gaps exist, significant deviations from ideal behavior are to be expected. In the present study, the activities of the components as a function of temperature and composition will be determined for systems of types 1 and 2.

The high chemical reactivity and chemical similarity of the alkali metals limit the number of possible experimental methods which may be used to determine thermodynamic activities. The vapor pressure method may be used provided that a means is available for the determination of the partial pressure of individual species which are present in the vapor phase. For binary alkali metal solutions the vapor is known to consist of atoms and diatomic molecules. Thus, for sodium-potassium solutions, the vapor will contain Na, K, Na_2, K_2, and NaK.

The optical absorption method permits the determination of the concentration of each of these species. In practice, it is only necessary to determine the concentration of either monatomic sodium (Na) or potassium (K) in the vapor, since all the others are in equilibrium. The optical absorption technique which will be used in this study permits exactly this to be done. In this method light of a frequency characteristic of Na alone is passed through the vapor above the solution NaK(ℓ). The amount of light absorbed at any temperature is proportional to P_{Na}, the partial pressure of sodium in the vapor at that temperature. The partial pressure of Na over the pure metal (P°_{Na}) can be obtained in the same way by replacing the solution NaK(ℓ) with pure sodium. The ratio of the absorbance by the vapor over the solution to the absorbance by the vapor over the pure metal gives P_{Na}/P°_{Na}, which is identical to the activity of sodium in the binary solution at some temperature T. The activity of the potassium can be determined in the same manner by measuring the light absorbed at frequencies which are characteristic of K(g) both above the binary solution, NaK(ℓ), and above pure potassium as a function of temperature. The Gibbs-Duhem relation will serve as a test of the internal consistency of the measurements. The instrument which will be used in this study consists of three parts: a liquid nitrogen-cooled hollow cathode lamp, a triple-zoned furnace which houses the absorption cell, and a monochromator.

A schematic diagram of the hollow-cathode lamp is shown in Figure I-28. The lamp consists of two parts: an upper anode and a lower cathode section, which are joined by a water-cooled standard-taper joint. The anode, which is housed in a glass envelope, consists of a cylinder of high-purity nickel which has an internal diameter of $\frac{5}{8}$ in. The anode is

held in place and sealed through the glass envelope by means of a tungsten rod which is welded to it. The tungsten rod also serves as the electrical connection of the anode.

Figure I-28

SCHEMATIC DIAGRAM OF HOLLOW CATHODE DISCHARGE LAMP

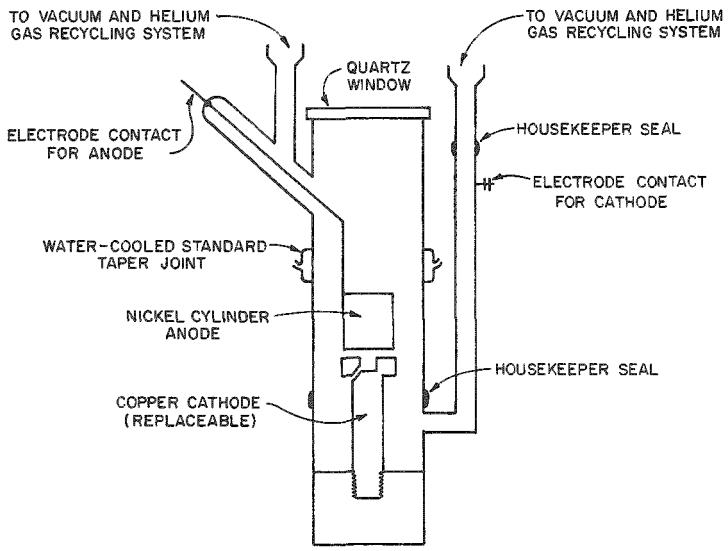

108-6893

The lower section which houses the cathode was fabricated from copper and glass joined together by a housekeeper seal. The cathode consists of a copper rod into which a cavity, $\frac{1}{4}$ in. deep and $\frac{3}{16}$ in. wide, and a channel (for the passage of helium) have been drilled. The discharge takes place in this cavity. A few crystals of sodium iodide placed in this cavity are sufficient to generate the sodium D lines.

A quartz window is held onto the upper section by Apiezon W Wax. This wax is also used to establish vacuum tightness at the standard taper joint. In order to warm the wax and thus prevent its fracture when the cathode is immersed in liquid nitrogen, water is circulated around the standard-taper joint.

The power for the lamp is generated by a regulated 1500-V, 200-ma, dc power supply (Kepco, model 1520B).

The absorption cells, which are made from high-purity quartz, are housed in a chrome-plated copper block provided with channels for a light path and slots to position the cells. Two absorption cells (sample and reference) may be placed in the block simultaneously. This block is located in the middle zone of a triple-zoned 15-in.-long Marshall Furnace. Two

additional blocks, each provided with light paths and thermocouple holes, reside in the two end zones. The temperature of each zone can be controlled separately. The furnace rests upon a table equipped with a micrometer thread drive which will permit the sample and reference cells to be accurately and alternately positioned in the light path.

The spectrometer is the Jarrell-Ash Model 8200, 0.5-m grating monochromator. This instrument, with a grating of 30,000 grooves per inch, has a resolution of at least 0.2 Å using a 10-μ slit.

The sodium-potassium system will be the first binary system studied. It is planned to make measurements at temperatures as close to the melting points of the alloys as possible. The deviations of a system from ideality may be expected to become more pronounced in the neighborhood of its melting point.

Intermediate Phases in the Rare Earth-Cadmium Systems (Effusion Studies)
(E. Veleckis, E. Van Deventer)

Studies of the phase relations of the binary systems of cadmium with lanthanum, cerium, and praseodymium by means of the recording effusion balance have been reported earlier (see ANL-6569, p. 88). In addition to the line compounds MCd_{11}, M_2Cd_9, MCd_2, and MCd, which are common to all three systems, several phases which have ranges of homogeneity were observed. Of the latter phases $MCd_{\sim 6}$ and $MCd_{\sim 3}$ are typical of cerium-cadmium and praseodymium-cadmium systems, whereas the phase $MCd_{\sim 8}$ is peculiar to the lanthanum-cadmium system.

Recently, these studies were resumed to include some representative elements of the heavier rare earths. Because significant changes were made in the apparatus and experimental procedure,* the results obtained for the systems already studied were also reviewed.

The effusion isotherms (at 445 C) for the systems lanthanum-cadmium, cerium-cadmium, praseodymium-cadmium, and neodymium-cadmium are shown in Figure I-29 as plots of the logarithm of the effusion rate vs. atom ratio (Cd/M). (To accommodate all four isotherms in one figure, the abscissae of the neighboring isotherms are offset by three units of the atom ratio.) The results of the studies made with the more sensitive equipment indicated the following:

---

*Improved sensitivity and reliability of the effusion apparatus were realized by recent installation of a new commercial recording balance. Also, the use of effusion crucibles having extremely small orifices (of 0.004-in. dia) has greatly facilitated the delineation of the exact phase-boundary locations.

1. A narrow phase having the stoichiometry La_2Cd_{17} exists rather than a phase with a wide solubility range as was reported previously.

2. The phases $MCd_{\sim 3}$ and $MCd_{\sim 6}$ that were previously observed in the cerium-cadmium and praseodymium-cadmium systems are line compounds M_4Cd_{13} and MCd_6. Analogous phases also exist in the neodymium-cadmium system.

3. All four systems form the compound having the stoichiometry M_3Cd_{13} rather than M_2Cd_9.

4. The sequence of compounds formed in the lanthanum-cadmium system is: $LaCd_{11}$, La_2Cd_{17}, La_3Cd_{13}, $LaCd_2$, and LaCd. The intermediate phases that exist in the binary systems of cadmium with cerium, praseodymium, and neodymium are: MCd_{11}, MCd_6, M_3Cd_{13}, M_4Cd_{13}, MCd_2, and MCd.

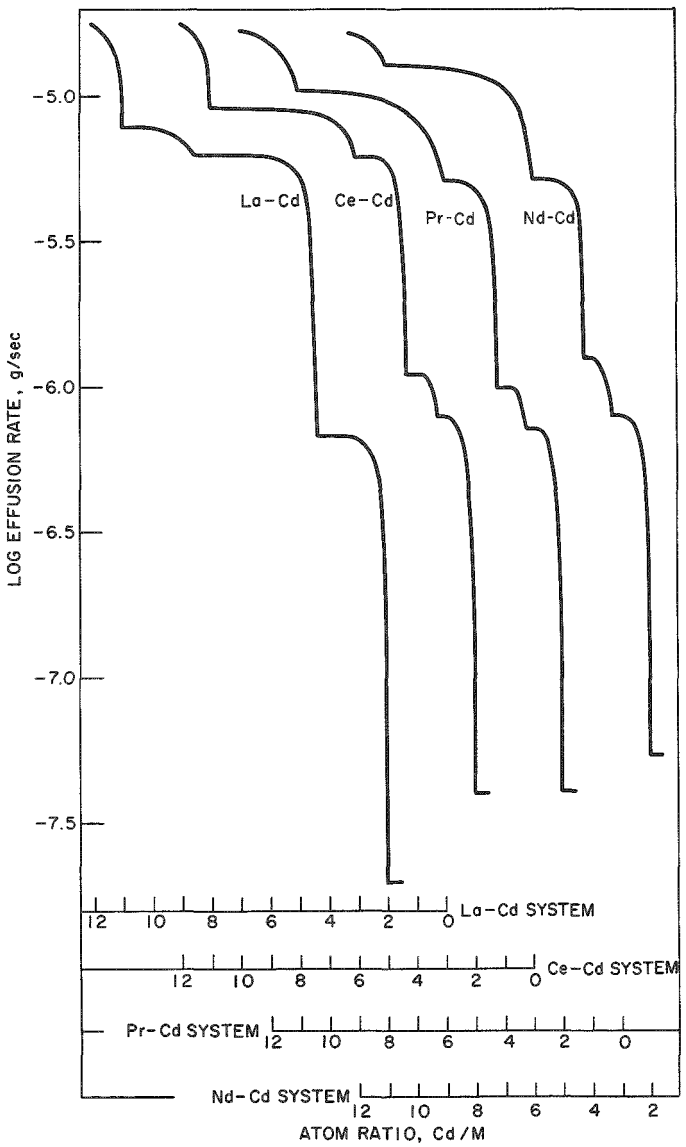

Figure I-29

RARE EARTH-CADMIUM SYSTEMS. TYPICAL EFFUSION ISOTHERMS AT 445 C

108-6843

II. FUEL CYCLE APPLICATIONS OF VOLATILITY AND FLUIDIZATION TECHNIQUES*

The development of a fluid-bed fluoride volatility process for the recovery of uranium and plutonium from spent uranium dioxide fuels was continued. In this process, uranium and plutonium dioxides are fluorinated to produce hexafluoride products, which are then decontaminated and separated by volatility techniques.

In the development of the fluid-bed fluoride volatility process for uranium dioxide-type fuels, current emphasis has been placed on the evaluation of a two-zone, oxidation-fluorination scheme as a means of improving performance of fluidized packed beds of uranium dioxide. In this scheme, which is carried out in a single reaction vessel, the lower (oxidation) zone of the reactor consists of a bed of uranium dioxide pellets with fused alumina grain filling the voids of the bed (fluidized packed bed) and the upper (fluorination) zone consists of a fluidized bed of fused alumina grain that extends above the fluidized packed bed. By passing an oxygen-nitrogen mixture through the lower zone, U_3O_8 fines are produced and transported to the upper fluidization zone, where the fines are fluorinated to uranium hexafluoride vapor. An evaluation of the two-zone technique for the processing of stainless steel-clad uranium dioxide pellets was also started.

Additional studies were carried out on the removal of uranium dioxide fuel from stainless steel cladding by converting the uranium dioxide to U_3O_8. In this reaction, the uranium dioxide pellets are transformed to a fine powder that is removed from the cladding.

Construction was continued of a plutonium-handling facility for engineering-scale investigation of the several steps of a fluid-bed fluoride volatility process for recovery of fissionable values from spent nuclear reactor fuel of the uranium dioxide type and for reconstitution of the oxide fuel material after it is freed from fission products.

Additional studies of a fluid-bed volatility process scheme for the recovery of enriched uranium from low uranium-high alloy fuel were carried out. The first fuel that is being studied is uranium-zirconium alloy fuel. In the process scheme, the zirconium is separated as the volatile tetrachloride during hydrochlorination of the alloy, and the uranium is recovered as the hexafluoride in a subsequent fluorination step. The reactions are conducted in an inert fluidized bed (currently, fused alumina grain is being used as the bed material) which serves as a heat transfer medium.

Studies were continued on the fluid-bed pyrohydrolysis reaction of zirconium tetrachloride with steam. The tetrachloride, which is produced during the chlorination of uranium-zirconium alloy fuels, is converted to the solid dioxide, a form which is more convenient for ultimate waste disposal.

---

* A summary of this section is given on pages 18 to 26.

Adaptability of the fluid-bed hydrolysis scheme to the conversion of aluminum chloride vapor (from the processing of aluminum-based alloy fuels) to the more readily stored oxide was demonstrated.

Installation was completed of the pilot-plant facility for the fluid-bed volatility reprocessing of highly enriched uranium-alloy fuel.

Additional studies were made of the conversion of uranium hexafluoride to high-density uranium dioxide by the simultaneous reaction of the hexafluoride with steam and hydrogen.

Supporting studies were carried out on the basic behavior of solids mixing in fluidized-bed systems for the purpose of assisting in the design and interpretation of process equipment operation.

The study of methods of removal of plutonium hexafluoride from air was continued.

Laboratory-scale fluorinations of U_3O_8 were carried out in a $1\frac{1}{2}$-in.-diameter fluid-bed fluorinator. This work is being performed to develop and to test apparatus and procedures for use in future work in which plutonium will be handled.

Reaction rates have been measured for the reaction of U_3O_8 with fluorine over the temperature range from 300 to 400 C employing a thermobalance.

The study of the effect that the addition of helium to plutonium hexafluoride has on the decomposition of plutonium hexafluoride by gamma irradiation was continued.

A. Laboratory Investigations of Fluoride Volatility Processes
(J. Fischer)

1. Fluid-bed Fluorination of U_3O_8
(A. V. Hariharan, R. L. Jarry, G. Manevy, J. J. Stockbar, T. D. Baker)

In the fluid-bed fluoride volatility process,[1] the uranium and plutonium content of spent oxide fuels will be recovered by fluorination to produce the volatile hexafluorides of uranium and plutonium. The process will employ a fluid-bed reactor as the fluorination vessel and will use fused alumina (Alundum, a product of the Norton Co., Worcester, Mass.) as the fluidized medium. One of the decladding schemes considered for this process would employ an oxidation step to remove the uranium dioxide and

[1] Jonke, A. A., Fischer, J., and Mecham, W. J., Fluoride Volatility Processing of Low-enriched Fuels, Trans. Am. Nuclear Soc. 4(2), 184-185 (1961).

plutonium dioxide from the stainless steel or Zircaloy cladding as a mixture of U_3O_8 and plutonium dioxide. The oxide mixture produced by such an oxidation process is a finely divided, free-flowing powder.

Two alternative schemes have been proposed for carrying out the combination of oxidation and fluorination reactions. In one, the oxidation and fluorination steps would be performed in the same fluid-bed reactor; the oxidation would be carried out in the lower section of the fluid bed, and the fluorination of the U_3O_8 product would be performed in the upper section of the bed. The transport of the U_3O_8 fines from the oxidation zone to the fluorination zone of the fluid bed would be accomplished by the fluidizing gas stream. The second scheme would employ a separate oxidation reactor, and the U_3O_8 powder formed would be fed into the fluid bed of a fluorination reactor by gas transport in a nitrogen stream used to fluidize the bed.

In the experimental work, the second scheme was used. A prototype fluid-bed fluorination reactor was set up to test and develop apparatus and procedures for subsequent work with mixtures of plutonium dioxide and U_3O_8. A gas and solids distributor described in a previous report (ANL-6648, p. 132) was used to produce a uniform dispersion of the oxide powder as it was fed into the fluidized alumina bed in a stream of nitrogen. The fluorinating gas entered the bed through holes in the distributor. A vibratory powder feeder, which was also described in ANL-6648, p. 133, was used to meter oxide powder into the fluidizing nitrogen stream at a controlled rate.

The U_3O_8 powder used in this work, obtained from a commercial source, had a surface area of 0.74 sq m/g, as measured by nitrogen adsorption, and an average particle diameter of 3.1 μ. Chemical analysis of the U_3O_8 powder showed a uranium content of 84.46 percent (theoretical, 84.80 percent), and spectrochemical analysis indicated that the principal contaminants, expressed in ppm, were: Al-30, Cr-10, Fe-50, Mo-30, Ni-50, and Si-30. Commercial-grade fluorine was first passed through a sodium fluoride trap at 100 C to remove hydrogen fluoride from the fluorine. Nitrogen, which was used as the fluidizing gas and also as a diluent for the fluorine, was passed through a trap containing Molecular Sieves to remove water before being introduced into the fluorination reactor. Fused alumina was used for the inert fluidized bed.

The fluorination apparatus consisted of the following major components: (1) a $1\frac{1}{2}$-in.-diameter fluid-bed fluorinator, (2) a vibratory powder feeder, (3) a system of cold traps and a sodium fluoride trap for trapping uranium hexafluoride, (4) a Lapp diaphragm pump for the circulation of the gas phase, (5) activated alumina traps for the disposal of fluorine, and (6) manifolds supplying fluorine, nitrogen, and vacuum service.

Figure II-1 is a schematic representation of the fluid-bed fluorination reactor. The lower section, which contains the inert bed of alumina, was fabricated from a 1-ft section of $1\frac{1}{2}$-in.-diameter schedule 40 nickel pipe.

The upper section of the reactor, the disengaging chamber, was fabricated from a 1-ft section of 3-in.-diameter schedule 40 nickel pipe. This section contained two sintered nickel bayonet filters through which the exiting reactor gases passed. The gas and solids distributor was located in the conical bottom of the reactor. The reactor was heated by a three-element resistance furnace. The lower resistance element was controlled by a thermocouple inside the reactor at the level of the fluorine inlet, whereas the upper two elements were controlled by a thermocouple placed at about the middle of the outside surface of the reactor.

Figure II-1

FLUID-BED FLUORINATION REACTOR

(The scale for the reactor sections is 3 in. = 1 ft)

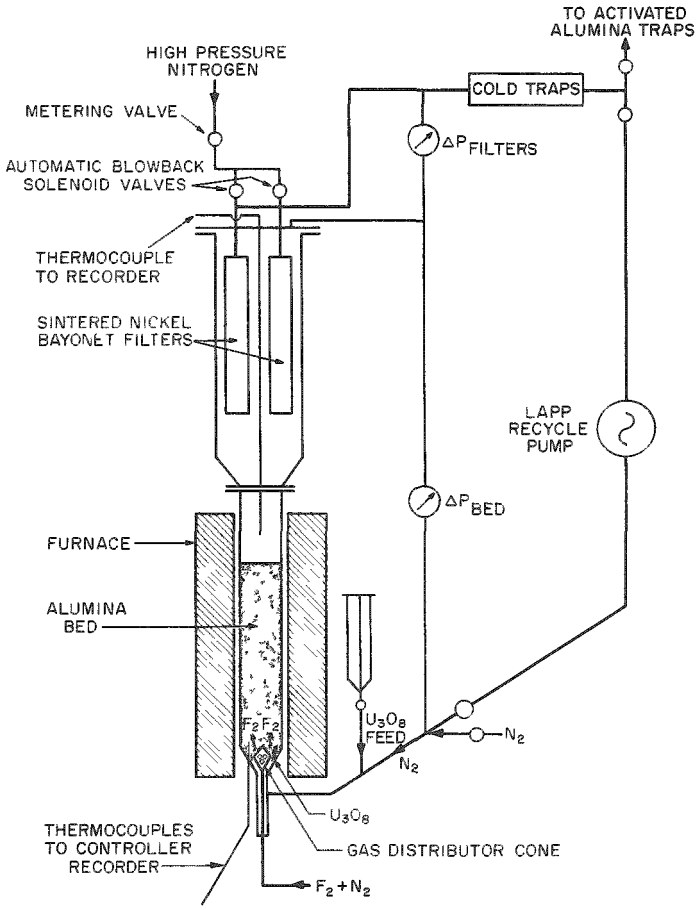

108-6887

An automatic blowback system* was employed to return solids which reached and were retained on the surface of the sintered nickel filters. A Venturi throat and jet were used in this system to deliver a high-velocity flow of nitrogen through the bayonet filter countercurrent to the normal gas flow of the system. The blowback procedure was alternated between the two filters and in this manner did not interfere with the normal flow of the reaction gases.

The cold traps used to condense the uranium hexafluoride consisted of three traps in series, which were maintained at about -80 C by means of a carbon dioxide-trichloroethylene slush. The first two traps were 4 in. in diameter and 1 ft in length; the third trap was 2 in. in diameter and 1 ft in length. In the second of the large traps, a sintered nickel bayonet filter was placed in the outlet line of the gas stream to retain any particulate matter. A trap packed with sodium fluoride was placed at the end of the series of cold traps. This trap was heated to 100 C to adsorb any uranium hexafluoride that was not condensed in the cold traps.

* J. W. Loeding et al., The Fluid-bed Calcination of Radioactive Waste, ANL-6322 (May 1961).

The U_3O_8 fluorination is conducted in two periods. During the first period, which will be referred to as the feeding-fluorination period, the U_3O_8 powder is injected into the fluid bed and most of the oxide is converted to uranium hexafluoride by reaction with a 20 v/o fluorine in nitrogen mixture. During the second period, which will be referred to as the recycle period, the fluorine content is raised to about 100 percent and the gas is recycled through the fluidized bed by means of the Lapp pump. The recycle period serves to remove the last traces of uranium from the fluid bed and will later serve to remove the plutonium from the bed.

The general operating procedure for the fluorination is as follows: about 400 to 500 g of 120 mesh fused alumina is placed in the fluid-bed fluorinator and the system is then heated to the operating temperature of 500 C. During the heating period, the nitrogen flow needed to fluidize the bed is started. The fluidizing nitrogen enters the bottom of the reactor, as shown in Figure II-1. A charge of a mixture of U_3O_8 and alumina in a 2:1 weight ratio is then placed in the vibratory powder feeder. When the fluid bed is at the proper operating temperature, the fluorine flow is started into the bed through the gas-distributor cone. The fluorine, which constitutes 20 v/o of the total gas flow, is diluted with an equal quantity of nitrogen before it enters the bed. The U_3O_8-alumina mixture is then injected into the fluidizing nitrogen stream and thence into the fluid bed at a rate of about 3 g U_3O_8/min. The gas velocity in the $\frac{3}{8}$-in.-diameter fluidizing nitrogen inlet line into which the uranosic oxide is fed is 5 ft/sec. Total flow through the fluid bed is 12 liters/min, with the fluidizing nitrogen contributing approximately 7 liters/min, and the mixture of fluorine and nitrogen contributing approximately 5 liters/min. The superficial velocity in the fluid bed is about 0.6 ft/sec at room temperature.

The Lapp diaphragm pump, which was used to recirculate the fluorine in the latter part of the fluorination procedure, had a rated flow capacity of 0.5 cu ft/min at a discharge pressure of 15 psig and atmospheric pressure intake. The remote head of the pump is constructed of Monel and nickel on the gas pumping side, and the impulse is transmitted from the compression head by means of a transmission line filled with fluorolube oil. Measurements of flow rates were made by means of a thermal flowmeter.* Flow calibration of the pump-flowmeter combination was accomplished by means of a wet test meter with nitrogen as the test gas.

The effluent gas stream from the fluorinator, when gas recirculation was not employed, passed through cold traps and a sodium fluoride trap to remove uranium hexafluoride. The gas then passed through an activated alumina trap where excess fluorine was removed before the effluent gas was exhausted to the atmosphere. This once-through flow was continued

* R. W. Kessie, The Design and Construction of Thermal Flowmeters. ANL-6531 (March 1962).

while the U_3O_8-alumina mixture was being fed into the fluid bed and for $\frac{1}{2}$ hr after the feeding has been completed. Following this feeding-fluorination period, the fluorine content of the gas phase was brought to approximately 100 percent and the recycle period started. The recycle flow was carried out for a period of 5 hr.

After the recycle period had been completed, the cold traps, while at -78 C, and the sodium fluoride trap were evacuated to remove the residual gas phase. The cold traps were then warmed to room temperature and the three cold traps and the sodium fluoride trap were weighed to assay the amount of uranium hexafluoride collected. No attempt was made to recover the uranium hexafluoride adsorbed on the sodium fluoride. The fluid-bed alumina was removed from the reactor and sampled for uranium analysis. The mixture of U_3O_8 and alumina retained in small amount in the disengaging section was removed and analyzed for uranium.

This experimental work, in which U_3O_8 alone was used, was preliminary to work with mixtures of plutonium dioxide and U_3O_8. The tests were designed to determine the optimum reaction conditions for efficient fluorination and to test the equipment. In the first series of experiments, the parameters affecting the elutriation of U_3O_8 from the alumina bed were explored. It is desirable to react the U_3O_8 with fluorine while it is in the bed. It is hoped that minimizing the elutriation will minimize the deposition of solids containing plutonium in the disengaging chamber of the reactor and on the filters. In tests of factors which might affect elutriation, the bayonet filters were removed from the disengaging chamber and any solids that passed through the disengaging chamber were trapped in a filter placed in a separate chamber outside of the reactor. By weighing the filter before and after the experiment, the quantity of unreacted U_3O_8 and alumina elutriated from the fluid bed could be determined. A determination of the quantity of U_3O_8 in the elutriated solids was made by dissolving the U_3O_8 in nitric acid. The residue of alumina was then dried and weighed, and the weight of U_3O_8 was obtained by difference.

The results obtained in experiments in which the effects of alumina particle size, bed height, and fluorine concentration on U_3O_8 elutriation were studied are shown in Table II-1. When the alumina particle size was decreased from 60 mesh (Experiment 18) to 120 mesh (Experiment 16), the elutriation of U_3O_8 from the bed was reduced from 19.5 to 9.0 percent of the U_3O_8 fed to the bed. When a 50-50 mixture of 60 and 120 mesh alumina (Experiment 19) was used, no significant decrease in the amount of U_3O_8 elutriated from the fluid bed was noted.

Variation of the height of the alumina bed also affected the elutriation of U_3O_8 from the bed. Increasing the bed height from 4 to 8 in. reduced the elutriation from 23 to 9 percent, as shown by the results of Experiments 20 and 16, respectively. A further increase in the height (to 12 in. in Experiment 21) did not result in a further reduction in the amount of U_3O_8 elutriated from the bed.

Table II-1

EXPERIMENTAL CONDITIONS AFFECTING ELUTRIATION OF U_3O_8 FROM A FLUIDIZED BED DURING FLUORINATION

Experimental Conditions

Fluid-bed Alumina:	520 g
U_3O_8:	100 g
U_3O_8 Feed Rate:	Approx 3 g/min
Bed Temperature:	500 C
Total Gas Flow Rate:	12 liters/min
Superficial Fluidizing Velocity:	0.6 ft/sec at 25 C
Gas Velocity in $\frac{3}{8}$-in.-dia Feed Line:	5 ft/sec at 25 C

Experiment No.	Al_2O_3 Particle Size (mesh)	Bed Height (in.)	F_2 Conc in Gas (v/o)	U_3O_8 Elutriated from Bed (g)
A. Al_2O_3 Mesh Size				
16	120	8	20	9.0
18	60	8	20	19.5
19	60 + 120 [a]	8	20	19.0
B. Bed Height				
20	120	4	20	23.0
16	120	8	20	9.0
21	120	12	20	9.5
C. Fluorine Concentration				
23	120	8	10	29.0
16	120	8	20	9.0
24	120	8	30	5.7

[a] Mixture: 50 w/o 60 mesh + 50 w/o 120 mesh.

The quantity of U_3O_8 elutriated from the reactor decreased as the concentration of fluorine in the reaction gas mixture was increased. The concentrations of fluorine in nitrogen in Experiments 23, 16, and 24, namely, 10, 20, and 30 v/o, respectively, resulted in elutriations of 29, 9.0, and 5.7 percent of the amounts of U_3O_8 fed to the reactor. From these data it is apparent that the elutriation of U_3O_8 from the fluid bed will decrease with decreasing particle size of the alumina, increasing bed height, and increasing concentration of fluorine in the gas phase.

In a second series of experiments, the effect of temperature on the fluorination reaction was examined. The bayonet filters were reinserted

in the disengaging chamber, and each filter was blown back with nitrogen every 5 min during the experiment. The fluorinations were carried out during the feeding-fluorination period. No recycle period was employed. Table II-2 lists the data obtained in experiments performed at 450, 500, and 550 C. An appreciable increase in conversion of U_3O_8 to uranium hexafluoride occurred when the temperature was increased from 450 C (Experiment 48) to 500 C (Experiment 45), from about 92 percent to 97.6 percent. When the temperature was increased to 550 C (Experiment 49), the percentage of U_3O_8 converted was not significantly greater than the percentage converted at 500 C.

Table II-2

EFFECT OF TEMPERATURE ON THE FLUID-BED FLUORINATION OF U_3O_8

Experimental Conditions

Bed:	Norton Refractory Al_2O_3, 120 mesh, 470 g
Feed Material:	100 g U_3O_8 (325 mesh), 50 g Al_2O_3 (120 mesh)
Total Gas Flow Rate ($F_2 + N_2$):	12 liters/min
F_2 Concentration:	20% (2.5 liters/min)
Linear Gas Flow in Bed:	0.575 ft/sec at 25 C

Filters alternately blown back every 5 min

Fluorinations continued for $\frac{1}{2}$ hr after feeding-fluorination period completed.

Run No.	U_3O_8 Feed Rate (g/min)	Bed Temperature (C)	% Conversion of U_3O_8 to UF_6 Based on UF_6 Collected
48	2.4	450	92.0
45	3.6	500	97.6
49	2.4	550	98.5

A series of experiments was performed at 500 C in which both the feeding-fluorination period and the 5-hr recycle period were employed. An automatic blowback system was used in these runs. During the recycle period, in which 100 percent fluorine was used, the portion of the feed line immediately adjacent to the reactor was heated to 450 C to facilitate the fluorination of any oxide which might be present in this area. The results obtained in these experiments and the experimental conditions used are listed in Table II-3. These data show that 99 percent or more of the U_3O_8 can be converted to uranium hexafluoride by a fluid-bed fluorination under the reaction conditions employed in these experiments. In Experiment 67, the

5-hr recycle period was performed at a temperature of 550 C; however, the use of this higher temperature did not result in a greater conversion of U_3O_8 to uranium hexafluoride.

Table II-3

FLUID-BED FLUORINATION OF U_3O_8

Experimental Conditions

Fluid-bed Alumina:	120 mesh; 520 g in Exp. 63 450 g in Exps. 65, 66, 67
U_3O_8-Al_2O_3 Feed Mixture:	2:1
Feeding-Fluorination Period:	
Bed Temperature:	500 C
Total Gas Flow Rate:	12 liters/min at 25 C
Fluidizing N_2	7 liters/min
Fluorine	2.5 liters/min
N_2 in Fluorine	2.5 liters/min
Superficial Fluidizing Velocity:	1.5 ft/sec at 500 C
Gas Velocity in $\frac{3}{8}$-in.-dia Feed Line:	5 ft/sec
Recycle Period:	
Bed Temperature:	500 C (550 C in Exp. 67)
Total Gas Flow Rate:	8 liters/min
Fluorine Conc in Gas Phase:	100 percent
Recycle Time:	5 hr
Temperature of Feed Line:	450 C

Experiment No.	U_3O_8 Charge (g)	U_3O_8 Feed Rate (g/min)	% Conversion of U_3O_8 to UF_6 on Basis of	
			UF_6 Collected	Analytical[a] Results
63	100	3.7	99.8	99.7
65	300	3.7	98.9	99.9
66	300	2.5	99.0	99.8
67	300	3.3	98.5	99.5

[a] Material retained in disengaging chamber and representative sample of bed material analyzed for uranium content; the total uranium content from both of these sources used to calculate the percent conversion.

The conversion values listed under Analytical Results in Table II-3 are based on uranium analyses performed on representative samples of the bed material and on the material deposited in the disengaging chamber. These values are somewhat higher than the values that are based on the amounts of uranium hexafluoride collected which is probably due to weighing inaccuracies.

Uranium retention in the alumina beds ranged from 0.02 to 0.05 w/o, corresponding to total uranium contents of 0.1 to 0.3 g for total weights of the recovered alumina beds of from 518 to 572 g. Samples of solids deposited in the disengaging chamber ranged in weight from 1 to 3 g and contained from 0.1 to 1.0 g of uranium. The total uranium contents of the alumina beds and samples from the disengaging chamber were 0.1 to 0.5 percent of the uranium fed to the reactor. The material balance figures were calculated from the values for the conversion of U_3O_8 to uranium hexafluoride based on the amount of uranium hexafluoride collected and on the uranium analysis of the bed and disengaging chamber material. The following equation was used:

$$\text{Material Balance \%} = \%\ U_3O_8 \text{ converted } (UF_6 \text{ base}) + 100 - \%\ U_3O_8 \text{ converted (Analytical base)}.$$

The somewhat lower conversion figures based on uranium hexafluoride collected are apparently not due to loss of hexafluoride, since the amounts found on the sodium fluoride (4.5, 0, 2.5, and 2 g for Experiments 63, 65, 66, and 67, respectively) were well below the tested capacity of the trap. It is probable that the discrepancy is due to weighing inaccuracies.

Future work will be carried out in the fluid-bed apparatus that has been assembled for plutonium operation. Initially, only U_3O_8 will be used to test the operation of the apparatus. This work will be followed by experiments in which mixtures of U_3O_8 and plutonium dioxide will be fluorinated. In these experiments, the principal objectives will be to determine the reaction conditions which will minimize the retention of plutonium on the surface of the alumina fluid-bed material and the deposition of plutonium on the surfaces and filters of the reactor and which will optimize the removal of plutonium as the volatile hexafluoride from the reaction system. In addition, determinations of the quantities of plutonium hexafluoride and uranium hexafluoride collected as products will be made. Separation of plutonium from uranium in the hexafluoride mixture by selective reduction of plutonium hexafluoride to the tetrafluoride by reaction with sulfur tetrafluoride may be used to determine analytically the quantities of plutonium and uranium present in the product mixtures.

2. Oxidative "Decladding" of Stainless Steel- and Zircaloy-clad Uranium Dioxide Pellets

(A. V. Hariharan, R. L. Jarry, T. D. Baker)

Removal of uranium dioxide and plutonium dioxide from stainless steel cladding by oxidation of the uranium dioxide to U_3O_8 is being considered as a step that would precede fluorination in the fluid-bed fluoride volatility process. Oxidation of uranium dioxide pellets results in an increase in volume and pulverization of the pellet material as U_3O_8 is formed. The feasibility of the process was demonstrated at Atomics International,[2] where successful decladding of uranium dioxide pellets clad in Type 304 stainless steel was achieved by oxidation at 400 to 500 C with air or oxygen as the oxidant. In these experiments, in which greater than 99 percent of the uranium dioxide was oxidatively removed from the cladding, holes at short intervals from each other were punched through the cladding along the long dimension of the fuel elements. As a result of this procedure, the cladding ruptured during oxidation, thus allowing greater access of the oxidizing gas to the uranium dioxide pellets. The U_3O_8 was separated from the cladding by means of mild vibration.

The present report covers work on the oxidative removal of uranium dioxide pellets from cladding in a fluid-bed reactor. Apart from its utility in the separation of uranium and plutonium oxides from cladding material, the oxidative process can also serve to produce a uniform feed for the fluid-bed fluorinator. Direct fluorination of spent uranium dioxide reactor fuel containing cracked and fragmented pellets would result in erratic fluorination conditions. The oxidation step, however, produces finely divided U_3O_8 powder with an average particle size of about 10 μ and a surface area of about 0.5 to 1.0 sq m/g.

Introduction of the powdered U_3O_8 to the fluid-bed fluorinator may be achieved by either of two methods. In one procedure, sections of the spent fuel elements are oxidized and declad in the lower section (oxidation zone) of a fluid-bed reactor. The oxide fines formed during the oxidation are transported by the fluidizing gas stream to the upper section (fluorination zone) of the reactor, where the fluorination step is carried out. In an alternative procedure, the oxidation step is performed in a separate reactor and the resulting oxide powder is then fed mechanically to a fluid-bed fluorinator.

Preliminary experiments on oxidative "decladding" were carried out in a horizontal tube furnace with uranium dioxide pellets clad in $\frac{3}{4}$-in.-long sections of Type 304 stainless steel tubing (wall thickness, 20 mils) which were open at both ends to simulate sheared fuel segments. The following information was derived from the experiments.

---

[2] Guon, J., et al., Low Decontamination Reprocessing Studies on Irradiated UO_2 Reactor Fuel, NAA-SR-7136 (Dec 15, 1961).

a) Complete conversion of uranium dioxide to U_3O_8 occurred in 3 to 4 hr at temperatures between 450 and 550 C in a flowing stream of air. The product was a finely divided, free-flowing oxide powder.

b) The oxidized material could be removed easily from the stainless steel cladding tube by gentle shaking.

c) Although oxidation at 450 to 500 C is slightly faster in a stream of pure oxygen than in air, the material obtained in reactions with pure oxygen has a tendency to cake and stick to the cladding.

Additional "decladding" work was carried out in a fluidized bed of alumina with uranium dioxide pellets clad in $5\frac{1}{2}$-in.-long sections of Type 304 stainless steel (wall thicknesses, 10 and 20 mils) or Zircaloy (wall thickness, 30 mils). Slots ($\frac{1}{8}$ in. x $\frac{1}{32}$ in.) were milled along the length of the cladding tubes. The distance between the ends of adjoining slots was $\frac{3}{8}$ in. The experiments were performed at 450 C with dry air as the fluidizing and oxidizing gas.

A single oxidation run with air was made at 550C with uranium dioxide pellets clad in Type 304 stainless steel tubing (wall thickness, 20 mils). The results of these experiments are given in Table II-4. In all cases an initial swelling of the cladding tube was followed by a partial and then complete splitting along the slit line. In runs made at 450 C with 10- and 20-mil stainless steel cladding, the tubing split open along its entire length after 2 and 4 hr of oxidation, respectively. Complete removal of the U_3O_8 product was accomplished by 1 or 2 hr of additional oxidation. In the runs with 30-mil Zircaloy cladding at 450 C and 20-mil stainless steel cladding at 550 C, the tubing was completely split after 6 hr of oxidation.

Table II-4

OXIDATIVE DECLADDING OF URANIUM DIOXIDE PELLETS CLAD IN TYPE 304 STAINLESS STEEL/ZIRCALOY

UO_2 Pellets	NUMEC, size 7/16-in dia, 7/16 in long
Fluid-bed Material	500 g 120 mesh Al_2O_3 (product of Norton Co.)
Fluidizing Gas	Air (linear velocity 0.3 ft/sec at 25 C)
Size of Cladding	5 1/2 in. long (slots 1/8 in. x 1/32 in. were milled along the length of cladding. Distance between ends of adjoining slots was 3/8 in.)
Number of Pellets	12, total wt UO_2 ~120 g

Temperature (C)	Type and Wall Thickness (mils) of Cladding	Percent Retention[a] of Uranium Dioxide in Cladding after Time (hr)						Average Rate of UO_2 Removal (g/hr)[b]
		2	4	5	6	7	8	
450	Type 304 SS, 10	65.7[c]	0.02	-	-	-	-	30[d]
450	Type 304 SS, 20	93.4	18.2[c]	0.03	-	-	-	24[d]
450	Zircaloy 30	98.6	87.2	-	10.0[c]	-	0.15	15[d]
550	Type 304 SS 20	91.4	91.1	-	10.0[c]	0.03	-	17

[a] Calculated on basis of initial weight of UO_2

[b] Calculation based on time necessary for complete removal of oxide from cladding

[c] Cladding split open completely at the end of this period

[d] Some uranium oxide fines remained in the fluid bed

The appearance of stainless steel-clad fuel segments at different stages of oxidation are shown in Figure II-2. The uranium dioxide pellets in these specimens were clad in stainless steel tubing having a wall thickness of 20 mils.

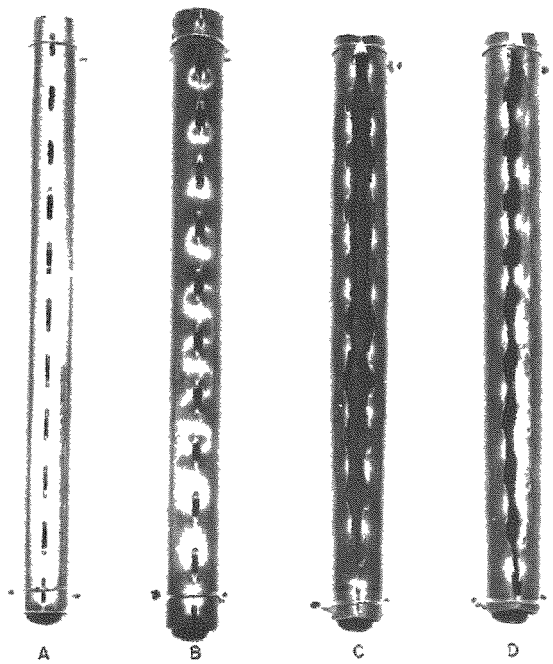

Figure II-2

SPECIMENS OF SIMULATED SEGMENTS OF STAINLESS STEEL-CLAD URANIUM DIOXIDE FUEL ELEMENTS AFTER VARIOUS STAGES OF OXIDATION

A - Original Element, 20-mil Stainless Steel Cladding
B - After 2 hr of Oxidation
C - After 4 hr of Oxidation
D - After 5 hr of Oxidation

108-6081

In Figure II-2, A is the fuel segment before treatment, B is a similar specimen after 2 hr of oxidation, C is a specimen after 4 hr of oxidation, and D is a specimen after 5 hr of oxidation. D shows the complete removal of the U_3O_8 powder from the cladding. Several observations can be made from the results of these experiments:

1) The removal of uranium dioxide pellets from Type 304 stainless steel or Zircaloy cladding by oxidation is feasible in a fluid bed at 450 C with air as the oxidant.

2) Slots milled along the length of the cladding allow greater access of the oxidizing gas to the uranium dioxide pellets and promote splitting of the cladding along the slot line, thereby also aiding the release of U_3O_8 from the cladding.

3) The time necessary for complete removal of the U_3O_8 formed appears to be dependent on the thickness of the cladding, i.e., the time necessary to achieve complete splitting of the cladding.

The Kinetics of Fluorination of U_3O_8

(R. L. Jarry, T. D. Baker)

The oxidative "decladding" of uranium dioxide fuel elements will produce finely divided, powdered U_3O_8. In a proposed fluid-bed fluoride volatility process, the U_3O_8 powder is to be fluorinated in a fluid-bed reactor. The U_3O_8 will either be produced in the same fluid bed in which the fluorination is to be carried out, or will be prepared in a separate reaction vessel and injected into the fluid bed of a fluorinator. It is necessary that the U_3O_8 be fluorinated during its residence time in the fluid-bed medium in order to minimize elutriation of powder to cooler portions of the reactor, where reaction would not take place. A study of the kinetics of the reaction of fluorine with U_3O_8 was made in order to obtain information from which the residence time necessary to completely react a particle of U_3O_8 with fluorine in a fluid bed could be calculated.

Two batches of U_3O_8 were used in this study. The first was a standard sample (designated as NB-15), which was prepared by the New Brunswick Laboratory of the AEC and which had a certified purity of 99 percent. The second batch (designated as UCN) was prepared by Union Carbide Nuclear Corp. Chemical analysis of this sample showed a uranium content of 84.99 percent (theoretical uranium content of U_3O_8 is 84.80 percent). The NB-15 and UCN samples had surface areas, as measured by nitrogen adsorption, of 0.14 and 0.28 sq m/g, respectively. The fluorine used was commercial grade from which hydrogen fluoride was removed by passing the gas through a trap filled with sodium fluoride heated to 100 C.

The fluorination experiments were performed with a thermobalance that was specially designed for use with fluorine. The main components of the thermobalance, which have been described in detail by Johnson and Fischer,[3] are a Sartorius Selecta analytical balance, equipped for autoweight recording, and a vertical, tubular nickel reaction chamber. A nickel sample pan, upon which the U_3O_8 powder was placed, was suspended in the reaction chamber by a Monel chain attached to the stirrup of the Sartorius balance. Fluorine was passed through a preheater before entering the reactor, and the flow rate was measured by means of a thermal flowmeter. A thermocouple positioned directly beneath the sample pan sensed the reaction temperature. The output of the thermocouple was measured by means of a Rubicon Type B potentiometer. A multipoint recording potentiometer was used to monitor the temperatures of the preheater, the reaction chamber furnace, and the output of the thermal flowmeter.

In a typical experiment, 400 mg of U_3O_8 was placed on a tared nickel pan and then lowered into the preheated reaction chamber. During this stage of the experiment, nitrogen flow was maintained through the

---

[3] Johnson, C. and Fischer, J., J. Phys. Chem., 65, 1849 (1961).

reactor. The weight of the oxide sample was checked on the Sartorius balance while temperature equilibrium between gas and solid was being attained. When the reaction system had reached a uniform temperature, the nitrogen flow was stopped and a flow of fluorine at a rate of 150 cc/min was started. During the reaction period, a continuous record of the weight change of the oxide sample versus reaction time was obtained.

The data obtained in these experiments was correlated by means of the diminishing-sphere model. This treatment of data was discussed in detail by Johnson and Fischer.[3] Briefly, the method assumes that in the gas-solid reaction the solid reactant consists of spherical particles of uniform diameter, and that the reaction occurs uniformly on all the particles simultaneously when the layer of solid is thin enough to allow saturation with the reactant gas. The reaction rate is then a function of the surface area of the particle. A mathematical treatment was developed for this kinetic model based on a gas-solid reaction which occurs at a continuously diminishing spherical interface. The final expression relates the reaction rate to a function of the fraction of the solid unreacted, as shown in the following equation:

$$(1 - F)^{1/3} = 1 - k't, \qquad (1)$$

in which

F = the fraction of solid reacted;

k' = $k/r_0 \rho$, where r_0 is the initial radius of a particle and ρ is the bulk density;

t = reaction time.

A plot of the function $(1 - F)^{1/3}$ versus t results in a straight line, and the reaction rate constant can be obtained from the slope of the line.

Seven experiments were performed with the UCN oxide and fourteen with the NB-15 oxide. The temperature range covered in the experiments was from 300 to 400 C. The fluorinations were completed in 2 or more hours at 300 C and in about 20 min at 400 C. The plot of $(1 - F)^{1/3}$ versus time t for each of these experiments gave a straight line over a significant portion of the data. A plot for a typical experiment is shown in Figure II-3. Deviation from the expected kinetics at the beginning of the experiment was due to dilution of the fluorine by the nitrogen initially present in the reactor. The deviation at the end of the reaction period is probably due to the small amount of sample remaining. X-ray diffraction analyses of the residues indicated that uranyl fluoride is an intermediate in this reaction.

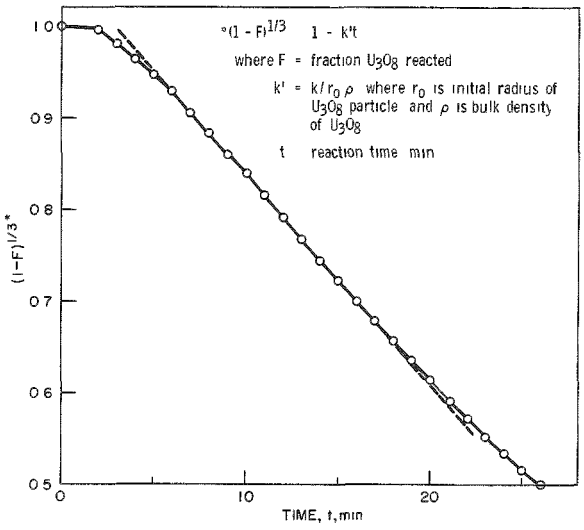

108-6878

Figure II-3

FLUORINATION OF U_3O_8

Temperature: 401 C

Fluorine Flow Rate: 120 ml/min

U_3O_8 Mesh Fraction: -100 +325

Rate constants were calculated from the slopes of the plots of the function $(1 - F)^{1/3}$ versus time t. The variations of the rate constants (k' of Equation 1) with temperature for the UCN and NB-15 samples of U_3O_8 are shown in Figure II-4. From the slopes of the lines drawn through the two sets of data points, values of the activation energy of 31 and 30 kcal/mole were calculated for the reactions of fluorine with NB-15 oxide and UCN oxide, respectively. The somewhat larger values of the reaction rate constants obtained for the UCN U_3O_8 is probably due to the larger surface

Figure II-4

VARIATION OF REACTION RATE CONSTANT k' WITH TEMPERATURE FOR THE FLUORINATION OF U_3O_8

Temperature Range: 300-400 C

Rate Equation: $(1 - F)^{1/3} = 1 - k't$

(see Figure II-3 for definition of symbols)

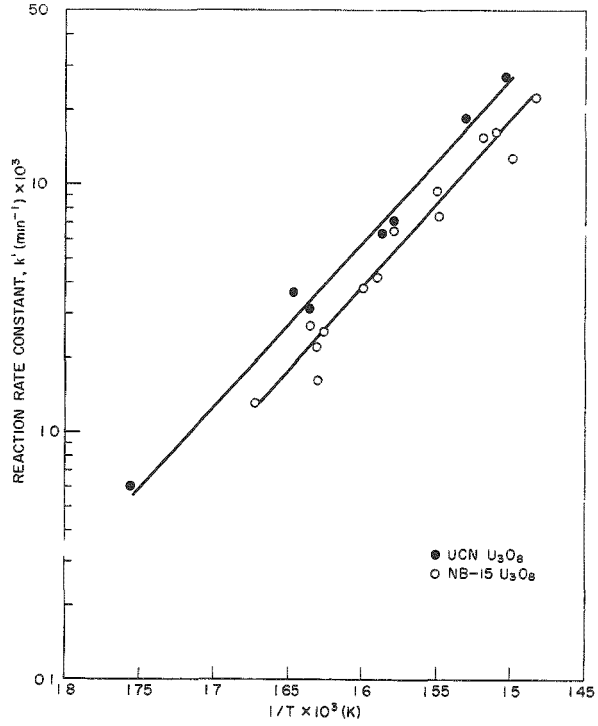

108-6836

area of that material. The integrated form of the Arrhenius equation was fitted to the two sets of data shown on Figure II-4 to obtain the following equations representing the change in rate constant with temperature:

$$\text{NB-15 oxide: } \log k' = -\frac{6787}{T} + 8.4438; \tag{2}$$

$$\text{UCN oxide: } \log k' = -\frac{6599}{T} + 8.3133. \tag{3}$$

By means of equation (3) an extrapolated value of 0.6 min^{-1} was calculated for the rate constant at 500 C, the temperature for the fluid-bed fluorination of U_3O_8. To estimate the time necessary to completely fluorinate a particle of U_3O_8, the kinetic equation in the following form was used:

$$1 - \frac{r}{r_0} = k't, \tag{4}$$

in which

r = radius of the particle at time t in the fluorination;

r_0 = initial radius of the particle.

When r is very small, that is, when the particle has been essentially completely converted to uranium hexafluoride, then the time is equal to the reciprocal of the rate constant. The solution of Equation (4) for t by use of the extrapolated rate for 500 C gave a value of 1.7 min. Therefore, if the extrapolated rate constant is reasonably accurate, a residence time that is several times greater than that needed for complete reaction is available. That this is so can be deduced from the data for the fluid-bed fluorination of U_3O_8 presented in another section of this report (p. 120). In these experiments, which were performed at 500 C and with a superficial fluidizing velocity of 1.5 ft/sec, more than 99 percent of the U_3O_8 was converted to uranium hexafluoride, and the alumina bed material contained no more than 0.05 w/o uranium.

Decomposition of Plutonium Hexafluoride by Gamma Radiation

(M. J. Steindler, D. Steidl)

In the fluid-bed fluoride volatility process, plutonium hexafluoride will be subjected to gamma radiation from fission products. The current investigation is intended to demonstrate the behavior of plutonium hexafluoride in a high gamma field under various process conditions and to serve as a fundamental study of the mechanism of the decomposition of plutonium hexafluoride by gamma radiation.

Plutonium hexafluoride at pressures of 80 to 100 mm Hg has been shown to decompose with a G value* of 7.5 ± 0.7 molecules in the range from zero to 37 x 10^{20} eV (see ANL-6687, p. 106). Both oxygen and fluorine, which will be present in process gas streams from the fluorination step of the fluid-bed fluoride volatility process, reduce the decomposition of plutonium hexafluoride by gamma radiation to rates that are nearly the same as those obtained for plutonium hexafluoride in the absence of gamma radiation (see ANL-6596, p. 126; ANL-6687, p. 109). The effect of added helium or krypton on the decomposition of plutonium hexafluoride by gamma irradiation has also been studied (see ANL-6596, p. 127; ANL-6687, p. 108). Current emphasis on the problem has been directed toward a detailed investigation of the effect of added helium on the decomposition of plutonium hexafluoride under gamma irradiation.

The experimental procedures employed in this work have been previously described (see Summary Report ANL-6477, p. 118). The results of current as well as previously reported experiments with helium are shown in Table II-5 and Figure II-5. These experiments were done at

Table II-5

DECOMPOSITION OF PLUTONIUM HEXAFLUORIDE BY GAMMA RADIATION IN THE PRESENCE OF HELIUM

Average Gamma Energy: 0.75 MeV
Dose Rate: 1 x 10^4 to 4 x 10^4 rad/min
Temperature: 60 to 70 C
PuF_6 Pressure: ~80 mm Hg at 25 C

Experiment	Initial PuF_6 (millimoles)	Initial He (millimoles)	Absorbed Dose (eV x 10^{-20}) In PuF_6	Absorbed Dose (eV x 10^{-20}) In He	PuF_6[b] Lost (millimoles)	PuF_4[c] Formed (millimoles)	G[d]
1199F-146	0.996	8.863	8.0	1.0	0.072	0.084	5.9
106	1.010	8.659	8.1	1.0	0.134	0.086	8.2
116	1.026	8.413	8.7	1.0	0.147	0.116	9.1
128	1 043	8.629	14.7	1.8	0.185	0.139	6.6
140	0.982	8.342	15.1	1.9	0.185	0.196	7.6
148	1.016	8.998	15.1	2.0	0.192	0.187	7.5
7	1.073[a]	8.132	15.6	1.8	0.252	0.222	9.1
40	0.964[a]	8.133	26.7	3.7	0.299	0.291	6.7
118	1.015	8.566	38.9	5.5	0.373	0.317	5.3
49	0.935[a]	8.298	40.5	6.2	0.361	0.436	5.9
34	1.035[a]	17.16	15.6	3.7	0.150	0.203	6.8
10	1.097[a]	17.29	16.8	4.0	0.184	0.183	6.6
122	0.967	17.22	25.7	7.5	0.315	0.223	6.3
158	1.045	17.58	28.2	7.6	0.314	0.315	6.7
130	1.010	17.31	28.6	7.6	0.242	0.236	5.0
152	1.022	18.14	30.6	8.3	0.216	0.231	4.4
154	1.005	17.78	40.8	11.8	0.324	0.347	4.9
132	1.018	17.58	40.8	11.9	0.391	0.389	5.7

[a] Presented previously.
[b] By tensiometric methods.
[c] By chemical analysis of solid residue.
[d] G value calculated from the average of PuF_6 lost and PuF_4 formed with energy absorbed in PuF_6 alone.

* Molecules decomposed per 100 eV of absorbed energy.

Figure II-5

DECOMPOSITION OF PLUTONIUM HEXAFLUORIDE BY GAMMA RADIATION IN MIXTURES WITH HELIUM

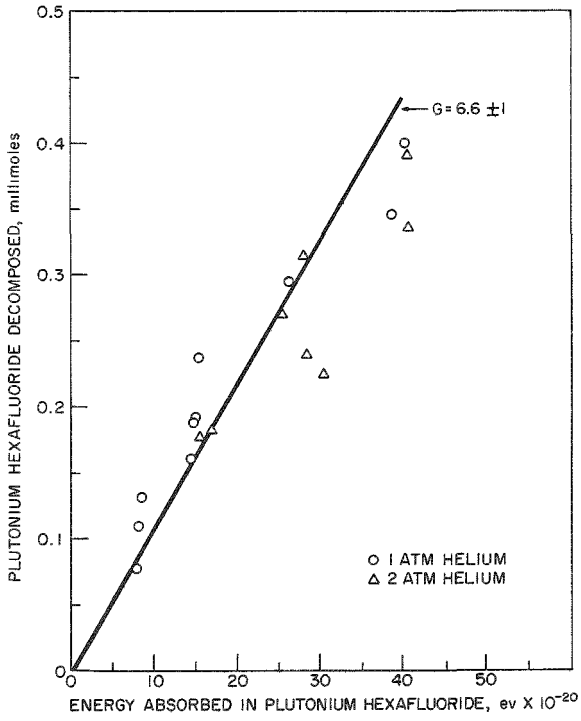

108-6883

helium pressures of approximately one atmosphere (~8.5 millimoles of helium) and two atmospheres (~17 millimoles of helium). The amount of plutonium hexafluoride decomposed appears to increase almost linearly with absorbed energy in the range studied (8×10^{20} to 41×10^{20} eV).

The data in Figure II-5 may be viewed as showing a deviation from linearity at high total dose. Such behavior has been observed in the study of the alpha decomposition of plutonium hexafluoride and may be attributed to the increasing importance of the back reaction as the products of the decomposition build-up. Evidence for the synthesis of plutonium hexafluoride from fluorine and plutonium tetrafluoride by gamma radiation has been presented previously (see ANL-6596, p. 130), and it is likely that the effective G for the decomposition will decrease at large doses. Although experiments done with one atmosphere of helium result in a G value that is slightly higher than that calculated from experiments with two atmospheres of helium, it is believed that the difference between values is not significant. Since no pronounced effect of the pressure of helium on the G value was found, a G value for all experiments with helium has been calculated. This value, $G = 6.6 \pm 1$, is not significantly different from that obtained from experiments with plutonium hexafluoride alone.

The data show, therefore, that when a vessel that contains plutonium hexafluoride only and a vessel that contains the same amount of plutonium hexafluoride together with one or two atmospheres of helium are subjected to the same external source of radiation for identical periods of time, the extent of decomposition of plutonium hexafluoride will be the same in both vessels, in spite of the fact that the total energy absorbed in the vessel containing helium is 10 to 20 percent greater than the energy absorbed in the absence of helium. Since plutonium hexafluoride has an estimated first ionization potential of 15 eV, and the first excited state of helium is approximately 20 eV, inhibition of plutonium hexafluoride decomposition by helium would involve deactivation of a plutonium hexafluoride

molecule which is both ionized and excited. On the basis that such excited ions are present in very small concentration, the slight effect of helium is in keeping with theoretical expectations.

The effect of krypton on the decomposition of plutonium hexafluoride is now being studied and will be reported in the next summary report.

The Alpha-radiation Decomposition Rate of Plutonium Hexafluoride
(R. Wagner, W. Shinn)

Studies of the decomposition of plutonium hexafluoride due to alpha radiation are continuing with an investigation of the effect of the gases nitrogen, oxygen, fluorine, helium, or krypton. Binary mixtures of 100 mm of plutonium hexafluoride and each of the above gases have been prepared at room temperature in 127-cc nickel spheres. Analysis of the products has begun and the results will be published in the next Chemical Engineering Summary Report.

B. Engineering-scale Investigation of Fluid-bed Fluoride Volatility Process
(A. A. Jonke)

1. Development of Fluid-bed Fluoride Volatility Processes for the Recovery of Uranium and Plutonium from Uranium Dioxide Fuels
(W. J. Mecham)

Development of a fluid-bed fluoride volatility process for the recovery of uranium and plutonium from irradiated uranium dioxide fuels has continued. In this process, uranium and plutonium oxides are reacted with fluorine to produce hexafluoride products, which are then decontaminated and separated by volatility techniques. The fluorination is carried out in a fluidized packed-bed reactor, in which the packed section is formed by uranium dioxide pellets. Alumina grain is used to fill the voids in the uranium dioxide pellet bed and to form a fluidized bed above the pellets. Development studies on an engineering scale have thus far been directed toward process optimization of the primary fluorination of uranium dioxide pellets. The major objectives of these studies have been to demonstrate short-time (less than 20 hr) batch fluorination and satisfactory fluorine utilization efficiencies (greater than 75 percent). During the present period, continued emphasis has been placed on the evaluation of a two-zone, oxidation-fluorination technique that is carried out in a single vessel.

In early one-zone system runs (see ANL-6596, pp. 136 to 139) with shallow beds (less than 6 in. deep) of reactor-grade (unirradiated) uranium dioxide fuel pellets, satisfactory heat removal, reaction control, and

the general effects of major process variables, such as temperature, reagent gas flow, and composition, were demonstrated. Although these runs were made mostly with batch charges of pellets, the semicontinuous feeding of pellets was also demonstrated. The introduction of oxygen along with fluorine in the fluidizing gas was shown to promote the fluorination reaction by the formation of uranium oxide (U_3O_8) fines of high specific surface area. Satisfactory process control was achieved by metering the inlet fluorine and oxygen gases. Although oxygen is a product of the fluorination reaction and must be bled from the system, a mathematical analysis (see Summary Report ANL-6543, pp. 131-134) of the use of process off-gas indicates that high fluorine efficiency can be obtained through off-gas recycle while holding recycle oxygen to a minimum.

In batch runs utilizing deeper pellet beds (18-in.-deep initial batch charges), caking tendencies were noted (see Summary Report ANL-6569, p. 109). These caking tendencies were apparently due to secondary reactions of uranium hexafluoride vapor with uranium-bearing intermediate compounds in the form of solid fines. To prevent caking in these deeper beds, low oxygen concentration was required, which in turn entailed the practical disadvantage of a relatively low rate of U_3O_8 production and a consequent low rate of uranium hexafluoride production and low efficiency of fluorine utilization. It has been found that caking can be prevented by the use of a two-zone oxidation-fluorination scheme. This scheme has been used successfully with 12-in.-deep beds and has allowed both high production rates and high fluorine efficiencies. Although the two-zone method is considered promising for beds deeper than 12 in., such tests have not yet been carried out.

In the two-zone process, two distinct reaction zones are utilized: The first is a bed of uranium dioxide pellets with fused alumina grain particles in the voids (oxidation zone); the second is a bed of fused alumina grain particles placed over the uranium dioxide pellet bed (fluorination zone). In the oxidation zone, U_3O_8 fines (about 10 to 20 μ in mean diameter) are produced by contacting the uranium dioxide pellets with a mixture of oxygen and nitrogen which also serves to fluidize the alumina particles. The U_3O_8 fines are transported from the lower zone by the oxygen-nitrogen gas stream and are reacted in the upper zone with fluorine, which is admitted to the fluidized bed of alumina just above the uranium dioxide pellet bed. The fluidized alumina serves as a heat transfer medium. A discussion of the two-zone method of operation and a summary of earlier runs are given in ANL-6687, pp. 112-124.

During the present period, improved process control was achieved in the batch fluorination of unclad pellets, as shown by satisfactorily high and uniform rates of uranium hexafluoride production and by high efficiency of fluorine utilization. The improvement in process control was aided by the use of a gas thermal conductivity instrument for the continuous monitoring of fluorine concentration in the process off-gas.

The fluid-bed oxidation-fluorination techniques under development for processing uranium dioxide fuel pellets may also be applied to metal-clad fuel elements that have been cut to expose the uranium dioxide to the reagent gases. In this way separate chemical decladding steps, such as chlorination for the removal of stainless steel, can be avoided. In an oxidation-fluorination process, the uranium dioxide would be removed from the unreacted cladding, which would be discarded with the solid waste from the fluorinator. Thus, by shearing fuel elements into approximately one-in. lengths, it is possible to react the exposed uranium dioxide with fluorine to form the volatile uranium hexafluoride or with oxygen to form a mobile powder of U_3O_8. Tests of the two-zone oxidation-fluorination scheme on variously cut fuel elements have been performed during the present period. In this method, the unreacted cladding is disposed of as solid waste after removal of the uranium.

Separate studies of the oxidation step for the removal of uranium dioxide fuel from stainless steel (Type 304) cladding were also made. Earlier oxidation studies (see Summary Report ANL-6477, p. 139) of unclad pellets showed that the oxidation of uranium dioxide to U_3O_8 proceeded rapidly to completion, requiring only about 4 hr for a bed of $\frac{1}{2}$-in. pellets at 500 C. Preliminary tests of the oxidation of one-in.-long segments of stainless steel-clad uranium dioxide fuel elements in a fluidized packed bed were reported in the preceding quarterly (ANL-6687, p. 124). The current work is directed toward the development of an oxidation step that may be incorporated into the two-zone oxidation-fluorination scheme in which uranium and plutonium hexafluorides are the product.

In the fluid-bed, oxidation-fluorination process, the transport of both heat and material is important, and depends on the mixing of solids and gas in this system. Because no previous work has been reported on the mixing behavior of such fluidized packed beds, basic studies in this area have been carried out as a part of process development. Rates of transport in the longitudinal (axial) and lateral (radial) directions are different and have been measured separately. When feasible, these studies have been carried out with materials that are more convenient to handle than uranium or fluorine. Earlier work on fluidized packed beds dealt with heat transfer and gas mixing. In the preceding quarterly (ANL-6687, p. 128), studies of rates of elutriation of fines from fluid beds were studied as a function of gas rates, fines concentration in the bed, size of fixed packing, and size of fluidized particles were reported. Studies of heat transfer rates as a function of fines concentration were also reported. During the present period, solids mixing rates in the lateral direction were investigated.

An engineering-scale high-alpha facility is being designed and installed for the purpose of studying the several steps involved in the fluid-bed fluoride volatility processing of uranium-plutonium oxide fuel. Process equipment is now being installed for the fluorination step; equipment for other separations steps is to be installed later.

2. Fluorination of Dense Uranium Dioxide Fuel Pellets in a Fluidized Bed

(L. Anastasia, B. Kullen, R. Kinzler, A. Rashinskas)

In order to improve reactor operation and control during the processing of uranium dioxide pellets by means of the two-zone oxidation-fluorination scheme, two modifications have been made in the 3-in.-diameter fluorinator system. One modification concerns the disengaging section and filter system, and is intended to minimize problems associated with the fluorination of fines of uranium intermediate compounds which may be elutriated from the fluid bed. The other modification provides a method whereby the fluorine concentration in the process off-gas is continuously measured.

Filter Modification

The function of the disengaging and filter sections is to prevent solids from escaping the fluorination zone of the reactor. The following steps are involved:

1) The freeboard immediately above the fluid bed provides a region in which lowered gas velocity (about $\frac{1}{2}$ that in the dense fluid bed) allows some of the larger, entrained particles to fall back into the fluid bed. This is most effective in practice for particles of +200 mesh which may acquire high velocity from bubble bursts or slugging in the fluid bed. The effectiveness of this freeboard increases with height of freeboard up to about 2 ft.

2) In general, disengaging sections of larger diameter would be expected to allow more effective settling of the finer particles because of the consequent decrease in gas velocity. In order to achieve a substantial reduction in the number of entrained particles of -200 mesh size, very large disengaging sections may be necessary. An increase in both the diameter (for reducing gas velocity) and the height (for increasing residence time) of the disengaging section would be advantageous. (Also, cyclones are sometimes used as an alternative to large disengaging sections.) The resulting low gas velocities may allow collected powders to accumulate. Vibration may be effective in reducing holdup of fines in this case.

Accumulations of uranium oxide or oxyfluoride in the disengaging section may be removed by fluorination at temperatures of 250 C or above. However, because of relatively poor heat transfer of such nonfluidized material, this method is considered to be limited in practice to thin ($\sim\frac{1}{8}$-in.) deposits.

Uranium or plutonium compounds that are carried through the disengaging section are collected on porous metal filters. These give good

separation performance due to filter cake action, and the cake can be removed from the filter and returned to the fluorination zone by reverse gas flow (blowback). These filters are mechanically weak (compared with solid metal) and are subject to corrosion. For use with fluorine, nickel or Monel filters have a long life only at temperatures below 200 C. Important in the control of temperature is (1) the cooling of hot gas from the reaction zone and (2) the prevention of any extensive fluorination of fines on the filter surface. The general approach has been to minimize the fines loading on the filter and to provide positive cooling of the filter chamber and of the gas before it contacts the filter.

In some recent runs, elutriated fines have accumulated in the disengaging and filter section because of low operating temperatures and because of internal surface configurations favoring powder holdup. The temperature of the disengaging section has been maintained at 100 to 200 C during fluorination experiments in order to maintain the physical integrity of the two porous metal filters. The tops of these filters with exposed pipe connections provided several areas suitable for fines buildup. In addition, a 19-in. length of Schedule 40, 3-in.-diameter pipe attached to the top flange of the reactor and perforated with sixty-eight 0.5-in.-diameter holes provided numerous horizontal surfaces and an additional vertical surface upon which fines have deposited. (The perforated pipe was originally intended as a mechanical guide for lowering solid charges into the fluorinator.) The pipe and filters have been removed from the disengaging section, and an external filter assembly has been constructed. Previous tests with external filters have been described in Summary Report ANL-6333, p. 184. A schematic diagram of the present system is shown in Figure II-6. The parts of the reactor system that have been removed are shown in dotted lines.

In the modified system, a single 3-in. x 18-in. bayonet filter surmounts the disengaging section to filter the process off-gas. A bypass gas path through a second external filter (non-blowback) has been provided to allow blowback of the process filter. The bypass is opened electrically by means of the blowback timer and a delay relay. Three seconds before each blowback, the timer actuates a solenoid that operates a pneumatic valve which in turn opens the bypass line; the delay relay then actuates the blowback system. This operation completes the timer cycle; the bypass is closed and normal gas flow through the process filter is resumed. The present location of the filters allows the use of higher temperatures for the fluorination of fines in the disengaging section; calrod heaters have been added to the disengaging section for this purpose.

Continuous Fluorine Analysis of Fluorinator Off-gas

Since fluorine is metered into the reactor system at a known rate, a continuous analysis of fluorine in the off-gas allows immediate knowledge of fluorine utilization efficiency. Also, since the uranium hexafluoride

collection rate is known independently, the rate of accumulation of fluorine as intermediate fluorides can be calculated. (In the two-zone system, uranyl fluoride is the chief intermediate compound resulting from the reaction between fluorine and U_3O_8 fines.)

Figure II-6

FLUORINATOR FOR URANIUM DIOXIDE PELLETS:
PIPING AND VALVE ARRANGEMENT FOR EXTERNAL FILTER

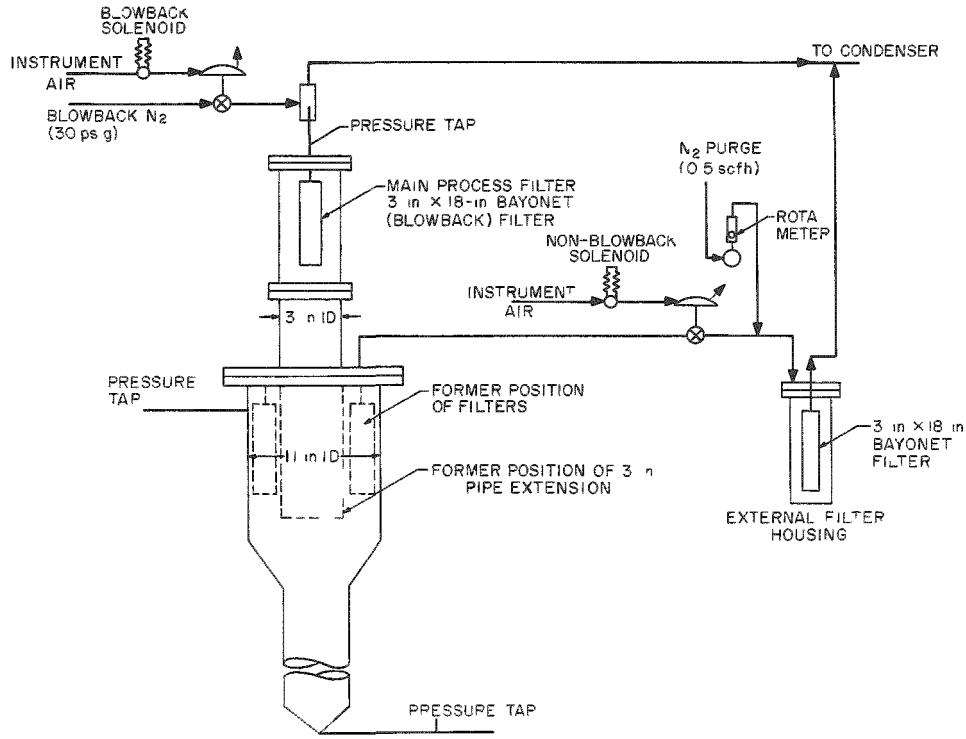

108-6841

From such information on the rate of fines accumulation, appropriate control action can be taken to limit the accumulation of fines in the system by reduction of the oxygen/fluorine ratio of the reagent gas input. However, an analytical time lag of $\frac{1}{2}$ to $\frac{3}{4}$ hr for a separate fluorine analysis is too long for fines control by regulation of the gas input. Hence, it is desirable to have a method of monitoring fluorine and uranium hexafluoride concentration in the off-gas continuously. For this purpose, a method employing thermal conductivity cells is currently being applied. With this system fluorine and uranium hexafluoride concentration in the off-gas can be plotted continuously on a strip-chart recorder.

In initial tests of the fluorine-analysis system, the gas feed for the thermal conductivity cell is taken from a point downstream of the uranium hexafluoride condenser and sodium fluoride traps. This gas contains oxygen, nitrogen, and fluorine. After the gas mixture passes through the

reference side of the cell, the fluorine in the mixture is replaced with chlorine (by reaction with sodium chloride) to form the sample gas analyzed by means of thermal conductivity. Output of the cell is, therefore, based on chlorine concentration, but the cell is calibrated to give readings in terms of fluorine concentration. Tests of the uranium hexafluoride analysis cell are to be made later.

Results of Fluorinations of Uranium Dioxide Pellets

Engineering-scale studies have continued on the development of a two-zone oxidation-fluorination scheme for the conversion of uranium dioxide pellets into uranium hexafluoride in a single reactor. In this scheme, the oxidation (lower) zone consists of uranium dioxide pellets with alumina grain filling the voids between the pellets. The fluorination (upper) zone consists of a fluidized bed of alumina grains which extends above the oxidation zone. By passing an oxygen-nitrogen mixture through the oxidation zone, U_3O_8 fines are produced. These fines are transported from the oxidation zone to the fluorination zone, where they are fluorinated to uranium hexafluoride vapor.

In two previous runs, 12-in.-deep beds of uranium dioxide pellets were converted to uranium hexafluoride in 15 hr when 4.5 percent oxygen in nitrogen was used as the oxidant and in 12.5 hr when 6 percent oxygen in nitrogen was used (see Runs UOF-68 and -69, ANL-6687, p. 117). Overall fluorine utilization efficiencies for these runs were 64.5 and 72.5 percent, respectively. In these runs, heat was conducted to the pellets from the fluorination zone, which was maintained at 500 C; no attempt was made to maintain predetermined temperatures in the oxidation zone. In these runs, fluorine input to the fluorination zone was diluted by a partial recycle of off-gas (0.25 cfm) to prevent plugging of the fluorine inlet. Gas pulsing was used to aid fines transport from the oxidation to the fluorination zone.

Another run (UOF-70) in this series has been completed with satisfactory results. A 12-in.-deep bed of pellets was completely reacted in 12.5 hr. The concentration of oxygen in nitrogen in the gas stream to the fluidized-packed bed was 8 percent. An overall fluorine efficiency of 75 percent was achieved. The operating conditions and results for Run UOF-70 are given in Table II-6 and in Figures II-7 and II-8. Good temperature control was achieved in this run, as in other recent two-zone runs.

The changes of the uranium hexafluoride production rates with time, shown in Figure II-7, were somewhat different than those obtained in the previous run, Run UOF-69. In Run UOF-69, production rates virtually doubled after 5.5 hr of operation, and reached a maximum of 107 lb UF_6/(hr)(sq ft) during the eighth hour, whereas in Run UOF-70, rate increases were more moderate and a maximum production rate of 82.5 lb UF_6/(hr)(sq ft) was achieved during the seventh hour. The uniformity in the rate of uranium hexafluoride production is shown by the plot of cumulative product gain with time in Figure II-8, and is taken to indicate good reaction control.

Table II 6

OPERATING CONDITIONS AND RESULTS FOR RUN UOF 70 A TWO ZONE OXIDATION FLUORINATION OF URANIUM DIOXIDE PELLETS WITH GAS PULSING

UO_2 Pellet Charge	Weight 8 8 kg Bed Height 12 in
Alumina Charge	Weight 7 1 kg (Blue Label Alundum) Static Height above Pellets 20 in Size Limits (U S Mesh) -40 +170
Temperatures	Fluorination Zone 500 C Oxidation Zone (Pellets) 340 ≤ T ≤ 480 C
Pulsing Conditions	Duration 0 04 sec Frequency 2 pulses/min Pressure 20 psig Gas Volume 0 016 cu ft/pulse
Oxygen Diluent	N_2
Fluorine Diluent	Process Off-gas (0 25 cfm)
Run Duration	12 5 hr (9 25 hr once through gas flow 3 25 hr total off-gas recycle)
Overall Fluorine Efficiency	75 percent

	Gas Flow					
	Oxidation Zone		Fluorination Zone			
Process Time (hr)	Rate (cfm)	O_2 (%)	Rate (cfm)	Average F_2 Input to Reactor (%)	Average Fluorine Utilization Efficiency[a] (%)	Average Production Rate [lb UF_6/(hr)(sq ft)]
0-3 5	1 04	8 0	1 44	10 2	69 4	37
3 5-8 5	1 04	8 0	1 51	14 4	85 8	68
8 5-9 25	1 04	8 0	1 42	9 4	46 4	23
9 25-12 5	(0 5 cfm gas recycle +0 06 cfm F_2)				42 3	9

[a] Fluorine utilization efficiency = $100 \left[\frac{3 \text{ (mole } UF_6 \text{ produced/hr)}}{\text{(mole } F_2 \text{ fed/hr)}}\right]$

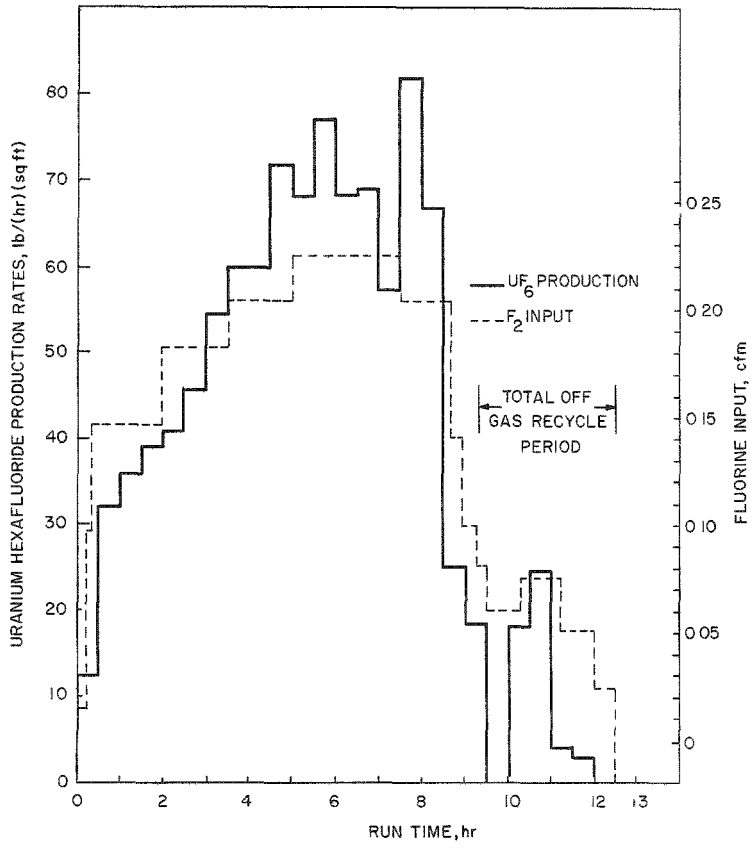

Figure II-7

URANIUM HEXAFLUORIDE PRODUCTION AND FLUORINE INPUT RATES FOR UOF-70. A TWO-ZONE OXIDATION-FLUORINATION OF URANIUM DIOXIDE PELLETS WITH GAS PULSING

(Run conditions in Table II-6)

108-6850

Figure II-8

CUMULATIVE URANIUM HEXAFLUORIDE PRODUCT COLLECTION FOR RUN UOF-70. A TWO-ZONE OXIDATION-FLUORINATION OF URANIUM OXIDE PELLETS WITH GAS PULSING

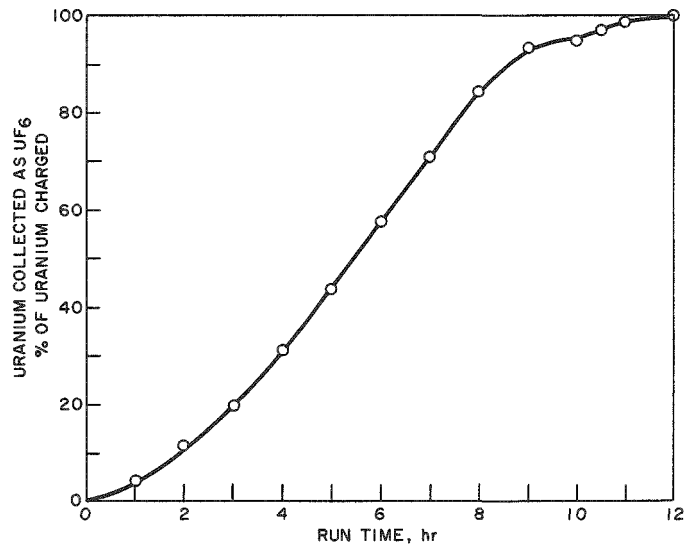

108-6896

During the first 9.25 hr of operation in Run UOF-70, once-through gas flow and a partial off-gas recycle of 0.25 cfm to the fluorination zone was used. During this period, a fluorine utilization efficiency of 78.6 percent (based on hexafluoride production) was achieved. The final 3.25 hr of the run was used to clean up the alumina bed with an enriched fluorine atmosphere using total off-gas recycle. This operation reduced the overall fluorine efficiency to 74.9 percent, which, nevertheless, is the highest efficiency yet obtained in two-zone oxidation-fluorination experiments.

The rates of fluorine input to the reactor are shown in Figure II-7. The average fluorine concentrations in the gas stream to the fluorination zone are given in Table II-6. In general, the method of comparing fluorine utilization efficiency for hexafluoride production with overall fluorine consumption calculated from fluorine analysis of the process off-gas was used to determine fluorine requirements needed to prevent fines accumulation. Continuous measurement of fluorine concentration in the off-gas was furnished by means of the thermal conductivity cell. The response time of the cell to a change in fluorine concentration at the reactor was determined to be approximately 4 min. Most of this time lag is due to the residence time of gas in the piping. This response time can be significantly reduced by shortening the length of the sample line.

Fluctuations in fluorine concentration in the process off-gas were apparent from the cell output. Because the thermal conductivity cell is sensitive to these fluctuations, it offers a significant improvement in process instrumentation over the previous grab-sample technique.

The use of a single, cooled, sintered-metal filter, a heated (400 C) disengaging section, and an alternate gas path during filter blowback gave very promising results during Run UOF-70. In general, pressure drop across the single filter was somewhat higher than that across the two parallel filters used previously. Although the total gas rate of 1.5 cfm (during the run period of 3.5 to 8.5 hr; see Table II-6) was 7 percent higher than that for a comparable period of uranium hexafluoride production during Run UOF-69, maximum differential pressures across the filter were 12 in. H_2O in Run UOF-70 and 7 in. H_2O in Run UOF-69. This result indicated that the solids loading of the exit gases had been reduced. At the same solids loading and gas rates, but with one-half the filter area, pressure drop is expected to increase by a factor of four.[4]

The bottom cone of the disengaging section was clean and the walls had a relatively light coating of solids. The single-process filter had a layer of solids which was similar to that normally obtained on each of the parallel filters previously used. The non-blowback filter in the bypass system had a barely discernible layer of oxide fines, thereby indicating that the non-blowback filter may not be necessary in similar operations.

Blowback frequency of the main process filter was once every 15 min; this compares with a blowback frequency of once every 30 min for each of the two filters in the previously used parallel arrangement (i.e., a blowback of a filter occurred every 15 min, alternating from one filter to the other).

The time required to collect 90 percent of the amount of uranium hexafluoride in tests with 12-in. deep beds of pellets is shown in Figure II-9 as a function of oxygen concentration in the oxidation zone. For purposes of comparison, it is noted that in Runs UOF-63 and UOF-64 (two-zone oxidation-fluorinations in which thermal gradients in the oxidation zone were present but in which no gas pulsing was used) the time required for 90 percent collection was 14 hr with 18 and 31 percent oxygen and 16 hr with 26 percent oxygen (see ANL-6648, pp. 137 to 143). As shown in Figure II-9, the required processing times were shorter with lower oxygen concentrations in two-zone oxidation-fluorinations with gas pulsing. These data also imply that the use of more than 8 percent oxygen with gas pulsing may not significantly reduce processing time, and that the concentration range 6 to 8 percent oxygen is satisfactory for high uranium fluoride production rates.

---

[4] D. B. Pall, Filtration of Fluid Catalyst Fines from Effluent Gases, Ind. Eng. Chem. 45 (6), 1197 (1953).

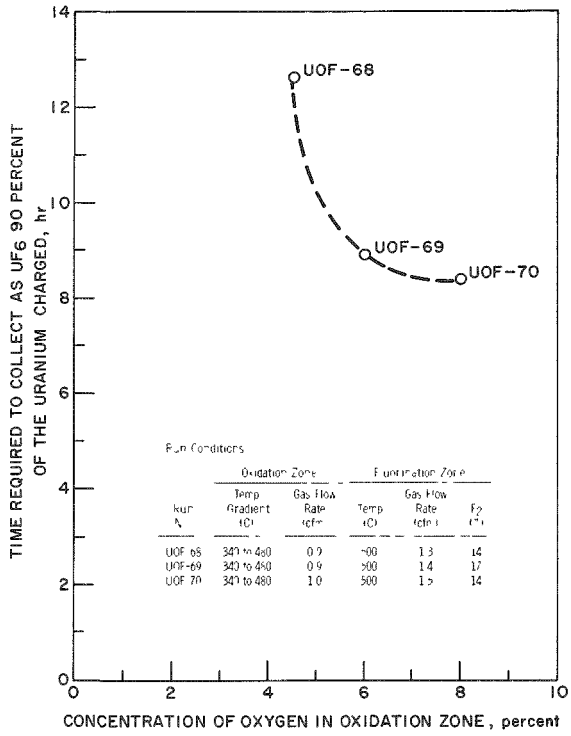

108-6879

Figure II-9

EFFECT OF OXYGEN CONCENTRATION ON THE TIME REQUIRED TO COLLECT 90 PERCENT OF THE CHARGED URANIUM AS URANIUM HEXAFLUORIDE

[For 12-in., fluidized packed beds of uranium dioxide pellets (8.8 kg UO_2) using two-zone oxidation-fluorination with gas pulsing.]

Uranium Material Balances for Runs UOF-68, UOF-69 and UOF-70

The uranium material balances for several recent two-zone oxidation-fluorinations utilizing 12-in.-deep beds of bare uranium dioxide pellets are shown in Table II-7. Material balances near 100 percent have been obtained since the recent addition of sodium fluoride traps downstream of the condenser; prior to the use of these traps, an empirical condenser efficiency of 96 percent was used for material-balance calculations. The average condenser efficiency for Runs UOF-68 to UOF-70 was 95.6 percent, whereas for individual runs the efficiencies were 95.0, 96.6, and 95.1 percent for Runs UOF-68, UOF-69, and UOF-70, respectively. For Runs UOF-68, UOF-69, and UOF-70, the overall uranium balances were 100 ± 0.4 percent.

Fluorination of Stainless Steel-clad Uranium Dioxide Pellets

The work described above has been directed toward the processing of beds of unclad uranium dioxide pellets. In the present period, work has been started on the evaluation of the two-zone technique for the processing of stainless steel-clad pellets. In these tests, uranium dioxide pellets are placed inside short lengths (about 1 to 2 in.) of stainless steel tubing to simulate sheared fuel elements. Longer-element sections with longitudinal slits are also being used in these experiments.

Table II-7

URANIUM MATERIAL BALANCES FOR RECENT TWO-ZONE OXIDATION-FLUORINATIONS OF 12-IN. DEEP URANIUM DIOXIDE IN FLUIDIZED PACKED BEDS

		Runs UOF-68 and UOF-69	Run UOF-70
Initial Weights (g)			
	UO_2 charged	17,610	8,851
	Al_2O_3 charged	7,087[a]	7,087
UO_2 Recovery			
As UF_6	in condenser (g UO_2)	16,726	8,407
	in NaF traps (g UO_2)	736	433
As Nonreacted UO_2 (g)		63	13[b]
As Uranium Compounds in Al_2O_3 (g UO_2)		20	28
Total U accounted for (as UO_2) (g)		17,545	8,881
Collection of UF_6 Product (% of U charged)		99.1	99.9
Final U Concentration in Al_2O_3 (w/o)		0.25	0.35
Overall Uranium Material Balance (%)		99.6	100.3

[a] Alumina was not removed from the reactor between Runs UOF-68 and UOF-69.

[b] 9.6 g of this material was UO_2 enclosed by a piece of stainless steel cladding.

Two experiments (Runs UOF-71 and UOF-72) have been completed in the 3-in.-diameter reactor with the objective of determining the completeness of removal of uranium dioxide pellets from short pieces of stainless steel cladding. These experiments were carried out by means of the two-zone oxidation-fluorination technique. In Run UOF-71, a 1.2-kg charge of pellets was used. The charge consisted of 40 stainless steel-clad elements which were $\frac{15}{16}$ in. long and contained two uranium dioxide pellets each, one segment which was $1\frac{3}{8}$ in. long and contained three pellets, and one which was $1\frac{13}{16}$ in. long and contained four pellets. Two stainless steel-clad pieces, which were about 5.2 in. and 10.3 in. long and which had been slit longitudinally, were also included in the charge. The height of the fluidized packed bed formed by the smaller pieces was about 2 in., with the longer pieces protruding above. A 100 percent removal of uranium dioxide from the cladding was achieved in 8.5 hr.

In the second experiment (Run UOF-72), a charge of 3.5 kg of uranium dioxide pellets was used. The pellets were clad in $\frac{15}{16}$ -in. long segments of Type 304 stainless steel (two pellets in each of 175 segments). The height of the fluidized packed bed was 6 in. In this run, 95 percent of the original uranium was removed from the cladding in 13.5 hr. Typical specimens of stainless steel-clad fuel segments before fluorination are shown in Figure II-10.

Figure II-10

TYPICAL SPECIMENS OF TYPE 304 STAINLESS STEEL-CLAD URANIUM DIOXIDE FUEL SEGMENTS

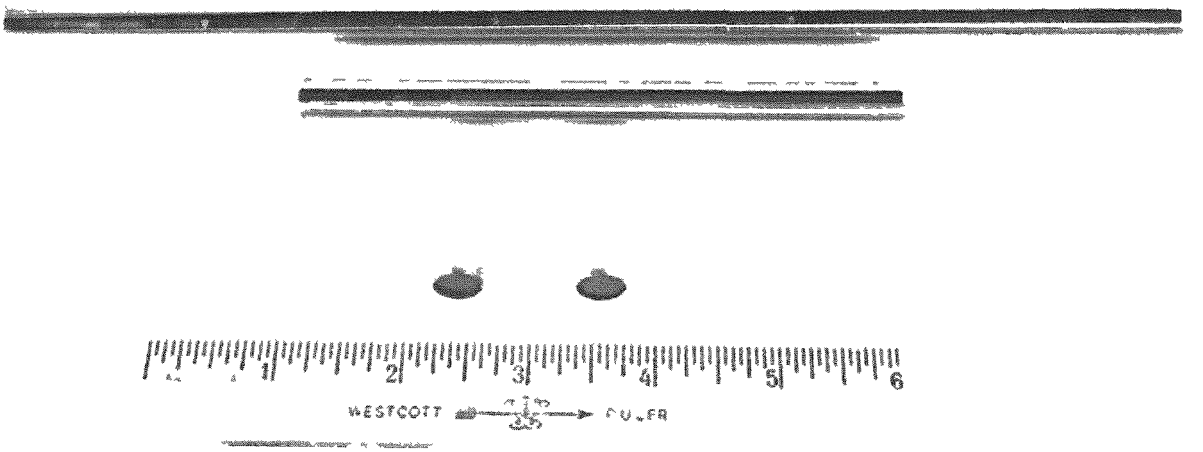

108-6163

The general operating conditions used in the decladding runs were similar to those used in recent runs with unclad pellets. However, the clad segments were exposed to higher oxygen concentrations than those used in runs with unclad pellets. In the present two runs, 22 percent oxygen in nitrogen was supplied to the oxidation zone, whereas 8 percent oxygen in nitrogen was used in typical earlier runs with unclad uranium dioxide pellets.

Run UOF-71

Operating conditions for Run UOF-71 are listed in Table II-8. With the oxidation zone (fluidized packed bed) at 450 C, the fluorination zone at 500 C, and with 22 percent oxygen being passed through the fluidized packed bed, a maximum uranium hexafluoride production rate of 31 lb UF_6/(hr)(sq ft) was obtained after 3 hr of operation After 4 5 hr of operation, the production rate dropped off to zero. At this point, 90 percent of the uranium originally present had been collected as the hexafluoride The remaining 10 percent of the uranium was fluorinated by passing fluorine through the fluidized packed bed and using total off-gas recycle. Overall fluorine efficiency, based on conversion to the hexafluoride, for Run UOF-71 was 26.6 percent.

Table II-8

OPERATING CONDITIONS FOR RUN UOF-71, A TWO-ZONE OXIDATION-FLUORINATION OF A FLUIDIZED PACKED BED OF STAINLESS STEEL-CLAD UO_2 PELLETS

UO_2 Pellets:	0.42-in. right cylinders	
Type 304 SS Cladding:	0.45-in. OD; 0.43-in. ID; 0.010 in. thick	
Materials Charged:	Weight of UO_2 Pellets:	1224 g
	Fixed Bed Height:	1.5 in.
	Weight of Cladding:	55 g
	Simulated Fuel Segments:	
	40 pieces 15/16 in. long (2 pellets each)	
	1 piece 22/16 in. long (3 pellets)	
	1 piece 29/16 in. long (4 pellets)	
	1 piece ~6 in. long (slit, 12 pellets)	
	1 piece ~12 in. long (slit, 24 pellets)	
	Weight of Alumina (Blue Label Alundum):	7.1 kg (size limits: -40 +170 mesh)
Pulsing Conditions:	Duration	0.04 sec
	Frequency	2 pulses/min
	Pressure	20 psig
	Gas Volume	0.016 cu ft/pulse
For Once-through Gas Flow (5.25 hr)		
Oxidation Zone:	Temperature	450 C
	Oxygen Concentration	22 percent
	Diluent	N_2
	Total Gas Rate	1.1 cfm
Fluorination Zone:	Temperature	500 C
	F_2 Concentration	4.2 to 10 percent
	Total Gas Rate	1.4 cfm
For Total Off-gas Recycle (3.25 hr)		
	Temperature	500 C
	Max F_2 Concentration	58 percent
	Total Gas Rate	0.59 cfm
Run Duration		8.5 hr

The forty-two smaller pieces of stainless steel cladding were recovered from the reactor in virtually the same form as charged; however, only small, thin fragments of the slit, longer sections of cladding were recovered. These fragments were about 1 sq in. in area by 0.003 in. thick. All of the stainless cladding sections had undergone fluorine attack, as was evident from surface scale formation. A photograph of the tubing elements after exposure to fluorine is shown in Figure II-11; one unexposed fuel segment is shown at the left. The reason is not known why in this run the stainless steel in the 6- and 12-in. segments were more severely attacked than the $\frac{15}{16}$-in. segments. Because the longer elements projected out of the packed bed and may have been carried upward out of the pellet bed, they may have been subjected to alternate oxidizing and fluorinating environments.

Figure II-11

APPEARANCE OF TYPICAL STAINLESS STEEL CLADDING RESIDUES AT END OF RUN UOF-71

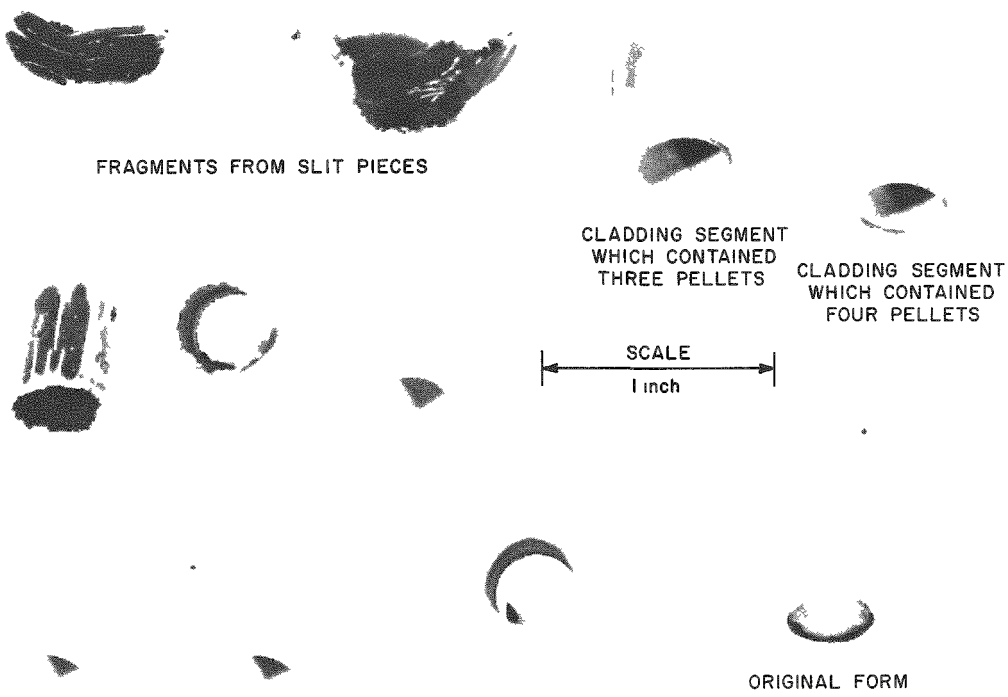

108-6899

Run UOF-72

For Run UOF-72, the height of the fluidized packed bed of clad pellets was increased to 6 in. The length of the stainless steel cladding segments was $\frac{15}{16}$ in. Operating conditions for this run are given in Table II-9.

Table II-9

OPERATING CONDITIONS FOR RUN UOF-72, A TWO-ZONE OXIDATION-FLUORINATION OF A FLUIDIZED PACKED BED OF STAINLESS STEEL-CLAD PELLETS

UO_2 Pellets:	0.42-in. right cylinders	
Type 304 SS Cladding:	0.45-in. OD; 0.43-in. ID; 0.010 in. thick	
Materials Charged:	Weight of UO_2 Pellets:	3484 g
	Fixed Bed Height:	6 in.
	Length and Weight of Cladding:	175 pieces 15/16 in. (length) 287 g
	Weight of Alumina (Blue Label Alundum):	7087 g (size limits: -40 + 170 mesh)
Pulsing Conditions:	Frequency	2 pulses/min
	Pressure	20, 30, and 40 psig
	Duration	0.04 sec
For Once-through Gas Flow (6.75 hr)		
Oxidation Zone:	Temperature	450 C
	Oxygen Concentration	22 percent
	Diluent	N_2
	Total Gas Rate	1.1 cfm
Fluorination Zone:	Temperature	500 C
	F_2 Concentration	4.0 to 10.3 percent
	Total Gas Rate	1.5 cfm
For Total Off-gas Recycle (6.75 hr)		
	Temperature	500 C
	Max F_2 Concentration	25 percent
	Total Gas Rate	0.56 cfm
Run Duration		13.5 hr

The initial operating conditions were identical with those used successfully in Run UOF-71; however, when the uranium hexafluoride production rates began to drop off after 3.5 hr of operation, pulsing pressures were increased in an effort to increase the rate of hexafluoride production. As shown in Figure II-12, the higher pulse pressures were not effective for this purpose.

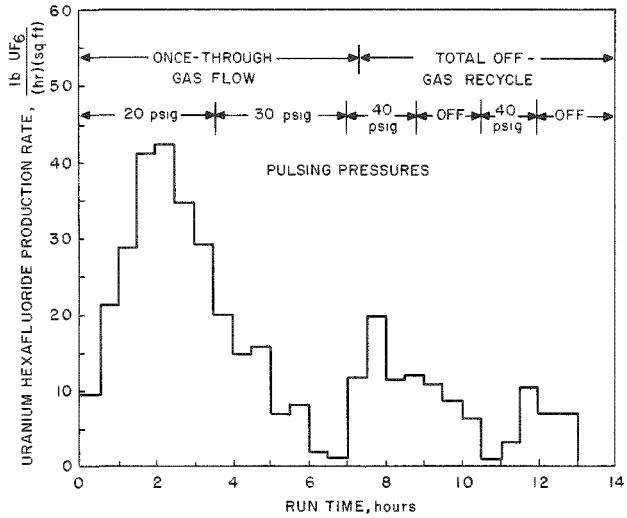

Figure II-12

URANIUM HEXAFLUORIDE PRODUCTION RATES FOR RUN UOF-72, A TWO-ZONE OXIDATION-FLUORINATION OF STAINLESS STEEL-CLAD URANIUM DIOXIDE PELLETS

(See Run Conditions in Table II-9)

108-6881

The maximum uranium hexafluoride production rate obtained in Run UOF-72 was 42 lb UF_6/(hr)(sq ft). In general, production rates were lower than those obtained in oxidation-fluorination experiments with bare pellets. The overall fluorine efficiency based on conversion to the hexafluoride was 51 percent in Run UOF-72.

In 6.75 hr, 67 percent of the uranium charge had been collected as uranium hexafluoride with oxygen passing through the oxidation zone (fluidized packed bed) and using once-through gas flow. The remaining 28 percent was fluorinated by passing fluorine through the fluidized packed bed and using total off-gas recycle. The total removal of uranium dioxide was 95 percent for a total run time of 13.5 hr.

Operationally, Run UOF-72 is not considered satisfactory because a high pressure drop occurred across the packed zone after 12.8 hr of operation, thereby indicating the formation of a caked bed. From subsequent examination of the bed, it appeared that cladding pieces at the bottom of the fluidized packed bed contained unreacted uranium oxide. From the appearance of this residual material, it is believed to be unconverted uranium dioxide. Incomplete conversion of the dioxide may have been caused by excessive cooling of the fluidized packed bed when larger quantities of ambient nitrogen were introduced into the system to increase the pulse pressure. Further studies of the two-zone scheme for the "decladding" and conversion of uranium dioxide fuels to uranium hexafluoride are being planned.

3. Oxidative Separation of Uranium Dioxide Fuel from Stainless Steel-clad Fuel Segments in a Fluidized Packed Bed

(M. Baerns, R. Kinzler)

Studies have been continued to determine the feasibility of the removal of uranium dioxide from stainless steel-clad fuel segments with both ends open by oxidation of the uranium dioxide to U_3O_8 in fluidized packed beds. The oxidation product, U_3O_8, tends to spall off the surface of the uranium dioxide because of the differences in density of the two oxides. In these tests, short fuel segments form a randomly packed (fixed) bed and alumina grain is fluidized in the voids of the packed bed. Air is used both as fluidizing and oxidizing gas. The U_3O_8 fines formed in this process mix with the fluid bed material and may be conveyed to a separate fluorination zone for the production of uranium hexafluoride.

The present studies of oxidative separation are intended to evaluate such a method of processing sheared or chopped fuel elements of the stainless steel-clad uranium dioxide type. This oxidation step could be performed as a separate step prior to the fluorination or incorporated into the two-zone oxidation-fluorination process carried out in a single vessel.

The results of the first five experiments of this type were presented in the preceding quarterly report (see ANL-6687, p. 124). In these experiments it was found that higher rates of removal were obtained by increasing the temperature from 350 C to about 450 C and by using gas pulsing. Removal rates were nearly constant for removals of up to approximately 80 percent of the uranium oxide. The runs were terminated before complete removals of uranium dioxide were obtained.

In the current tests, the emphasis was placed upon finding the conditions for complete removal of the oxide from the cladding. Additional runs were made in which the effect of bed temperature and of gas pulsing was studied further. However, a complete removal of the oxide was not achieved in any of these runs made thus far. A further effort is under way to investigate additional techniques for improving the oxide removal from sections of cladding. Three methods appear worthy of investigation:

(1) the fluorination of oxide residues (mainly U_3O_8) to uranium hexafluoride;

(2) mechanical agitation or vibration to loosen the oxide residues from the cladding;

(3) loosening of oxide residues by density changes involved in the reduction to UO_2 followed by reoxidation to U_3O_8.

Preliminary tests of method (1) are discussed in the previous section of this report. In this section are reported some scouting tests showing that methods (2) and (3) result in improved separation of the uranium dioxide from the cladding.

Experimental

The 2-in.-diameter reactor system used for these experiments was described in the preceding quarterly report (see ANL-6687, p. 125). In the first series of fluidized packed bed runs (Runs XO-1 to XO-14), the batch charge of each run consisted of a randomly packed bed (about 6 in. deep) of forty simulated fuel segments and fused alumina grain, which was fluidized in the voids of of the packed bed and above it. Each fuel segment consisted of two dense uranium dioxide pellets (0.42 in. in diameter and 0.42 in. in length) placed in close-fitting stainless steel (Type 304) tubes ($1\frac{1}{8}$ in. long by 0.5 in. in OD). The wall thickness of these tubes was 0.035 in. in Runs XO-1 to XO-8 and 0.010 in. in Runs XO-9 to XO-16. In Runs XO-15 and XO-16, the reactor was charged with 32 fuel segments and alumina grain. In these two runs, the packed bed of fuel segments was divided into four sections (see Figure II-13). Each section was approximately 1.5 in. high and was supported by a perforated plate.

Figure II-13

FLUIDIZED PACKED BED CONSISTING OF FOUR INDIVIDUAL PACKED SECTIONS

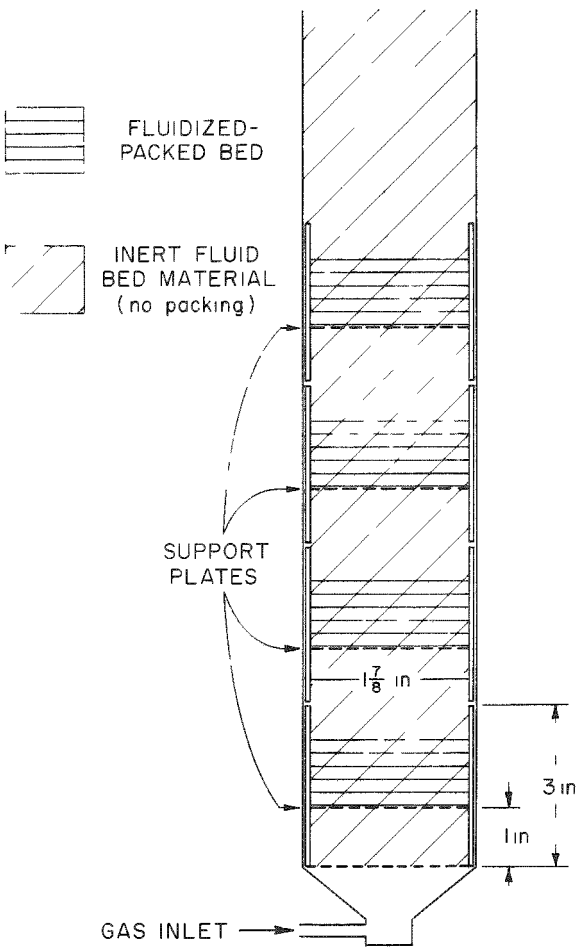

108-6858

The alumina grain was fluidized throughout the voids of the four sections. This arrangement was expected to improve the circulation of the alumina grain and to allow the fuel segments to have greater freedom of motion with gas pulsing. The bed was fluidized with nitrogen during the preheating period and with air during the oxidation. In the experiment in which U_3O_8 was reduced to uranium dioxide, a mixture of approximately 5 v/o hydrogen in nitrogen was used as fluidizing gas. Oxygen consumption in the fluidizing air was measured by a gas thermal conductivity cell in several experiments.

The primary purpose of measuring the oxygen consumption was to indicate the time at which oxygen consumption ceased.

A description of Runs XO-6 to XO-16, which were performed in this report period, is given below. Detailed conditions and experimental results are summarized in Tables II-10 and II-11. Runs XO-7

Table II-10

OPERATING CONDITIONS AND RESULTS OF OXIDATION RUNS FOR REMOVAL OF URANIUM DIOXIDE FROM STAINLESS STEEL CLADDING

Equipment: 2-in -diameter column
Inert Bed Charge: 740 g of fused alumina grain -40 +170 mesh
Oxidizing Gas: Air

Run No	Weight of UO_2 Pellets[a] (g)	Temperature (C)	Superficial Gas Velocity[b] (ft/sec)	Time of Reaction (hr)	UO_2 Removed (%)	Elutriated Fines (%)
XO-5 (pulsed)[c]	796	445 ± 10	0 75	9	86	53
XO-6 (pulsed)[c]	782	452 ± 10	0 75	14 75	86	54
XO-9 (nonpulsed)	795	550 ± 10	0 77	9	53	36 4
XO-10 (pulsed)[c]	798	400 to 490	Approx 0 75	15	67	30 5
XO-11 (pulsed)[d]	795 5	450 to 400	Approx 0 1	9	71	21 0
XO-12 (pulsed)[e]	797	Approx 390	Approx 0 74	9	58	6 4

[a]Added as forty random-packed pieces of simulated sheared fuel segments which were made by placing two UO_2 pellets (0 42-in diameter and length) in close-fitting stainless steel tubes These tubes were open at both ends

[b]Corresponding to reaction temperature and pressure

[c]Gas pulses introduced into bottom of reactor column Ten gas pulses of air every 15 min at a frequency of 10 pulses/min and a pulse duration of 1 sec

[d]Gas pulses were introduced into the bottom of reactor column throughout the run at a frequency of 6 pulses/min and a pulse duration of 1 sec

[e]Gas pulses were introduced into the bottom of reactor column after 2 5 hr of process time for the remainder of the run at a frequency of 6 pulses/min and a duration of 1 sec

Table II-11

OPERATING CONDITIONS AND RESULTS OF EXPERIMENTS FOR REMOVAL OF URANIUM DIOXIDE FROM STAINLESS STEEL CLADDING USING OXIDATION REDUCTION AND REOXIDATION OF THE FUEL

Equipment: 2 in -diameter column
Inert Bed Charge: 740 g (Run XO-13) and 1500 g (Run XO-14 to XO-16) of alumina grain (40 +170 mesh)
Oxidizing Gas: Air
Reduction Gas: 5 v/o hydrogen and 95 v/o nitrogen

Run No and Reaction Sequence	Weight of UO_2 Pellets[a] (g)	Temperature (C)	Superficial Gas Velocity[b] (ft/sec)	Time of Reaction (hr)	UO_2 Removed (%)	Elutriated U_3O_8 Fines (%)
XO-13	795					
Oxidation		410 to 480	2 0	5 75		
Reduction		500 to 600	1 8	4 25	65	
Reduction		550 to 600	1 9	2 5		
Reoxidation		430 to 460	1 6	4 5	80	64
				Total 17		
XO-14[c]	794					
Oxidation		420 to 470	0 8	6 5		
Reduction		580 to 610	1 1	3 75		
Reoxidation		435 to 465	0 8	3 5	74	26
Reduction		>10 to 590	1 8	3 75		
Reoxidation		440 to 455	1 6	3 75	80	37
				Total 21 25		
XO-15[c d]	639					
Oxidation		430 to 465	0 8	7 3	91	
Reduction		580 to 610	2 2	2 75	96	36
Reoxidation		445 to 465	0 8	3 25	100	39
				Total 13 3		
XO-16[c d]	641					
Oxidation		430 to 465	1 6	5 0		
Reduction		540 to 600	1 9	1 75		
Reoxidation		440 to 465	1 6	2 25	88	43
Reduction		580 to 605	2 0	1 33		
Reoxidation		435 to 450	1 6	2 00	98 8	50
				Total 12 33		

[a]Added as forty (Runs XO-13 and XO-14) and thirty-two (Runs XO 15 and XO-16) respectively random packed pieces of simulated sheared fuel segments which were made by placing two UO_2 pellets (0 42 in diameter and length) in close fitting stainless steel tubes These tubes were open at both ends

[b]Corresponding to reaction temperature and pressure

[c]Gas pulses introduced into the bottom of reactor column (frequency 2/min, duration 0 5 sec) Pulsing gas was air during oxidation and nitrogen during reduction

[d]Packed bed was divided into four individual 1 5-in -high sections (see text pp 149 and 153 and Figure II-14)

and XO-8 were eliminated from analysis because of malfunction of the temperature-measurement instruments.

Run XO-6

The conditions of gas pulsing in Run XO-6 were the same as in the previous Run XO-5: ten gas pulses of air were introduced into the column below the gas distribution plate (see ANL-6687, p. 125, Figure II-8) every 15 min at a frequency of 10 pulses/min and a pulse duration of 1 sec. During the pulsing period the continuous flow of fluidizing gas was turned off to maximize the pulse effect. On the basis of earlier observations made with this mode of pulsing, the upper fuel segments in the packed section of the bed are believed to be lifted and agitated by the gas pulsing. Final removal in this run was 86 percent.

Run XO-9

This run was performed at 550 C without gas pulsing. Poor removal of uranium oxide from the cladding is believed to be due to highly compressed U_3O_8 inside the cladding. Such a condition is consistent with the observation of bulging of the cladding which occurred in this run. Final removal was 53 percent.

Run XO-10

Gas pulsing was applied in the same manner as in Runs XO-5 and XO-6. However, after 1.6 hr of operation the bed became partially caked, as indicated by a temperature gradient (400 to 490 C) in the bed. This gradient persisted during the remainder of the run. Final removal was 67 percent.

Run XO-11

Gas pulses of air (frequency, 6/min; duration, 1 sec) were introduced into the reactor throughout the run. In addition, air at a constant velocity was fed into the bottom of the bed to provide enough oxygen for the oxidation reaction during the intervals between pulses. The velocity of the air stream (about 0.1 ft/sec) was less than the minimum gas velocity required for fluidization. This low velocity was used because earlier tests showed that gas pulsing moved pellets more effectively if the bed is not fluidized. In this run, a uniform bed temperature could not be maintained after 4 hr of reaction, probably because of poor fluidization. The temperature of the fluidized packed bed was initially 450 C, but as the run proceeded the temperature in the upper part of the bed dropped to 400 C. Final removal was 71 percent.

Run XO-12

It was planned to carry out Run XO-12 at 400 C without applying gas pulsing. However, a uniform temperature could not be maintained throughout the bed after 2.5 hr of reaction; to promote solids movement, gas pulses (frequency, 6/min; duration, 1 sec) were then introduced for the balance of the run. The maintenance of a uniform temperature (about 400 C) throughout the fluidized-packed bed was aided by the pulsing. Final removal was 58 percent.

Run XO-13

In this run higher gas velocities and an oxidation-reduction-oxidation cycle were used. The presence of U_3O_8 fines at sufficiently high concentrations in the alumina is believed to impair fluidization quality. In order to elutriate U_3O_8 fines from the bed in this run, the velocity of the fluidizing air was increased to approximately 2 ft/sec, which was about $2\frac{1}{2}$ times greater than that used in the previous oxidation runs. The oxidation, carried out at about 450 C, was terminated after 5.75 hr, since no further oxygen consumption occurred after this time (as indicated by the gas thermal conductivity cell). After the reactor system had been evacuated twice at room temperature to remove traces of oxygen, the temperature of the fluidized packed bed was increased while passing a stream of nitrogen through the bed. At 500 C, hydrogen was added to the nitrogen flow in an amount sufficient to give a concentration of about 5 v/o for the reduction. The reduction was terminated after 4.25 hr. The bed was then cooled, drained, and examined. Since it was not certain that the residues remaining in the cladding were completely reduced back to UO_2, the reduction was continued after recharging the reactor for an additional 2.5 hr under the same experimental conditions as those described above. The residual uranium dioxide was then oxidized again to U_3O_8. The oxidation stopped after 4.5 hr, as indicated by oxygen consumption. Final removal was 80 percent.

Run XO-14

Gas pulses of air (frequency, 2/min; duration, 0.5 sec) were here superimposed upon the fluidizing air stream. In this run, as in the following ones, the reactor was charged with twice the weight of alumina grain used in the previous Runs XO-1 to XO-13, because it was thought that the quality and temperature control of the fluidized bed might be improved by decreasing the concentration of U_3O_8 fines in the bed during oxidation. Temperature control did appear to improve. The complete treatment consisted of 6.5 hr of oxidation, followed by 3.75 hr of reduction, and finally, 3.5 hr of oxidation. However, a removal of only 74 percent of the oxide was obtained in this run, and the residual charge material was returned to the reactor, and the reduction (3.75 hr) and reoxidation (3.75 hr) procedures were repeated. The final oxide removal was 80 percent.

Runs XO-15 and XO-16

In these two runs the packed section of the bed was divided into four sections in the arrangement mentioned above. Gas pulsing (frequency, 2/min; duration, 0.5 sec) was superimposed upon the fluidizing gas. The reduction and reoxidation procedures were again applied (see Table II-11). No difficulties were experienced in maintaining a reasonable constant temperature throughout the bed. In Run XO-15, the U_3O_8 fines were separated from alumina grain after the first oxidation to improve the fluidization quality. This procedure is justified because the fines would be continuously transported from the oxidation zone in the two-zone oxidation-fluorination process. The final removal was complete in Run XO-15. At the end of Run XO-16, after the fluid bed was drained, an inspection of the fuel segments showed that some of the fuel segments had become wedged together in the two lower packed sections. These segments could not be moved by gas pulsing. The uranium oxide was not removed from these immobilized pieces, while the uranium oxide was completely removed from the other fuel segments, which were free and therefore capable of moving by pulsing. In Run XO-16, an additional reduction step and reoxidation step were performed to further improve the removal. The final removal was about 99 percent.

Discussion

The experimental results are summarized in Tables II-10 and II-11 in terms of the percentage of uranium dioxide that was removed from the stainless steel cladding in the various runs. The results are discussed below.

Effect of Temperature on the Separation

The results of the nonpulsed Run XO-9 and those of previous nonpulsed runs (Runs XO-2 and XO-3, ANL-6687, p. 126, Table II-12) indicate that the optimum temperature for the oxidative separation of UO_2 from metal cladding is between 400 and 500 C. Although the oxidation rate increases further with increasing temperature, the overall rate of removal decreases, probably because of compaction of the oxide in the cladding.

Effect of Gas Pulsing on the Separation

Gas pulsing increased the initial rate of removal of UO_2 as was shown in the preceding quarterly report (see ANL-6687, p. 127, Figure II-9), but the final amount of removed UO_2 could not be improved significantly. Comparison of the results of Run XO-5 with those obtained in Run XO-6 indicates that no improvement in separation occurred in Run XO-6 in spite of the 5 hr of additional run time. This is taken to indicate that gas pulsing

is not capable of achieving complete removal for the packed bed as a whole. The effect of pulsing is not uniform throughout the whole packed section of the fluidized packed bed. In several experiments, the stainless steel cladding tubes containing the UO_2 pellets were numbered, and the position of each tube in the reactor was known. In each experiment, the 40 tubes were divided into four parts, each containing ten tubes. The removal of UO_2 from the layer of fuel segments (Nos. 1 to 10) just above the gas distribution plate was poorer than the removal from the topmost layer of fuel pieces (Nos. 31 to 40). Some of these results, which are given in Table II-12, may be explained by the degree of movement or vibration of the fuel segments. The upper fuel segments are more readily moved and agitated than the lower ones. The motion of the fuel pieces, in turn, promotes the loosening and separation of the oxide residues from the cladding. A lesser degree of movability of the lower fuel pieces is certainly caused by the weight of the total bed that is resting on them. That this is actually the case was shown in Runs XO-15 and XO-16, in which the movability of the fuel pieces was assured by using very shallow beds with gas pulsing.

Table II-12

EFFECT OF POSITION OF SIMULATED 304 STAINLESS STEEL-CLAD FUEL SEGMENTS IN A FLUIDIZED PACKED BED ON THE OXIDATIVE REMOVAL OF URANIUM DIOXIDE FROM THE CLADDING

Run No.	Percent of Uranium Dioxide Removed from Each of Four Layers of Stainless Steel-clad Fuel Segments[a]			
	1st Layer (Nos. 1 to 10)	2nd Layer (Nos. 11 to 20)	3rd Layer (Nos. 21 to 30)	4th Layer (Nos. 31 to 40)
XO-9	41	55	49	68
XO-10	46	61	72	88
XO-11	51	74	88	70
XO-12	43	45	57	85

[a]A total of 40 stainless steel-clad fuel segments, each containing two UO_2 pellets, was divided into four layers, each layer consisting of ten segments. Segments No. 1 to 10 formed the bottom layer, and segments 31 to 40 formed the top layer in the packed bed.

Effect of the Reduction-Oxidation Cycles on the Separation

As a basis for this approach, it was assumed that the U_3O_8 which was not removed from the cladding by oxidation may be loosened enough that further oxidation is more effective in achieving separation from the cladding. A possible advantage of this reduction method over the fluorination method (see p. 150) is that the stainless steel cladding undergoes less reaction with hydrogen or oxygen than it does with fluorine. The results of the four experiments XO-13, XO-14, XO-15, and XO-16 indicate that some improvement can be obtained by the oxidation-reduction-reoxidation procedure.

Conclusions and Future Work

Complete separation of uranium dioxide from sheared fuel segments was not obtained by oxidation of the UO_2 fuel to U_3O_8 in a fluidized packed bed in these tests. Gas pulsing and a reduction-oxidation cycle were auxiliary techniques which resulted only in minor improvement in removal. However, it was shown that the separation can be significantly improved if the fuel segments are moved and agitated during the process. Therefore, some further considerations will be given to mechanical vibration of the fuel segments during the process to promote removal of uranium dioxide from stainless steel cladding under oxidizing conditions in fluidized packed beds.

4. Design and Construction of Plutonium Facility
(G. J. Vogel, E. L. Carls, W. Murphy)

Construction is under way of a facility for engineering-scale investigation of the several steps of a fluid-bed fluoride volatility process for recovery of fissionable values from spent nuclear reactor fuel of the uranium dioxide type and for reconstitution of the oxide fuel material after it is freed from fission products. In this process, the dioxides of uranium and plutonium are fluorinated to form volatile hexafluoride products. Subsequently, the hexafluorides are further purified by fractional distillation and converted back to dioxides by reaction with steam and hydrogen.

Because of the high toxicity of plutonium, it must be completely contained. Therefore, all equipment is being installed inside a large glovebox, 17 ft high by 25 ft long. The fluorination equipment is now being installed. The principal features of the facility have been described previously (see Summary Report ANL-6569, p. 110).

Essentially all of the process piping and valve installations in the large alpha-containment box and in the fluorine gas storage and supply system located in the fluorine cabinet have been completed. Current work is concerned chiefly with the instrumentation and auxiliary lines inside the glovebox. The installation and mounting of the fluorine pump has also begun.

The elevator lifts which provide personnel with complete access to glove ports at all levels of the large alpha box have been received and installed.

The Phase II subcontract for the installation of services and ventilation has been awarded. This work is scheduled to be completed early in September 1963.

Testing of process valves under extended use has been started. First results are described below.

Performance Tests of Process Valves

The Hoke LM 744 angle valve is being tested. These valves may be operated manually or, in remote operations, by air. Gas flowing through the valve is prevented from leaking to the atmosphere by a Monel sealing bellows which connects the valve stem to the body. A secondary Teflon packing seal at the stem is provided should the bellows fail. In the pilot plant, leakage through either will be determined by a pressure-drop method. Pressurized gas from a fixed volume will be supplied to the cavity between the bellows and the body.

Tests are underway to determine the number of times a valve can be cycled (that is, opened and closed) before the secondary Teflon seal leaks. The effect of cycling on seat wear will also be noted. In these tests, which were carried out at room temperature, the packing leakage was determined by pressurizing the cavity between the bellows and the secondary Teflon-packed stem seal with 15 psig He. The seat leakage was checked by connecting the outlet of the valve to a helium mass spectrometer leak detector, evacuating and spraying inlet of valve with helium. Table II-13 summarizes the results of the first cycling tests on an air-operated valve.

Table II-13

RESULTS OF LEAK TESTS OF PROCESS VALVES

Cycling Conditions: Valve opened and closed by automatic timer, 1 cycle/5 sec

Temperature: Approx 25 C

Time	Number of Cycles	Seat Leakage	Bellows Leakage	Leakage at Stem Packing
Specifications	-	0.1 μ cu ft/hr	0.0005 μ cu ft/hr	-
Initially	-	0.1 μ cu ft/hr	No detectable leak He leak detector	Not detectable leak with bubble test
4 hr	2880	Not checked	No detectable leak He leak detector	Not detectable leak with bubble test
20 hr	14400	High	No detectable leak He leak detector	High

The stem leakage which occurred between 2880 and 14,400 cycles of opening and closing the valve, was easily corrected by lightly tightening the packing nut, after which no escaping helium was detected by the mass spectrometer.

Examination of the seat and plug after disassembly of the valve disclosed an uneven groove formed on one side of the K Monel plug and an

apparent wearing down of the edge of the seating surface of the seat, which is made of standard Monel. Tests are being planned for the investigation of the duration of leak tightness of the valve seats and stem seals under elevated temperatures and of the means of servicing the valves after process installation.

5. Cleanup of Plutonium Hexafluoride from Cell Exhaust Air (R. W. Kessie)

A study is under way of methods of removal of plutonium hexafluoride (PuF_6) from air. The objective of this study is to obtain information needed for the design of equipment capable of cleaning up the ventilation air exhausted from gloveboxes or other plutonium-handling areas which might become contaminated with plutonium fluorides. The method studied was to react plutonium hexafluoride with water in the vapor phase to yield solid plutonyl fluoride ($PuOF_2$) and to pass the air through a high-efficiency filter. In a previous report (ANL-6596, pp. 123-125), the results were presented of experiments in which small-scale controlled releases of plutonium hexafluoride, 25 mg or less, were made into an atmosphere of known moisture content. The resulting air mixtures were passed at a controlled flow rate through AEC filters, a water bubbler, and Millepore filters in series. Alpha and gamma counts of filters were used to determine the penetration of plutonium hexafluoride through the filters. These earlier data are shown in Figure II-14.

Figure II-14

FRACTION OF RELEASED PLUTONIUM HEXAFLUORIDE PASSING THROUGH TWO AEC FILTERS

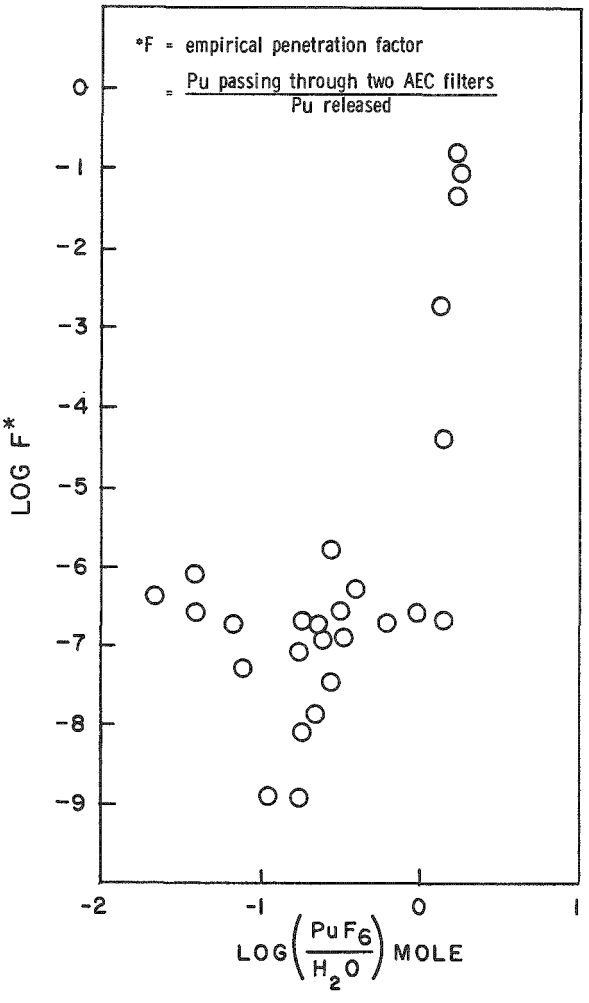

108-6852

The data in Figure II-14 show considerable scatter. One source of this variation is the different amounts of PuF_6 released into the moisture-containing atmosphere. The resulting differences in the production of plutonyl fluoride may affect the filtration by two mechanisms:

(1) The particles of the hydrolysis product may agglomerate at different rates before reaching the filter.

(2) Solid product may accumulate on the filter at different rates and may thereby affect the filter efficiency.

In order to obtain an improved correlation of filter efficiency by including the amount of PuF_6 released, a mathematical model was developed for the processes of agglomeration and of filtration under loading. This model may also serve to indicate the range of operating conditions in which the effects of agglomeration and filter loading are appreciable.

a. Model of the Agglomeration Process Affecting Filtration

In the model developed below, the change with time in the number of particles in the mixing chamber (up stream of the filter) is expressed in terms of simple mathematical relations for the processes of agglomeration and gas purging of the mixing chamber. The assumptions involved in deriving the mathematical expressions are given below:

1. The plutonium hexafluoride and water vapor are combined in a reaction chamber, where they are instantly reacted and the solid product is perfectly mixed, i.e., evenly distributed in the chamber. Subsequently, the product particles are swept out by air passing through the chamber and to the filters. The gas purge sweeps out particles regardless of size.

2. The hydrolysis product particles are initially of the same size (unagglomerated), and the range of sizes of the agglomerated particles may be described by a Poisson distribution.

3. All the penetration of the filter is due to unagglomerated particles, that is, the agglomerated particles make a negligible contribution to amount of material penetrating the filter. A penetration factor for unagglomerated particles is taken as a property of the filter.

Other workers have found that, when agglomeration alone is considered, the particle concentration varies with time as follows:[5]

$$\frac{1}{n} = \frac{1}{n_0} + Kt, \qquad (1)$$

where n is the number of particles per unit volume at time t, $n = n_0$ at $t = 0$, and

$$K = 4k\,TC/3\,\mu, \qquad (2)$$

[5]Handbook on Aerosols, United States Atomic Energy Commission, Washington, D. C., p. 69.

with k the Boltzmann constant, T the absolute temperature, C Cunningham's correction factor to Stokes' law, and μ the gas viscosity.

Differentiation of Equation (1) gives

$$-\frac{dn}{dt} = Kn^2. \tag{3}$$

This describes the change in particle concentration due to agglomeration alone.

The loss of particles in the mixing chamber due to the gas purge is treated as follows. Perfect mixing without agglomeration would give

$$-\frac{dn}{dt} = \frac{Rn}{V}, \tag{4}$$

where R is the gas flow rate and V is the volume of the mixing chamber. For both agglomeration and mixing, we have

$$-\frac{dn}{dt} = Kn^2 + (R/V)\, n. \tag{5}$$

Integration gives

$$-\int_{n_0}^{n} \frac{dn}{Kn^2 + (R/V)\, n} = \int_0^t dt, \tag{6}$$

or

$$n = \frac{n_0\, e^{-Rt/V}}{1 + (KVn_0/R)\left(1 - e^{-Rt/V}\right)}. \tag{7}$$

The effect of gas purge in Equation (4) may be expressed also in mass terms, in which form it is independent of agglomeration. The weight w of plutonium in the mixing chamber is independent of agglomeration, and the rate of decrease of w is given by

$$-\frac{dw}{dt} = \frac{R}{V} w \tag{8}$$

or

$$w = w_0\, e^{-Rt/V}, \tag{9}$$

where w_0 is the initial weight released at $t = 0$.

For the whole collection of particles in the mixing chamber, the initial (unagglomerated) particle weight m_0 is given by

$$m_0 = w_0/n_0V. \tag{10}$$

Similarly, the average particle weight m at any time is given by

$$m = w/nV. \tag{11}$$

The average number of particles, M, per agglomerate is the ratio of the average particle weight to the weight of the initial particle, and is given by

$$M = \frac{m}{m_0} = \frac{wn_0}{w_0n}. \tag{12}$$

Substitution of (7) and (9) in (12) gives

$$M = 1 + \frac{KVn_0}{R}\left(1 - e^{-Rt/V}\right). \tag{13}$$

The fraction p of unagglomerated particles is obtained by assuming that there is a Poisson distribution of the number x of (original) particles in an agglomerate. By the well-known statistical property of the mean we may write this as

$$p(x - 1) = \frac{(M - 1)^{(x - 1)}\, e^{-(M - 1)}}{(x - 1)!}. \tag{14}$$

Substitution of (13) in (14) and setting $x = 1$ for unagglomerated particles gives

$$p = e^{-(KVn_0/R)\left(1 - e^{-Rt/V}\right)}. \tag{15}$$

The total amount of plutonium passing through the filter is that fraction of unagglomerated material swept out of the mixing chamber which also is not trapped on the filter. Thus,

$$w_0P = \int_0^\infty np\,(w_0/n_0V)P_0R\,dt, \tag{16}$$

where P is the average weight fraction penetration measured and P_0 is the weight fraction of unagglomerated material that passes through the filter. This P_0 is a standard property of the filter (for a particular particle size) and is not the empirical, overall penetration P measured for agglomeration. The ratio P/P_0 is greater than one in all actual cases in

which some agglomeration occurs. Substitution of Equations (7) and (15) in (16) and letting

$$KVn_0/R = a \tag{17}$$

gives

$$\frac{P}{P_0} = \int_0^{\infty} \frac{e^{-Rt/V} + a\left(1 - e^{-Rt/V}\right) dt}{1 + a\left(1 - e^{-Rt/V}\right)}. \tag{18}$$

The change of variables

$$Z = 1 + a\left(1 - e^{-Rt/V}\right) \tag{19}$$

gives

$$\frac{P}{P_0} = \frac{e}{a} \int_1^{1+a} \frac{e^{-Z}\, dZ}{Z}. \tag{20}$$

This integral is known as the exponential integral and has been tabulated.[6] The function is plotted in Figure II-15.

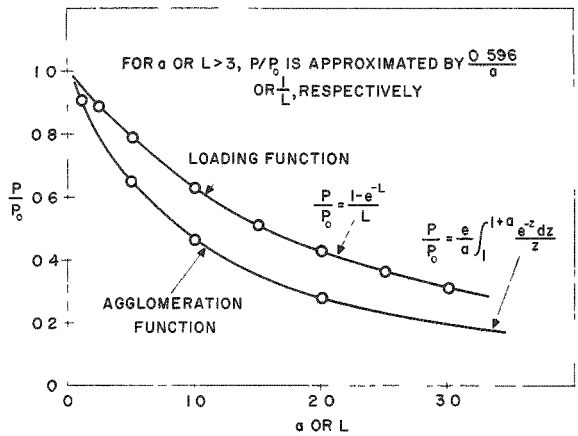

Figure II-15

AGGLOMERATION AND LOADING FUNCTIONS

108-6870

The function P/P_0 is the ratio of the weight fractions:

$$\frac{\text{measured penetration}}{\text{penetration by unagglomerated particles}}.$$

The abscissa a in Figure II-15 is the dimensionless agglomeration number defined in Equations (17) and (2) above in terms of physical constants, gas properties, flow rate, and the initial quantity of particles released.

---

[6] Tables of Sine, Cosine and Exponential Integrals, Federal Works Agency Work Projects Administration, New York City (1940).

b. Model of the Effect of Filter Loading on Filtration Efficiency

A model for filter loading was developed along the same lines as those used for the agglomeration process. A mathematical relation was initially taken for the instantaneous penetration of the filter and the total surface of the filter (including the loading of trapped solid); subsequently an integrated relation including the weight fraction of filter penetration was developed. Finally, in a subsequent discussion, a new correlation of experimental filtration data is discussed with reference to these models.

The following assumptions were made for filter loading:

1. For the type of filter and fume particles of interest, the diffusion mechanism of filtration is controlling.

2. The filtration performance at any instant of time is a function of the total surface of the filter, which includes both the surface of the filter medium and of the collected fume particles.

The diffusion mechanism gives for the instantaneous weight penetration

$$P_i = e^{-kA_t}, \tag{21}$$

where k is a diffusion constant for the process and

$$A_t = A_f + A_c w. \tag{22}$$

Here A_f is internal filter area and A_c is the specific surface area per unit weight w of the deposited fume particles.

The average penetration P integrated over the total collection of a single release starting with a clean filter is

$$P\, w_0 = \int_0^{w_0} P_i \, dw. \tag{23}$$

For a clean filter without loading

$$P_0 = e^{-kA_f}; \qquad k = \frac{\ln (1/P_0)}{A_f}. \tag{24}$$

Substitution in (21) gives

$$P_i = e^{-\frac{\ln (1/P_0)}{A_f}(A_f + A_c w)} \tag{25}$$

$$= P_0 \, e^{-A_c (w/A_f) \ln 1/P_0}. \tag{26}$$

Combination of (26) and (23) yields

$$\frac{P}{P_0} = \frac{1}{w_0} \int_0^{w_0} e^{-A_c (w/A_f) \ln (1/P_0)} \, dw \tag{27}$$

$$= \frac{1 - e^{-A_c (w_0/A_f) \ln (1/P_0)}}{\left(\frac{A_c w_0}{A_f}\right) \ln \frac{1}{P_0}}. \tag{28}$$

This function is plotted in Figure II-15 as

$$\frac{P}{P_0} = \frac{1 - e^{-L}}{L}, \tag{29}$$

where P/P_0 is the ratio of the same quantities defined in Section a above. However, the ratio here describes the decrease in the penetration of the filter due to loading. In Figure II-15, the abscissa L is the dimensionless loading number:

$$L = \frac{A_c w_0}{A_f} \ln \frac{1}{P_0}. \tag{30}$$

Thus, L relates P/P_0 to the specific area of the filter medium and of the fume, to the filtration efficiency of the unloaded filter, and to the weight of particles released.

c. Discussion of Experimental Results

The models developed above may be used as a basis for estimating the experimental conditions under which agglomeration and filter loading have important effects on filtration efficiency. For this application of the model, information is required about the surface area and size of the fume particles and the filter medium.

The size distribution of particles resulting from the vapor-phase hydrolysis of plutonium hexafluoride has been determined for one of the experiments of the type summarized in Figure II-14 and described

earlier in Summary Report ANL-6543, pp. 122-126. The particulate matter was produced from the release of 6.0 mg of plutonium hexafluoride into a 385-ml volume containing air at one atmosphere and water vapor at 7.66 mm Hg. The particles resulting from the hydrolysis were collected by an electrostatic precipitator, with a carbon film collector. From a photograph made by an electron microscope, the particle size distribution of the hydrolysis fume particles was determined; this result is shown in Figure II-16. The same figure shows the fiber size distribution of AEC filter media as determined in a separate electron photomicrograph. The electrostatic precipitator and the photographs of the filter were described previously in Summary Report ANL-6477, pp. 114 and 115. In Figure II-16, the ordinate values are the integrals of the frequency factor f from zero diameter to the diameter indicated on the abscissa. The data indicate that both frequency distributions are accurately described by the log normal frequency distribution. In Figure II-16 the mean particle size, dg, is based on the number of particles. Also shown is σg, the geometric standard deviation. Because of the high resolution (20 Å) of the electron microscope used in these measurements, it was possible to estimate the size of individual particles from the photograph even in the cases of agglomerates made of several particles. The size distribution of Figure II-16 is for unagglomerated particles.

Figure II-16

SIZE DISTRIBUTION OF HYDROLYZED PuF_6 AND AEC FILTER FIBERS

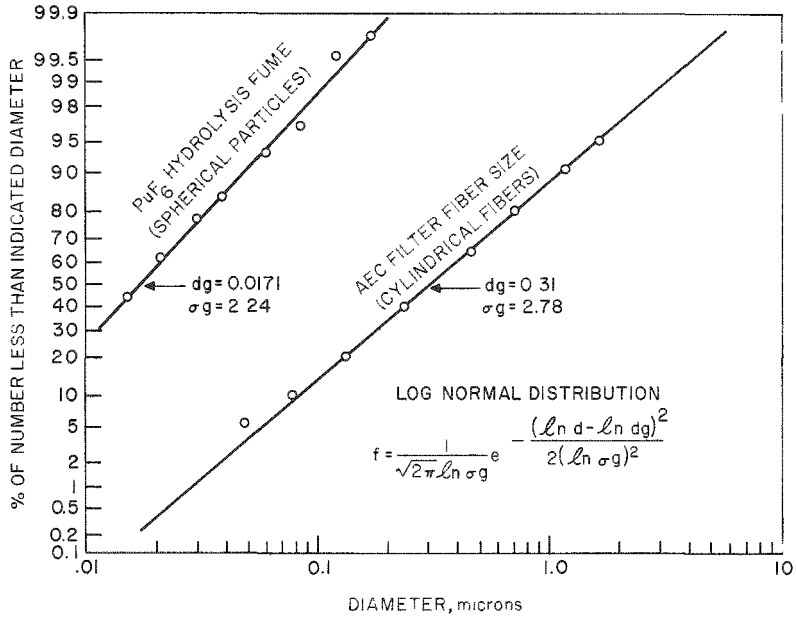

108-6890

The agglomeration effects of experiments made thus far may be evaluated in terms of the above determination of unagglomerated

particle size and the theoretical model developed in Section a above. The particle size distribution of Figure II-16 was converted to a weight basis, and the dimensionless agglomeration factor a was calculated from Equation (17) above, with the result that $a = 0.02 (w_0/R)$, where w_0 is the initial weight release of plutonium hexafluoride in milligrams and R is the air flow rate in ml/sec. In this form, the agglomeration factor does not contain the volume of the mixing chamber explicitly. In the experiments summarized in Figure II-14, releases up to 25 mg PuF_6 were used, and the values of a ranged from 8 to 140. Therefore, it appears that agglomeration has a significant effect. An important result here is that the value of a can be estimated for other operating systems.

The loading effect is evaluated in terms of surface areas according to the model in Section b above. The diameter of the particle of mean weight (derived from the distribution of Figure II-16) was approximately 0.1 μ. From this mean diameter it was estimated that the hydrolysis product of this particle size from 1 mg of PuF_6 had a surface area of 75 cm^2. The AEC filter medium had a total fiber surface of 77 cm^2/cm^2 of the superficial area. Thus, the total surface area of the filter was approximately doubled when the product from 1 mg PuF_6 was collected on one cm^2 of superficial surface area. In terms of the model, loading would be considered controlling when the loading factor L [see Equation (30) and Figure II-15] is greater than one.

In order to apply this agglomeration model to the plutonium-release experiments referred to above, L was calculated for the above-mentioned specific surface areas of the filter medium and the particles resulting from the hydrolysis of plutonium hexafluoride. A value of 10^{-4} was taken for the penetration factor P_0, which also enters into the calculation of L by Equation (30). The values of L calculated for the plutonium release experiments varied from 2 to 30. This result is taken to indicate that filter loading is just enough to be controlling in these experiments. From the same data, it was estimated that filter loading would have a significant effect on similar plutonium-release experiments where

$$w_0/A > 5,$$

where w_0 is the release of PuF_6 in milligrams and A is the superficial area of the AEC filter in square centimeters.

According to the above analysis, an effect of the quantity of PuF_6 released would be expected to appear in the filter penetration results shown in Figure II-14. Consequently, a function including both the overall penetration factor F and the weight w_0 of PuF_6 released may give a better correlation (against the PuF_6/H_2O mole ratio) than does F alone. Tests were made of Fw_0, Fw_0^2, and Fw_0^3; the best correlation was obtained

with Fw_0^2, which is plotted in Figure II-17. Although a good deal of scatter remains in Figure II-17, a greater regularity of the data points are shown here than in Figure II-14, and it is believed that this correlation is superior to the original one. The dependence of P/P_0 on the square of w_0 is what would be expected when the effects of agglomeration and loading take place simultaneously, since each factor (a or L) is proportional to w_0. Further experimental study will include the kinetics of the hydrolysis reaction, and attempts to improve and to generalize the correlation of results.

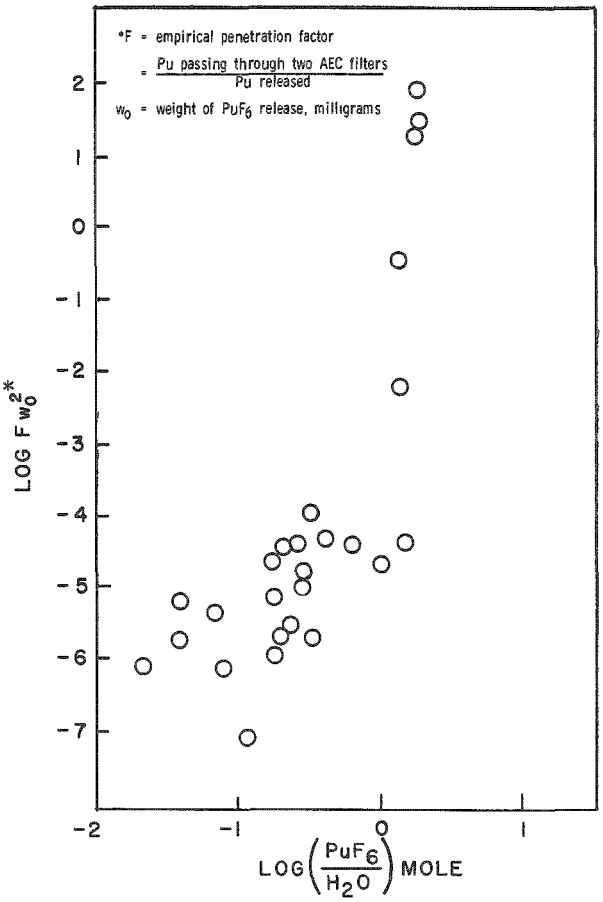

Figure II-17

CORRELATION OF DATA OF FILTER PENETRATION IN PuF_6 RELEASE EXPERIMENTS

108-6840

6. Basic Studies of Fluidized-bed Behavior Related to Process Operations: Solids Mixing
(J. D. Gabor, P. L. Katz,* and J. Savage)

A study was made of the mixing of particulate solids fluidized in the voids of a packed bed of larger, nonfluidized bodies. This study was carried out in support of work at Argonne National Laboratory on the application of inert fluidized particles in chemical reactor systems to improve the removal of the heat generated by the exothermic reaction of larger bodies. Heat transfer rates are dependent on the movement of

*Student Aide, Illinois Institute of Technology.

fluidized particles in such a system. A measure of the particle movement was achieved in this study by the determination of diffusion coefficients for the rates of solids mixing in the lateral direction for metal shot fluidized in the voids of spherical and cylindrical packing. Experimental data showed that the particle mixing was related to the void structure of the packed bed by a random-walk model. A general correlation was made for fluidized solids diffusivity in spherically packed beds.

There are few references to fluidized packed beds in the literature. Sutherland and Osberg[7] were interested in fluidized packed beds because the baffling effect of the fixed packing permits smooth fluidization (without slugging) for large height-to-diameter ratios. However, the baffling has some adverse effects in that it hinders the movement of the fluidized material. Recently, Ziegler[8] has published data and discussed the mechanism of radial heat transfer in fluidized packed beds. This work was performed at Argonne National Laboratory in cooperation with Northwestern University.

No work on solids mixing in fluidized packed beds was found. However, investigations of solids mixing have been made with fluidized beds (without packing). Bart,[9] Massimilla and Bracale,[10] and Hayakawa et al.[11] obtained quantitative measurements for longitudinal solids mixing in the fluidized beds. Work on solids mixing in fluidized beds in the lateral direction was done by Brötz.[12] Although the above references are interesting as to analysis and technique, the references do not indicate the effect that fixed packing would have on mixing rates.

In general, fluidized packed beds would be expected to show features which are combinations of those of packed beds and of fluidized beds. The primary motion of the fluidized material is determined by particle size and gas velocity, whereas the dimensions of the packed material determine the void structure within which fluidization takes place. The

---

[7]Sutherland, J. P., and Osberg, G. L., The Effect of Fixed Packing in a Fluidized Bed, Forty-Seventh Annual Meeting, AIChE, Baltimore (May 1962).

[8]Ziegler, E. N., Radial Heat Transfer in a Packed-Fluidized Bed, M. S. Thesis, Northwestern University (1961).

[9]Bart, R., Ph. D. thesis, Cambridge, Massachusetts Institute of Technology (1950).

[10]Massimilla, L., and Bracale, S., Ricerca Sci., 26, 487 (1956).

[11]Hayakawa, T., Graham, W., and Osberg, G. L., Canadian Research Council, unpublished data.

[12]Brötz, W., Chem. Ing. Tech., 28, 165 (1956).

present study concerns the measurement of mixing in the lateral (or radial) direction of solids fluidized in the voids of a fixed bed and the effect of system variables on the rate of this mixing.

Experimental Design

In the present study, the experimental method of measuring the rate of solids mixing was patterned after that of Brötz. The general method is based on the use of two solids which are similar with respect to the physical properties that determine mixing behavior, but which are different with respect to some property that is usable for analysis of composition. The analytical property employed by Brötz was color. In the present study, the differences in magnetic properties of nickel and copper were used. Since nickel and copper have the same density (8.9 gm/cc), it would be expected that nickel and copper particles having the same size and shape would exhibit identical fluidizing characteristics.

Determination of Solids Composition by Magnetic Separation

Pure copper and nickel particles are placed in a rectangular cell and are separated from each other by a centrally located partition. The particles are fluidized and when the partition is removed, mixing occurs on each side of the center line. After a certain mixing time, the fluidizing gas is cut off and the mixing is arrested. Bed samples are then taken at points of known distance from the original partition location. The samples are analyzed for weight concentration by magnetic separation. From the sample analyses and the locations at which the samples were withdrawn a concentration profile can be determined.

Diffusion Equation for Solids Mixing

A diffusion coefficient for the bed of fluidized solids was used to characterize the rate of solids mixing. The usual differential equation for diffusion in one dimension is

$$\frac{\delta C}{\delta \theta} = - \frac{\delta^2 C}{\delta x^2}. \qquad (1)$$

The key to the symbols used in the above equation and below is

C	Concentration, fractional weight
d	Diameter of fluidized particle, ft
D	Diffusion coefficient, sq ft/sec
D_p	Fixed packing diameter, ft
R	Half-width of column, ft

V_0	Superficial gas velocity, ft/sec
V_{0mf}	Minimum superficial gas fluidization velocity, ft/sec
x	Distance from center of column, ft
ϵ	Packing void space
θ	Time, sec

The solution of the above equation is given by Sherwood and Reed:[13]

$$C = \frac{1}{2} + \frac{2}{\pi}\left[\exp\left(-\left(\frac{\pi}{2}\right)^2 \frac{D\theta^2}{R^2}\right)\sin\frac{\pi x}{2R} + \frac{1}{3}\exp\left(-9\left(\frac{\pi}{2}\right)^2 \frac{D\theta^2}{R^2}\right)\sin\frac{3\pi x}{2R} + \frac{1}{5}\exp\left(-25\left(\frac{\pi}{2}\right)^2 \frac{D\theta^2}{R^2}\right)\sin\frac{5\pi x}{2R} + \text{-----}\right]. \quad (2)$$

In this equation, values of C are related to values of diffusion distance x in terms of the diffusivity D, one half the column width R, and the time θ of mixing. Thus, D was found from the value of the parameter which fit the experimentally measured profile of C as a function of x.

Apparatus and Procedure

A schematic diagram of the apparatus is shown in Figure II-18. Nitrogen, the fluidizing gas, was distributed by a porous metal plate

Figure II-18

SCHEMATIC DIAGRAM OF APPARATUS USED IN STUDIES OF MIXING OF FLUIDIZED PARTICULATE SOLIDS

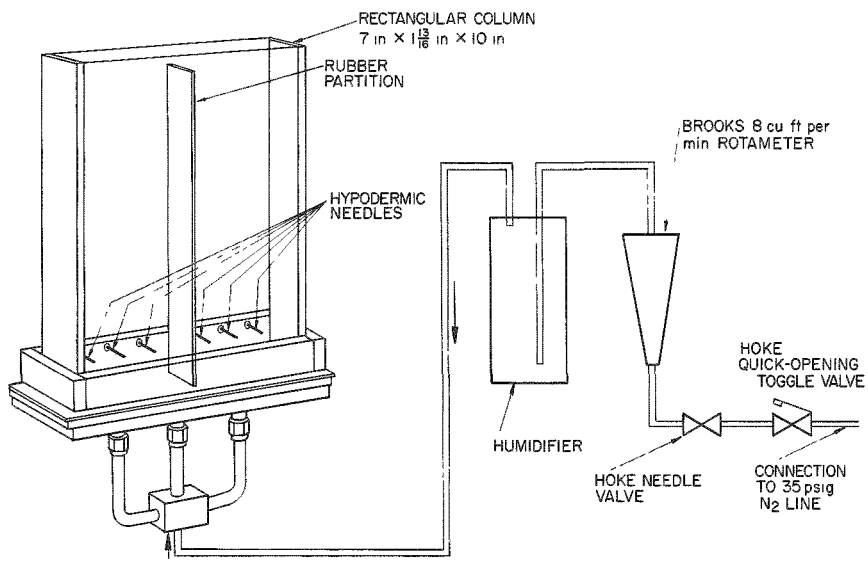

108-6193 Rev. 2

[13] Sherwood, T. K., and Reed, C. E., Applied Mathematics in Chemical Engineering, McGraw-Hill Book Co., Inc., New York (1939).

(not shown in figure). A rotameter measured gas flow rates. Sampling was accomplished by a horizontal row of $1\frac{1}{2}$-in.-long, fixed hypodermic needles, which were located $\frac{3}{4}$ in. above the bottom of the column, and were spaced 1 in. apart. Also, samples were taken by a 9-in.-long needle which was injected into the bed to the desired position. The concentration profile was invariant with respect to height because of high vertical mixing rates.

The fluidizing gas was humidified to prevent static charges on the fluidized particles by a separate 1-ft packed column partially filled with water.

The fluidizing material consisted of copper and nickel shot of -40 +50, -100 +120, -120 +200, and -140 +170 mesh sizes. Fixed packing consisted of $\frac{1}{2}$-, $\frac{3}{8}$-, $\frac{1}{4}$-, and $\frac{3}{16}$-in.-diameter steel spheres and $\frac{1}{2}$ in. x $\frac{1}{2}$ in., $\frac{3}{8}$ in. x $\frac{3}{8}$ in., and $\frac{1}{4}$ in. x $\frac{1}{4}$ in. brass cylinders. A set of runs was also made without fixed packing, i.e., a normal open-tube fluidized bed was used. The run time varied from 0.5 to 20 min depending on the gas velocity and the sizes of the fluidized particles. Smooth fluidization was attained in the order of about a second after introduction of the fluidizing gas. It was, therefore, expected that initial startup disturbance would have negligible effect on the data.

Experimental Results

The mixing experiments performed resulted in obtaining values of the diffusion coefficient D as a function of gas velocities for various fluidized packed bed systems. Variations of D were investigated for different sizes of spherical and of cylindrical packings as well as different sizes and heights of fluidized material. The results are presented also in the form of a general correlation which is closely related to the random-walk theoretical model. Reference cases for fluidization without packing are also presented.

Effect of Size of Spherical Packing

A series of runs was made with packing consisting of $\frac{1}{2}$-, $\frac{3}{8}$-, $\frac{1}{4}$-, and $\frac{3}{16}$-in.-diameter steel spheres and with 0.0038-in.-diameter copper and nickel shot. The data for the several packings are plotted as the diffusion constant D versus average gas velocity in Figure II-19. The diffusion coefficients increased with packing size over the range tested. Fluidization was also attempted in a bed of $\frac{1}{8}$-in.-diameter spheres, but the particle motion was greatly inhibited and channeling occurred. For open-tube fluidization (no packing), bed diffusion coefficients are about three and one-half times higher than for the same fluidized particles at the same superficial gas velocity in a bed containing $\frac{1}{2}$-in.-diameter

packing. These fluidized-bed data were for an expanded bed height of approximately 1 in. The open-tube fluidized bed mixing rate increased strongly with bed height; this effect is discussed further in a later section.

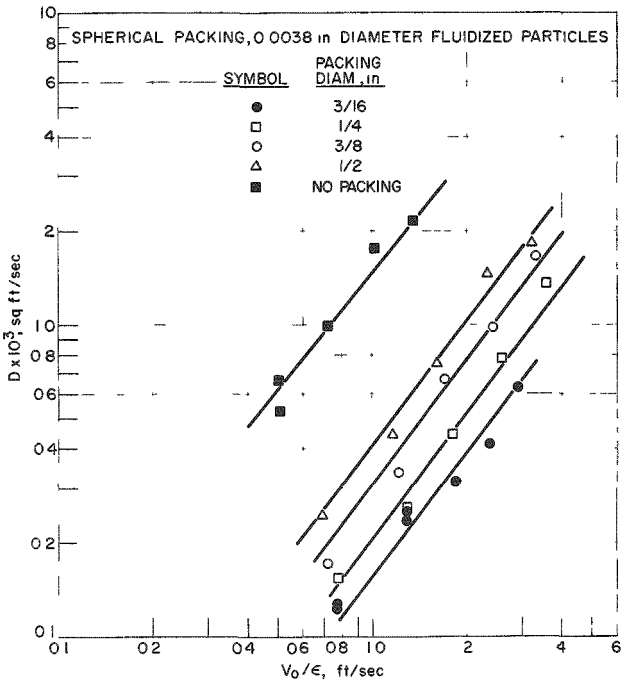

Figure II-19

EFFECT OF SIZE OF FIXED PACKING ON SOLIDS MIXING

108-6189 Rev. 2

The data in Figure II-19 indicate that the diffusivity D is directly proportional to the packing diameter D_p over the range of gas velocities used. This appears to be a general relation holding between the mixing rates of fluidized particles and the void structure of a packed bed of spheres in which the fluidization takes place. A mathematical theory of this effect has been developed and will be presented in a topical report. The mean particle velocities predicted by this theory are consistent with independent observations of particle velocity made photographically.

Effect of Cylindrical Packing

The solids diffusivities of 0.0038-in.-diameter fluidized particles in voids of cylindrical packing having the following dimensions: $\frac{1}{2}$ in. x $\frac{1}{2}$ in., $\frac{3}{8}$ in. x $\frac{3}{8}$ in., and $\frac{1}{4}$ in. x $\frac{1}{4}$ in., are plotted in Figure II-20. The slopes for these curves are somewhat less than those for spherical packing (see Figure II-19). Aside from the difference in shape, the larger cylinders exhibited a greater tendency for "bridging" than spheres when randomly packed. This bridging resulted in nonuniform void fractions throughout the bed and caused the results to be slightly erratic.

In order to determine if length of time of fluidization affected the solids diffusivity, a run was made with the $\frac{1}{4}$ in. x $\frac{1}{4}$ in. cylindrical

packing in which samples were taken after 2.15, 3.84, and 4.84 min of fluidization. The diffusivity was found to be time-invariant to within about 1.5 percent.

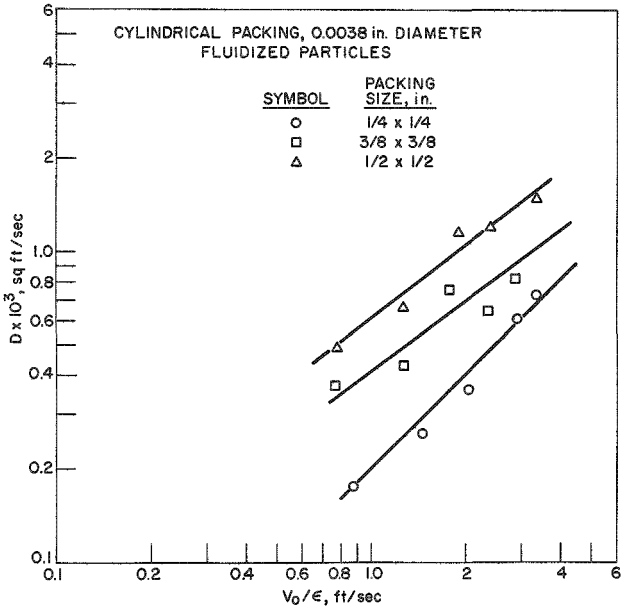

Figure II-20

DIFFUSION COEFFICIENTS FOR FLUIDIZED PACKED BED WITH CYLINDRICAL PACKING

108-6191 Rev.

Effect of Fluidized Particle Size

Runs were made with -40 +50, -100 +120, and -140 +170 mesh copper and nickel in the voids of $\frac{3}{8}$-in.-diameter spherical packing to determine the effect of particle size on mixing rates. Diffusivities versus superficial gas velocities for the various particle sizes are given in Figure II-21. The smaller-sized fluidized particles showed higher diffusivities.

Generalized Correlation

From the above data on the dependencies of solids diffusivity on system variables, a generalized correlation was made relating D/D_p to the fluidized particle diameter d and the average gas velocity in the voids of the packed bed, V_0/ϵ, as corrected for the minimum fluidization average gas velocity, V_{0mf}/ϵ. A plot is given in Figure II-22. In numerical terms the correlation is

$$D = D_p\left[\frac{V_0 - V_{0mf}}{d\epsilon}\right]^{1.15} \quad (1.22 \times 10^{-6}) \text{ sq ft/sec.}$$

In this dimensional equation, all units of dimension are in feet and seconds.

The effects of gas viscosity and fluidized particle density were not considered here.

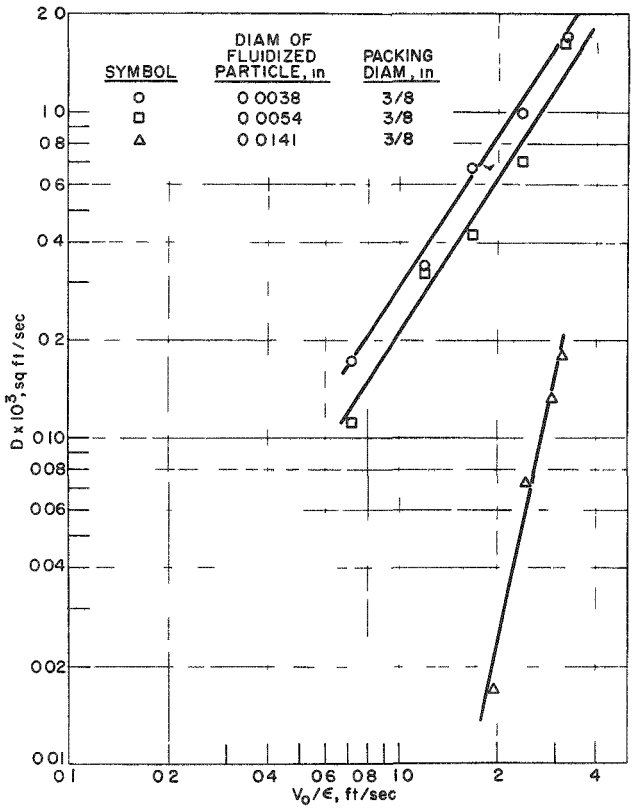

Figure II-21

EFFECT OF SIZE OF FLUIDIZED PARTICLES ON SOLIDS MIXING

108-6184 Rev. 3

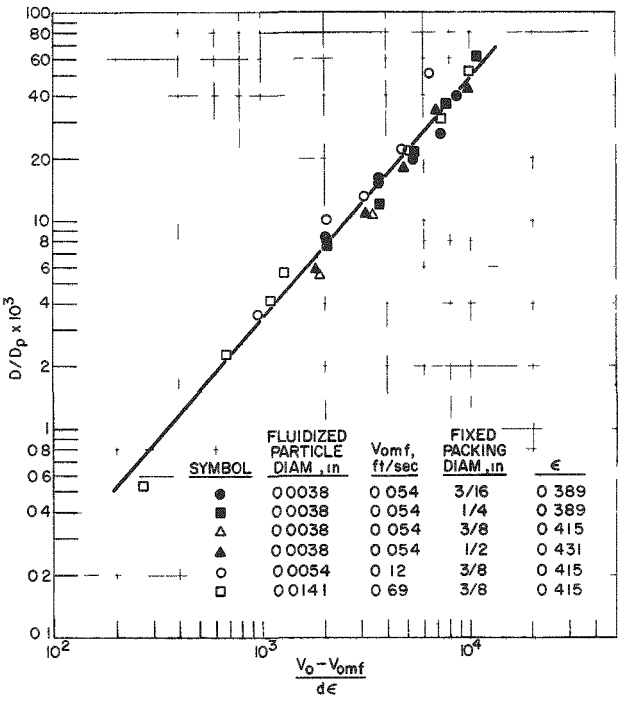

Figure II-22

GENERAL CORRELATION FOR SOLIDS MIXING IN A FLUIDIZED PACKED BED

108-6182 Rev. 2

The above correlation was made with narrow cuts in screen sizes. Several runs were made with -120 +200 mesh particles which have approximately the same average diameter as -140 +170 mesh particles (0.0038 in.) but have a greater spread in size distribution. A comparison was made of the effect of particle size distribution on the solids mixing for fixed packings of $\frac{1}{2}$-in.- and $\frac{1}{4}$-in.-diameter spheres (see Figure II-23). It was found that mixing is greater with -120 +200 mesh particles, i.e., with particles having a wider size spread. Also, it appeared that the diffusion coefficient for the -120 +200 mesh particles was not a simple logarithmic function of gas velocity. It was observed that with particles of this mesh size, the fluidized bed segregated into two phases when the gas velocities were increased sufficiently. There was a dilute, highly agitated phase in the upper portion of the packed bed, and a denser phase in the lower portion of the column.

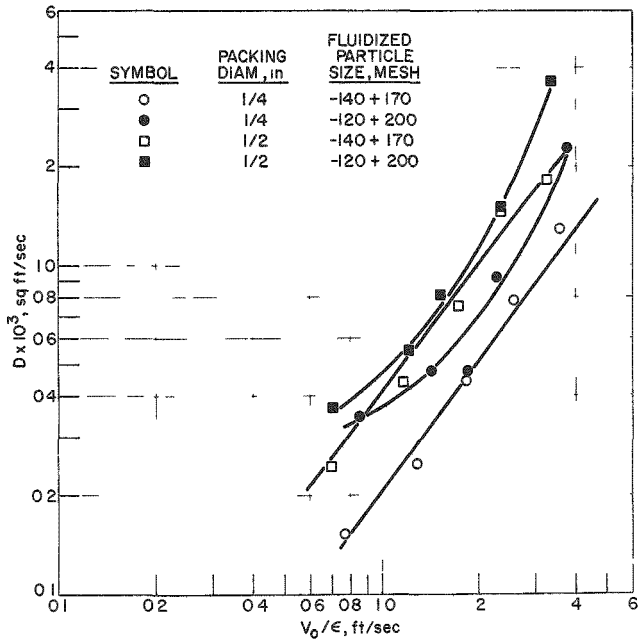

Figure II-23

EFFECT OF SIZE DISTRIBUTION OF FLUIDIZED PARTICLES ON SOLIDS MIXING

108-6188 Rev. 2

Effect of Bed Height for Fluidized and for Fluidized Packed Beds

A brief examination was made of fluidized-bed mixing, i.e., mixing with no fixed packing present. In Figure II-19, a comparison was made of the mixing rates of a fluidized bed (static height of 0.7 in.) and of fluidized packed beds. The mixing rate was greater for the fluidized bed because of the absence of baffling effects of fixed packing.

In the studies with the fluidized bed, it was also observed that slugging increased with depth of bed. As the slugging increased, the motion of the particles became more vigorous, and an increased incidence of

Figure II-24

EFFECT OF BED HEIGHT ON RATE OF LATERAL SOLIDS MIXING IN A FLUIDIZED BED

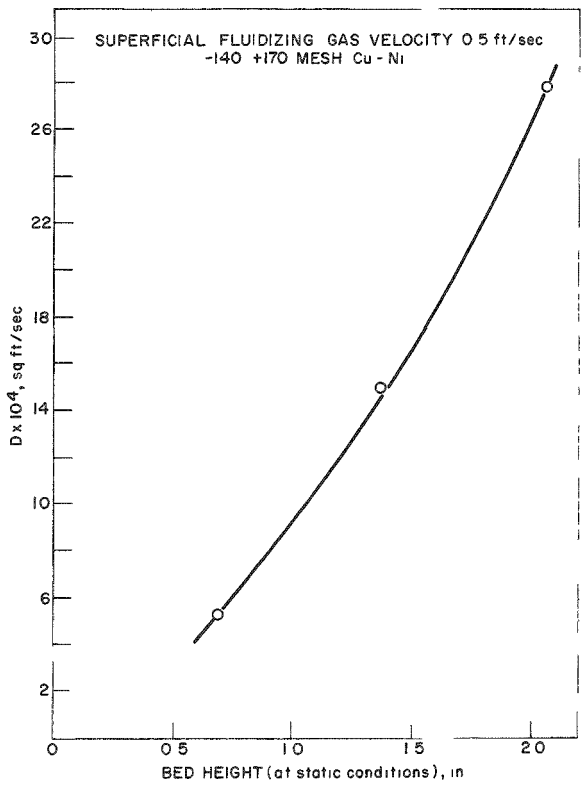

108-6190 Rev.

particles being thrown into the air occurred as a result of bubble bursts at the surface. Runs were therefore made to determine the effect of bed height on solids mixing for both the fluidized bed and the packed fluidized bed. Figure II-24 shows the relation of the solids diffusion coefficient to bed height for a fluidized bed. The fluidizing gas velocity was the same (0.5 ft/sec) in each of three runs. The bed depths were measured in the static condition. There was a very significant increase in solids mixing with increased height of bed. The expansion ratio for the fluidized bed at a gas velocity of 0.5 ft/sec was 1.4.

The mixing diffusion coefficients for three different initial fluidized particle bed depths ($1\frac{1}{8}$ in., $2\frac{1}{4}$ in., and $3\frac{3}{8}$ in.) for a fluidized packed bed with $\frac{3}{8}$-in.-diameter spherical packing were measured. Within the experimental accuracy there was no effect of height of fluidized bed on the diffusivity. The packing effectively baffles the slugs in the fluidized bed and, as a result, a smooth, uniform fluidization occurs. From the above data it is expected in practical cases that mixing in open-tube fluidization would be considerably greater than in fluidized packed beds.

Conclusions

1. The lateral mixing behavior of particles fluidized in the voids of a packed bed is not analogous to the random motion of gas molecules, but resembles eddy diffusion in a flowing gas stream.

2. A random-walk model may be used to relate these solids diffusivities to the void structure of the packed bed. Mean particle velocities calculated from this theoretical model appeared to be consistent with observations of particle velocity made photographically. Depending on the size of the particle, the particle velocity is a factor of four to two hundred lower than the average linear gas velocity in the packed bed.

3. A dimensional correlation for solids diffusivity in a spherically packed bed was empirically deduced and has the following form:

$$D = D_p \left[\frac{V_0 - V_{0mf}}{d\epsilon} \right]^{1.15} \quad (1.22 \times 10^{-6}) \text{ sq ft/sec.}$$

Velocity dimensions are in feet per second, and particle sizes are in feet. Further experimental work involving variation of gas properties and fluidized-particle densities is necessary before a completely generalized correlation can be made.

4. The rate of change of solids diffusivity with gas velocity is less for cylindrically packed beds than for spherically packed beds.

5. The rate of solids mixing increases with bed height for open-tube fluidization (no packing), but is virtually independent of height for fluidized packed beds.

7. Process Studies on the Recovery of Uranium from Highly Enriched Uranium Alloy Fuels
(N. Levitz)

A fluid-bed volatility process for the recovery of uranium from highly enriched uranium alloy fuels is being developed. Initial studies are being performed with uranium-zirconium alloy fuel. The process involves two highly exothermic reactions carried out in sequence, namely, hydrochlorination of the alloy, followed by fluorination of the residues to recover the uranium. During hydrochlorination, the zirconium is separated as the volatile tetrachloride (sublimation point, 331 C at 14.7 psia), while the uranium is retained as particulate chlorides. The uranium is recovered as the volatile hexafluoride during the fluorination step. The reactions are conducted in a fluidized bed of granular alumina which serves as a heat transfer medium. Solids entrained from the fluid bed are retained by a packed bed of granular alumina which serves as a filter.

The process studies are being conducted in a bench-scale fluid-bed reactor unit consisting of a $1\frac{1}{2}$-in.-diameter fluid-bed reactor connected in series with a $1\frac{1}{2}$-in.-diameter packed-bed filter section. The progress of the reactions is followed by the continuous measurement of the concentration of key reaction products by thermal conductivity cells.

Previous experimental results proved the feasibility of this fluid-bed volatility process. Granular, fused alumina (Alundum, a product of the Norton Company) has been found to be a satisfactory inert bed material under all the process conditions tested. High (~99 percent) overall recoveries of uranium have been achieved (see ANL-6648, p. 154, and ANL-6687, p. 141). Uranium losses were due primarily to: (a) retention of uranium by the alumina in the fluid bed and filter bed at the end of the reaction sequence, and (b) passage of uranium through the packed-bed

filter during the hydrochlorination step, either as a volatile chloride species or as particulate solids by entrainment in the gas stream. Generally, the uranium losses have been less than 0.2 percent of the uranium in the initial charge.

An aim of these studies has been to find conditions which would result in a minimal amount of uranium being retained by the alumina after a single reaction cycle. The concentration limit that has been set is a value corresponding to a loss of one percent or less of the uranium in the initial charge. In the current flowsheet, this loss is equivalent to a concentration of about 0.01 w/o uranium retained by alumina. A level of 0.03 w/o uranium in alumina was achieved in previous studies (see Summary Report ANL-6569, p. 115) when large quantities of hydrogen chloride and long hydrochlorination times (11 to 25 times stoichiometric, run duration up to 28 hr) were used prior to a two-step fluorination (the first step at 400 C and the second at 500 C). However, these conditions are unsuitable, because uranium loss appears to be a direct function of hydrochlorination time. In other studies, residual uranium levels in the range from 0.03 to 0.1 w/o were achieved by fluorination at 350 to 400 C; these levels were reduced to values in the range of 0.02 to 0.03 w/o by a follow-up high-temperature (500 C) fluorination (see ANL-6569, p. 149).

The following procedures were successful in limiting the retention losses to about one percent of the uranium in the initial charge:

(1) use of the same bed for successive hydrochlorination-fluorination cycles; in a series of five runs, the uranium concentration leveled off after the second use of the bed (see Summary Report ANL-6543, p. 150);

(2) use of a single fluorination after several successive hydrochlorinations, a modification of (1) above (see ANL-6648, p. 154, and ANL-6687, p. 141).

In current work, attempts were made to reduce the uranium retention further by employing a modified fluorination procedure in which the initial fluorination temperature was lowered and in which a high initial fluorine concentration was used. A series of runs is being made in which miniature multiplate fuel element subassemblies are being processed. The first two runs of this series have been completed, and the results obtained are reported below.

The early packed-bed filtration studies (see Summary Report ANL-6413, p. 138) were made with relatively fine alumina (-40 +200 mesh) in the filter beds. However, severe plugging of the filter occurred as a result of filling of the voids by the particulate solids entrained from the fluid bed (see Summary Reports ANL-6543, p. 150, and ANL-6569, p. 115).

Subsequently, use of graded alumina beds (-14 +20 mesh along with finer mesh material) that had larger voids was successful in reducing the plugging problem (see ANL-6648, p. 168). Currently, beds consisting entirely of -14 +20 mesh alumina are being used.

Related studies during this period were concerned with the fluid-bed hydrolysis of aluminum chloride, which simulated the processing of the off-gas from hydrochlorination of aluminum-based fuels. Also, installation was completed of the pilot-plant facility that is intended for a demonstration of the fluid-bed volatility process for enriched uranium alloy fuels. Shakedown work will be started soon with nonirradiated fuel material. Design of equipment for reprocessing studies of highly irradiated uranium-zirconium alloy fuel specimens is nearly complete. The study of the conversion of uranium hexafluoride to dense uranium dioxide particles was continued. The course of increase in density of a bed of uranium dioxide particles of relatively low initial density was investigated.

a. Hydrochlorination and Fluorination Reaction Studies on Uranium-Zirconium Alloy Fuels and Evaluation of Fixed-bed Filters
(D. Ramaswami, D. Goeser)

Process development studies of the hydrochlorination and fluorination steps of a fluid-bed volatility process for the recovery of enriched uranium from low uranium-high alloy fuels are being carried out in nickel equipment. Initial studies are being conducted on uranium-zirconium-alloy fuel. The assembly consists of a $1\frac{1}{2}$-in.-diameter fluid-bed reactor connected in series with a $1\frac{1}{2}$-in.-diameter packed-bed filter section. Granular alumina (Norton Company's Alundum) is being used as a heat transfer medium in the fluid-bed reactor and as a filter medium in the packed-bed filter section. The progress of the reactions is followed by means of thermal conductivity cells. Details of the apparatus, the associated equipment, and the experimental procedure were described previously (see Summary Report ANL-6569, pp. 114 to 118). The first two of a current series of runs with miniature uranium-Zircaloy-alloy fuel element subassemblies were made during this quarter; previously, alloy chips had been used.

Current Process Studies

A total of three fuel element subassemblies were processed (one in Run 37 and two in Run 38) in further attempts to improve the hydrogen chloride-fluorine reaction cycle. The effect of a modified fluorination procedure on uranium removal from two types of alumina (Type RR Alundum and the less costly Type 38 Alundum) was investigated. A lower initial fluorination temperature (250 C as opposed to 350 C) was coupled with high initial fluorine concentrations (about 50 percent from the outset instead of an initial concentration of about 10 percent).

The fuel element subassemblies consisted of three or four 5-in.-long by $\frac{7}{8}$- to 1-in.-wide, Zircaloy-clad, uranium-Zircaloy plates welded together.

The weights of the subassemblies were 160 or 183 g. Each subassembly was placed in the fluid bed (320 g of -40 +60 mesh, Type RR Alundum for Run 37 and 320 g of -80 +100 mesh, Type 38 Alundum for Run 38). The packed-bed filter contained 320 g of -14 +20 mesh alumina (Type 38 Alundum). The same filter bed was used for both runs.

The hydrochlorinations were conducted with the reactor wall temperatures maintained in the range from 300 to 415 C. The temperature of the fluid bed ranged from 335 to 500 C, depending upon the reaction rate. Alloy temperatures up to 750 C were noted during periods when the rates were highest. The two-step fluorination procedure was employed, a period at 250 C, followed by a period at 500 C. In both periods relatively high fluorine concentrations (50 to 90 percent) were used. The process conditions are summarized in Table II-14.

Table II-14

REACTION CONDITIONS FOR HYDROCHLORINATION AND FLUORINATION OF MINIATURE MULTIPLATE URANIUM-ZIRCONIUM FUEL ELEMENT SUBASSEMBLIES

Equipment:	$1\frac{1}{2}$-in.-diameter fluid-bed and $1\frac{1}{2}$-in.-diameter filter-bed sections.
Fuel Charge:	Uranium-Zircaloy-alloy subassemblies weighing 160 to 183 g each. One subassembly in Run 37 and two subassemblies in succession in Run 38. Average concentration of uranium - 1.0 w/o.
Fluid Bed:	320 g of fused alumina (Type RR Alundum) -40 +60 mesh for Run 37; Type 38 Alundum, -80 +100 mesh for Run 38.
Packed-bed Filter Bed:	320 g of fused alumina (Type 38 Alundum), -14 +20 mesh for Run 37; filter bed from Run 37 reused for Run 38.
Superficial Gas Velocity in Fluid Bed:	0.5 to 0.8 ft/sec.

	Reactant			Temperature (C)	
Run No.	Type	Concentration[a] (v/o)	Time (hr)	Fluid Bed	Filter Bed
37	HCl	0 to 76.0	7.3[c]	400 to 500	400
	F_2	50 to 65.0	2.0	250	250
	F_2	50 and 95.0[b]	2.0	500	500
38	HCl	0 to 90	13.6[c]	335 to 500	350
	F_2	50 and 90	1.0	250	250
	F_2	50 and 90	2.0	500	500

[a]Remainder nitrogen.

[b]Higher concentration of fluorine was used for the fluid bed only.

[c]The overall time for hydrochlorination was not optimum due to a planned shutdown to allow examination of the fuel charge.

The subassembly processed in Run 37 was examined after one stoichiometric amount of hydrogen chloride had been fed to the column. Penetration of all three plates was found to be relatively uniform and was more pronounced at the bottom of the subassembly, the region that was first contacted by the inlet gas. The top of the subassembly appeared completely unreacted, thereby indicating that very high utilization of the reactant gas was achieved during this period (2.5 hr). For Run 38, each subassembly was reacted to completion and then a single fluorination was conducted.

Results and Discussion

In the current experiments, the operations proceeded without difficulty, and the retentions of uranium by alumina were the lowest that have thus far been achieved; the concentration of uranium in alumina was reduced to less than 0.01 w/o (limit of detection by an X-ray spectrographic method). Although most of the fluorination periods were of 2-hr duration, analytical results of fluid-bed samples taken at intermediate times showed, with one exception, that only one hour at each temperature was needed to reach an equilibrium uranium value. The exception was the 2-hr fluorination at the higher temperature when Type 38 Alundum was in use (Run 38). The new fluorination procedure thus appears to enhance overall uranium recovery when either of these two types of alumina are used.

The final concentration of uranium in the packed-bed filter (-14 +20 mesh, Type 38 Alundum) after Run 37 was 0.007 w/o (as determined by wet chemical analyses). It is also of significance that the uranium concentration remained at this level after re-use during Run 38. No pressure buildup across the all-coarse Alundum down-flow filter bed occurred in either run. In view of the encouraging results obtained for Type 38 Alundum, this material will continue to be used in both the fluid bed and the filter bed.

Uranium Losses during Hydrochlorination

Correlation of the experimental data that have been accumulated to date indicates that the uranium loss through the packed-bed filter during hydrochlorination is a function only of the lowest temperature downstream of the fluid bed (but within the reactor system). A semi-log dependency was found (see Figure II-25), indicating that loss by vaporization is the probable mechanism. The probable vaporizing species is uranium tetrachloride (since the vapor pressure of uranium trichloride is negligible in this temperature range from 320 to 390 C). This dependency, plotted as average rate of uranium lost (as determined from the uranium content of the condensed zirconium tetrachloride phase) against $1/T$, appears to be unaffected by:

(a) the total mass of uranium in the initial charge (2 to 36 g);

(b) the rate at which the alloy is hydrochlorinated (average rates of 9 to 70 g of alloy per hour with instantaneous rates up to 110 g of alloy per hour);

(c) the quantity and mesh size of alumina in the filter section (in the range 90 to 14 mesh);

(d) the temperature of the filter bed alone (325 to 550 C).

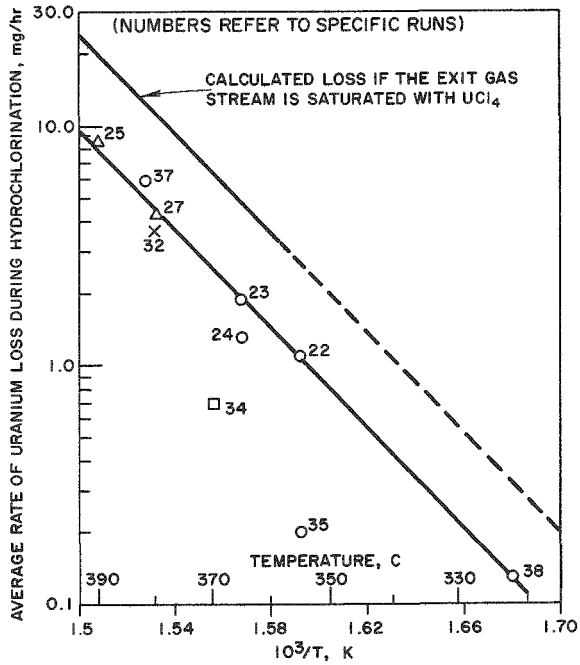

108-6885

Figure II-25

URANIUM LOSS DURING HYDROCHLORINATION OF URANIUM-ZIRCONIUM ALLOY FUELS

Average rate of uranium loss vs. 1/T, where T(K) the lowest temperature measured in the reactor assembly between the fluid bed and the distal side of packed-bed filter.

○ Hydrochlorination with packed-bed filter connected in series with the fluid bed.

× An empty 1-1/2-in. "settling" chamber installed between the fluid-bed reactor and the packed-bed filter.

△ Packed-bed filter connected in series with the fluid bed but contained no bed.

□ Hydrogen introduced along with the feed; packed-bed filter connected in series with the fluid bed.

Calculations based on reported values for the vapor pressure[14] of uranium tetrachloride indicate that the exit gas was about 50 percent saturated under most of the run conditions. The main conclusion to be drawn from this information is that to minimize losses the unit should be operated at as low a temperature as possible, especially in the region of the disengaging section above the fluid bed, in the connecting line between the two reactor sections, and in the filter section. In future studies, operating conditions will be modified with this in mind.

These results further suggest that the solution of the overall problem of retaining uranium in the system may not depend on filtration alone, but rather on a combination of filtration and condensation of a volatile species, with the latter being possibly of greater importance. This is somewhat indicated by the results of those runs in which an empty filter

---

[14]Stoller, S. M., and R. B. Richards, Reactor Handbook, Vol. II, Fuel Reprocessing, Interscience Publishers, Inc., New York (1961), p. 267.

chamber, maintained at operating temperature, was used (Runs 27 and 32, Figure II-25); for these runs the uranium losses were not extreme. The bare walls apparently provided sufficient surface for condensation.

Formation of Interhalogen Compounds during Fluorination

Infrared analyses* and mass spectrometric analyses** of the contents of the uranium hexafluoride cold traps from Run 38 were made to establish the extent of formation of interhalogen compounds under the current process conditions. The infrared analyses indicated that the cold traps contained the same fluorination products as those found during a previous run, in which treatment with phosgene and hydrogen chloride prior to fluorination was included. These products were uranium hexafluoride, chlorine trifluoride, and an unidentified material whose wave numbers were in the range of 535 to 560 cm^{-1} (see ANL-6596, pp. 151 and 152).

In addition to confirming the results obtained by infrared analysis, the mass spectrometric analyses revealed the presence of: (a) a large amount of chlorine and an insignificant amount of chlorine monofluoride, and (b) unidentified compounds with mass numbers 47, 51, 67, 83, 119, 131, and 169 (no further identification of these was made). Calculations indicate that about seven percent of the chlorine initially associated with the uranium after hydrochlorination was converted to chlorine trifluoride during fluorination. Further consideration will be given to treating the uranium chlorides with hydrogen fluoride as a safe means of removing the bulk of the chlorine (the uranium will be converted to the tetrafluoride) prior to the introduction of fluorine, thereby precluding the formation of chlorine trifluoride.

Future Work

Studies will be concerned with the effects of water vapor (at concentrations of the order of 1000 ppm) in the hydrogen chloride feed (a) on the hydrochlorination rates and (b) on overall uranium recovery, and with the effect of simulated fission products on overall uranium recovery and bed behavior (caking effects). Process studies on other types of fuels (e.g., uranium-aluminum alloy and UO_2-ZrO_2, clad with Zircaloy) are planned.

---

*Carried out by Dr. Martin J. Steindler and W. H. Gunther, Chemical Engineering Division, Argonne National Laboratory.

**Carried out by Dr. Martin H. Studier, Chemistry Division, Argonne National Laboratory.

b. Fluid-bed Hydrolysis of Zirconium Tetrachloride and Aluminum Trichloride
(K. S. Sutherland, D. J. Raue)

In the proposed fluid-bed volatility scheme for processing reactor fuels consisting of uranium alloyed with either zirconium or aluminum, the first step is the hydrochlorination of the fuel element. The resulting zirconium tetrachloride or aluminum trichloride vapor is a reactive waste product and must be converted to a stable solid form for satisfactory storage. One of the most stable forms is the oxide, and it is proposed that conversion of the chloride to oxide be effected by the hydrolysis reaction with steam in a fluidized bed.

Previous work (see ANL-6648, pp. 169 to 172, and ANL-6687, pp. 144 to 147) has demonstrated the feasibility of the process for zirconium tetrachloride for a wide variety of operating conditions. However, in the most recent runs (Run CO-45 to Run CO-48, see ANL-6687, p. 146) unexpectedly large quantities of fines (-200 mesh) were found in the final bed. Two further runs, made during this period in an attempt to discover the reason for the excessive fines production, were inconclusive for reasons discussed below.

In other current work the hydrolysis process was tested with aluminum trichloride.

Hydrolysis of Zirconium Tetrachloride

The two runs with zirconium tetrachloride (Runs CO-49 and CO-50) were carried out in a 6-in.-diameter reactor column under conditions identical with those of Run CO-48. At the end of each run a considerable quantity of unsublimed solid in the form of fine powder was found in the sublimation furnace, in the line between the furnace and the reactor, and in the section of the reactor below the distributor plate (see Summary Report ANL-6569, p. 119). Subsequent tests showed that between 7.5 and 10 percent of the feed material had remained unsublimed at 500 C ($ZrCl_4$ sublimes at 331 C). This batch of tetrachloride had been used in Run CO-45 and subsequent runs, and it is now believed that the presence of this unsublimable material was the cause of the high rate of fines formation. The fines were produced in the bed partly by transport of the fine unsublimed material into the bed and partly by attrition of bed material near the distributor plate. The majority of the 48 holes in the gas distributor plate were found to be plugged, and significant attrition in the region of the plate could have occurred as a result of higher-than-normal inlet gas velocities through the few (possibly as few as four) remaining unblocked holes.

Nevertheless, the work on the fluid-bed hydrolysis of zirconium tetrachloride has demonstrated that tetrachloride feed rates of

between 4 and 5 kg/hr can be processed in a 6-in.-diameter unit containing a bed of alumina or sand, 24 in. in depth and having a particle size distribution such that 90 percent is -60 +200 mesh. The bed should be maintained at a temperature near 350 C, and about three times the stoichiometric requirement of steam should be supplied, with an overall gas flow rate approximately twice the minimum fluidization value. In view of this satisfactory state of the zirconium tetrachloride hydrolysis work, the study of this reaction in the 6-in.-diameter unit was concluded. Any further investigation that might become necessary can be performed in the pilot plant now under construction.

Hydrolysis of Aluminum Trichloride

Insofar as a hydrochlorination processing plant might be called upon to handle aluminum alloy fuels in addition to those of zirconium, it was considered advisable to test the hydrolysis of aluminum trichloride under conditions similar to those used for zirconium tetrachloride. Accordingly, three runs were made with the equipment exactly as in Runs CO-49 and CO-50. Sand was used as the starting bed; a bed temperature of 300 C and a feed rate of about 4 kg/hr of aluminum trichloride were used. The steam rate was equivalent to four times stoichiometric.* Duration of the three runs totalled 9.5 hr. The runs were troublefree in operation, and excellent overall mass balances were obtained. No trace of aluminum was found in the off-gas stream.

It has thus been demonstrated that aluminum trichloride vapor can be hydrolyzed readily in a fluidized bed under conditions similar to those used for zirconium tetrachloride and at satisfactorily high rates. No further hydrolysis work in the unit is planned.

c. Pilot Plant Facility for Demonstration of the Fluid-bed Volatility Process for Recovery of Uranium from Enriched Uranium-Alloy Fuels

(N. Levitz, J. Barghusen, J. Holmes, C. Schoffstoll, W. Kremsner)

Installation of the pilot-plant facility for demonstration of the fluid-bed volatility process for reprocessing enriched uranium-alloy fuel has been completed. Final leak-checking of the equipment is in progress. During the ensuing quarter, operational tests of system components, such as the cold traps and the coolant system on the main reactor, will be made and will be followed by pre-fluorination and shake-down experiments. The planned program on nonirradiated uranium-zirconium and uranium-aluminum fuel material (up to 30 kg of alloy per charge) will then be initiated.

---

*Based on the reaction: $2AlCl_3 + 3H_2O \rightarrow Al_2O_3 + 6HCl$.

d. High-activity-level Studies of Enriched Uranium-Alloy Fuels
(J. W. Loeding, K. S. Turner)

Efforts directed toward the installation of a bench-scale, high-radiation-level facility to study the fluid-bed volatility process for highly enriched uranium-alloy fuels are continuing. Equipment design is nearly complete, and detailing of the design drawings is underway. Fabrication of the process equipment is expected to start during the next quarter. Irradiated fuel specimens will be used in resolving the following: (a) the distribution of fission products throughout the various process steps and the decontamination factors that may be realized, (b) the behavior of irradiated fuel with respect to reaction rate and the effect of radiation on uranium recovery and retention (losses) by the bed material, and (c) the short-term effects of radiation on process equipment and components, in general. In addition, experience in the design and operation of remotely operable equipment will be gained.

The equipment is similar to that currently in use for inactive fuel-reprocessing studies (see Summary Report ANL-6569, p. 114) and includes a $1\frac{1}{2}$-in.-diameter fluid-bed reactor and a packed-bed filter with associated equipment for the containment of volatile chlorides and uranium hexafluoride produced in the process. It is planned to install the proposed unit in an existing cave in the Chemical Engineering Division facilities during the latter half of 1963. Manipulators will be used for the operation and maintenance of the equipment.

8. Conversion of Uranium Hexafluoride to Uranium Dioxide: Preparation of High-density Particles
(I. Knudsen, N. Levitz, J. Kincinas)

A fluid-bed process for preparing high-density, spheroidal uranium dioxide particles directly from uranium hexafluoride is being studied. The process involves the reaction of uranium hexafluoride with a mixture of steam and hydrogen at temperatures of 650 to 700 C. Uranium dioxide particles with densities of 89 percent of theoretical density have been produced directly at 700 C; final particle densities of 96.5 percent of theoretical density were obtained by sintering in hydrogen at 1725 C. The dense uranium dioxide particles would be intended for use in dispersion fuels or in bulk form in packed fuel elements.

Previous work* has been concerned primarily with establishing the effect of process variables such as reactant concentration, reactant rates, reactor temperature, and bed height, on the density of the uranium dioxide product. The amount of steam in the reactant stream was found

*See Summary Reports ANL-6569, p. 121; ANL-6596, p. 158; ANL-6648, p. 173; ANL-6687, p. 149.

to have a pronounced effect on the particle density, near-stoichiometric* quantities resulting in maximum density. Other process variables had only minor effects on the density of the uranium dioxide product.

In earlier work, unusually rapid increases in particle density were noted when the starting bed was initiated. The aim of this study was to determine whether a procedure could be established for densifying a low-density material and to obtain data to aid in understanding the densification mechanism.

The studies are being conducted in a 3-in.-diameter cone-bottom Monel column described previously (see Summary Report ANL-6379, p. 183). In this unit, uranium hexafluoride is fed directly into a bed of uranium dioxide particles which are fluidized with the steam and hydrogen. The operating procedure involves alternating 30-min periods of uranium hexafluoride feed with 30-min periods of fluoride cleanup. During the cleanup period, only steam and hydrogen are fed in order to complete the conversion of the deposited solids to the dioxide. Product is removed semicontinuously (at the end of each cleanup period) in such an amount that the bed weight remains approximately constant.

In the current study (Run PY-72), the uranium dioxide used as a starting bed was of relatively low particle density, 6.7 g/cc (61 percent of theoretical density), and in the size range -20 +325 mesh [average particle diameter (volume/surface) of 192 μ]. The bed weight averaged about 5.5 kg during the run, thus providing a bed height (static) of about 8 in. The bed was pretreated with steam and hydrogen at 650 C for 4 hr. The pretreatment period was followed by 8 hr of run time at 650 C with a uranium hexafluoride feed rate of 25 g/min. The steam rate was 3.3 g/min (corresponding to about 1.3 times the stoichiometric requirement), and the hydrogen rate was 1.0 scfm. The combined steam and hydrogen flows, exclusive of nitrogen purges and uranium hexafluoride feed, gave a superficial velocity of 1.0 ft/sec. No seed particles were added during the run so that the changes in the starting material could be observed more readily. The uranium dioxide products were analyzed for changes in particle size, density, and surface area, and photomicrographs were made of sectioned particles.

Results

A 24 percent increase in particle density from about 6.92 to about 8.58 g/cc (values obtained for composite bed samples) was effected during the 8-hr hexafluoride feed portion of the run; little or no density change occurred during the 4-hr pretreatment with steam and hydrogen. The smaller particles were found to be more dense than the coarser material, about a 13 percent difference in density being noted between the

*Based on the reaction $UF_6 + 2H_2O + H_2 \rightarrow UO_2 + 6HF$.

-40 +60 mesh fraction and the -100 +140 mesh fraction (see Figure II-26). Density measurements of samples taken from the bed immediately after a hexafluoride feed period and again after the cleanup period gave similar results, indicating that densification occurred primarily during the hexafluoride feed period. The change in surface area of the material reflected the increases in density, for example, the area of -40 +60 mesh samples decreased from 0.7 sq m/g to 0.3 sq m/g during the run period. A total of about 0.84 bed equivalent of uranium dioxide was produced. Fines equivalent to 12 percent of the hexafluoride feed were found in the filter vessel.

Figure II-26

INCREASE IN DENSITY OF URANIUM DIOXIDE BED PARTICLES OCCURRING DURING DEPOSITION OF HIGH-DENSITY OXIDE FROM CONVERSION OF URANIUM HEXAFLUORIDE WITH STEAM AND HYDROGEN

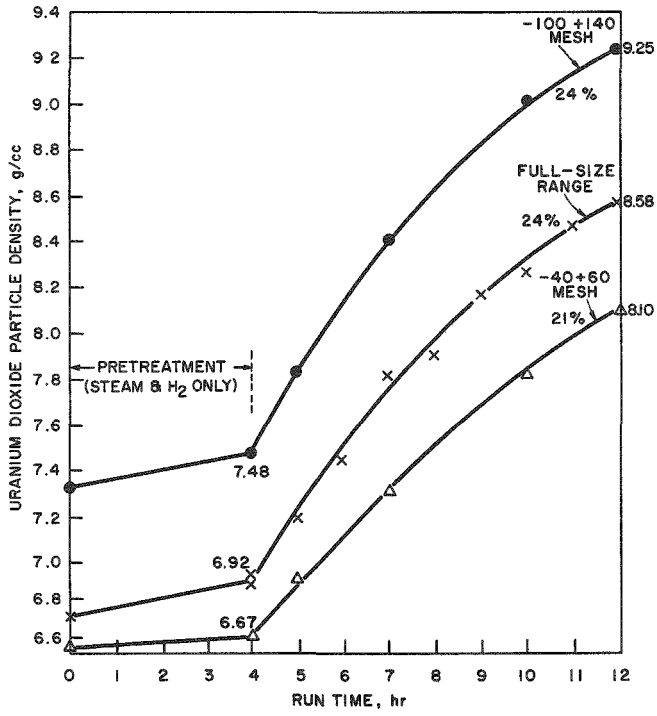

Run PY-72 Conditions

Temperature:	650 C
UF_6 Feed Rate:	25 g/min for 30 min/hr
Steam Feed Rate:	1.3 times stoichiometric requirement
Hydrogen Feed Rate:	1.0 scfm

108-6877

The behavior of individual particle size fractions of the bed during the run period is shown in Figure II-27. Unexpectedly, some breakup of the coarser mesh fractions (the -40 +60 mesh fraction and possibly also the +40 mesh fraction) was noted during the initial 2 hr of the pretreatment period. No overall particle growth was observed, although, during the latter part of the run, the -100 +140 mesh fraction increased as the next smaller fraction (-140 +200 mesh) decreased.

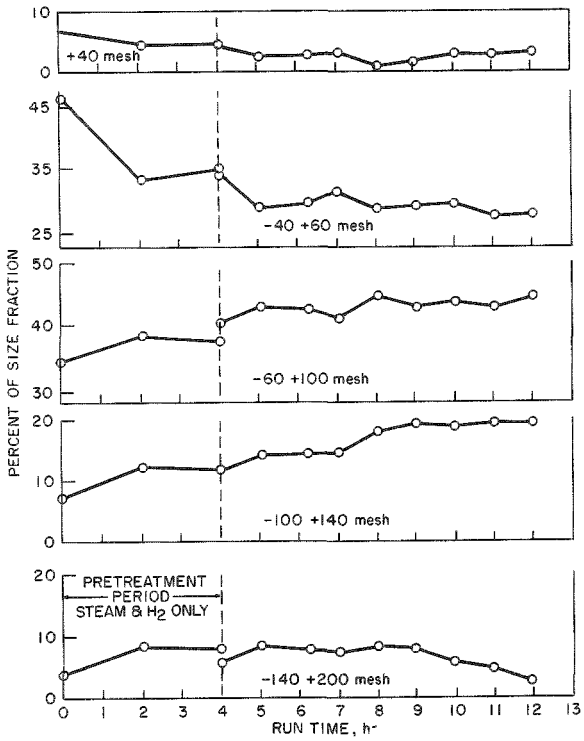

108-6853

Figure II-27

PARTICLE SIZE BEHAVIOR DURING THE CONVERSION OF URANIUM HEXAFLUORIDE TO URANIUM DIOXIDE IN A FLUIDIZED BED - RUN PY-72

After 4 hr, additional UO_2 was added to increase the size of the bed and sieve analysis of the bed was retaken.

Discussion

Calculations based on operational data (such as the quantity of hexafluoride fed, the rate of bed displacement, the average starting particle size) predicted a 19 percent increase in particle diameter and an overall increase in particle density of 12 percent. These calculations assumed the density of the deposited material to be 9.3 g/cc, the value achieved in previous studies under conditions similar to those used in the current run. The rapid and continued increase in particle density (up to 24 percent, see Figure II-26) and the unexpected phenomenon of no overall particle growth suggest that the entire particle mass was undergoing densification (referred to subsequently as "particle sintering") during the entire run. A concurrent process, "surface sintering," is believed to have occurred; low-melting mixtures of uranium dioxide and uranium tetrafluoride were presumably formed[15,16] during the deposition of the newly formed solids.

Evidence that "particle sintering" occurred is shown in the photomicrographs of sectioned particles (see Figure II-28). Particles from the starting bed (see Figures II-28a and II-28b) clearly exhibited large

[15]Ewing, R. A., and Bearse, A. E., Differential Thermal Analysis of Uranium Tetrafluoride-Uranium Dioxide Mixtures, BMI-1103 (June 1956).

[16]Barber, E. J., Solid-Liquid Equilibrium and Sintering Temperatures of Uranium Tetrafluoride-Uranium Dioxide Mixtures, KLI-3588 (1955).

Figure II-28

PHOTOMICROGRAPHS OF SECTIONED URANIUM DIOXIDE PARTICLES
BEFORE AND AFTER DENSIFICATION DURING RUN PY-72

Starting Material

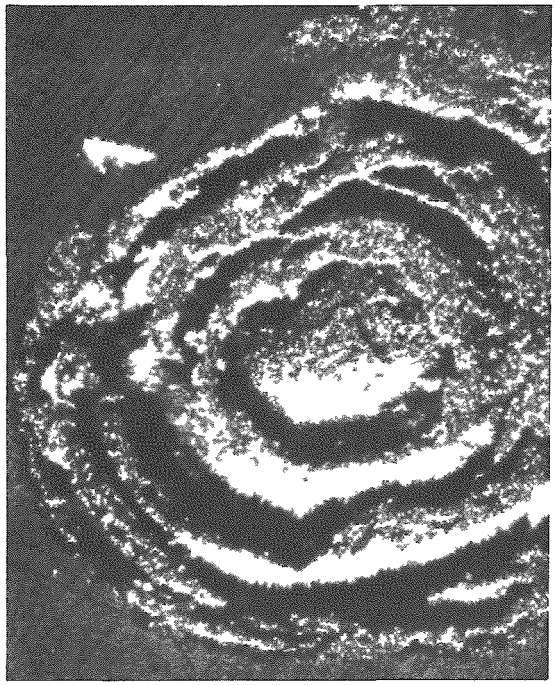

(a) -40 +60 mesh 266X

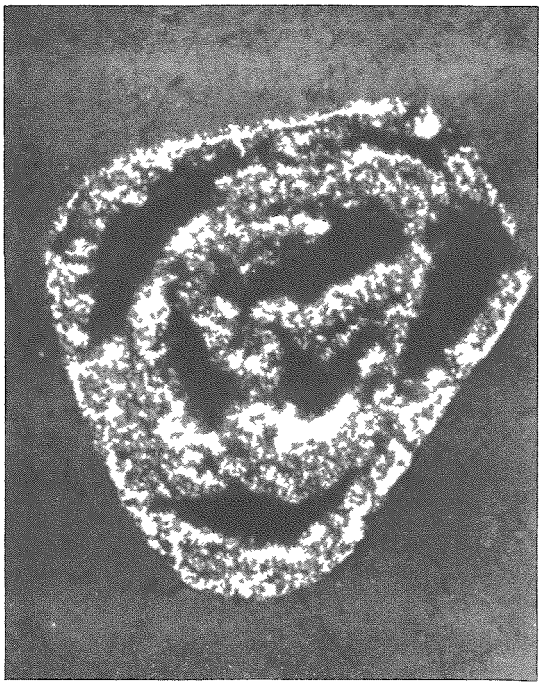

(b) -100 +140 mesh 400X

Final Product

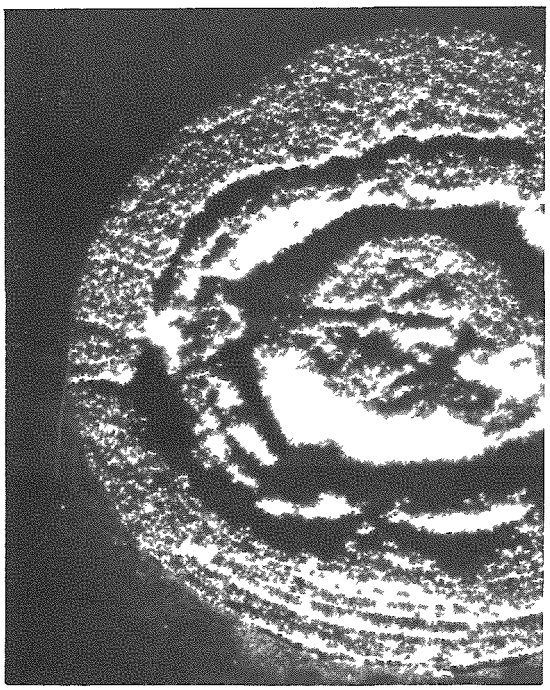

(c) -40 +60 mesh 266X

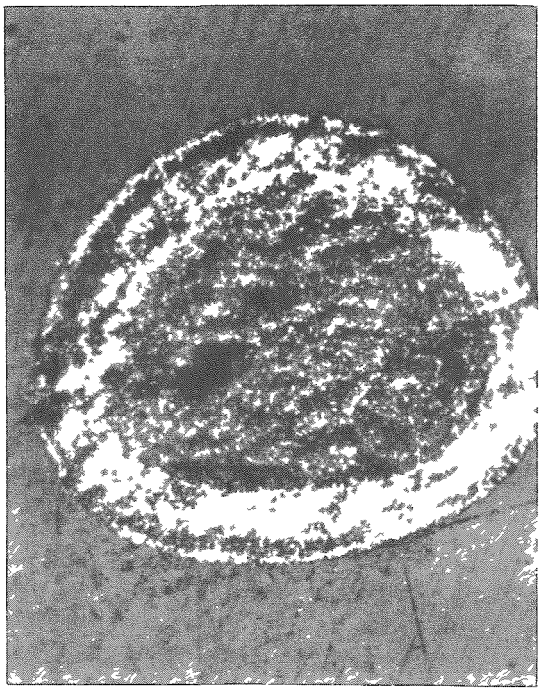

(d) -100 +140 mesh 400X

108-6898

voids and would be of relatively low density, whereas particles taken from the bed at the end of the run (see Figures II-28c and II-28d) showed a dense layer structure, the smaller particle appearing to be dense throughout. With such a densification mechanism in effect, the density of the smaller particles would reach a maximum first; particle growth would then commence. This was found to be the case in this experiment (see Figure II-27). With additional time, the particles in the remaining fractions would also reach a maximum (or steady-state) density value. The current scheme thus appears to be suitable for upgrading low-density material.

Future Work

Future work will be concerned with determining the effect of the return of filter fines to the bed on the preparation of dense particles. The filter vessel will be relocated directly above the reactor to facilitate this work. Evaluation of the product in compaction tests is planned.

The feasibility of preparing, by the current fluid-bed techniques, "homogeneous" UO_2-PuO_2 solids for plutonium recycle applications will be determined in a unit now being designed. Operations will involve the feeding of mixtures of uranium and plutonium hexafluoride.

III. CALORIMETRY*

(W. N. Hubbard, H. M. Feder)

Thermodynamic data are lacking for many compounds of interest in high-temperature chemistry because of the experimental difficulties involved in making the necessary measurements. A program has been undertaken to determine some of these data.

The basic data needed are heats of formation at 25 C. Part of the program of the group consists of determinations of heats of formation by the method of oxygen bomb calorimetry. However, many of the compounds of interest are difficult to burn in oxygen and, consequently, cannot be studied by oxygen bomb calorimetry. To study compounds of interest that are difficult to burn in oxygen and thus not amenable to oxygen bomb calorimetry, the techniques of the bomb calorimetric method (a method which has been developed to a high degree of precision and accuracy) have been modified so that fluorine can be used as the oxidant.

The accumulation of basic heat of formation data for fluorides is a necessary preliminary adjunct to the general use of fluorine bomb calorimetry for the study of compounds and is a valuable program in its own merit. To date, heat of formation values have been determined for the following fluorides: the difluorides of cadmium, magnesium, and zinc; the trifluorides of boron and aluminum; the tetrafluorides of titanium, zirconium, hafnium and silicon; and the hexafluorides of molybdenum and uranium. The heats of formation of three compounds: boron nitride, silicon dioxide, and zirconium diboride, have also been determined by fluorine bomb calorimetry. To obtain the heat of formation for boron nitride required the use of the value obtained previously for boron trifluoride; for silicon dioxide, the value for silicon tetrafluoride was required; and for zirconium diboride, the values for boron trifluoride and zirconium tetrafluoride were required.

To determine thermodynamic properties at high temperatures, the heats of formation at 25 C from oxygen or fluorine combustion calorimetry will be combined with the change in enthalpy values measured by a high-temperature enthalpy calorimeter. The calorimetric system, which is to be used for measurements up to 1500 C, has been designed and is now being assembled and tested. Design concepts for an electron beam furnace for a drop calorimeter to operate up to 2500 C are being tested in the laboratory.

---

*A summary of this section is given on page 26.

A. Revised Value of the Enthalpy of Formation of Uranium Hexafluoride (J. Settle)

Recalculation of the experimental data obtained from the combustion of uranium in fluorine has resulted in a slight revision of the previously reported derived standard thermal data for the formation of uranium hexafluoride from the elements at 25 C (see ANL-6648, p. 179). The revised values, in kcal/mole, are:

	$UF_6(c)$	$UF_6(g)$
$\Delta Ef°$	$-520.7_9 \pm 0.4_4$	$-509.5_1 \pm 0.4_6$
$\Delta Hf°$	$-522.5_7 \pm 0.4_4$	$-510.7_0 \pm 0.4_6$
$\Delta Gf°$	$-491.8_9 \pm 0.4_4$	$-490.7_2 \pm 0.4_6$

B. Exploratory Combustion of Uranium Monosulfide in Fluorine (J. Settle)

With the determination of the standard thermal data for the formation of uranium hexafluoride, it is now possible to measure the enthalpies of formation of various uranium compounds for which adequate thermochemical data is not now available. One of the compounds of interest in high-temperature reactor technology is uranium monosulfide (US).

Experiments have been performed to indicate (a) the extent of spontaneous reaction between uranium monosulfide and fluorine at room temperature and (b) the effect of certain variables on the combustion characteristics of uranium monosulfide in fluorine. The uranium monosulfide used in these experiments was in powdered form, making it necessary to use a support dish.

To determine the extent of reaction between fluorine and uranium monosulfide in a bomb prior to intentional ignition, 0.5-g samples of uranium monosulfide were exposed to fluorine at 5 atm pressure. The samples gained weight at a rate of approximately 0.52 mg/hr. The fluorination products were not determined, but the experiments demonstrated that it will be necessary to protect uranium monosulfide from exposure to fluorine before intentional ignition is carried out in the calorimetric combustions. One way of providing protection is to enclose the sample in a bag made of du Pont's heat-sealable Teflon-FEP fluorocarbon film. Preliminary tests indicate that leak-free bags can be made by conventional heat-sealing techniques. If this method of protecting the sample is adopted, the energy of combustion of Teflon-FEP film will have to be determined.

The results of exploratory combustions, in which uranium monosulfide was not protected from fluorine before ignition, are summaried

in Table III-1. As may be seen, the variables investigated to date are: the support dish material, the mass of sample, and the initial fluorine pressure in the bomb. The values for the mass of solid residue listed in column 4 are the weights of nonvolatile products of combustion, such as uranium tetrafluoride. Several milligrams of apparently unreacted uranium monosulfide were recovered when a prefluorinated zirconium support dish was used. No unreacted uranium monosulfide was recovered when a quartz dish was used. The support dish was always fluorinated to some extent during a combustion. The extent of reaction is given in the next two columns. It is assumed that the volatile products of combustion are uranium hexafluoride and sulfur hexafluoride, but this has not yet been confirmed by analyses. The extent of conversion to volatile products is given in the last column.

Table III-1

EXPLORATORY COMBUSTIONS OF URANIUM MONOSULFIDE IN FLUORINE

Support Dish Material	Mass of US (g)	Initial F_2 Pressure (atm)	Mass of Solid Residue (g)	Zr Reacted (g)	SiO_2 Reacted (g)	Conversion of US to Volatile Products (%)
Zr	0.551	5.0	0.2	>0.005	-	35
Zr	0.967	7.5	0.2	>0.003	-	80
Zr	0.898	10.0	0.2	>0.002	-	80
Zr	1.297	12.5	0.063	>0.006	-	95
Zr	1.507	15.0	0.149	>0.001	-	90
Zr	1.477	19.5	0.184	>0.006	-	88
Zr	2.016	12.5	0.328	>0.004	-	84
Zr	1.955	15.0	0.088	>0.004	-	95
Zr	1.968	20.0	0.252	>0.009	-	87
SiO_2	0.524	5.0	0.2	-	1.5	62
SiO_2	0.80237	10.0	0.00098	-	1.77095	99.86
SiO_2	1.40204	10.0	0.0224	-	0.51772	98.41
SiO_2	1.42582	15.0	0.00061	-	3.56424	99.96
SiO_2	1.34912	12.5	<0.001	-	1.827	>99.9

In each of the combustions done with a zirconium dish, a large amount of solid residue was left. The analysis of such residues, consisting of mixtures of uranium monosulfide, several uranium fluorides, and zirconium tetrafluoride, presents a difficult problem. Consequently, a zirconium support dish is not very satisfactory.

Of the combustions on quartz dishes, three were excellent in that 99.9 percent of the uranium monosulfide was converted to volatile products. However, so much quartz reacted that more energy was produced from this source than from the fluorination of the sulfide. This fact seems to require a more precise determination of the energy of combustion of glassy quartz than has been made thus far. It is intended to investigate several other metals and ceramics as support dish material in an effort to find the one which will yield the best combustion of uranium monosulfide while itself suffering minimum attack.

These experiments have indicated that the sample size is not critical, but the fluorine pressure must be in the region of 10 to 15 atm in order to obtain complete combustion of uranium monosulfide.

In summary, it has been found that application of the techniques of fluorine bomb calorimetry may yield a precise value for the enthalpy of formation of uranium monosulfide as refinements in the combustion method are made.

C. Exploratory Combustions of Carbon and Silicon Carbide in Fluorine
(E. Greenberg, C. Natke)

During this past quarter, a suitable technique was developed for the combustion of powdered silicon carbide in fluorine. Progress was also made in working out analytical methods for identifying and determining the gaseous products from the combustion of either carbon or silicon carbide in fluorine. A new bomb head, designed for the combustion of silicon carbide, has been fitted to bomb Ni-T-A. The calorimetric system is currently being calibrated. Work has been resumed on the development of a suitable technique for combustion of carbon in fluorine.

Exposure to fluorine of a weighed sample of the silicon carbide indicated no significant spontaneous reaction. As indicated in ANL-6687, p. 161, molybdenum fuse wire placed just above the sample has been successfully used for ignition of silicon carbide. Quartz dishes of various thicknesses were tried as sample supports, but in each case extensive reaction of the quartz was obtained. Nickel dishes, on the other hand, were virtually unreacted when used as supports. Quantitative studies indicate that a nickel dish gains less than one milligram per combustion. This is quite satisfactory for calorimetric work. In order to promote more complete combustion, the sample is confined to the center of the dish by means of a thick nickel ring. No technique has been found for burning the silicon carbide sample completely, but combustion of more than 99 percent of the sample has been achieved in some cases. Over the range of about 80 to 200 mesh, there appears to be no significant difference in the combustion characteristics of the sample.

In exploratory work utilizing the glass bomb,[1] difficulty was experienced because some of the silicon carbide sample was swept out of the support dish during combustion. The use of a nickel cover or shield over the dish reduced the problem. Under these conditions, it is expected that the quantity of unburned silicon carbide can be determined by simply weighing the dish and contents after combustion. It is suspected that part of the scattering of the sample is caused by gas currents created during charging of the glass bomb, because of the relative locations of the bomb valves and the sample dish. In the nickel bomb, the situation is much more favorable; recent experiments indicate that it may be possible to eliminate the cover over the sample dish.

A problem common to the combustions of both carbon and silicon carbide is the quantitative determination of the various carbon-containing compounds that are formed. Approximately 99 percent of the carbon is converted to tetrafluoromethane, with the remainder forming higher homologs. The relative amount of these higher fluorocarbons depends very much on the combustion conditions employed. A suitable gas chromatographic method has been developed[2] for analyzing this mixture of fluorocarbons. The higher fluorocarbon combustion products have been identified as C_2F_6 and C_3F_8, and the amounts of these can be determined to about 5 percent relative accuracy, which is sufficient for our calorimetric work.

No suitable gas chromatographic column has been found for analysis of the silicon fluorides. However, mass spectrometric analysis of the gaseous products from a typical silicon carbide combustion revealed only silicon tetrafluoride, with no evidence of any higher homologs. The combustion gases from typical calorimetric experiments will therefore be submitted for analysis by mass spectrometry in order to ascertain that all of the silicon has been burned to silicon tetrafluoride.

A new rotating bomb calorimeter (ANL-R2) has been installed in the laboratory and now appears to be in satisfactory operating condition.

D. Thermodynamic Properties of Hydrogen Fluoride
(E. Rudzitis)

Hydrogen Fluoride (gas). The standard enthalpy of formation of gaseous hydrogen fluoride, $\Delta Hf°$ (HF),* is a fundamental constant in the thermochemistry of fluorine-containing compounds. It is an essential quantity for correlating data obtained by fluorine bomb calorimetry with those derived by other means. To be useful in making correlations, the

---

*All values refer to 298.16 K.

[1]R. L. Nuttall, M. A. Frisch, and W. N. Hubbard, Rev. Sci. Instr., 31, 461 (1960).

[2]M. Runner, Chemical Research Services, Inc., Addison, Illinois.

reliability of the $\Delta Hf°(HF)$ value should be within the attainable precision limits of fluorine bomb calorimetry, i.e., within approximately 0.1%. The data found in the literature vary from -63.8 to -65.1 kcal/mole. To some extent, the variations are due to uncertainties in the nonideality correction for the gas due to a tendency toward extreme association.

Elimination of the data requiring such corrections leaves the following $\Delta Hf°(HF)$ values (kcal/mole): -64.45 ± 0.1,[3] -64.92 ± 0.12,[4] and -65.1 ± 0.4.[5]

The first of those values, -64.45 kcal/mole, was obtained by measuring the heat of Reaction 1 directly:

$$1/2\ H_2(g) + 1/2\ F_2(g) = HF(g), \qquad (1)$$

in a flow calorimeter at 100 C. At this temperature, no significant nonideality corrections are required.

The value of -64.92 kcal/mole was derived from combination of the thermochemical data of Reactions 2, 3, 4, and 5:

$$SiO_2\ (\alpha\text{-quartz}) + 2\ F_2(g) = SiF_4(g) + O_2(g) \qquad (2)$$

$$SiO_2\ (\text{crystobalite}) = SiO_2\ (\alpha\text{-quartz}) \qquad (3)$$

$$2\ H_2(g) + O_2(g) = 2\ H_2O(g) \qquad (4)$$

$$SiF_4(g) + 2\ H_2O(g) = SiO_2\ (\text{crystobalite}) + 4\ HF(g) \qquad (5)$$

The standard enthalpy of Reaction 5, which includes hydrogen fluoride gas, has been derived from equilibrium measurements at elevated temperatures, again without the need for nonideality correction.

The value -65.1 kcal/mole resulted from the analysis of the ultraviolet spectra of HF(g) in helium under ideal conditions. It is difficult to rationalize the almost 0.5-kcal/mole variance between the directly measured value[3] and the values of -64.92 and -65.1 which are in reasonable agreement with each other. This illustrates the fact that the reliability of the standard enthalpy of formation of gaseous hydrogen fluoride is not commensurate with its fundamental importance.

---

[3]H. Wartenberg and H. Schütza, Z. anorg. allgem. Chem. 206, 65 (1932).

[4]H. M. Feder, W. N. Hubbard, S. S. Wise, and J. L. Margrave, J. Phys. Chem. 67, 1148 (1963).

[5]J. W. C. Johns and R. F. Barrow, Proc. Roy. Soc. (London), A251, 504 (1959).

Hydrogen Fluoride (aqueous). Another important constant in the thermochemistry of fluorine-containing compounds is the standard enthalpy of formation of aqueous HF, $\Delta Hf°$ ($HF \cdot xH_2O$), Reaction 6.

$$1/2\ H_2(g) + 1/2\ F_2(g) + xH_2O(liq) = HF \cdot xH_2O(liq). \quad (6)$$

This quantity is particularly useful for the correlation of values between nonaqueous and aqueous fluorine thermochemistry. In NBS Circular 500[6] $\Delta Hf°$ values are tabulated over a concentration range of $HF \cdot 2\ H_2O$ to $HF \cdot \infty H_2O$; these data are given to the nearest 0.01 kcal. Examination of the cited references revealed that Reaction 6 is a summation of Reactions 1, 7, and 8:

$$HF(g) + 400\ H_2O(liq) = HF \cdot 400\ H_2O\ (liq) \quad (7)$$

$$HF \cdot 400\ H_2O + (x - 400)\ H_2O(liq) = HF \cdot xH_2O(liq) \quad (8)$$

To obtain a $\Delta Hf°$(HF gas) value, the compilers of Circular 500 averaged three reported values (kcal/mole): -63.8 ± 0.3,[7,9] -64.2 ± 0.3[8,9] and -64.45 ± 0.1,[3] obtaining -64.2 kcal/mole as the "best" value. The first two values were obtained by the reaction of fluorine with hydrogen under conditions where appreciable (0.5 to 1 kcal) nonideality corrections were required. Reaction 7 also required a nonideality correction of the same magnitude, a condition which in itself would be favorable because of cancelling out of the nonideality corrections of Reactions 1 and 7, provided that the averaging of $\Delta Hf°$(HF gas) values would not have included -64.45 ± 0.1 kcal/mole which was derived without the necessity for nonideality corrections.[3] An additional uncertainty remains because the conditions of Reaction 7 required extrapolation of HF pressure from its original saturated vapor pressure in the range between -21 C and 0 C to the pressure at the dissolution temperature of 32 C. Since no experimental data were available, the calculations were based on a simple association model which is now recognized as incorrect.

The heat effect of Reaction 8, which is of relatively minor importance, both numerically and for this discussion, seems to have been reliably measured and interpreted by W. A. Roth and coworkers (for original references see Circular 500).[6]

---

[6] F. D. Rossini, D. D. Wagman, W. H. Evans, S. Levine, and I. Jaffe, Selected Values of Chemical Thermodynamic Properties, NBS Circular 500 (1952).

[7] H. V. Wartenberg and O. Fitzner, Z. anorg. allgem. Chem. 151, 313 (1926).

[8] O. Ruff and F. Laass, ibid., 183, 217 (1929).

[9] O. Ruff and W. Menzel, ibid., 198, 375 (1931).

It is evident that although the number of significant figures given for the listed $\Delta Hf°(HF \cdot xH_2O)$ values,[6] e.g., $\Delta Hf°(HF \cdot 400\ H_2O)$ = -75.74 kcal (mole HF)$^{-1}$, is necessary for relating data of aqueous thermochemistry, the absolute accuracy implied by the significant figures is unrealistic for comparing values between aqueous and nonaqueous fluorine thermochemistry. An indication of the magnitude of uncertainty associated with $\Delta Hf°(HF \cdot 400\ H_2O)$ was obtained by combining and averaging individual pairs of data for Reactions 1 and 7 obtained under comparable conditions. Nineteen data pairs yielded an average value of $\Delta Hf°(HF \cdot 400\ H_2O)$ = -75.6 kcal (mole HF)$^{-1}$ with an uncertainty interval (twice the standard deviation) of ± 0.4 kcal. Although it is possible that the absolute value of $\Delta Hf°$ may change due to the refinements in calculations, it is less likely that the uncertainty interval will change appreciably.

In conclusion, it can be stated that at the present time the thermochemical data for hydrogen fluoride are unsatisfactory for supplementing data obtained by fluorine bomb calorimetry. This evaluation will be continued, and attempts will be made to correlate the extensive experimental and theoretical information on hydrogen fluoride in terms of thermodynamics of association.

E. High-temperature (1500 C) Enthalpy Calorimeter

(D. R. Fredrickson, R. L. Nuttall, R. Kleb, and J. E. Brugger)

In the preceding quarterly report (ANL-6687, p. 164), mention was made of the increasing difficulty in controlling the temperature of the furnace of the high-temperature drop calorimeter. When the deterioration of temperature control culminated in the loss of the main shield control thermocouple, the furnace was opened and its internal components examined (for drawings of the furnace, see ANL-6477, p. 165, and ANL-6648, p. 184). The outer radiation shields - five of aluminum followed by three of silver - were extensively damaged by melting and by the action of a low-melting silver-aluminum alloy. The three inner molybdenum radiation shields, the alumina-filled tantalum dust shield, and the molybdenum core were intact. One thermocouple had melted at the junction, two others had opened through mechanical strain, and all exposed thermocouples showed evidence of surface attack. The tantalum heater windings had embrittled, and X-ray analysis indicated that some tantalum nitride had formed. This failure of furnace components was not a major setback and presumably arose from an overestimation of the effectiveness of the dust shield and from a misalignment of the shields.

In order to obtain heat transfer data for the original dust shield, which consists of two nested tantalum cans having a $\frac{3}{4}$-in. annular space filled with bubbled Alundum grain (Norton type E 163 -8 +72 mesh 99.5% alumina), a simplified version of the furnace was assembled. The molybdenum core was replaced by a 12-in. length of grooved Alundum tube

having two 5-in. windings of platinum wire. Three pairs of ears fashioned from alumina thermocouple tubing were cemented near the top of the Alundum tube to position it within the dust shield. Of the radiation shields, only the three (undamaged) molybdenum shields were installed. At the top, the center, and the bottom of the core, platinum-10% rhodium, platinum thermocouples were fastened. Thermocouples were also attached to the inner and the outer walls of the dust shield and to the outermost molybdenum shield. All thermocouple leads were taken to the cold portion of the furnace in alumina tubing and then out of the furnace at the rubber gasket of the junction box.

Pertinent temperature and power input data are summarized in Table III-2. These data were used to compute the coefficient of thermal conductivity, K, for the dust shield by a standard formula. Figure III-1 is a plot of the coefficient of thermal conductivity in W cm^{-1} deg C^{-1} versus the mean temperature of the dust (average of Col. 2 and 3 of Table III-2).

It was believed that this heat transfer across the dust was primarily by radiation rather than conduction. To test the validity of this belief, the quantity $Z(\text{deg } K^4 W^{-1}) = [(T_1 + 273)^4 - (T_2 + 273)^4]/\dot{Q}$ was calculated. The constancy of Z, as shown in the sixth column of Table III-2, indicates that heat transfer across the dust shield is essentially by radiation. The curvature of the plot in Figure III-1 further corroborates this hypothesis.

Experiments are now underway to evaluate the effectiveness of finer mesh powders and of different filler materials (Morganite-brand alumina and Carborundum-brand silicon carbide) for the dust shield.

Table III-2

HEAT TRANSFER CHARACTERISTICS OF DUST SHIELD

	Temperature (C)				
Power $\dot{Q}$ (W)	Inner Surface of Dust Shield, T_1	Outer Surface of Dust Shield, T_2	ΔT, $T_1 - T_2$	Outermost Molybdenum Shield, T_3	Z (deg $K^4 W^{-1} \times 10^{-9}$)
30	396	175	221	69	5.4
68	555	271	284	121	5.6
260	896.	485	411	250	5.9
400	1021	550	471	285	5.9
512	1102	599	503	308	5.9
905	1317	708	609	342	5.3

Figure III-1

THERMAL CONDUCTIVITY OF DUST SHIELD
VS. MEAN TEMPERATURE

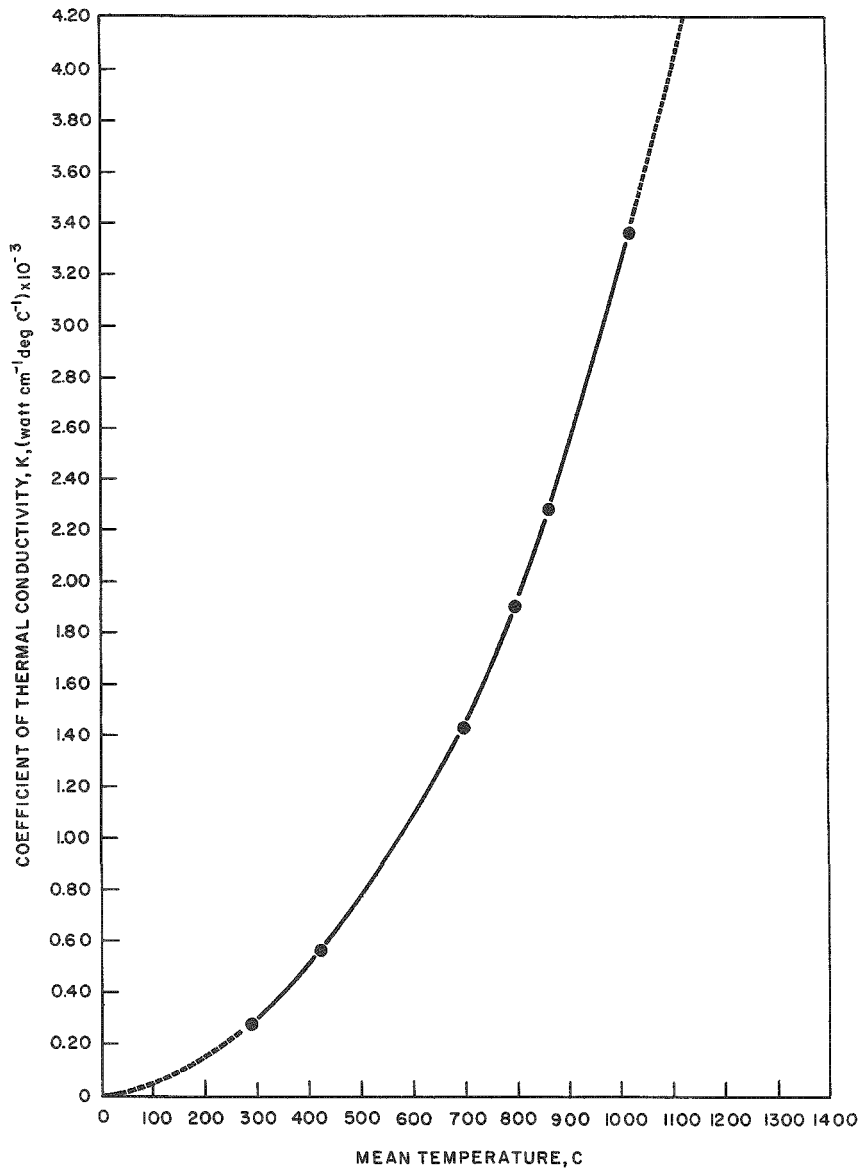

108-6839

F. High-temperature (2500 C) Enthalpy Calorimeter
(R. L. Nuttall)

A calorimetric system is being developed for measurements of enthalpy changes between 25 and 2500 C (see ANL-6687, p. 165). The power supply for the electron guns (used to heat the sample) has been repaired, and testing is continuing. Design for the calorimeter part of the system is nearly complete. Design of a preliminary test calorimeter receiver which can be used for preliminary measurements has been started.

IV. REACTOR SAFETY*

The oxidation, ignition, and combustion processes of substances used in nuclear technology are being studied to provide information needed to minimize the hazards associated with the handling of these materials.

A. Metal-oxidation and -ignition Kinetics
(L. Baker)

1. Isothermal Oxidation of Uranium in Air at Temperatures of 500 C and Above
(R. Wilson, L. Baker, R. Koonz)

The air oxidation of uranium at temperatures above 500 C is being studied in order to determine the nature and degree of protectiveness of oxide films formed at high temperatures. The existence of protective oxide films at high temperatures is indicated by the cyclic variations of temperature that have been observed in ignition studies.[1] These protective oxide films are effective in preventing a rapid sustained burning of massive specimens of uranium which have ignited. Ignition results have suggested that the oxide is more protective in air than in pure oxygen. An important part of this study is therefore an assessment of the role of nitrogen in the oxidation reaction. A preliminary phase of this program was reported in the previous quarterly report (ANL-6687, p. 167). The preliminary studies were performed by passing a gas consisting of 94 v/o air and 6 v/o argon over induction-heated uranium cubes in a once-through flow system. The reaction rate was determined by mass spectrometric measurement of the concentration of oxygen and nitrogen relative to the argon present in the effluent gas.

In the preliminary study (see ANL-6687, p. 167), mass spectrometric analyses indicated that there was no measurable uptake of nitrogen by the uranium specimens over the entire temperature range studied (500 to 1000 C). Individual analyses of the composition of the effluent stream were made at 2-min intervals, the frequency of analyses being limited by the time required to scan the mass spectra from mass-to-charge ratios of 14 to 40. This limitation prevented accurate determination of the initial rates of oxidation. A new experimental procedure was therefore devised which permitted more detailed studies of the initial oxidation reaction and took advantage of the observation that nitrogen does not react to a measurable degree with uranium in the presence of oxygen.

---

*A summary of this section is given on pp. 27 to 29.

[1] Schnizlein, J.G., et al., Ignition Behavior and Kinetics of the Reactor Metals, Uranium, Zirconium, Plutonium and Thorium, and Binary Alloys of Each, ANL-5974 (June 1959), p. 31.

a. Apparatus and Procedure

Studies of the intial rate of the uranium-air reaction employed a closed system, with a recording pressure transducer to indicate the disappearance of oxygen from the gas phase. To prevent localized depletion of oxygen in the vicinity of each sample, the reaction cell was arranged in the form of a convective loop, as shown in Figure IV-1. The sample was a nominal one-cm cube of uranium* which was supported on a stainless steel-clad thermocouple and was contained in a quartz tube in the lower portion of the left-hand vertical leg of the loop. The remainder of the loop was constructed of $1\frac{1}{4}$-in.-diameter copper tubing. The upper portion of the left-hand vertical leg of the loop was heated by external nichrome heating wire to temperatures of about 400 C. The right-hand vertical leg of the loop was cooled by an external coil containing flowing tap water. Simultaneous heating of the left leg of the loop and cooling of the right leg resulted in vigorous circulation of the oxidizing gas.

Figure IV-1

APPARATUS TO DETERMINE THE URANIUM-AIR REACTION KINETICS

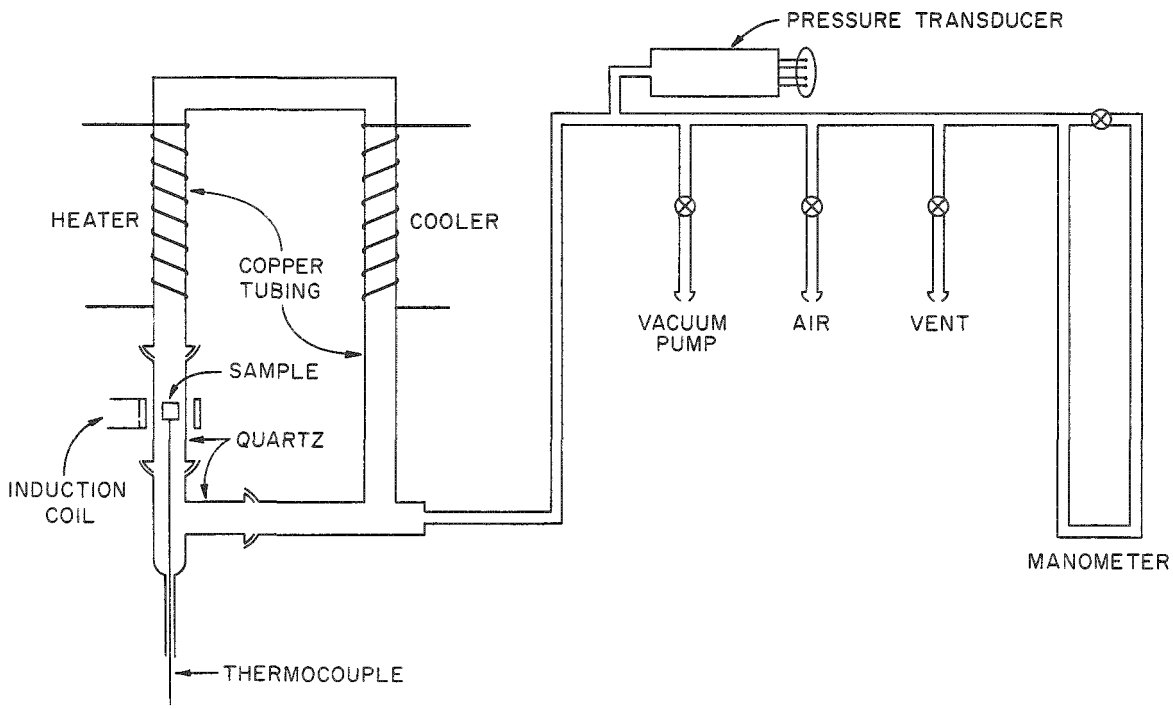

108-6767

Three different oxidizing gas compositions were used: (a) pure oxygen at an initial pressure of 200 mm, (b) dry air at one atm, and (c) a synthetic "air" consisting of 20 v/o oxygen-80 v/o argon at one atm. In addition, a few experiments were performed with air in which the

*The total impurity content of the uranium is about 250 ppm. A detailed analysis of the metal may be found in Ref. 1, p. 146.

bottom of the loop contained Drierite and Ascarite to ensure that there were no traces of water vapor and carbon dioxide in the oxidizing gas.

Samples were heated to 500, 600, 700, 800, 900, and 1000 C by induction from a single-turn coil which was external to the reaction cell loop. The sample was brought to the test temperature in 15 to 30 sec and was maintained at a constant temperature by manual adjustment of the power of the induction generator. In this way, it was possible to compensate for heat generated by the oxidation reaction. Pressure decrease in the system was recorded as a function of time, using a strain-gage-type pressure transducer* from which a signal was fed into a strip-chart recorder having a relatively rapid response.** The results of blank runs with a 1-cm platinum cube were used to correct the pressure-time curves for the initial changes of pressure resulting from sample heating. In the blank runs, it was shown that the heated portion of the copper tubing in the reaction cell loop did not oxidize at a significant rate.

b. Results and Discussion

The duration of individual experiments was limited by oxygen depletion of the oxidizing gas mixtures. Runs were discontinued when approximately one-half of the oxygen in the reaction cell was consumed. The preliminary experiments, in which mass spectrometry was employed (see ANL-6687, p. 167), had not been limited in duration, being continued until approximately 80% of each sample cube was oxidized in the 600 to 1000 C range.

The results of both studies are summarized in digest form in Table IV-1. Reactions with pure oxygen and with oxygen-argon mixtures were studied only in the loop apparatus for short periods of time. The results showed that there were as many as three distinct stages to the oxidation reactions. Although the character of the oxidation reaction (linear, parabolic, or cubic) was reproducible for a given oxidizing gas and for a given specimen temperature, there was considerable variation from one run to another in the rate constants and the times corresponding to the transition from one stage to another. The ranges of rate constant values and transition times listed in Table IV-1 indicate the magnitude of experimental scatter. Eight runs at various temperatures were performed with Ascarite and Drierite present in the reaction cell loop. The results of these runs were indistinguishable from those of the other runs.

*Statham, Model 5870, 0-15 psia.

**Minneapolis-Honeywell Brown Recorder, $\frac{1}{4}$-sec response.

Table IV-1

RESULTS OF ISOTHERMAL STUDIES OF THE REACTION OF URANIUM WITH AIR, OXYGEN, and 20 v/o OXYGEN-80 v/o ARGON MIXTURE

(Nominal one-cm Uranium Cube Specimens)

			Isothermal Reaction Rate Law and Range of Rate Constants[a]					
Temperature (C)	Number of Runs	Oxidizing Gas	First Stage	Duration of Experiment or Transition Time (min)	Second Stage	Duration of Experiment or Transition Time (min)	Third Stage	Duration of Experiment (min)
500	6	O_2	Linear (0.8-1.5)	~30[b]	-	-	-	-
500	3	O_2-Ar	Linear (0.7-1.0)	8-21	Linear (0.9-1.2)	27-36[b]	-	-
500	6	Air	Linear (1.1-2.3)	18-35	Linear (1.5-3.4)	40-60[b]	-	-
600	6	O_2	Linear (2.4-6.6)	~20[b]	-	-	-	-
600	4	O_2-Ar	Parabolic (26-94)	3-4	Linear (1.8-3.0)	~15[b]	-	-
600	13	Air	Parabolic (29-58)	2-5	Linear (1.6-4.4)	20-30	Linear (3.8-4.4)	45-60[b]
700	5	O_2-Ar	Parabolic (171-211)	~10[b]	-	-	-	-
700	13	Air	Parabolic (124-172)	2-4	Linear (1.8-8.8)	45-60[b]	-	-
800	4	O_2-Ar	Parabolic (234-308)	~5[b]	-	-	-	-
800	9	Air	Parabolic (229-273)	3-4	Linear (5.1-7.7)	40-60[b]	-	-
900	3	O_2-Ar	Parabolic (341-387)	~3[b]	-	-	-	-
900	7	Air	Parabolic (354-1053)	18-27	Linear (2.1-3.0)	60-90[b]	-	-
1000	3	O_2-Ar	Cubic (15,000-22,000)	~3[b]	-	-	-	-
1000	7	Air	Parabolic (790-1640)	16-40	Linear (2.7-4.5)	60-90[b]	-	-

[a]Linear rate constants in (mgO_2/sq cm)/min Parabolic rate constants in (mg O_2/sq cm)^2/min Cubic rate constants in (mg O_2/sq cm)^3/min

[b]End of experiment.

Results at 500 C indicated that there was no significant difference in reaction between pure oxygen, air, and the 20 v/o oxygen-80 v/o argon mixture. The reaction followed a nearly linear rate in all cases, although the rate values scattered considerably. The reaction rate was not appreciably different from that reported to occur in pure oxygen in previous studies using a heat sink reaction cell (see Summary Report ANL-6543, p. 168). Reaction rates in the latter study were reported to be decelerating slightly in the 500-600 C range. At 600 C in the present study, the nearly linear reaction in pure oxygen persisted, in agreement with the previous study. The reaction of uranium with air and with the oxygen-argon mixture at 600 C was initially parabolic and became linear only after 2 to 5 min. There was no difference, however, between the reaction with air and with the oxygen-argon mixture at 600 C.

Reaction of uranium with pure oxygen could not be studied accurately at temperatures above 600 C because of self-heating and ignition. In several attempts to study the reaction at higher temperatures, the formation of protective oxides was indicated, although it was not possible to obtain accurate rate data.

At 700, 800, and 900 C, the reaction with the oxygen-argon mixture was parabolic, whereas at 1000 C the reaction was best described by the cubic rate law. The reaction with air was initially parabolic over the 600 to 1000 C range; however, a transition to a linear reaction occurred at each temperature. At 600, 700, and 800 C, the transition to a linear reaction occurred in 2 to 5 min and corresponded to the consumption of between 8 and 33 mg O_2/sq cm reaction. At 900 and 1000 C, the parabolic reaction in air persisted for 16 to 40 min and corresponded to the consumption of between 125 and 217 mg O_2/sq cm reaction. The values of the parabolic rate constants obtained for the initial reaction of uranium with air and with 20 v/o oxygen-80 v/o argon mixture are plotted as ranges in Figure IV-2 as a function of reciprocal temperature. The nature of the plot suggests that the initial reaction with both air and the oxygen-argon mixture is controlled by the same mechanism over the temperature range from 600 to 1000 C.

The kinetics of the high-temperature uranium reaction with oxygen-containing gases can be accounted for by a mechanism involving adsorption and solid-state diffusion. The initial stage of reactions with air and the oxygen-argon mixture at 600 C and above can be correlated by means of a parabolic rate law, suggesting that the reaction rate variation with time is controlled by the solid-state diffusion of oxygen ions. The absolute value of the reaction rate is probably also determined by an adsorption equilibrium at the oxide-gas interface. The competition for adsorption sites by nitrogen and argon molecules in the gas mixtures is probably responsible for the differences between the reaction rate with pure oxygen at 600 C and that with the gas mixtures at 600 C. It was concluded

in a previous study[2] that adsorption at the oxide-gas interface is a key factor in the reaction mechanism at lower temperatures.

Figure IV-2

PARABOLIC RATE CONSTANTS FOR THE INITIAL REACTION OF URANIUM WITH AIR AND WITH 20 v/o OXYGEN-80 v/o ARGON MIXTURE

(One-cm Cubes of Uranium)

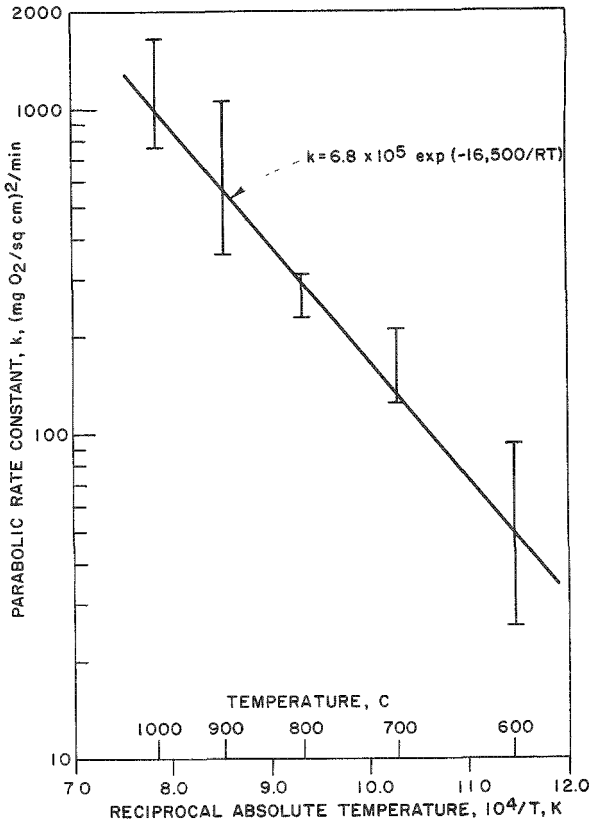

108-6766

The results reported previously for the uranium-steam reaction are also consistent with this mechanism (see Summary Report ANL-6569, p. 148). The steam reaction was also parabolic above 600 C with an activation energy (18.6 kcal/mole) which is experimentally identical with the value obtained for the air reaction (16.5 kcal/mole). The reaction rate with air (or with the oxygen-argon mixture) was about ten times more rapid than the rate with steam. This would result from the greater partial pressure of oxygen in air than that in equilibrium with water for activated adsorption.

The change from a parabolic to a linear reaction is usually taken to imply that the diffusion barrier film develops cracks at a more or less definite film thickness which depends on the plasticity and adherence of the film. On this basis, it can be concluded that the oxide film produced in air oxidation has a much greater plasticity and adherence at 900 and 1000 C than it does at lower temperatures. The experimental results at 700 and 800 C would indicate that the nitrogen in the air causes cracking and transition to the linear reaction to occur at an earlier time than does the argon in the oxygen-argon mixture. The marked protectiveness of the oxide film formed in air at 900 and 1000 C would account for the cyclic variations of temperature observed in ignition experiments and the failure of massive pieces of uranium to undergo sustained burning in air.

---

[2]Leibowitz, L., Schnizlein, J. G. Bingle, J. D., and Vogel, R. C., J. Electrochem. Soc. 108, 1155 (1961).

2. Plutonium-ignition Studies
(J. G. Schnizlein, D. F. Fischer)

The increasing use of plutonium in the nuclear energy program makes safe handling procedures imperative. Detailed knowledge of the oxidation and ignition characteristics of plutonium and plutonium alloys is being acquired to allow appraisal of the hazards. Studies of the isothermal oxidation of plutonium between 140 and 450 C were reported in the previous quarterly report (ANL-6687, p. 171). The present report describes results of ignition studies with specimens of pure plutonium.

The facilities, including the gloveboxes and the specially constructed thermobalance used in the experiments, were described previously (see Summary Report ANL-6413, p. 168). The plutonium cubes and foil specimens used in the experiments were prepared at Hanford.* The specimens were 5-mm cubes and 3 x 20-mm sections of foil having thicknesses of 1, 0.5, 0.22, 0.17, and 0.12 mm. The specific area of the specimens ranged from 0.65 to 11 sq cm/g.

Burning-curve experiments and shielded-ignition experiments were performed with the pure plutonium specimens in both air and oxygen. In a burning-curve experiment, the specimen is supported on a thermocouple and is heated at a uniform rate (usually 10 C/min) in a flowing oxidizing gas until ignition occurs. Ignition temperature is determined graphically as the intersection of the pre-ignition heating curve with the post-ignition self-heating curve.

In a shielded-ignition experiment, the sample is heated to the test temperature in a protective atmosphere of helium. The protective gas is then rapidly replaced by the oxidant to determine whether ignition occurs at the test temperature. Ignition temperature is given as the range between the highest temperature at which ignition does not occur and the lowest temperature at which ignition does occur.

Results of ignition temperatures determined by both methods are listed in Table IV-2. Ignition temperatures obtained by the burning-curve method are plotted as a function of specific area in Figure IV-3. Some of the data for 5-mm cubes included in Figure IV-3 were reported previously (see ANL-6648, p. 193). Ignition data from Dempsey and Kay[3] and from Carter, Foy, and Stewart[4] are also included in Figure IV-3. The ignition temperatures ranged from 535 to 280 C. The variation of ignition

*Preparations were under the supervision of R. R. King, P. G. Pallmer, T. Nelson, and O. J. Wick, General Electric Co., Hanford Atomic Products Division, Richland, Washington.

[3]Dempsey, E., and Kay, A. E., J. Institute Metals 86, 379 (1958).

[4]Carter, R. F., Foy, B., and Stewart, K., The Particulate Material Formed by Oxidation of Plutonium, AERO-Conf/8 (1960).

Table IV-2

IGNITION TEMPERATURES OF PLUTONIUM IN AIR AND OXYGEN

Foil Thickness (mm)	Specific Area (sq cm/g)	Burning-curve Ignition Temperatures (C)		Shielded Ignition Temperatures[a] (C)	
		Air	O_2	Air	O_2
~5 (cube)	0 65	520 508	512 494	442-492	-
1 0	1 5	492 322	490	378-408	327-374
0 52	2 5	310 314	468 505	303-337	353-398
0 22	5 3	518 520 535 519[b] 521[b]	524 527	375-403	322-350
0 17	6 7	282	299		
0 12	11 0	282	305	266-280	273-284

[a]Indicated as the highest temperature at which ignition did not occur and the lowest temperature at which ignition did occur

[b]Samples were polished with 600 grit SiC paper, all others as received

Figure IV-3

IGNITION TEMPERATURES OF PLUTONIUM BY THE BURNING CURVE METHOD

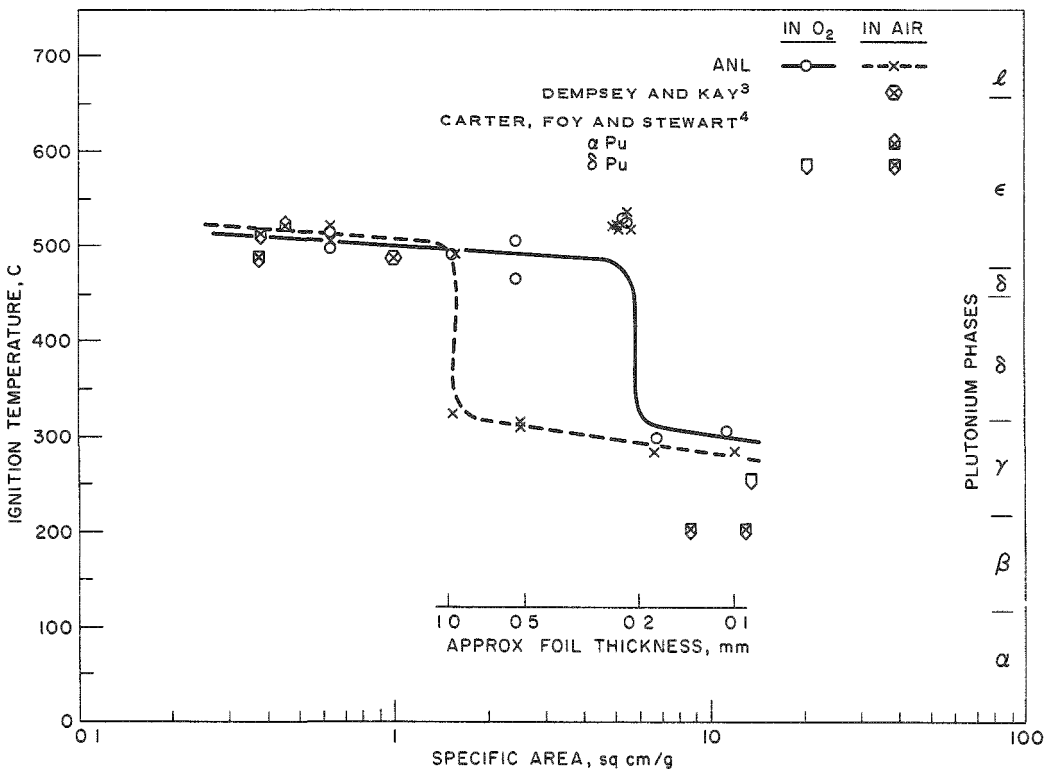

108-6764

temperature with specific area, however, is not smooth. Ignition occurs in one of two regimes, one at approximately 300 C and the other at approximately 500 C.

Results of a pair of burning-curve ignition experiments with 1.0-mm-thick (1.5-sq cm/g) foil specimens in air (shown in Figure IV-4) illustrate the manner in which ignition might occur in either regime. The sharpness of the change of ignition temperature from the low-temperature regime to the high-temperature regime is emphasized by the fact that the difference of specific area of the two samples was indistinguishable. A discontinuity in ignition temperatures in air occurs at a specific area of 1.5 sq cm/g and at 6.0 sq cm/g if the specimen is in oxygen. The 0.22-mm-thick foil was exceptional in that it ignited consistently in the high-temperature regime in air, even though its specific area, 5.3 sq cm/g, was considerably greater than the 1.5-sq cm/g dividing line. Possible causes of this anomalous ignition behavior, which are being explored, might be unique heat treatment during fabrication that tends to stabilize delta-phase plutonium, or contamination with aluminum or silicon which could cause increased ignition temperatures.

Figure IV-4

BURNING-CURVE IGNITIONS IN AIR OF ONE-mm-THICK PURE PLUTONIUM FOIL SPECIMENS
(Specific Area, 1.5 sq cm/g)

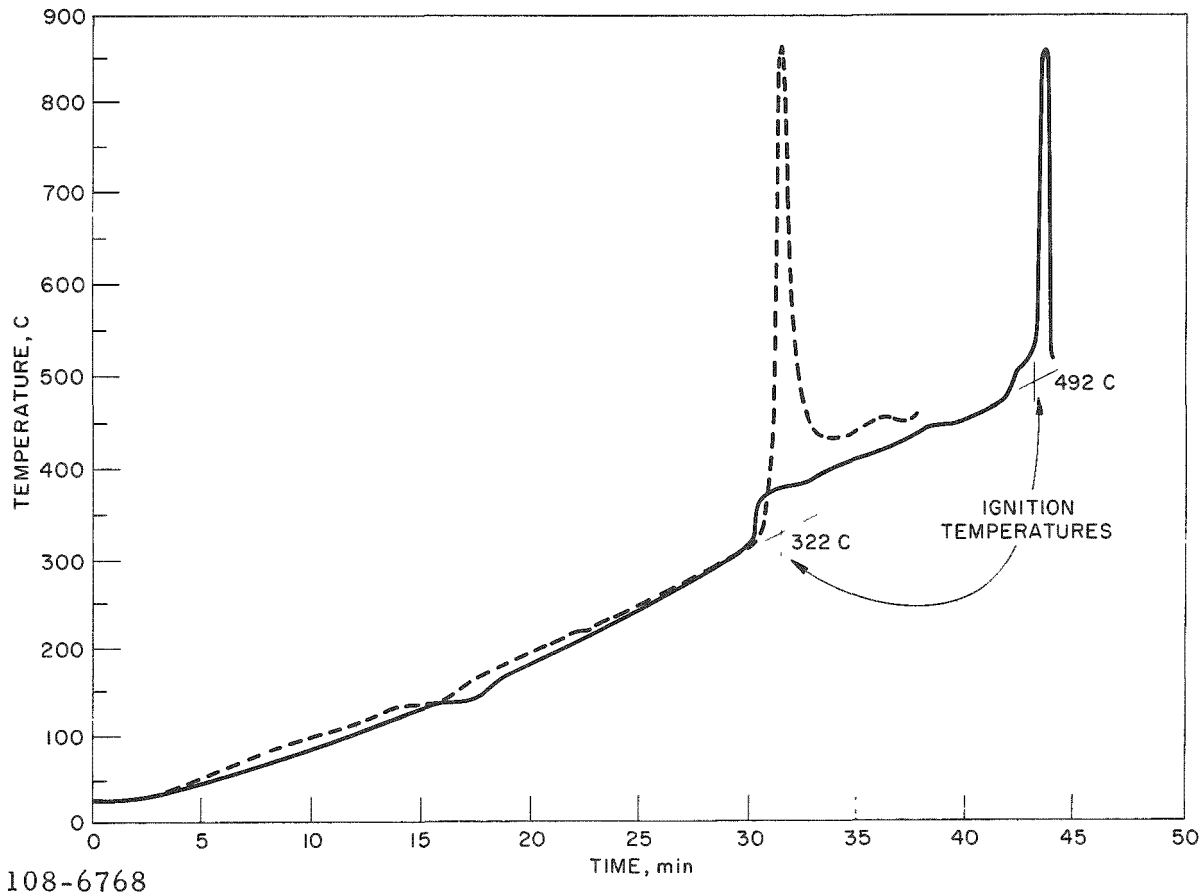

The ignition results by Dempsey and Kay[3] and Carter, Foy, and Stewart[4] were generally consistent with the other results plotted in Figure IV-3. The ignition observed by Dempsey and Kay during an experiment intended to be isothermal at 487 C occurred after oxidation had proceeded for about 300 min. The tests by Carter et al. were performed with both alpha plutonium and delta-stabilized plutonium in two forms: 10-g billets and 1-g to 2-g collections of turnings.

The existence of two regimes of ignition is consistent with the oxidation behavior of plutonium. During the oxidation of plutonium, a change in the isothermal oxidation kinetics occurs just above 300 C (see ANL-6687, p. 171). The oxidation rate was shown to decrease sharply between 350 and 450 C. Evidently, the rate of heat generation by oxidation in the region of 300 C is just sufficient to cause ignition of specimens having large specific areas. Specimens having smaller specific areas have greater thermal inertia, and the temperature increase caused by self-heating occurs more slowly. This allows the formation of more protective oxide at temperatures near 400 C, where there is a minimum in the oxidation rate. The decreased oxidation rate prevents ignition from occurring until the sample temperature is increased by external heating beyond 450 C, and the oxidation rate again rapidly increases with increasing temperature.

Ignition studies are continuing with a series of binary plutonium alloys which contain 2 a/o each of aluminum, carbon, chromium, cerium, cobalt, iron, nickel, silicon, and uranium.

B. Metal-Water Reactions
(L. Baker)

1. Studies of Metal-Water Reactions by the Laser Heating Method
(L. Leibowitz, R. E. Wilson, L. Mishler)

The laser heating experiment is an attempt to obtain fundamental data concerning the rates of chemical reaction and heat transfer between metal particles and water. In the experiment, an intense beam of light from a ruby laser is focused on a small particle of metal in a water environment. Nearly instantaneous heating simulates the rapid contacting of heated particles with water that would occur in a water-cooled nuclear reactor in the event of a violent meltdown. (Either a nuclear runaway or a sudden loss of coolant might result in the injection of heated particles of cladding or fuel into the water.) Knowledge of the rate of exchange of both chemical and thermal energy from individual particles to the water is of prime importance in the analysis of reactor accidents.

Considerable information concerning the reaction of heated particles of zirconium, uranium, and stainless steel with water was obtained by the condenser-discharge method and reported in ANL-6687 and preceding

quarterly reports. The condenser-discharge experiment has the disadvantage that a number of particles are generated in each run, whereas only one particle is involved in a laser experiment. Also, condenser-discharge experiments with aluminum wires were unsuccessful: nonuniform heating of aluminum occurred in attempted runs, and very little of the aluminum reacted (see Summary Report ANL-6101, p. 142). It is expected that the laser experiment will be applicable to studies of the aluminum-water reaction. Also, the laser experiment should be applicable to nonmetals as well as metals; the condenser-discharge experiment could be performed only with materials having a high electrical conductivity, i.e., metals.

Descriptions of the theory and practice of laser operation are widely available,[5] and no repetition of this information is given here. It is sufficient to note that a laser beam is a highly directional, easily focused, brief pulse of high-intensity light. With commercially available ruby laser systems, outputs of 30 J (7.2 cal) at 6943 Å may be obtained in about 0.001 sec. This energy is sufficient to heat a 2-mm-diameter aluminum sphere from room temperature to about 2000 C, which is slightly below the boiling point of aluminum. In principle, the laser as a heating device seems well suited to these studies.

For this work, a Maser Optics* 3020 laser system has been obtained. This system employs a $6\frac{5}{8}$ x $\frac{3}{8}$-in. ruby rod, uncoated on one end and with a reflecting dielectric coating on the other. The rod is closely coupled by means of a highly polished elliptical cavity to an Edgerton, Germeshausen, and Grier, Inc.** FX-45 xenon flashlamp with a 6-in. arc gap. The laser head employs liquid nitrogen cooling, and flashlamp outputs up to 3500 J may be used. Laser outputs up to 26 J are reported.

Preliminary energy determinations have been carried out. The temperature rise of a polished tantalum disc was measured by means of a thermocouple spotwelded to the rear face of the disc, while the unfocused laser beam impinged on the front face. The energy absorbed was proportional to the temperature rise. The temperature rise was used to calculate the energy after correcting for the emissivity of the disc material. These preliminary measurements verified the reported output of about 25 J. It is planned to carry out more precise energy measurements by using commercially available optical calorimeters or still more precisely by using light-scattering methods. The latter technique involves scattering of the laser beam by an MgO surface and measurement of the light intensity some distance from the MgO. With suitable calibrations, the intensity of the original beam may be found.

---

*Maser Optics, Inc., 89 Brighton Avenue, Boston 34, Mass.

**Edgerton, Germeshausen, and Grier, Inc., 160 Brookline Avenue, Boston 15, Mass.

[5]Lengyel, B. A., Lasers, John Wiley and Sons, Inc., New York (1962).

The arrangement of the apparatus for studying metal-water reactions is the following: Two optical benches have been carefully aligned, one horizontally along the laser beam and the other perpendicular to it. A prism mounted on the horizontal optical bench reflects the laser beam along the perpendicular bench. A simple lens then focuses the beam onto the metal sample held in a suitable container. Lenses of various focal lengths have been used. A modified microscope mechanical stage is used for precise alignment. The image of the ruby holder focused on a ground glass screen allows for precise alignment.

Numerous scouting tests have been performed with laser beams to heat various metals while the metals were submerged in water. It has been shown that zirconium and stainless steel foil can be melted under water in this way. Also, aluminum pellets have been melted on one side while the other side was evidently not affected. Tests with smaller particles will be carried out to determine the conditions necessary to melt aluminum particles completely. Uranium foil was partially destroyed, i.e., part of the foil was reduced to powder and the remainder was not changed. Further tests are planned to find optimum experimental conditions for heating the metal specimens. In quantitative experiments, metal samples will be exposed to laser beams of varying intensities, and hydrogen evolution will be measured.

A micro gas-analysis system has been constructed for measurement of the small quantities of hydrogen expected to be evolved. This system, which was taken from the system described by Stover, Partridge, and Garrison,[6] is a constant-volume system of conventional design. The pressure of the gas sample is measured at a known volume, hydrogen is removed from the sample by oxidation over hot CuO, and then the pressure of the remaining gas is measured. The amount of hydrogen that was present is found by difference. Tests have shown that 0.01 ml (STP) of hydrogen can be measured in this apparatus. This represents 0.1% reaction with water of an aluminum sphere 2 mm in diameter. Metallographic examination of the residue from experiments involving laser heating will also be carried out. Measurement of the temperature of the metal particles will be attempted with a fast-response two-color pyrometer currently being built. This device will employ two RCA 7102 photomultiplier tubes.

2. Studies of the Aluminum-Water Reaction in TREAT
(R. O. Ivins, F. J. Testa, P. Krause)

The use of the TREAT (Transient REActor Test facility) reactor at the NRTS, Idaho, to study the reaction of various metals with water is continuing. The technique consists of subjecting fuel specimens immersed in water to a transient nuclear burst. The objectives of this program are:

---

[6]Stover, C. N., Jr., Partridge, W. S., and Garrison, W. M., Anal. Chem. 21, 1013 (1949).

1. to determine the extent of reaction between the metal and water;
2. to determine the fuel temperature and pressure history during the excursion;
3. to determine the physical damage that occurs as a result of the transient; this is accomplished by such means as metallographic and particle size evaluations.

The results of several experiments in which aluminum-uranium alloy fuel plates were subjected to destructive transients in TREAT have been reported in previous quarterly reports (ANL-6648, p. 201, and ANL-6687, p. 179). These studies were performed with the sample fuel plates submerged in room-temperature water. These results will be compared with those of current runs in which samples were immersed in water at 286 C (pressure of 1000 psia). The same two types of alloy plates were tested in the earlier studies as were tested in the current quarter's work in which heated water was used. They were:

(1) a 6061 aluminum-clad, 77 w/o aluminum-23 w/o uranium (fully enriched) plate cut from a standard SPERT-ID plate. Each cladding layer and the core material were 20 mils thick. These plates had the nominal dimensions of 0.06 by 0.5 by 1.4 in. The edges of these plates were not clad.

(2) an unclad 81 w/o aluminum-17 w/o uranium (fully enriched)-2 w/o nickel alloy, which was the core material of the SL-1 fuel plates. These plates had the nominal dimensions of 0.2 by 0.5 by 0.5 in.

a. Experiments in Heated Water

Four experiments were conducted in water which was heated to 285 C and had a pressure of 1000 psia (saturated steam). Two experiments were conducted with SPERT plates, and two with samples of SL-1 core material. The parameters and the results of these experiments are summarized in Table IV-3. The samples were subjected to neutron bursts in TREAT at energy levels selected to correspond with experiments previously conducted in room-temperature water.

For each of the two types of samples, one transient (CEN 141H and 142H) was run at a reactor energy calculated to supply only enough energy to melt the plate. In these runs, the plates reacted with water in only negligible amounts, as was the case in the previous room-temperature-water experiments.

Table IV-3

RESULTS OF TREAT EXPERIMENTS WITH ALUMINUM-URANIUM ALLOY PLATES

TREAT Exp. CEN No.	Fuel Wt (g)	Initial Water Temp (C)	Reactor Characteristics		Calc Energy Input (cal/g)	Peak Temp Adiabatic[d] (C)	Appearance of Fuel after Transient	Extent of Reaction (%)
			Period (ms)	Int Power (MW-sec)				
141H	2.4850[a]	285 (1000 psig)	87	236	350	1130	Melted, bulged; retained a resemblance to its original shape	0.24
140H	2.3885[a]	285 (1000 psig)	86	348	500	1700	Melted into a single porous globule	76.0
142H	2.1605[b]	285 (1000 psig)	63	430	390	1275	Melted, sagged; retained a resemblance to its original shape	0.35
143H	1.9295[b]	285 (1000 psig)	46	650	570	1975	Melted into a single porous globule	89.0
144-1[c]	6.64	25 (20 psia He)	118	109	92	400	-	-
144-2[c]	6.64	25 (20 psia He)	62	410	353	1375	Melted into a single globule	0.4
145[c]	6.32	25 (20 psia He)	50	543	467	1875	Melted into a single porous globule	5.0

[a]Unclad SL-1 core material: 81 w/o Al-17 w/o U-2 w/o Ni; 0.2 x 0.2 x 0.5 in.

[b]Al-clad SPERT-ID plate: 77 w/o Al-23 w/o U; 0.06 x 0.5 x 1.4 in.

[c]Three SPERT-ID plates held in a stainless steel holder.

[d]These temperatures are calculated from the energy input and thermodynamic data, and are considerably higher than that actually reached by the sample due to heat losses.

Two other experiments (CEN-140H and -143H) were run at energies sufficient to cause complete melting and to generate actual fuel temperatures of the order of 1200 C or more. The extents of reaction (76 and 89%) in heated water were more extensive than in the experiments with room-temperature water (< 20%) at similar nuclear energy inputs. These results are shown as heated-water data in Figure IV-5, in which the extent of reaction of the plates is plotted as a function of the nuclear energy input. The data (reported in previous quarterlies) for runs with room-temperature water are included for comparison. For the heated-water experiments, the energy supplied by the autoclave heating system to raise the temperature of the plates from room temperature to 285 C was added to the nuclear energy input to allow comparison of the results. It is obvious from Figure IV-5 that in the two heated-water experiments conducted at the higher energies (one with a sample of SL-1 core material and one with a sample of SPERT-ID plate), reaction was much more extensive than in previous experiments. The two samples did not break up violently. The residue from each sample was a single globule contained in the alumina crucible which originally held the sample. The plate from experiment CEN-140H is shown in Figure IV-6. The crucibles were cracked, and a deposit of a fine alumina dust was found on inner surfaces of the autoclave.

Figure IV-5

NUCLEAR ENERGY INPUT VS. EXTENT OF REACTION FOR ALUMINUM-URANIUM ALLOY PLATE MELTDOWN EXPERIMENTS IN TREAT

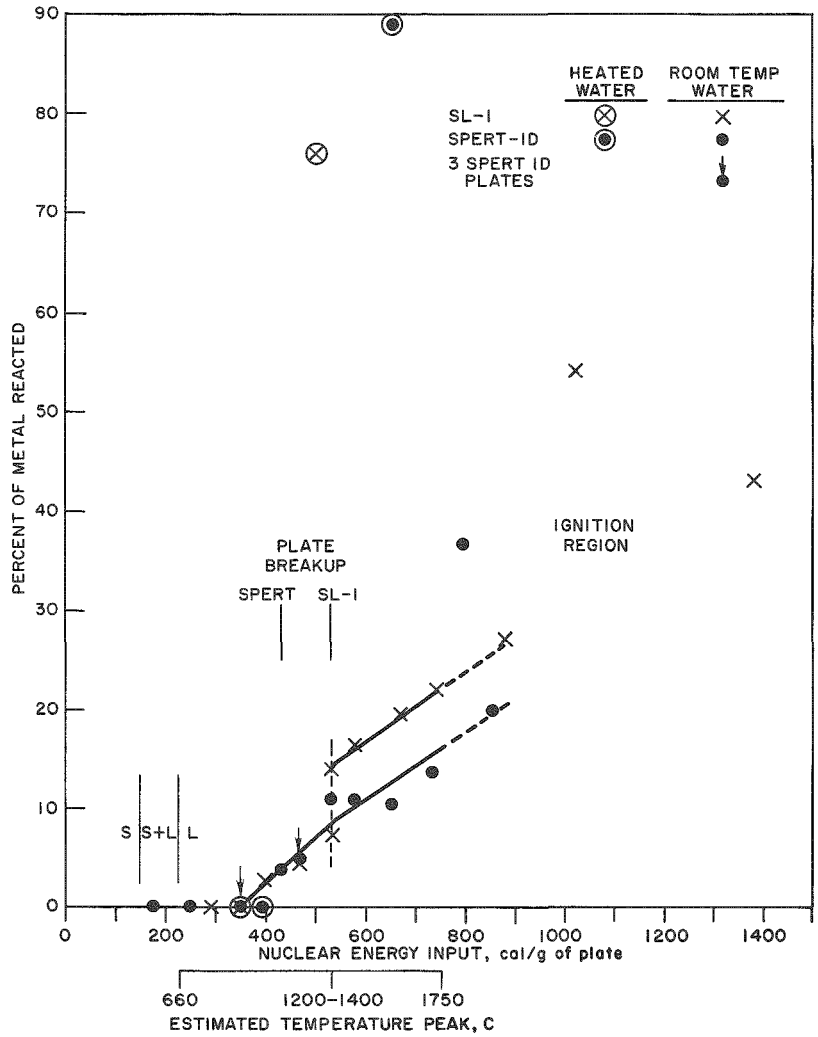

108-6765

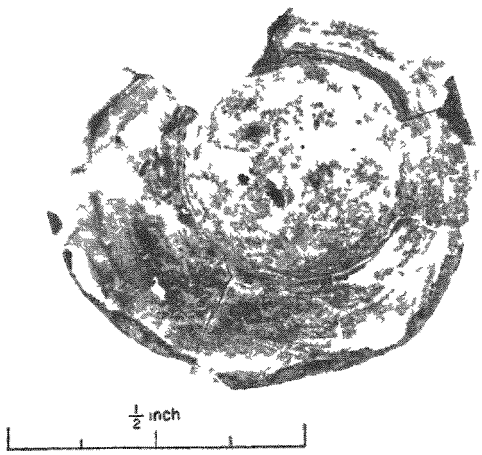

Figure IV-6

ALUMINUM-URANIUM ALLOY (UNCLAD SL-1 MATERIAL) AFTER MELTDOWN EXPERIMENT CEN-140H

108-6110

The reasons for extensive reaction are elusive. The possibility exists that the pressure and temperature used created a kinetic effect unlike any previously noted in these studies. It is thought that the difference in reaction rates may be related not only to differences in pressure in the autoclaves, but also to the fact that the heat losses in subcooled boiling (room-temperature water) are much greater than in saturated boiling (heated water). This difference in heat loss may have the effect of greatly diminishing the net energy input to specimens in room-temperature water. To overcome the heat loss in the experiments with room-temperature water, a nuclear heating rate much higher than in the experiments conducted in heated water may be required. Several investigators[7] have reported unusually high "burnout" heat fluxes (i.e., more recently referred to as DNB or Departure from Nucleate Boiling). The difference in the heat flux required to exceed the "burnout" temperature causes a difference in the effective nuclear energy input and the resulting sample temperature, depending on the initial water temperature. Further study is required in order to interpret the results of the experiments in heated water.

Transient-pressure measurements indicated that no explosive pressure increases occurred. Detailed reaction rates could not be derived from the pressure-time traces because of electrical interference of the transient neutron flux on the strain-gage circuitry. Methods for locating pressure transducers out of the high-flux region of the reactor core in future experiments are currently under study. It is anticipated that decreased fidelity resulting from placing the transducer at the end of a long tube will be more than offset by the decreased interference from the transient flux.

b. Experiments with Clusters of Fuel Plates

In each of two additional experiments, three SPERT-ID plates rather than one were irradiated (see Table IV-3) to determine the effect of multiple plates on the extent of reaction. Three plates, submerged in room-temperature water and held vertically in a slotted U-shaped stainless steel support, were subjected to transient bursts of the TREAT reactor.

The autoclave used in the first experiment (CEN-144) was subjected to two transients, the first imparting an energy of 92 cal/g to the plates (heating the plates to ~400 C) and the second melting the plates with an energy of 353 cal/g. The plates reacted to the extent of 0.4%, based on the amount of hydrogen evolved.

In the second experiment (CEN-145) the transient imparted an energy of 467 cal/g to the plates. These plates reacted to the extent of 5.0%. In Figure IV-5, the extent of reaction for these tests is compared with the previously reported experiments with individual SPERT-ID plates. The increase in the number of plates did not affect the extent of reaction.

[7]Drew, T. B., and Hoopes, J. W., Jr., Advances in Chemical Engineering, Vol. 11, Academic Press, New York, pp. 21-27 (1958).

In each case the three plates melted to form one large globule. The appearance of the resultant partially oxidized metal was similar to that for single-plate experiments conducted at like energy inputs. The melted plates from the lower-energy experiment, CEN-144, are shown in Figure IV-7.

Figure IV-7

THREE SPERT ID PLATES HELD IN STAINLESS STEEL HOLDER: IN ORIGINAL CONDITION AND AFTER MELTDOWN EXPERIMENT CEN-144

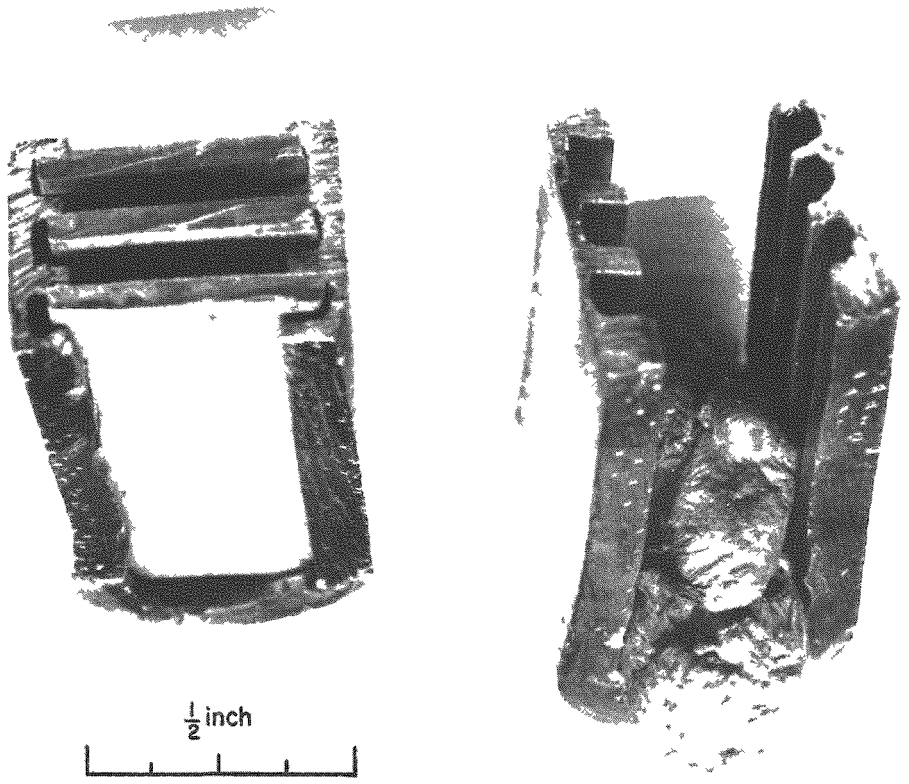

108-6166

Each of these experiments was instrumented with an unbonded strain-gage pressure transducer. The open top of the tubular alumina crucible in which the plates were held vertically faced the pressure transducer. Although the plates in experiment CEN-145 reached temperatures exceeding those estimated as a peak (~1250 C) in the recent SPERT-ID destructive test,[8] there was no indication of a rapid pressure rise. Radiation effects on the transducers prevented the determination of a small and gradual pressure rise.

[8] Report on SPERT-1 Destructive Test Results, Trans. Amer. Nucl. Soc. 6 (1), 137-141 (1963).

c. Breakup and Particle Size Determinations

In order to evaluate the metal-water reaction and to calculate the heat transfer to the coolant that would occur during an actual core destruction, a determination of the size distribution of the particles created is necessary. Unfortunately, there appears to be no satisfactory theoretical approach to predicting the size of particles produced in an excursion.

As part of the post-transient examination, a sieve screen analysis of TREAT specimens in which breakup occurred has been made in order to determine the particle size distribution. The distribution data have been presented in the form of histograms in preceding quarterly reports. The weight percent of particles versus particle diameter and the mean surface-volume diameters* (Sauter mean diameters) were tabulated (see ANL-6648, p. 201, and ANL-6687, p. 179). This average diameter is based on the specific surface per unit volume (i.e., the diameter of a sphere having the same surface-to-volume ratio as the group of particles it represents).

In Figure IV-8, the mean surface-volume diameter is plotted as a function of nuclear energy input for the SL-1 and SPERT plates whose percent reaction is correlated with nuclear energy input in Figure IV-5. For a sample in which breakup did not occur, the diameter chosen was that of a hypothetical sphere of the same mass as the original sample.

In Figure IV-8 it can be seen that a tenfold decrease in diameter (an increase in surface area by a factor of 100) occurred with a small increase in energy above that required for breakup. The threshold of breakup occurred at about 450 and 530 cal/g for the two types of samples.

d. Calculation of the Extent of Aluminum-Water Reaction Occurring in the SL-1 and SPERT-ID Destructive Transients

The rate and extent of metal-water reaction occurring during a reactor accident are ultimately analyzed by a synthesis of reactor kinetic and chemical reaction calculations. Although considerable knowledge exists in both areas, no rigorous means has been developed to analyze an accident involving core meltdown. The principal stumbling block has been uncertainty regarding the mechanism of fragmentation of the core and, in particular, the particle sizes produced. Knowledge is limited to the results obtained in small-scale meltdown experiments such as those described in the preceding sections of this report. In these studies, the effect of scale-up on the fragmentation of the materials has not been determined.

*$d_{sv} = \Sigma nd^3/\Sigma nd^2$ where n is the number of particles of diameter d.

Figure IV-8

AVERAGE PARTICLE SIZE OF ALUMINUM-URANIUM ALLOY PLATES AFTER IRRADIATION IN TREAT VERSUS NUCLEAR ENERGY INPUT

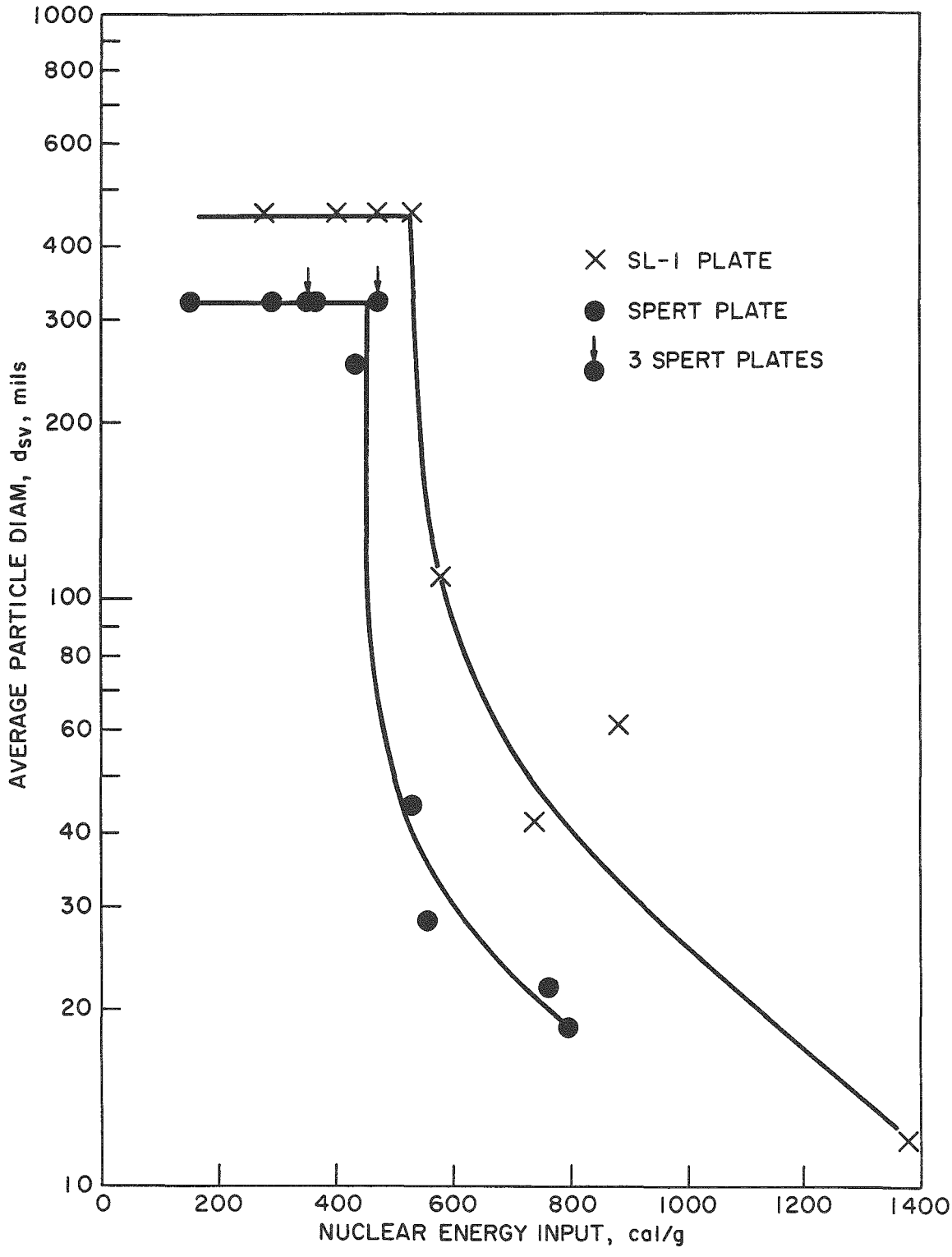

108-6763

In three separate facilities, aluminum-uranium alloy reactor cores have sustained nuclear excursions (see Table IV-4), resulting in extensive damage. Two of these excursions, those in Borax-I[9] and in SPERT-I[8,10,11] reactors, were full-scale excursion experiments; one, that in the SL-1 reactor,[12-14] was an accident.

Table IV-4

COMPARISON OF THE NUCLEAR EXCURSIONS OF THE BORAX-I, SL-1, AND SPERT-1 REACTORS

	Reactor		
	Borax-I	SL-1	SPERT-1
Date of Event	7/22/54	1/3/61	12/5/62
Category of Event	experiment	accident	experiment
Aluminum Present in Core, kg	~60	185	51
Uranium Present in Core, kg	~5.0	14.0	4.0
Reactor Period, ms	2.6	~4	3.2
Peak Power, MW	19,000(est.)	19,000 (est.)	2,300
Integrated Power, MW-sec	135	130	31
Chem Energy Release, MW-sec	-	24 ± 10	3-4
Peak Core Energy Density, cal/g	-	500	380
Peak Core Temperature, C (estimated)	-	>2000	1200-1300
Percent of Core Melted	-	32	35

The three incidents were very similar. Each reactor had a core of aluminum-clad, aluminum-uranium alloy plates. The excursion was initiated in each case by the rapid removal of a control rod. A large portion of the center of the core was melted and fragmented. Violent movement of a large portion of the coolant up and out of the reactor core occurred in each incident. In all three excursions, the core debris had a similar appearance. Portions of core that had been completely melted were spongy, and considerable quantities of metallic oxides were present.

---

[9]Dietrich J. R., Experimental Investigation of the Self-limitation of Power during Reactivity Transients in a Subcooled Water Moderated Reactor, Borax I Experiments, AECD-3668 (1954).

[10]Wilson T. R., An Engineering Description of the SPERT-1 Reactor Facility, IDO-16318 (1957).

[11]Quarterly Technical Report, SPERT Project, Jan., Feb., March, 1963, IDO-16893 (1963).

[12]Final Report of SL-1 Recovery Operation, IDO-19331 (1962), p. IV-21.

[13]Buchanan, J. R., SL-1 Final Report, Nuclear Safety; A Quarterly Progress Review, 4, No. 3, 83 (March 1963).

[14]Report on the Nuclear Incident at the SL-1 Reactor, January 3, 1961 at the National Reactor Testing Station, IDO-19302 (1962).

Whereas no attempt to determine the extent of reaction of the core with water in the Borax-I experiment has been reported, in the post-excursion analysis of both the SL-1 and SPERT-1 destructive excursions, portions of the debris were analyzed for alpha alumina. (Alpha alumina is the reaction product formed at temperatures above 600 C.) Based on the results of these analyses, combined with an overall material balance, chemical energy releases were estimated to be 24 ± 10 MW-sec and 3 to 4 MW-sec for the SL-1 and SPERT-1 excursions, respectively.

In order to estimate the extent of metal-water reaction which occurred in the SPERT and SL-1 excursions from the TREAT data, a calculation was made as follows:

1) The portion of core which became molten was assumed to be spherical, with x = 0 at the center and x = 1 at the surface. Therefore, the volume = $4\pi/3$.

2) The energy density was assumed to vary linearly with the distance from the center of the sphere. This assumption is probably valid as a first approximation. This relationship was expressed as

$$E_x = E_{max} - Ax,$$

where

E_x = Energy density at position x

E_{max} = Energy density at center (maximum)

A = Constant.

3) The maximum energy densities were taken from the literature as

a) E_{max}(SL-1) = 500 cal/g;[12]

b) E_{max}(SPERT-1) = 380 cal/g.[8]

4) The energy density at the surface of the sphere (x = 1) was taken as 220 cal/g, the energy required to heat aluminum to its melting point and completely melt it.* The equations for energy distribution were then determined to be

$$(SL\text{-}1)\ E_x = 500 - 280\ x;$$

$$(SPERT\text{-}1)\ E_x = 380 - 160\ x.$$

---

*Energies based on E = 0 at 25 C.

These equations were then used to calculate the energy distribution in the sphere by calculating the distances from the center of the sphere that achieved energies corresponding to various temperatures. The fraction of the sphere attaining a selected temperature or higher was then calculated as x^3. In steps of 100 C, the amounts of metal that achieved various energy levels were calculated.

The extent of reaction was then calculated from the TREAT data (see Figure IV-5). This was done by assuming the following:

1) A TREAT energy input of 220 cal/g results in complete melting of the material.

2) The break point of 530 cal/g (see Figure IV-8) in the TREAT data corresponds to the temperature range of 1200 to 1400 C.

3) The marked increase in extent of reaction at 750 cal/g in the TREAT data corresponds to a temperature of 1750 C.

The temperatures between these points were linearly interpolated. These assumptions were based on physical observations and metallographic examinations of the TREAT samples. The abscissa in Figure IV-5 includes both TREAT energies and assumed temperatures. The calculations are summarized in Tables IV-5 and IV-6. The estimates of chemical energy release calculated from TREAT data are in excellent agreement with the values (see Table IV-4) obtained by the post-excursion analyses of the SPERT-1 and SL-1 debris. The analysis of debris for α-alumina yielded 3.5 MW-sec of chemical energy release for SPERT-1 and 24 ± 10 MW-sec for SL-1. The calculations based on TREAT data yielded values of 2 MW-sec for SPERT-1 and 26 MW-sec for SL-1.

In this estimation, the extent of reaction is based on the peak temperatures reached by the molten core. This is necessary because the duration of the transients differed, being 40 to 100 ms in the TREAT experiments and 2 to 4 ms in the excursions. This method is applicable to other materials of core construction. Considerable experimental data obtained with the TREAT reactor has been published.[15]

---

[15] R. C. Liimatainen et al., ANL-6250 (Jan. 1962).

Table IV-5

CALCULATION OF EXTENT OF ALUMINUM-WATER REACTION IN THE SPERT-1 EXCURSION

(Based on 18 kg of molten core material)

Temperature Reached T (C)	Energy Density E(cal/g)	Distance from Reactor Center, x	x^3	Weight of Metal within Sphere of Radius x, W (kg)	Differential Weight ΔW (kg)	Percent Reaction	Metal Reacted (kg)
1250	380	0	0	0	-	-	0
1200	368	0.075	0.0004	0.0072	0.0072	10.0	0.0007
1100	342	0.238	0.0105	0.189	0.182	7.0	0.0127
1000	316	0.400	0.064	1.15	0.96	3.4	0.0326
900	290	0.562	0.178	3.24	2.09	1.2	0.0251
800	264	0.725	0.382	6.88	3.64	0.6	0.0218
700	238	0.888	0.700	12.60	5.72	0.2	0.0114
660	220	1.000	1.000	18.00	5.40	0.1	0.0054
						Total metal reacted	0.1097

0.1097 kg x 18 MW-sec/kg = 2.0 MW-sec chemical energy release

Table IV-6

CALCULATION OF EXTENT OF ALUMINUM-WATER REACTION IN THE SL-1 EXCURSION

(Based on 60 kg of molten core material)

Temperature Reached T (C)	Energy Density E(cal/g)	Distance from Reactor Center, x	x^3	Weight of Metal within Sphere of Radius x, W (kg)	Differential Weight ΔW (kg)	Percent Reaction	Metal Reacted (kg)
1700	500	0	0	0	-	-	0
1600	474	0.093	0.0008	0.048	0.048	19.9	0.010
1500	448	0.186	0.0066	0.395	0.347	17.2	0.060
1400	422	0.279	0.023	1.39	0.99	11.0	0.109
1300	396	0.372	0.051	3.06	1.67	11.0	0.184
1200	368	0.472	0.105	6.29	3.23	11.0	0.355
1100	342	0.564	0.180	10.8	4.5	7.0	0.315
1000	316	0.658	0.284	17.0	6.2	3.4	0.211
900	290	0.750	0.422	25.3	8.3	1.2	0.100
800	264	0.843	0.600	35.9	10.6	0.6	0.064
700	238	0.935	0.817	48.9	13.0	0.2	0.026
660	220	1.000	1.000	60.0	11.1	0.1	0 011
						Total metal reacted	1.445

1.445 kg x 18 MW-sec/kg = 26.0 MW-sec chemical energy release

V. ENERGY CONVERSION*

Two methods of directly converting nuclear energy into electricity are being investigated. One method involves the use of thermally regenerative cells; the other method, involving less effort, depends upon the thermocouple effect for the conversion.

A. Regenerative Emf Cell
(C. E. Crouthamel)

The basic studies of a regenerative cell system to convert heat into electricity are continuing, the eventual goal being to couple a thermally regenerative emf cell with a reactor heat source in a closed cyclic operation. The systems which appear to have the best chance of succeeding in this application are (1) the lithium hydride cell and (2) bimetallic cells employing fused salt electrolytes and liquid metal electrodes. Many of the basic chemical and physical properties of these systems are unknown, so that a considerable amount of basic research is necessary to provide an adequate foundation for both cell design and cyclic operations.

The basic studies that were carried out during the quarter were related to the following major categories of research: (1) development of regenerative bimetallic cells, (2) development of a regenerative lithium hydride cell, and (3) studies of cell regeneration at high temperatures.

The emf-temperature-composition diagram for a lithium-bismuth bimetallic cell is complete, and analysis of the data is in progress. The emf-temperature-composition diagram for the lithium-tin cell has been partially completed.

In the solid-liquid equilibrium studies of the binary lithium hydride-lithium chloride system, a difficulty (an additional unexplainable break in the cooling curve which appeared only on the lithium chloride solid-liquid equilibrium side of the phase diagram) was experienced when lithium chloride-rich mixtures were cooled. This difficulty may be typical of other fused-salt cooling-curve data in the literature in which lithium chloride is a component. Data in the literature on several fused salt binary systems involving lithium chloride as one of the components are being checked.

The equilibration of two liquid phases by the isopiestic technique is being examined for possible application in liquid metal-salt equilibrations. Of particular interest in the regenerative cell program are metal-salt solubilities at cell operating temperature (isothermal equilibration) and the vapor-phase equilibration of a bimetallic solution at high temperature (up to 1000°C) with a pure liquid (usually alkali metal) at lower temperature. Metal solubility in the cell electrolyte will transfer the anode liquid to the cathode by an irreversible process, and thereby lower the cell

*A summary of this section is given on pages 29 and 30.

voltage and efficiency. The high-temperature vapor-phase equilibria will determine the parameters for the regeneration of the cell reactants from the bimetallic cell product. An evaluation of the results is still incomplete.

1. Bimetallic Cells
(M. Foster, R. Eppley)

Thermodynamic functions of binary liquid metal systems and the associated solid intermetallic compounds which may be of interest in a regenerative cell system are under investigation. Two bimetallic systems are being studied: the lithium-bismuth and the lithium-tin systems. Galvanic cells in which the electrolytes are molten salts are being used in these studies.

Measurements of the lithium-bismuth system have been continued. The electrolyte was the eutectic mixture of LiCl-LiF. The data for a galvanic cell having a pure lithium anode and a bismuth cathode saturated with $Li_3Bi(s)$ were reported previously (see ANL-6687, p. 191). The cathode in the previous measurements remained saturated with $Li_3Bi(s)$ up to 60 a/o lithium in bismuth. This composition is a homogeneous solution at 775 C; below this temperature Li_3Bi solid precipitates, according to the known phase diagram. Reproducible data were obtained up to a temperature of 825 C.

This anode was then used as a reference anode for cells with various unsaturated liquid metal cathodes in which the mole fractions of lithium (X_{Li}) were 0.05, 0.20, 0.30 and 0.40. By use of this technique, the activity of lithium in the anode is reduced considerably over that of pure lithium metal, and thus the activity of lithium in solution (due to solubility) is correspondingly reduced. Finally, the irreversible transfer of lithium from the anode to the cathode is greatly reduced. These cells, with Li_3Bi-saturated anodes and dilute cathodes, yielded voltages which were quite stable with respect to time, even at the higher temperatures. The data were adjusted to yield the points shown in Figure V-1. The curves corresponding to $X_{Li} = 0.05$ and liquid bismuth saturated with Li_3Bi are derived from data taken in two independent runs at each concentration; the other curves are derived from data taken from single experiments. Thermodynamic quantities are being calculated from these data.

Owing to an insufficient difference in the vapor pressure of the two metals, it may be impractical to regenerate the cell by vaporizing lithium from the lithium-bismuth alloy. For example, at 900 C the equilibrium vapor pressures of pure lithium and bismuth are 12 mm and 0.5 mm, respectively. This would appreciably lower the cell output by returning a lithium-rich alloy of lithium and bismuth to the anode (and a bismuth-rich alloy to the cathode). A metal which has a lower vapor pressure than bismuth appears attractive in that the vapor separation of nearly pure lithium

might be much easier. Such a metal is tin, which has a normal boiling point of 2780 K[1] and at 900 C an equilibrium vapor pressure of 2×10^{-5} mm.

Figure V-1

POTENTIAL-TEMPERATURE CURVES OF THE CELL

Li(l)/LiCl-LiF(l)/Bi(l) with X_{Li}
(X_{Li} = Mole Fraction of Lithium)

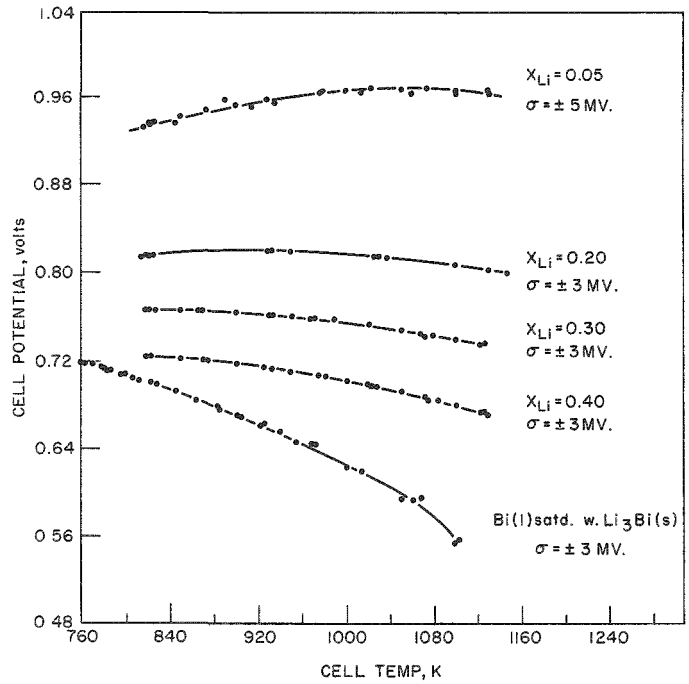

108-6875

Laboratory studies of lithium-tin cells are underway. The methods used are identical with those used previously. Data for cells utilizing LiCl-LiF eutectic as electrolyte in which a pure lithium anode and a saturated lithium-tin cathode were used are shown in Figure V-2.

Pronounced breaks in the emf-temperature plot are attributed to phase changes occurring in the cathode, e.g., in the upper curve, breaks are shown at 775 K and 963 K. At 775 K, the solid in equilibrium with a liquid alloy changes from Li_2Sn to Li_5Sn_2, and at ~963 K there is a transition from a two-phase system to a single liquid phase (unsaturated). It should be noted that in Figure V-2 the peritectic temperature (or the lower phase change) remains the same when the mole fraction of the lithium in the cathode is changed from 0.65 to 0.70. However, the transition to a one-phase

[1] J. A. Cahill and A. D. Kirshenbaum, J. Inorg. Nucl. Chem. 25, 501 (1963).

system occurs at a higher temperature when $X_{Li} = 0.70$ than when $X_{Li} = 0.65$, as would be expected. According to the phase diagram,[2] the upper transition in each respective cell should take place at the temperatures marked with triangles on Figure V-2. These are slightly lower than the temperatures observed - indeed, the observed temperature (~1003 K) of highest transformation is higher than the reported melting point (993 K) of solid Li_5Sn_2. Investigations of the phase diagram will be conducted to clarify this difference. Further thermodynamic studies of the lithium-tin system are continuing.

Figure V-2

POTENTIAL-TEMPERATURE CURVES OF THE CELL

Li(l)/LiCl-LiF/Sn(l) with X_{Li}
(X_{Li} = Mole Fraction of Lithium)

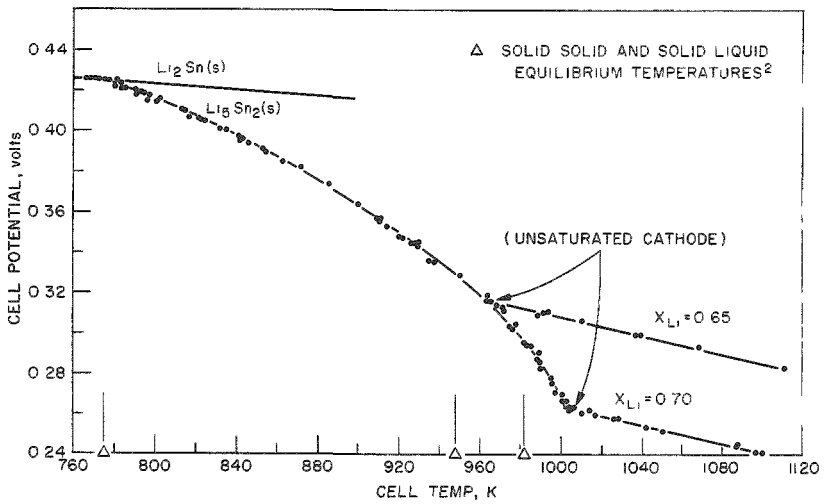

108-6833

A comparison of the saturated lithium-bismuth electrode potentials (Figure V-1) with the saturated lithium-tin electrode potentials (Figure V-2) shows a decrease of approximately 0.25 V for the latter. Both potentials were measured with reference to a pure liquid lithium metal anode, and both saturated electrodes contain comparable amounts of lithium, i.e., mole fractions of lithium in each saturated system at 1000 K is between 0.6 to 0.7. At comparable concentrations of the unsaturated electrodes the lithium-tin system will remain about 0.25 V below the lithium-bismuth electrode potential. This difference may be offset by the better vapor-phase separation of lithium from tin.

---

[2]Hansen, M., and K. Anderko, Constitution of Binary Alloys, Second Ed., McGraw-Hill Book Co., Inc., New York (1958)

2. Lithium Hydride-Lithium Chloride Solid-Liquid Equilibrium Studies

(C. Johnson, J. Allen)

The solid-liquid equilibrium curves of various electrolyte salt systems are needed for the design of both the lithium hydride cell and the bimetallic cell. The data of the LiH-LiCl binary system were obtained by apparatus previously described in ANL-6596, p. 203, and the method described in ANL-6648, p. 214. The phase diagram given in ANL-6687, p. 195, indicated higher solid-liquid equilibrium temperatures at the lithium chloride-rich side of the diagram than does Table V-1, which presents the final data. The eutectic melting point, 495.6 C, and the eutectic composition, 34.0 percent lithium hydride, remain unchanged.

Table V-1

LITHIUM HYDRIDE-LITHIUM CHLORIDE SOLID-LIQUID EQUILIBRIUM

LiH (mole fraction)	Solid-liquid Equilibrium Temperature (C)	LiH (mole fraction)	Solid-liquid Equilibrium Temperature (C)
0	606.8	0.401	529.1
0.050	595.0	0.495	561.6
0.061	592.4	0.522	572.3
0.101	581.5	0.576	585.8
0.151	567.5	0.654	605.9
0.210	551.6	0.698	619.7
0.249	538.5	0.786	639.5
0.289	521.7	0.852	655.9
0.340	495.6	0.901	665.1
0.382	523.2	1.00	685.8

A typical cooling curve on the lithium chloride-rich side of the solid-liquid equilibrium diagram always contained two exothermic breaks in addition to the eutectic halt. This anomalous behavior was completely absent with the lithium hydride-rich side of the solid-liquid equilibrium diagram.

If the first break was assumed to reflect the precipitation of a pure solid phase, lithium chloride, the second exothermic break in the cooling curve above the eutectic halt was difficult to explain. The problem is illustrated in Figure V-3 by three typical cooling curves obtained with a sample cup of the original design, and plots of the anomalous breaks compared with the final solid-liquid equilibrium data obtained with a sample cup of modified design.

On the cooling curves for salt mixtures containing 5, 20, and 33 m/o lithium hydride, there were three regions above the eutectic halt. Each line AB in Figure V-3 represents a binary fused salt system cooling as a homogeneous liquid mixture. The system was mechanically stirred

at the high temperature to insure complete mixing of the liquid salts and then was cooled with no additional stirring. At point B, precipitation of the pure solid-phase lithium chloride started and was expected to continue until the eutectic halt was reached at point D. However, at point C in each of the three curves, a second unexpected exothermic break appeared. The break at point C was sharper than the first one at point B, and when plotted gave the lower anomalous curve in Figure V-3.

Figure V-3

ANOMALY IN LiH-LiCl SOLID-LIQUID EQUILIBRIUM DATA

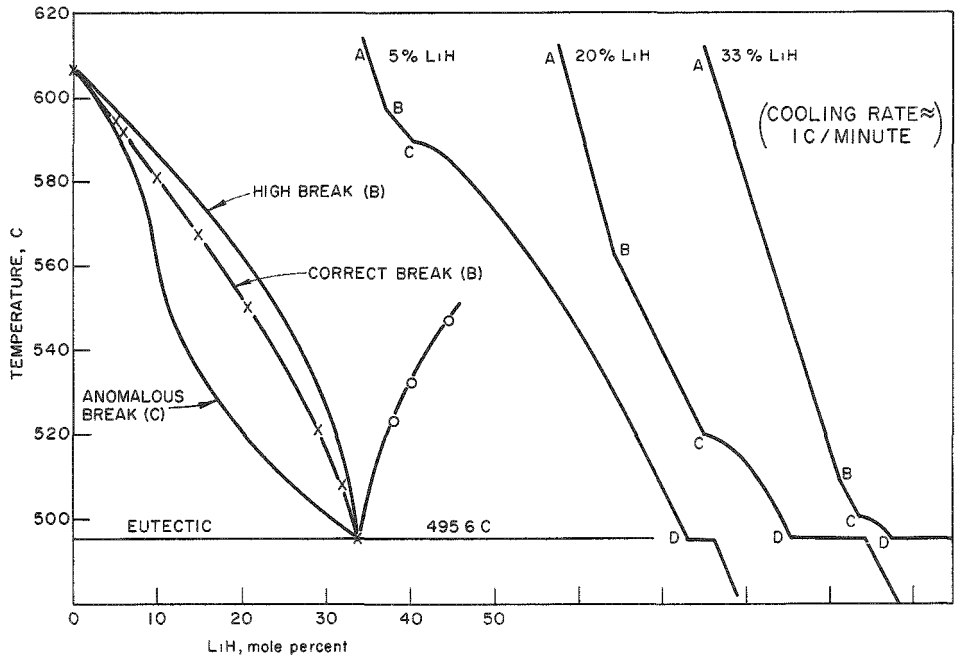

108-6895

Experiments have been done with a newly designed sample holder containing two circular heat-conducting fins and a thermocouple well which extends to the base of the cup. The two sample holder arrangements are shown in Figure V-4. When the new sample holder (B in Figure V-4) was used, the two breaks above the eutectic halt were replaced with a single break. In Figure V-4, the configuration of the salt mixture on cooling in the first cup used is depicted to aid in the understanding of the reason underlying the occurrence of the anomalous breaks. Solid lithium chloride forms initially on the walls of the container. When the first lithium chloride appears, the thermocouple in the centrally located well records a temperature somewhat above the true solid-liquid equilibrium temperature. The unexpected and sharp break at point C in Figure V-3 appears when sufficient solidification has occurred so that the liquid salts trapped in the shell of lithium chloride solid lose wet contact with the iron vessel, as depicted in Figure V-4A. Heat transfer through solid lithium chloride is low, and therefore the anomalous exothermic break in the cooling curve is very sharp. In contrast, conduction of heat through lithium

hydride solid was good enough so that no appreciable errors appeared in cooling curves on the lithium hydride side of the phase diagram. Nevertheless, with the old sample holder A in Figure V-4, heating curves were very poor on both sides of the phase diagram. Using sample holder B in Figure V-4, we were able to eliminate the anomalous break and to obtain corresponding solid-liquid breaks on both heating and cooling. Figure V-5 shows typical heating and cooling curves on the lithium chloride side of the phase diagram. The liquid-solid breaks were sharp on both curves and differ by less than 3 C.

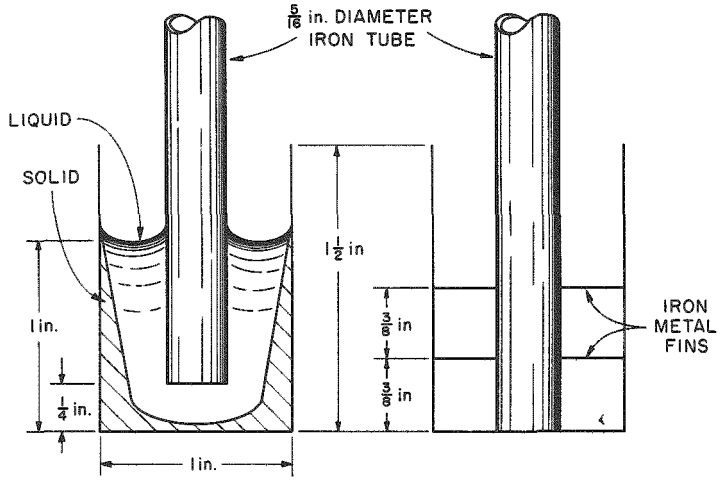

108-6859

Figure V-4

SAMPLE CONFIGURATION DURING TIME OF SOLIDIFICATION

Figure V-5

COMPARISON OF HEATING AND COOLING CURVES IN LiCl-LiH SYSTEM WITH SPECIALLY DESIGNED SAMPLE HOLDER

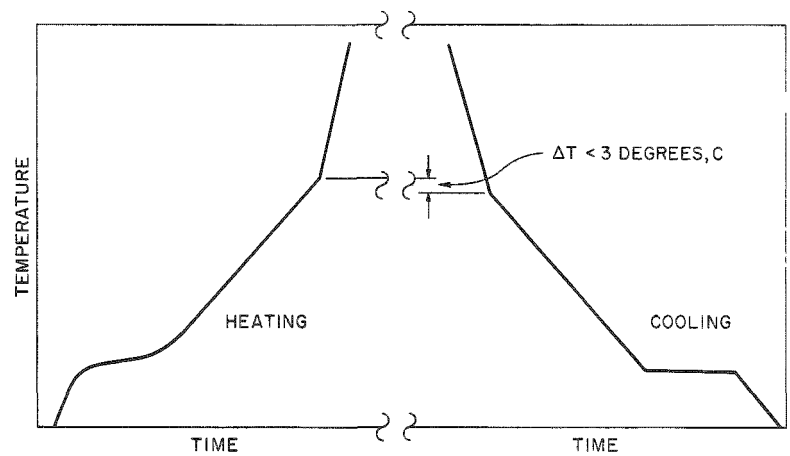

108-6891

Thermodynamic functions for each component were obtained from the liquid-solid equilibrium data by the method outlined by Wagner.[3] In the analysis of these data, only the heterogeneous equilibrium between pure solid and a binary liquid mixture was considered. With no evidence for solid solution in the heating and cooling curves, it was assumed that only pure solids precipitated from solution. The data are given in Tables V-2 and V-3. An integrated form of the Gibbs-Duhem equation was used to obtain the excess chemical potential of one component in the region of the other, as given in Figure V-6.

Table V-2

THERMODYNAMIC DATA FOR LiH IN LiH-LiCl SYSTEM

LiH (mole fraction)	T_e(a) (K)	$\overline{F}_1^M$(b) (cal/mole)	μ_1^{xs}(c) (cal/mole)	γ(d) at 1000 C
0.340(e)	768.8	-1089.8	558.4	1.324
0.382	796.4	-926.9	597.1	1.350
0.401	802.3	-892.7	565.2	1.329
0.495	834.8	-701.7	464.2	1.263
0.522	845.5	-648.4	442.7	1.250
0.576	859.0	-561.9	379.9	1.211
0.654	889.1	-447.2	294.6	1.160
0.698	892.9	-368.0	269.4	1.145
0.786	912.7	-256.7	178.9	1.094
0.852	929.1	-163.9	132.0	1.069
0.901	938.3	-114.3	79.8	1.041
1.0	959.0	-	-	1.00

(a) T_e = Solid-liquid equilibrium temperature

(b) $\overline{F}_1^M$ = Relative partial molar free energy of lithium hydride

(c) μ_1^{xs} - Excess partial molar free energy of lithium hydride

(d) γ - Activity coefficient, γ = 1 for pure LiH

(e) Eutectic composition

Table V-3

THERMODYNAMIC DATA FOR LiCl IN LiH-LiCl SYSTEM

LiCl (mole fraction)	T_e(a) (K)	$\overline{F}_2^M$(b) (cal/mole)	μ_2^{xs}(c) (cal/mole)	γ(d) at 1000 C
0.660(e)	768.8	-59.7	44.3	1.023
0.711	794.9	-453.9	84.9	1.044
0.751	811.7	-348.1	113.8	1.059
0.790	824.8	-295.2	91.2	1.047
0.849	840.7	-205.1	68.7	1.035
0.899	854.7	-135.4	45.4	1.023
0.939	865.6	-76.8	31.5	1.016
0.950	868.2	-64.3	24.2	1.012
1.0	879.9	-	-	1.00

(a) T_e = Solid-liquid equilibrium temperature

(b) $\overline{F}_2^M$ - Relative partial molar free energy of lithium chloride

(c) μ_2^{xs} Excess partial molar free energy of lithium chloride

(d) γ - Activity coefficient, γ = 1.00 for pure LiCl

(e) Eutectic composition

[3] Wagner, C., Thermodynamics of Alloys, Addison-Wesley Press, Cambridge, Mass. (1952).

Figure V-6

EXCESS FREE ENERGIES IN THE
LiH-LiCl BINARY SYSTEM

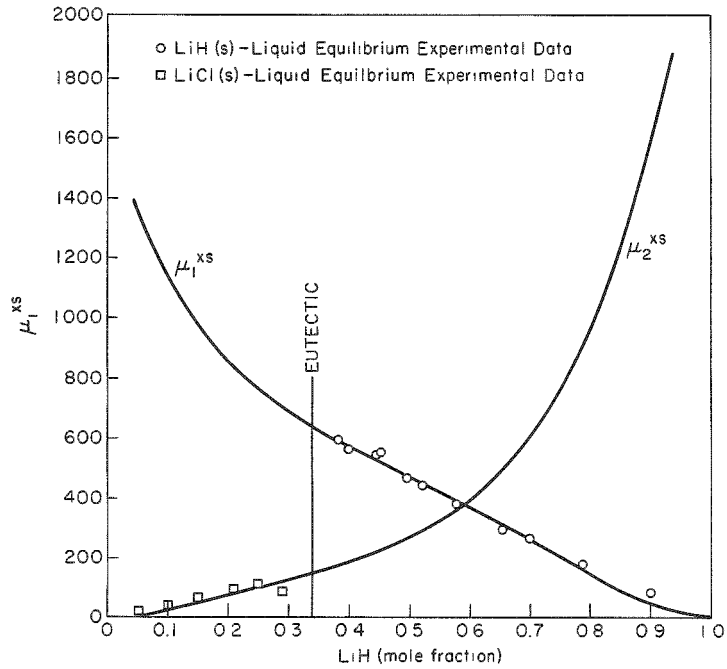

108-6854

Consideration of these data indicates that the system is close to an ideal solution. Examination of the activity coefficients for each component shows a drop in the neighborhood of the eutectic. This area of the phase diagram has been examined quite rigorously, and although it is believed that the experimental data are quite reliable, the exact nature of the behavior is not known. The system acts as if the eutectic melting point were depressed by some unknown means, but this seems unlikely, since no deviation in eutectic melting point has been observed in going from 5 to 95 m/o lithium hydride.

3. Isopiestic and Transpiration Techniques in the Study of Some Aspects of the Regenerative Emf Cell Problem
(A. K. Fischer, S. Johnson)

The isopiestic technique of phase equilibration and the transpiration technique of vapor-pressure measurement are well-suited to the study of certain problems connected with the conception and design of a regenerative fuel cell. These problems are: (1) the determination of solubilities of metals in each other and in a pure or mixed fused salt electrolyte; for this purpose and for the likely systems to arise, the isopiestic technique is, in principle, suitable; (2) the determination of the vapor pressures of the components in a cell product and thus the determination of the activity of these components in the cell product at various

temperatures; for this purpose, the transpiration technique is one of several which may be used, depending on the nature of the system of interest.

The first problem, the determination of solubilities of metals in fused salts and of metals in each other, is associated with the regenerative emf cell problem in that the degree of solubility of the reactive electrode in the electrolyte places a limit on the potential and output of the cell, and thus needs to be known. Development and evaluation of the isopiestic technique for these solubility measurements has been undertaken.

The isopiestic technique is well established for work with aqueous systems near room temperature, but little work has been reported in which the isopiestic technique has been applied at high temperatures. Nonapplication of the method in high-temperature work has apparently stemmed from the lack, until fairly recently, of means to enclose samples in envelopes which are inert and vacuum-tight at high temperatures. Provision of a uniform high-temperature field, though troublesome, has not been impossible. This accomplishment has led to further study on our part of the high-temperature isopiestic method with the uncovering of other difficulties.

In preparation for the application of the isopiestic technique to problems in the regenerative emf cell program, the following work has been done: (1) a furnace tube and a system of copper blocks which serve as a high-temperature thermostat has been designed, and (2) a crucible and enclosing tube system which can be sealed under vacuum and then placed in the high-temperature thermostat, has also been designed. The copper blocks, crucibles, and enclosing tube are placed in a furnace tube provided with an argon atmosphere to protect the copper from oxidation. The Marshall furnace windings are controlled in sections to provide a uniform temperature zone.

As a preliminary check on the isopiestic technique, some solubility determinations on the lithium-lithium chloride system have been undertaken. This system is of interest in regenerative cells with a lithium electrode and with lithium chloride as the electrolyte or as an electrolyte component. The small amount of data on the lithium-lithium chloride system available in the literature can be compared with experimental values as a partial check on the reliability of the technique. Three measurements of the solubility of lithium in lithium chloride have been completed to date. The results are: 1.3 a/o at 609 C, 3.1 a/o at 727 C, and 2.6 a/o at 770 C. At the opposite ends of the tie lines, the solubilities of lithium chloride in lithium were found to be 8.5 a/o at 609 C, 9.6 a/o at 727 C, and 8.8 a/o at 770 C. Additional experiments are needed to appraise the technique adequately and to characterize the lithium-lithium chloride system. The only literature values for the solubility of lithium in lithium chloride are 0.5 ± 0.2 a/o at 650 C and 2.0 ± 0.2 a/o at 1000 C.[4]

[4]A. S. Dworkin, H. R. Bronstein, and M. A. Bredig, J. Phys. Chem. 66, 572 (1962).

Because of the scarcity of data on the lithium-lithium chloride system, a more thoroughly reported system (such as potassium-potassium chloride) may be studied to permit more accurate testing of the isopiestic technique. The potassium-potassium chloride system has no direct bearing on any of the regenerative cells that are now being studied.

During the preliminary testing of the equipment, analyses of the upper and lower regions of the sample tube, and of the outsides of the crucibles, have shown that "wild" distillation (distillation to sites other than in the equilibrating phases) is low and apparently is not a major source of error as we conduct the experiment. At the present time, it is believed that the data obtained in the isopiestic experiments are fairly reliable, but that a number of variables, such as duration of equilibration, quenching rate, and sample size ratio, need to be tested to gain assurance of the validity of results. If the isopiestic procedure is reliable at high temperatures, a versatile tool will be available for solubility measurements and, thus, for tracing the miscibility gap in phase diagrams of binary liquid systems.

In contrast with the isopiestic technique, which is relatively neglected, the transpiration technique is widely applied in high-temperature chemistry and is used to measure vapor pressures. Materials having vapor pressures that are too high to be measured by the Knudsen method may be studied by the transpiration method. Materials having high vapor pressures are likely to be used in thermally regenerative emf cells in which a cell product is to be decomposed thermally. (Low vapor pressure for components would argue against the feasibility of the desired regeneration.) Measurement of the vapor pressure of, for example, lithium and/or bismuth over Li_3Bi and over Li_3Bi-Li mixtures at various temperatures will permit calculation of the activities of both components in the cell product at the various temperatures. This information, then, would be used to determine the feasibility and the optimum conditions for the regeneration.

A transpiration apparatus has been assembled and has been tested for leaks. Essentially, the transpiration apparatus is of conventional design, being a vertical-tube type with a fritted disc to support the sample and to permit argon to pass through the sample.

B. Thermoelectricity Research
(R. K. Edwards and H. M. Feder)

Studies in thermoelectricity are underway to contribute to the future technological development of direct conversion of nuclear reactor heat energy into electrical power by means of the thermocouple effect.

Two limited materials areas have been selected as of special interest. Liquid thermocouple materials are under investigation because of

favorable experimental factors. Refractory solid thermocouple systems form the other major area, since they are considered to be of particular interest to reactor energy conversion.

The personnel associated with thermoelectricity research are undertaking additional research in the area of high-temperature materials. A program of high-temperature chemistry has been begun which is centered about likely high-performance fuels in their operating environments. Currently, equipment planning and acquisition are in progress. The following studies of refractory materials are planned: (a) effusion and mass spectrometric studies of the gaseous decomposition products, (b) gaseous transpiration studies, (c) phase diagram and interdiffusion studies.

1. Liquid Systems
(R. K. Edwards, P. Danielson)

The studies of Seebeck coefficients in liquid systems were deferred during this report period in favor of equipment planning, designing, and acquisition for projected high-temperature studies.

Future plans are to carry out measurements of Seebeck coefficient values in the liquid indium-bismuth system at 750 C so that the results of the three related systems: indium-bismuth, indium-antimony, and antimony-bismuth, may be compared for the same temperature. Plans are also underway for measurement of electrical conductivities in these systems, and equipment is being modified for this purpose.

2. Refractory Solid Thermocouple Systems
(M. Tetenbaum, F. Mrazek)

For energy-conversion devices that are to be used at high temperatures, as in certain nuclear reactor systems, materials possessing high melting points and low vapor pressures are desirable. The lanthanide and actinide sulfide systems are highly refractory and have phases with carrier concentrations in the semiconducting range. The uranium sulfide and thorium sulfide systems and their solid solutions have been selected for the initial studies. In addition, preliminary studies on uranium monophosphide have been initiated during the past quarter.

Preparation of Uranium Monosulfide

A 100-g batch of relatively high-purity uranium monosulfide was prepared during the past quarter for measurements of the heat of formation of uranium monosulfide by the Calorimetry Group and for thermoelectric parameter measurements. The pertinent steps involved in the preparation are as follows: 1) preparation of the hydride, 2) its thermal decomposition to give finely divided metal, 3) reaction of the finely divided metal with hydrogen sulfide to give a mixture of metal and higher sulfides, and 4) homogenizing by

heating this mixture in a tungsten crucible to approximately 2000 C in vacuum (~10^{-5} mm Hg) to produce sintered crystalline uranium monosulfide. Certain modifications in handling techniques were incorporated into the procedure in order to minimize exposure of the crude sulfide product to air when the charge is transferred into the NRC furnace.* This was accomplished as follows: After the sulfiding step and prior to homogenization, the crude sulfide product was loaded into tungsten crucibles in a dry box, and the crucibles were sealed in plastic bags. The crucibles in their plastic bags were removed from the dry box, inserted into the NRC furnace, and the package fired by slowly heating to ~2000 C. The plastic volatilized at approximately 500 C. A liquid nitrogen trap was incorporated into the NRC furnace unit to minimize back diffusion of oil vapor from the diffusion pump.

Because of the limitation of crucible size, the 100-g batch of crude sulfide product was divided into five equal batches which were fired individually in order to homogenize the material. The maximum homogenization temperature was approximately 1900-1950 C. After homogenization, the ingots were all bright and shiny. Analytical results obtained thus far are shown below.

Batch	Insolubles (%)	S (%)	Atom Ratio, S/U
1	0.00	12.39	1.05
2	0.00	12.10	1.02
3	0.14	12.30	1.04
4	0.56	12.70	1.08
5	0.00	12.55	1.07

X-ray analysis of Batch 2 gave a lattice parameter of $a_0 = 5.488 \pm 0.005$ Å.

The uranium monosulfide product represented by Batch 2 was ultimately used to prepare some of the specimens for the thermoelectric parameter studies described below. The remainder of the batch will be used by the Calorimetry Group for measuring the heat of formation of uranium monosulfide.

Determination of Seebeck Coefficients

The essential features of the apparatus used for Seebeck measurements are shown schematically in Figure V-7. The specimens were pressed between two tantalum plates by means of a spring-operated thrust rod impinging on the surface of the upper tantalum plate. Platinum-platinum, 10 percent rhodium thermocouples, spot-welded on the tantalum plates, were used to measure both the temperature gradient and the Seebeck voltage (relative to platinum) across the samples. The emf's developed were measured by means of a Leeds and Northrup K3 potentiometer. The temperature

*Manufactured by NRC Equipment Corporation, Newton, Massachusetts.

Figure V-7

SCHEMATIC DIAGRAM OF APPARATUS USED FOR MEASUREMENTS OF SEEBECK COEFFICIENT AND RESISTIVITY AS A FUNCTION OF TEMPERATURE

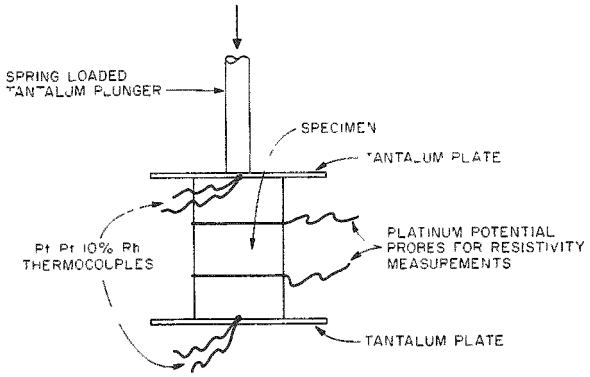

108-6861

gradient existing in the furnace* was used to generate the Seebeck potential. The temperature gradient across the specimen generally was 10 to 15 C. The specimen and assembly shown in Figure V-7 were housed in an Inconel tube, and all measurements were made in vacuum (10^{-4} to 10^{-5} mm Hg). The differential Seebeck coefficient α_{S-Pt} of the specimen S relative to platinum is defined by

$$\alpha_{S-Pt} \equiv \lim_{\Delta T \to 0} \frac{\Delta V}{\Delta T},$$

and is taken to be effectively $\Delta V/\Delta T$ for the small ΔT values used, where ΔV is the Seebeck voltage developed as a result of the temperature difference ΔT. The absolute Seebeck coefficient of the specimen can be obtained by algebraically subtracting the Seebeck coefficient value of platinum from the differential Seebeck coefficient.

Resistivity Measurements

The resistivity was measured by passing a direct current (generally 50-100 mA) through the specimen and measuring the voltage produced between the two platinum probes wrapped around the specimen (Figure V-7). (A leg from each thermocouple at the ends of the specimen served as current leads.) The current was reversed, and a second voltage reading was taken immediately; the mean voltage was used to calculate the resistivity ρ by means of the following formula:

$$\rho = VA/Id,$$

where

V = mean voltage measured between probes
I = current
A = cross-sectional area of the specimen
d = distance between probes

The voltage drop across the probes was measured with either an L & N K3 potentiometer or an L & N DC Microvolt Indicating Amplifier (Model 9835B). The current through the specimen was determined by measuring the voltage drop across a standard resistance in series with the specimen, with a conventional potentiometer.

*Manufactured by the Marshall Furnace Company, Columbus, Ohio.

Thermoelectric Power Measurements on Uranium Monosulfide

Measurements of the Seebeck coefficient as a function of temperature have been made for a sintered pellet of relatively high-purity (see section, Preparation of Uranium Monosulfide) monosulfide (negligible insolubles content; S/U, ~1.02) and for a slab of uranium monosulfide (7.8-mm length and 2.6-mm width) which was fabricated from a melted ingot* (1.1 percent insolubles; S/U. ~ 0.97). The results are shown in Figure V-8. It is apparent from Figure V-8 that the trend and magnitude of the Seebeck coefficient values with temperature are approximately the same for the sintered specimen as for the melted specimen.

Figure V-8

COMPARISON OF ABSOLUTE SEEBECK COEFFICIENT AS A FUNCTION OF TEMPERATURE FOR URANIUM MONOSULFIDE SPECIMENS

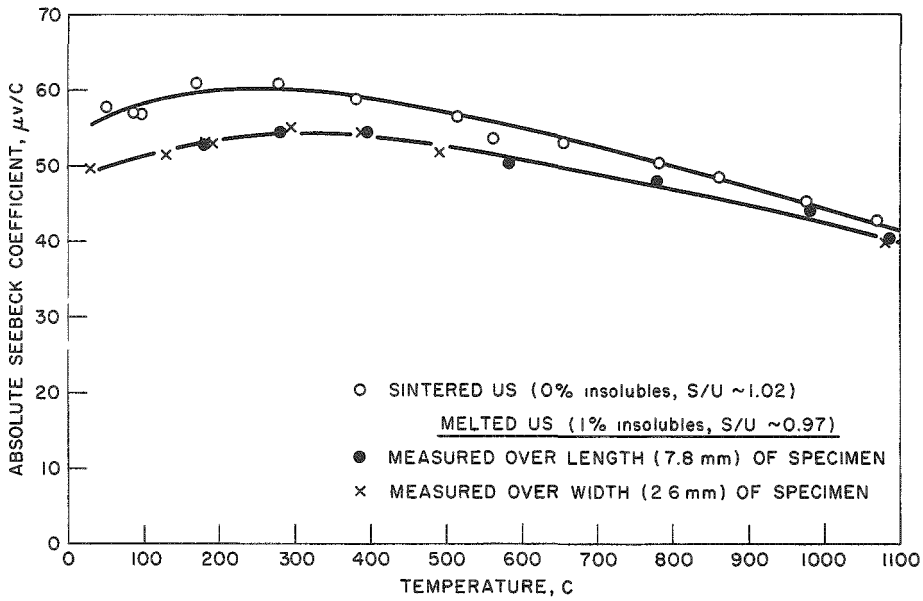

108-6844

It should be noted that the Seebeck data shown for the uranium monosulfide slab were obtained by two independent sets of measurements. In one set, the specimen was sandwiched lengthwise between the tantalum plates; in the second set of measurements, the specimen was sandwiched widthwise. Table V-4 allows a comparison of the differential Seebeck coefficient values obtained when measuring over the length or the width of the specimen at roughly corresponding temperatures but with different temperature gradients across the specimen. It is apparent that agreement for the two sets of measurements is good, and that the Seebeck apparatus (Figure V-7) is capable of yielding reproducible data.

*We are indebted to R. Noland of the Metallurgy Division for supplying the ingot.

Table V-4

COMPARISON OF SEEBECK COEFFICIENTS FOR MELTED URANIUM MONOSULFIDE SPECIMEN

Length of Specimen: 7.8 mm
Width of Specimen: 2.6 mm

	Average Temperature (C)	Temperature Gradient across Specimen (C)	Differential Seebeck Coefficient (μV/C)
Length	172.1	22.0	62.8
Width	179.7	5.7	61.6
Length	282.8	12.8	65.6
Width	295.1	10.1	66.2
Length	387.0	12.3	67.2
Width	386.6	9.0	67.2
Length	1086.2	9.5	63.3
Width	1080.7	7.1	61.6

Effect of Higher Sulfides in Uranium Monosulfide on Seebeck Coefficient Values

A cursory examination of the effect of higher sulfides on the thermoelectric power of uranium monosulfide was made during this quarter. X-ray analysis of the uranium monosulfide powder (S/U = 1.3) containing higher sulfides revealed the presence of the following phases: US, U_2S_3, and U_3S_5. The powder was cold pressed into a pellet and was sintered for approximately one hour at 1200 C in vacuum. Seebeck coefficient values as a function of temperature for the sintered pellet and for pure uranium monosulfide were determined and are shown in Figure V-9. The presence of higher sulfides in uranium monosulfide apparently results in a considerable decrease in the value of the Seebeck coefficient as the temperature is increased. Ultimately, in the vicinity of 600 C, the sign of the Seebeck coefficient changes. Slightly higher values were obtained during the cooling cycle, apparently because of composition changes occurring during the measurements.

Resistivity of Thorium Monosulfide and 50-50 US-ThS Solid Solution

Resistivity has been measured as a function of temperature for sintered specimens of thorium monosulfide and a 50-50 m/o solid solution of uranium monosulfide and thorium monosulfide. The results are shown on Figure V-10. The thorium monosulfide specimen showed a linear increase of resistivity with increasing temperature, which is characteristic of metallic behavior, and is also consistent with the trend in Seebeck values obtained

Figure V-9

EFFECT OF HIGHER SULFIDES ON THE THERMOELECTRIC POWER OF URANIUM MONOSULFIDE

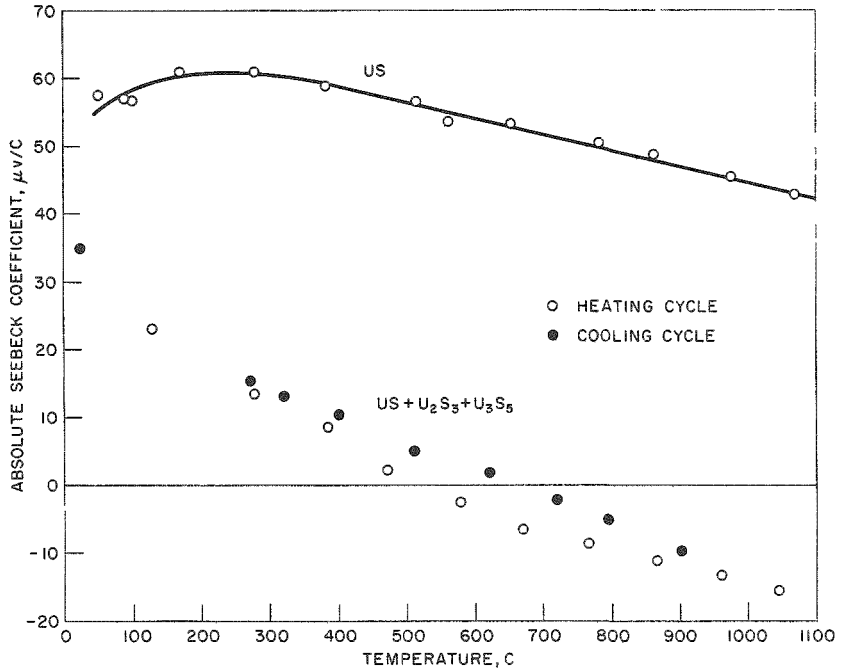

108-6857

Figure V-10

RESISTIVITY AS A FUNCTION OF TEMPERATURE FOR SINTERED SPECIMENS OF THORIUM MONOSULFIDE AND 50-50 m/o US-ThS SOLID SOLUTION

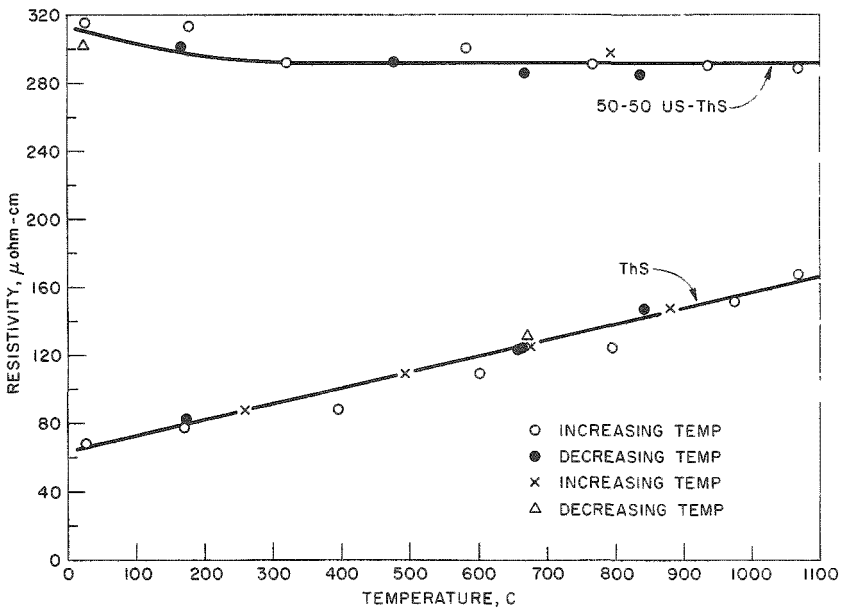

108-6847

with this material, namely, an increase in Seebeck coefficient with temperature (at 25 C, $\alpha \cong -5$ μV/deg; at 1000 C, $\alpha \cong -12$ μV/deg). For the 50-50 solid solution, the resistivity is nearly constant with temperature. Similar behavior was previously reported for a sintered specimen of uranium monosulfide containing approximately 5 w/o insolubles (see ANL-6648, p. 230).

The temperature dependence of resistivity for specimens of compositions (mole percent) 25 US-75 ThS and 75 US-25 ThS is to be measured.

Thermoelectric Parameter Measurements on Uranium Monophosphide

Determinations of the Seebeck coefficient as a function of temperature and measurements of the room temperature resistivity of a sintered pellet of uranium monophosphide* have been made. The magnitude and trend in Seebeck coefficient values for uranium monophosphide (see Figure V-11) are almost identical with the values obtained with uranium monosulfide. The room-temperature resistivity of uranium monophosphide was found to be approximately 250 x 10^{-6} ohm-cm, which is also comparable with the room-temperature resistivity of uranium monosulfide.

Figure V-11

ABSOLUTE SEEBECK COEFFICIENT VS. TEMPERATURE FOR URANIUM MONOPHOSPHIDE

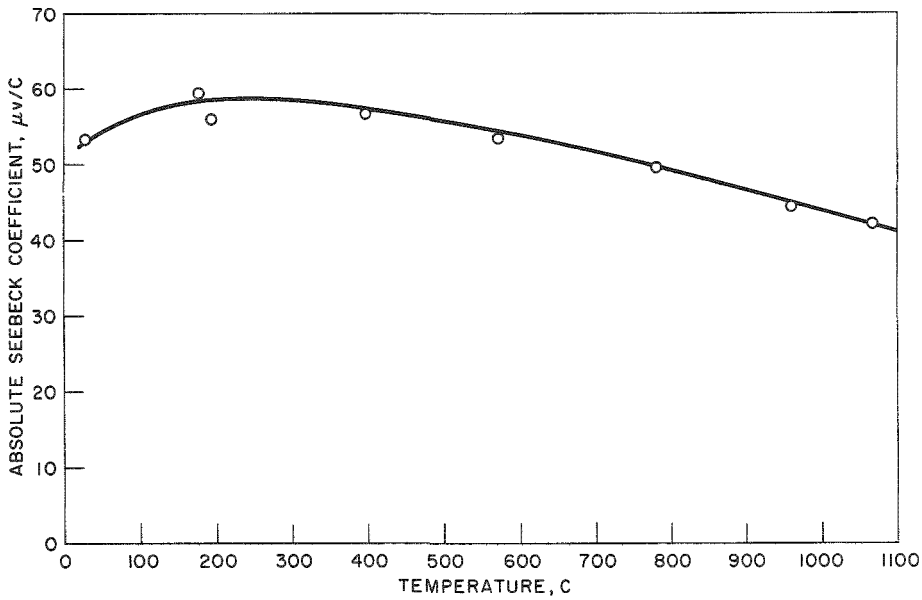

108-6860

*We are indebted to Yehuda Baskin of the Metallurgy Division for preparing the specimen.

The room-temperature Seebeck coefficient and resistivity values measured by other investigators[5] are shown below to allow comparison with ANL values.

Experiment No.	Material[a]	Seebeck Coefficient (μV/C)	Resistivity (ohm-cm x 10^6)
114	UP	+52.6	1460
115	UP	+50.0	1180

[a]The composition of the uranium phosphide compacts is unknown.

The room-temperature Seebeck values shown in the table are in good agreement with our measurements; however, the resistivity value measured by us is lower by a factor of approximately five. The Seebeck coefficients determined at ANL with various specimens of uranium monosulfide were also found to be relatively insensitive to the resistivity of the specimens investigated.

The Canadian Report[5] gives a value of approximately 0.0571 W/cm-deg for the room-temperature thermal conductivity of uranium monophosphide. With the use of this value and the values of the average Seebeck coefficient and resistivity obtained from the above table, the value for the figure of merit Z of uranium monophosphide at room temperature was calculated to be approximately 3.5×10^{-5}. This figure of merit value is about three times lower than the room-temperature Z value obtained with uranium monosulfide from ANL measurements of thermoelectric parameters. In addition, with the use of the Canadian data, a Wiedemann-Franz ratio of approximately 25.2×10^{-8} $(V/deg)^2$ was calculated for uranium monosulfide. With our resistivity value, the ratio was found to be about 4.8×10^{-8} $(V/deg)^2$. For a degenerate (carrier density $\geqq 10^{21}$/cc) material, the theoretical value is 2.45×10^{-8} $(V/deg)^2$. It appears, therefore, that the lower resistivity value is more nearly the correct one. Using the ANL resistivity value to estimate the room-temperature figure of merit for uranium monophosphide, we find $Z \cong 1.2 \times 10^{-4}$, which is comparable with the Z value obtained with uranium monosulfide. However, these room-temperature values for the figure of merit are too low for useful power generation by a factor of approximately ten.

[5]Progress Report No. 3, Department of Metallurgy, University of British Columbia, September 1961.

VI. DETERMINATION OF NUCLEAR CONSTANTS*

(C. E. Crouthamel)

The fast reactor program continues to require fast neutron cross section data as new elements begin to receive consideration for use in reactor construction. Total neutron cross sections are being measured for neutron energies between about 10 keV and 2 MeV, and capture cross sections as a function of neutron energy between 0.2 MeV and 2 MeV.

Recent work with rhenium has yielded capture cross sections for neutron energies between 150 keV and 2 MeV; total neutron cross-section measurements for this element are in progress. Results are also given for the total neutron cross sections of gadolinium and the neutron capture cross sections of erbium-170.

Fast Neutron Cross Sections

(C. E. Crouthamel, D. C. Stupegia, A. A. Madson, and M. Jones)

Rhenium: This dense metal has recently received attention for possible use as a reactor material because of its favorable high-temperature properties. It is being considered for use in an alloy with tungsten as a fuel element matrix material. A study of its fast neutron cross sections has therefore been undertaken, and preliminary neutron capture cross section values have been determined.

Rhenium consists isotopically of 37.07 percent rhenium-185 and 62.93 percent rhenium-187. Neutron irradiation of rhenium produces the following three capture reactions:

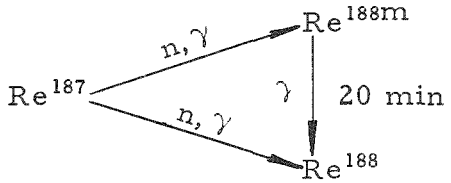

$$\xrightarrow[\beta,\gamma]{17\ \text{hr}} Os^{188};$$

$$Re^{185} \xrightarrow{n,\gamma} Re^{186} \xrightarrow[\beta,\gamma]{90\ \text{hr}} Os^{186}.$$

By suitable choice of length of irradiation and gamma analyses following irradiation, the cross sections for all three processes can be measured.

In this work the monoenergetic neutron source was the reaction $Li^7(p,n)Be^7$ produced when protons from the Van de Graaff accelerator bombard a lithium target. The neutron flux was measured with a fission chamber which counted fissions in a sample of uranium. After irradiation,

*A summary of this section is given on page 30.

the target was analyzed for the gamma-ray spectrum of its activation products by means of a NaI crystal and multichannel analyzer. The absolute disintegration rate corresponding to the gamma spectrum of the irradiated target was determined by comparing this spectrum with that of a known activity of the same species counted in the same geometry, the activity of the latter having been determined by absolute beta counting.

Irradiations of several hours were carried out, following which gamma analyses were done on the targets. These irradiations yielded the data necessary for the determination of the cross section of rhenium-185 and of the cross section for the production of both states of rhenium-187. Irradiations of 20-min duration were carried out and the targets were analyzed for the gamma ray of 20-min rhenium-188m. Thus when the cross sections for the production of the 20-min state and of the sum of both rhenium-188 states are known, the cross section for each state alone can be calculated.

Preliminary data for the capture cross section of rhenium-187 are given in Figure VI-1. The cross sections given represent the sum for the production of both states of rhenium-188. The absolute calibration of the rhenium-187 cross section has not yet been completed, but the values given in the figure have been estimated to be accurate to ±50%. The values of the points relative to each other are believed to be correct to ±7%. The data have not yet been analyzed to the point where the cross sections for the production of the two states of rhenium-188 can be given separately, nor has the cross section of rhenium-185 been calculated. These analyses are in progress.

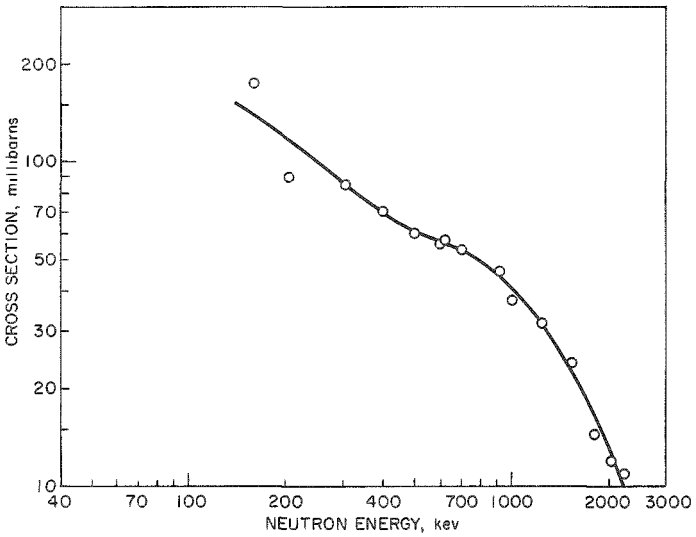

Figure VI-1

NEUTRON CAPTURE CROSS SECTIONS OF RHENIUM-187

108-6832

Total neutron cross sections of rhenium as a function of neutron energy are also being determined in this program. The results of this work will be reported when more data are available.

Cross Sections of Rare Earth Elements

Some of the rare earths, such as Gd, Sm, Eu, and Dy, have been considered as possible reactor control materials and as constituents of ceramic control elements (see Summary Report ANL-6379, p. 226). In the present report, total neutron cross sections of gadolinium and neutron capture cross sections of erbium are given.

Gadolinium: The total neutron cross section of gadolinium has been determined as a function of neutron energy between 9 keV and 1880 keV. The results are shown in Figure VI-2. The standard deviations of the cross section values are about ±2%, and the neutron-energy spreads at each point are generally such that they just overlap between successive points. This work was done with use of the Van de Graaff accelerator of the Physics Division.

Figure VI-2

NEUTRON TOTAL CROSS SECTION OF GADOLINIUM

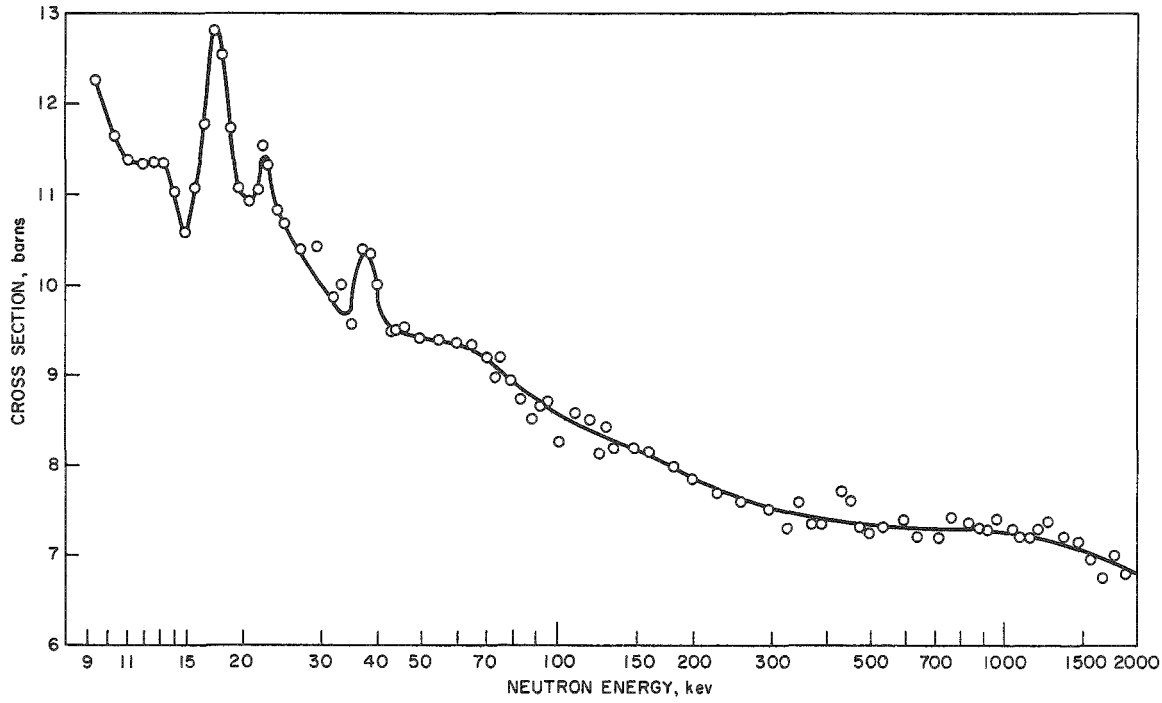

108-6845

Erbium-170: The neutron capture cross section of erbium-170 has been determined for neutron energies between 0.34 and 1.9 MeV. The results are given in Figure VI-3. The neutron-energy spreads at each point are about ±25 keV. Standard deviations of the cross sections are about ±8%. The experimental procedures were basically the same as those described above for rhenium.

Figure VI-3

NEUTRON CAPTURE CROSS SECTION OF ERBIUM-170

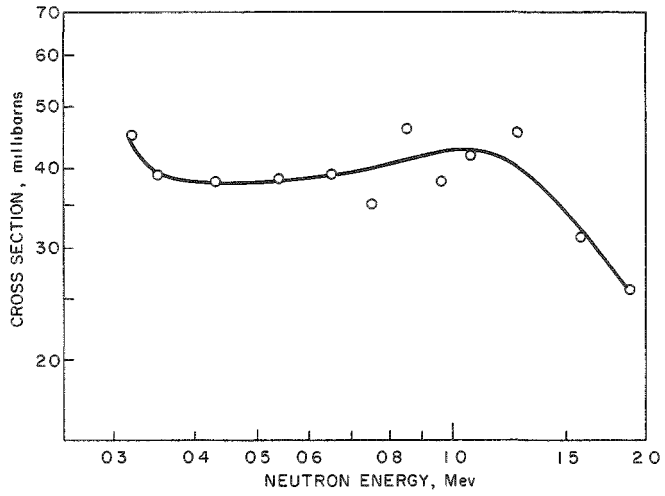

108-6834